AN ABSTRACT OF THE THESIS OF

Anthony G. Hafner for the degree of Master of Science in Civil Engineering presented on March 20, 2012

Title: Experimental Research on the Behavior and Strength of Large-Scale Steel Gusset Plates in Sway-buckling Response Including Effects of Corrosion and Retrofit Options

Abstract approved:

Christopher C. Higgins

The collapse of the I-35W Bridge in Minneapolis, MN on August 1, 2007 brought into question the design and inspection of gusset plates in steel truss bridges. The experimental tests performed in this research study the sway-buckling strength and behavior of large-scale steel gusset plates in an isolated truss connection. Parameters studied include plate thickness, combination member loading, initial out-of-plane imperfection, diagonal compression member out-of-plane flexural stiffness, corrosion, and alternative retrofits to increase lateral stiffness. The flexural stiffness of the diagonal compression member and retrofit designs were unique to the testing program. The variables monitored during testing include gusset plate surface stresses and strains, member axial strains, out-of-plane displacement of the gusset plate free edge, and buckling capacity. The results were compared with previously established design models for predicting buckling capacity of gusset plates which include the Whitmore effective

width, the Modified-Thornton method, and the FHWA Load Rating Guidelines. A parametric finite element model was developed to determine the lateral stiffness of the gusset plate connection and the additional stiffness provided by the alternative retrofit options.

The results showed interaction between the diagonal compression member and gusset plate occurs, which affects sway-buckling capacity. Combination of member loads showed evidence of detrimental effects on sway-buckling capacity. Corrosion of the gusset plates along the top edge of the bottom chord did not lead to significant reduction in sway-buckling capacity. The two retrofit designs showed increases in both lateral stiffness and buckling capacity as well as economic benefits over traditional retrofit methods. Comparison of the results to the current design guidelines showed that the current methods are conservative and do not accurately represent the true behavior of gusset plate connections. The research concludes with two proposed models for future use in design and retrofit of gusset plates. The first is a member-gusset plate interaction model based on a stepped column analogy that takes into account the effects of member flexural stiffness and gusset plate stiffness. The second is a general design guideline developed for retrofit of gusset plate connections dominated by sway-buckling behavior which uses a stiffness based approach to increase the capacity of gusset plate connections.

Experimental Research on the Behavior and Strength of Large-Scale Steel Gusset Plates with Sway-buckling Response Including Effects of Corrosion and Retrofit Options

by
Anthony G. Hafner

A THESIS

submitted to

Oregon State University

in partial fulfillment of
the requirements for the
degree of

Master of Science

Presented March 20, 2012
Commencement June 2012

Master of Science thesis of Anthony G. Hafner presented on March 20, 2011.

APPROVED:

Major Professor, representing Civil Engineering

Head of the School of Civil and Construction Engineering

Dean of the Graduate School

I understand that my thesis will become part of the permanent collection of Oregon State University libraries. My signature below authorizes release of my thesis to any reader upon request.

Anthony G. Hafner, Author

ACKNOWLEDGMENTS

The author wishes to express the sincerest appreciation to Dr. Chris Higgins for the guidance and assistance provided throughout the entirety of the research process. Without his guidance and support this research would not have been possible. Thanks are also given to Dr. Thomas Schumacher and Dr. O. Tugrul Turan who were responsible for writing the grant proposal and designing the original experiment and testing setup. This research was funded by the Oregon Transportation Research Consortium with match funding provided by the Oregon Department of Transportation.

CONTRIBUTION OF AUTHORS

Dr. Christopher Higgins assisted with experimental design, data collection, interpretation of results, and writing of Chapter 2 and Chapter 3. Dr. O. Tugrul Turan assisted with experimental design and data collection. Dr. Thomas Schumacher of the University of Delaware assisted with the experimental design.

TABLE OF CONTENTS

Page

TABLE OF CONTENTS (Continued)

Page

LIST OF FIGURES

Figure Page

LIST OF FIGURES (Continued)

<u>Figure</u> <u>Page</u>

LIST OF TABLES

LIST OF APPENDICES

LIST OF APPENDIX FIGURES

LIST OF APPENDIX FIGURES (Continued)

Figure Page

LIST OF APPENDIX FIGURES (Continued)

Figure Page

LIST OF APPENDIX FIGURES (Continued)

Figure Page

LIST OF APPENDIX FIGURES (Continued)

LIST OF APPENDIX FIGURES (Continued)

Figure Page

LIST OF APPENDIX TABLES

1 GENERAL INTRODUCTION

When the I-35W bridge over the Mississippi River in Minneapolis, MN collapsed on August 1, 2007, the state of the infrastructure throughout the entire United States was brought into question. After a thorough investigation of the collapse that was undertaken by the National Transportation Safety Board, the cause of the failure was determined to be an under-designed gusset plate at node U10 which failed due to sway buckling (NTSB 2008). This was one of the first times a design flaw was implicated as the cause of collapse of a steel truss bridge. The gusset plate at the failed node was found to have insufficient capacity to carry the loads being applied during the deck overlay that was occurring at the time of collapse. Despite routine inspections performed as prescribed by the FHWA for fracture critical structures, such as steel truss bridges, no report was made of the deficient gusset plate.

The collapse prompted funding for research into the behavior and strength of gusset plates under compression loading and is the driving force behind the research presented in this thesis, which is broken down into two separate manuscripts. The first manuscript addresses the behavior and strength of gusset plates through large-scale experimental testing. The experimental program looked at different variables that could contribute to the buckling capacity of gusset plate connections and include: plate thickness, initial out-of-plane imperfection of the gusset plate free edge, combination loading of different truss members, and out-of-plane flexural stiffness of the diagonal compression member. The variation of the diagonal compression member stiffness was a unique component for the research program as current design codes do not take this variable into account. Current design standards such as the FHWA Design Guide use a combination of buckling stress and column theory to predict the buckling load (FHWA 2009); however, the interaction between the gusset plate and member may have significant impact on the overall capacity of the connection. The results were compared to the FHWA Design Guide, Whitmore effective width method, and Modified-Thornton method to check the adequacy of each in predicting gusset plate connection buckling capacity.

Using the behavior observed in the first phase of the experimental testing program, the second manuscript looks at the effects of corrosion on the buckling capacity as well as alternative retrofit options for preventing sway buckling. Corrosion is considered to be the most common contributor to capacity reduction of gusset plate connections and is a key point in bridge inspections. The experimental program looked at how the introduction of corrosion typically seen in truss bridge connections affects the buckling capacity of the gusset plate. Accurate assessment of the effects will help determine better load rating guidelines for inspections conducted on existing bridges in the future.

Finding simple retrofits to help strengthen the connections is also critical. The alternative retrofit options detailed in the second manuscript were designed to increase the sway-buckling capacity of the connection by increasing the lateral stiffness of the gusset plates. Current practice in retrofitting deficient gusset plates typically involves costly replacement of the existing plates with new, thicker plates to add capacity (Curtis 2009). While effective this method is very time consuming and expensive. The retrofit designs investigated are relatively inexpensive and are easily applied to existing bridges.

While the design of the retrofits for the specific connection used in the laboratory was empirically based off of previous tests, any design guidelines for the retrofits would need to rely on theory and accurate modeling to produce a reliable design for existing bridge connections. To aid in the development of such a design guide, a small parametric finite element model was developed to determine a stiffness based approach to design the retrofits. This study is also a part of the second manuscript.

The appendices at the end of this thesis provide additional data gathered throughout the experimental testing program not presented in either manuscript. Additional data includes: full instrumentation plans, digital image correlation data, bolt slip displacements, member displacement relative to the work point, strain gage data, additional gusset plate stress comparisons, calibration data, threshold determination for plate bending, and finite element modeling data. These data are not discussed explicitly, but are provided for future reference.

The combination of the two manuscripts presented in this thesis will help future engineers better understand how gusset plate connections behave in compression and also to prevent the catastrophic failure exhibited by the I-35W bridge collapse. While further research is needed these papers provide a solid base of data from which to move forward.

EXPERIMENTAL TESTS OF GUSSET PLATE CONNECTIONS WITH SWAY-BUCKLING RESPONSE

Anthony G. Hafner, Christopher Higgins, O. Tugrul Turan, Thomas Schumacher

Journal of Bridge Engineering, ASCE

1801 Alexander Bell Dr.

Reston, VA 20191-4400

Issue not yet determined

2 EXPERIMENTAL TESTS OF GUSSET PLATE CONNECTIONS WITH SWAY–BUCKLING RESPONSE

Anthony Hafner[1] S.M.ASCE, Christopher Higgins[2] P.E. M.ASCE, O. Tugrul Turan[3], Thomas Schumacher A.M.ASCE[4]

2.1 Abstract

The collapse of the I-35W Bridge in Minneapolis, MN in 2007 brought into question the strength of large-size gusset plates in steel truss bridges. To provide new data on behavior and strength of large size bridge-type gusset plates, experimental tests were performed and are described here. The research program focused on sway-buckling behavior and test variables included: plate thickness, member stiffness, initial out-of-plane imperfection, and member load combinations. Unique to this test program was the direct consideration of different compression diagonal out-of-plane flexural stiffness on plate buckling behavior and capacity. Results showed that sway-buckling behavior and ultimate capacity were affected by initial out-of-plane imperfections of the plate and the out-of-plane bending stiffness of the truss member. Results also showed that the effective length factor, *K*, a parameter used in present load rating guides, did not accurately predict sway-buckling capacity and the Whitmore section approach may not be the best approximation for use in plate sway-buckling behavior. A stepped column approach was shown to illustrate and predict the plate-member stiffness interaction on buckling capacity.

2.2 Introduction

On August 1, 2007 the I-35W Bridge over the Mississippi River in Minneapolis, MN

[1] Graduate Research Assistant at Oregon State University
[2] Professor and Slayden Construction Faculty Fellow, School of Civil and Construction Engineering, Oregon State University
[3] Former Postdoctoral Research Assistant at Oregon State University
[4] Assistant Professor at the University of Delaware

collapsed resulting in 13 deaths and 145 injuries. The failure was attributed to a design flaw that resulted in under-strength gusset plates at connection U10 (NTSB 2008). The failure was precipitated by placement of construction loads that resulted in overloading of the design-deficient connection. This unexpected failure prompted transportation agencies to inspect and evaluate steel truss bridge connections and this effort continues to present. Early after the collapse, it was recognized that experimental data were lacking to support the application of available design methods for evaluation of large-sized truss bridge gusset plates and the rating outcomes using such methods were uncertain.

To address some of the questions related to gusset plate connection strength and to help better assess existing truss bridge connections, an experimental research program was undertaken. The focus of the work was on sway-buckling behavior and the key variables selected for this study included truss member out-of-plane stiffness, initial out-of-plane imperfection, plate thickness, and member loading combinations. A large-size steel gusset plate connection in an isolated truss joint was developed and the members and proportioning were inspired by the connection geometry of joint U10 in the I-35W bridge. This paper discusses previous research, the experimental design and setup, significant findings and interpretation of the results, and concludes with a proposed stepped column analogy for analysis of gusset plates to include member stiffness interactions on the connection buckling strength.

2.3 Background

Present gusset plate design guidelines originate from work performed by Whitmore (1952) that resulted in the widespread acceptance of the previously understood assumption of stress distribution now known as the Whitmore effective width, *w* (see Fig. 2-1). Tests conducted by Irvan (1957) and Hardin (1958) corroborated these results with only slight differences. All of the tests conducted were performed on small scale dual plate models representative of Warren truss bridges. Vasarhelyi (1971) followed after and was one of the first to use a finite element analysis (FEA) model of gusset plates and compared them with experimental findings. The FEA model showed that the elementary design models being used at the time gave a good approximation of capacity with the only differences coming in the precise locations of maximum stress.

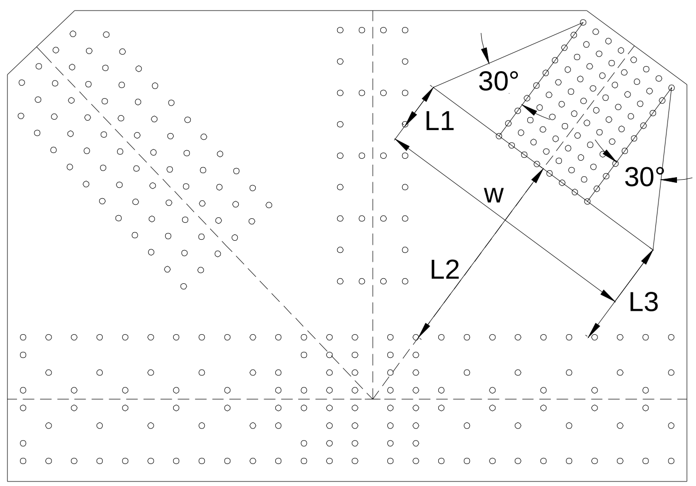

Fig. 2-1: Whitmore effective width, *w*, and lengths (L_1=6 in, L_2=26.7 in, L_3=15.5 in)

Thornton (1984) provided an alternate method to Whitmore using a column based approach where a unit width column was represented by the length, L_2, as shown in Fig. 2-1. Studies by Yam and Cheng (1994) proposed a Modified-Thornton method which used a 45° dispersion angle instead of an equivalent column of unit width to approximate the stress distribution in the plates. Both the Thornton and Modified-Thornton methods rely on a column surrogate for plate behavior. Studies at the National Institute of Standards and Technology (NIST) showed that Whitmore's method underestimated the actual buckling capacity of gusset plates by a significant amount (Gross 1990).

Currently, evaluation of gusset plates is being performed by transportation agencies and consultants using the FHWA Load Rating Guidelines (FHWA 2009), which will be referred to here as the *FHWA Guide*. The *FHWA Guide* was issued to provide consistent guidelines for gusset plate connection evaluation and relies significantly on past design practice. The *FHWA Guide* uses the Whitmore section and an effective column analogy to evaluate gusset plate buckling as:

$$l = \frac{L_1 + L_2 + L_3}{3} \tag{2-1}$$

$$I_g = \frac{wt^3}{12} \tag{2-2}$$

$$A_g = wt \tag{2-3}$$

$$r_s = \sqrt{\frac{I_g}{A_g}} \tag{2-4}$$

$$\lambda = \left(\frac{Kl}{r_s \pi}\right)^2 \frac{F_y}{E} \tag{2-5}$$

If $\lambda < 2.25$
$$P_n = 0.66^{\lambda} F_y A_g \tag{2-6}$$

If $\lambda \geq 2.25$
$$P_n = \frac{0.88 F_y A_g}{\lambda} \tag{2-7}$$

where L_1, L_2, L_3 = lengths from Whitmore section as shown in Fig. 2-1 (in), l = effective length (in), w = Whitmore section width (in), t = thickness of plate (in), I_g = moment of inertia of section (in^4), A_g = gross area of section (in^2), r_s = radius of gyration of section (in), F_y = yield strength (ksi), E = elastic section modulus (ksi), K = effective length factor, and P_n = nominal compressive buckling capacity of single gusset plate (kips). The effective length factor, K, is based on conventional column buckling theory for both sway and non-sway conditions with design values ranging from 1.2-2.1 and 0.65-1.0 based on boundary conditions, respectively. Limited data are available for large-sized gusset plate connections to provide clear guidance to analysts for selection of the effective length factor or for development of alternative analysis procedures that can more effectively incorporate plate behavior into capacity prediction models. To provide empirical data for evaluation of gusset plate buckling behavior and strength, experimental tests were conducted on large-size gusset plates and the findings are reported here. These data help clarify analytical approaches and improve rating methods.

2.4 Experimental Design, Setup and Testing Methods

Based on the identified cause of failure for the I-35W Bridge, the experimental program focused on the buckling response of double-sided gusset plates typical of bridges. The actual size and strength of connection U10 makes full-size testing difficult and costly. While it was not the intent of this study to test a reduced-scale replica of the original connection, the selected laboratory gusset plate configuration and proportions were inspired by the original U10 connection in the I-35W Bridge which produced buckling failure. Modifications to fastener patterns, member framing angles, and member lengths were made to allow it to fit within the laboratory capability. An elevation view of the overall test setup is shown in Fig. 2-2. The connection consists of double-sided gusset plates joined to tubular truss members using high-strength bolts. The truss members are attached to a test frame that reacts against the applied forces and the generated member forces. The setup allows over 4448 kN (1 million pounds) of force to be generated within the setup. A lateral brace was positioned on the west gusset plate at the work point. The brace allowed vertical motion but restricts out-of-plane displacement of the truss and represents the lateral support available to a real truss gusset connection due to floor beams or wind bracing. Slotted holes in the connection angles use to join the brace to the gusset ensured that significant forces cannot flow through the connection angles.

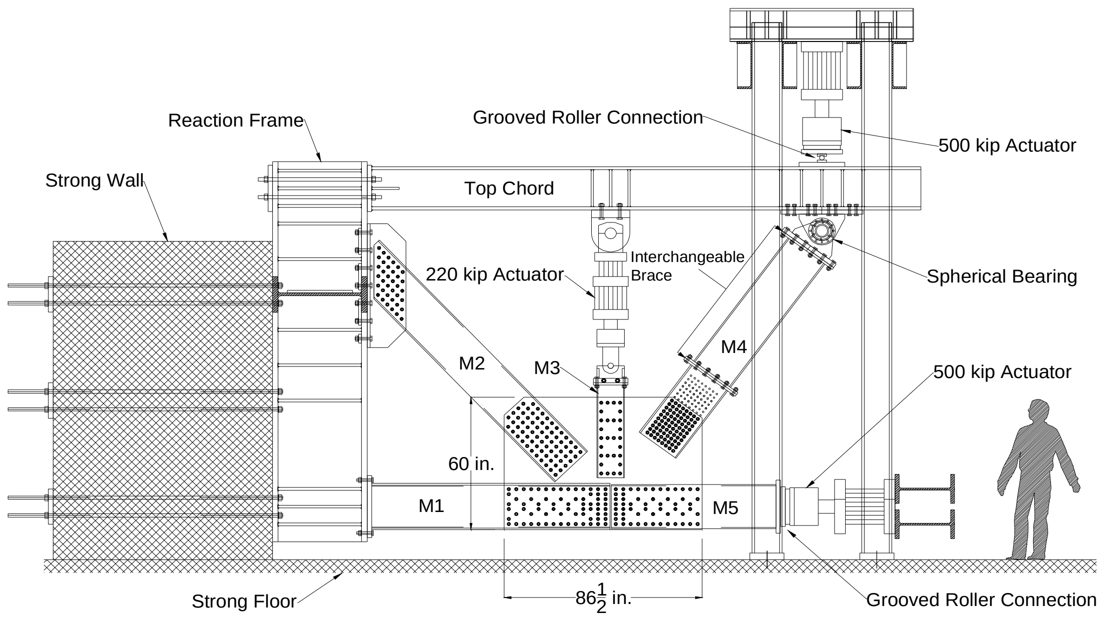

Fig. 2-2: Overall elevation view of experimental setup

Five truss members were joined by the gusset plates in the setup: members M1 and M5 represented a top or bottom chord, M2 a tension diagonal, M3 a vertical member, and M4 a compression diagonal (Fig. 2-2). The gusset plates were designed so that sway-buckling failures could occur at the M4 connection. The dimensions and bolt patterns are detailed in Fig. 2-3. Member M1 was a built-up box member made of four 31.75 mm (1.25 in.) thick A36 steel plates with overall member dimensions of 533.4 mm x 304.8 mm (21 in. x 12 in.). The weak bending axis is oriented in the plane of the truss. Members M2, M4, and M5 were HSS508x304.8x15.9 (HSS20x12x5/8) rectangular tubes with the weak axis oriented in the plane of the truss. Member M3 was an HSS304.8x304.8x9.5 (HSS12x12x3/8) square tube. The tube sections were A500 steel and all members were designed to remain elastic at the full capacity of the available hydraulic actuators. All of the connections were bolted with 19 mm (3/4 in.) diameter A325 bolts and tightened with a pneumatic impact wrench except for the M4 connection, which was hand-torqued to a relatively low 0.136 kN-m (100 ft-lbs) to allow fastener bearing rather than slip-critical behavior such as that expected for riveted connections. The M4 stand-off distance was specifically designed to allow the entire Whitmore section to be effective in the plate and facilitate buckling of the connection. All the gusset plates tested were A36 steel and two thicknesses were tested: 6.4 mm (0.25 in.) and 9.5 mm (0.375 in.). The mechanical properties of the plates were determined according to ASTM A370 (1997) and are shown in Table 2-1.

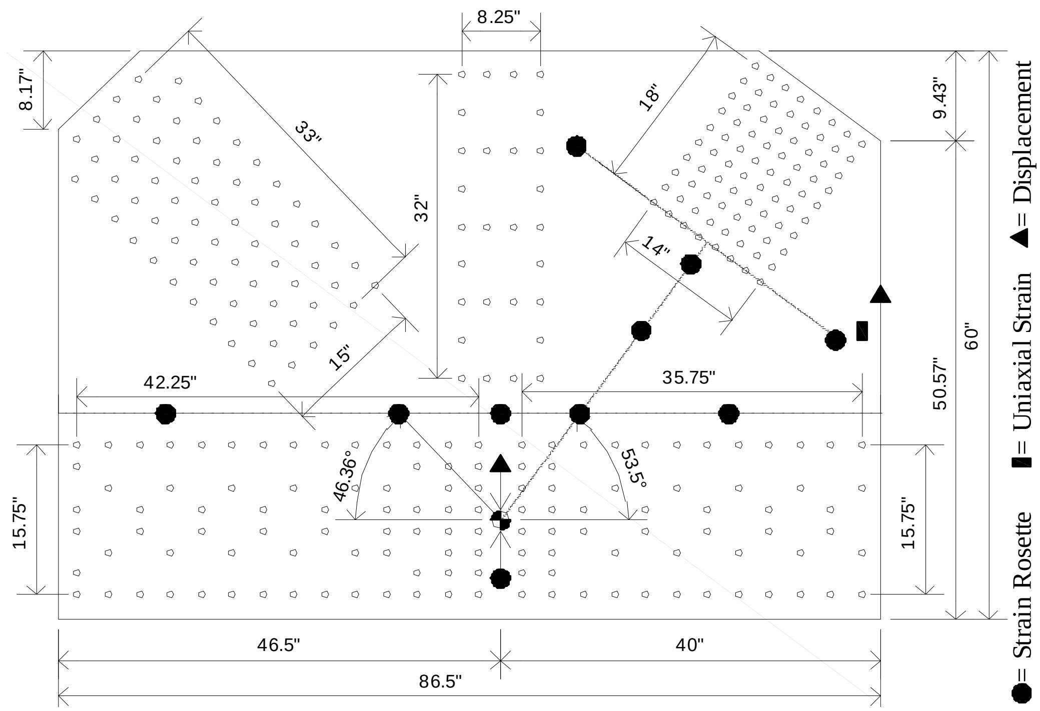

Fig. 2-3: Gusset plate details and relevant strain gage and displacement locations

Table 2-1: Mechanical properties of test specimens

Specimen #	Average F_y, MPa (ksi)	Std. Dev.	Average F_u, MPa (ksi)	Std. Dev.
1	323.9 (47.02)	1.73	501.2 (72.74)	0.90
2	310.9 (45.12)	1.95	472.6 (68.59)	0.46
3	316.5 (45.93)	0.34	466.8 (67.76)	0.31
4	310.7 (45.10)	1.55	482.0 (69.96)	0.31
5	317.9 (46.13)	0.66	467.3 (67.83)	0.34
6	318.8 (46.27)	0.19	467.8 (67.90)	0.16

In addition to the five truss members described, an interchangeable M4 section with different stiffness properties was used in this study. This was done to evaluate the effects of the compression diagonal out-of-plane flexural stiffness on the connection strength. The diagonal compression member stiffness was investigated because real truss bridge members are much longer than those used in laboratory investigations. Further, laboratory connection tests generally have members that are over-designed in order to ensure failure of the connection. As a result, the translational and rotational stiffnesses of the members cannot be properly modeled simultaneously in the laboratory environment without full-size tests with full-length members. In order to compare both stiffness effects, two different cross sections were used for member M4 in the present research. Out-of-plane stiffnesses (both rotational and translational) of existing truss bridge compression diagonal members were investigated for a suite of existing steel truss bridges from around the country and are reported in Table 2-2. Based on these values, a cross section consisting of back-to-back MC408x86 (MC18x58) A36 steel channel sections was selected for the interchangeable M4. This provided approximately the same axial stiffness (AE/L) and strong axis second moment of area (orthogonal to the plane of the truss), but had a weak axis second moment of area equal to 7%

of the original tubular HSS508x304.8x15.9 (HSS20x12x5/8) member. For these two different compression diagonals, the flexurally-stiff tubular M4 section resembles the translational stiffness and the flexurally-soft back-to-back channels M4 section resembles the rotational stiffness of the real truss members considered in Table 2-2.

Table 2-2: Comparison of truss member stiffness in experiment and existing bridges, $k_T = EI/L^3$, $k_R = EI/L$

Bridge Name	Member Number	Member Shape	Moment of Inertia, I, cm^4 (in^4)	Length, L m (ft)	Translational Stiffness, k_T, kN/mm (kip/in)	Rotational Stiffness, k_R, kN-m (kip-ft)
OSU experiment	M4 (Stiff)	Box	3.54 (851)	2.8 (9.2)	3.22 (13.38)	25,300 (18,700)
	M4 (Soft)	I-shape	0.25 (60.6)	2.8 (9.2)	0.23 (1.31)	1,800 (1,300)
I-94 over Little Calumet River, IL	L2-U3	Box	34.83 (8367)	21.2 (69.5)	0.07 (0.42)	32,900 (24,300)
	L0-U1	Box	40.53 (9737)	21.2 (69.5)	0.09 (0.49)	38,300 (28,300)
I-275 over Ohio River, KT	L2-U3	Box	36.21 (8700)	23.8 (78.2)	0.05 (0.30)	30,400 (22,400)
	M15-L16	Box	53.19 (12779)	16.8 (55.0)	0.23 (1.29)	63,500 (46,800)
Clarion River Bridge, PA	U6-L5	Box	37.79 (9079)	18.7 (61.3)	0.12 (0.66)	40,400 (29,800)
	U12-L13	Box	47.2 (11341)	17.7 (58.0)	0.17 (0.98)	53,300 (39,300)
St. Highway 57, Watooga Rriver, TN	U11-L12	Box	14.21 (3413)	18.8 (61.6)	0.04 (0.25)	25,300 (18,700)
Booth Ranch Bridge, #7841A, OR	U1-L0	Box	5.77 (1386)	11.6 (38.2)	0.07 (0.42)	9,900 (7,300)
	U3-L2	I-shape	4.65 (1116)	11.6 (38.2)	0.06 (0.34)	8,000 (5,900)
Caney Fork River, HWY #56, TN	L1-U2	I-shape	7.06 (1697)	13.0 (42.7)	0.06 (0.37)	10,800 (8,000)
	L15-U16	I-shape	20.19 (4850)	16.6 (54.3)	0.09 (0.51)	24,400 (18,000)

2.4.1 Instrumentation Plan

The instrumentation plan was developed to acquire data for the plate stresses, plate and member displacements, and member forces and interactions and is illustrated in Fig. 2-3. The plate was instrumented with uniaxial and 45 degree rosette strain gages. The uniaxial gages were placed along the free edges of the plate and within the bolt pattern of member M4. Uniaxial strain gages were placed on all truss members except M3 to capture strains near the midpoint of the member to measure member axial force and bending. Member M3 was not instrumented since the hydraulic actuator and attached load cell effectively act as the member and the member force transducer. Member M4 was calibrated by directly applying a compression force to the member (as a single column) that allowed calibration of the attached uniaxial strain gages to allow precise measurement of the member force. To measure out-of-plane displacement of the plate, displacement sensors were positioned along the free edges of the gussets. Rigid body motion was captured by displacement sensors at the work point and at the base of the gusset plates. There were also displacement sensors positioned between the members and gusset plates to measure relative slip and between the member and gusset plate at the work point to measure overall member deformations. In addition to the discrete displacement measurements, a digital image correlation (DIC) system monitored plate deformations on the west side of the connection.

2.4.2 Loading Protocols

Up to three different hydraulic actuators were used in the experiments and are illustrated in Fig. 2-2. They consist of a 979 kN (220 kip) actuator positioned over member M3, and two 2240 kN (500 kip) actuators: one placed vertically over member M4 and the other placed horizontally in line with members M5 and M1. Henceforth the actuators will be referred to by the name of the member they impart load to, e.g. the 500 kip actuator over member M4 will be the ‘M4 actuator’. To minimize bending in the compression diagonal M4, a special high-force spherical bearing was fabricated to connect the end of the member to the loading frame as seen in Fig. 2-2. The spherical bearing provided no rotational restraint.

Two different loading protocols were used in the tests. Two tests (specimens #1 and #3) were conducted with a combination of all three actuators using an increasing amplitude cyclic loading sequence (loading with unloading) and all other tests were conducted with a monotonic loading history using only actuator M4. The combination load history was based on the relative amplitude between the individual actuators and a set sequence of actuator loading and unloading. Each load cycle consisted of the following steps: all loads at zero, load M4, load M3, unload M3, load M5, unload M5, load M3 and load M5, unload M3, unload M5, unload M4. In subsequent steps the loads were incrementally increased and the process repeated until failure. The relative actuator load values for Test 1 went as follows: M4 = 111 kN (25 kip), M3 = 27 kN (6 kip), M5 = 100 kN (22.5 kip). The initial loading values for Test 3 went as follows: M4 = 222.4 kN (50 kip), M3 = 53.4 kN (12 kip), M5 = 155.6 kN (35 kip). The combination loading rate was set at 4.4 kN/sec (1 kip/sec) for lower values and was increased to 8.9 kN/sec (2 kip/sec) later in the test. The monotonic tests were continuously loaded until failure at a rate of 4.4 kN/sec (1 kip/sec).

2.4.3 Measurement of Initial Imperfections

Prior to conducting tests, the initial out-of-plane imperfections in the gusset plate were measured using a DIC system. The initial imperfections were somewhat random and did not correspond to the predicted fundamental buckling mode shape. Peak amplitudes for each of the specimens are shown in Fig. 2-4. For specimen #3, imperfections were imposed on the specimen and Fig. 2-5 shows two different stages of imposed imperfection: a) the maximum applied load with no additional imposed imperfection, and b) 102% initially imposed additional imperfection prior to application of the loading that caused failure. The image correlation system was also used to track the progression of out-of-plane deformations as loads were applied to the truss members.

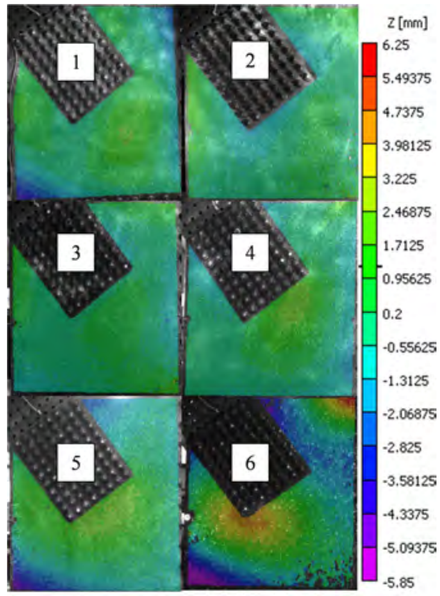

Fig. 2-4: DIC measured initial out-of-plane plate imperfections (prior to any imposed deformations on specimens 3 and 6)

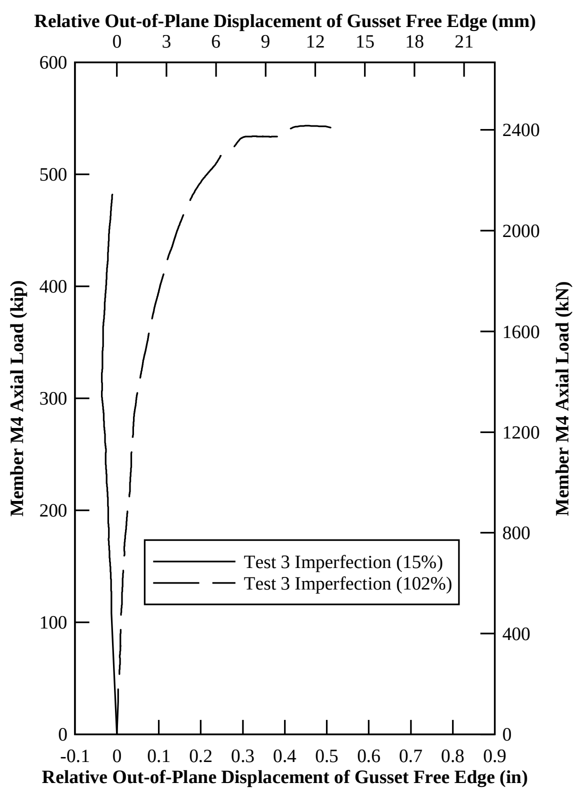

Fig. 2-5: Compression diagonal load and corresponding out-of-plane displacement at the free-edge for Test 3 showing effects of initial imperfections

2.5 Experimental Results

Six specimens were tested to failure in this study. Key properties and findings are summarized in Table 2-3. This table shows the test variables, the axial load in member M4 at failure, amplitude of the out-of-plane displacement at the free edge of the gusset plate at failure, and average stress across the Whitmore width. All specimens failed due to sway buckling at the M4 connection. Five specimens sway-buckled in the direction of the floor brace and specimen #1 sway-buckled in a direction away from the floor brace. These indicate limited bias in the experimental setup. An example of the connection after failure is shown in Fig. 2-6.

Table 2-3: Test matrix with results

	Test 1	Test 2	Test 3	Test 4	Test 5	Test 6
Plate Thickness, mm (in)	6.4 (0.25)	6.4 (0.25)	9.5 (0.375)	6.4 (0.25)	9.5 (0.375)	9.5 (0.375)
Loading Protocol [a]	1	2	1	2	2	2
M4 Brace Section	Stiff	Stiff	Stiff	Soft	Soft	Soft
Max. Initial Plate Imperfection, % plate thickness	50%	19%	102%[b]	43%	40%	98%[b]
Gusset Free Edge Out-of-Plane Displacement at Failure, mm (in)	14.5 (0.57)	4.1 (0.16)	12.7 (0.50)	21.6 (0.85)	15.2 (0.60)	16.3 (0.64)
M4 Axial Load at Failure, kN (kip)	1294 (291)	1446 (325)	2424 (545)	1139 (256)	2575 (579)	2215 (498)
σ_w at Failure, MPa (ksi)	115.3 (16.7)	128.8 (18.7)	144.0 (20.9)	101.4 (14.7)	152.9 (22.2)	131.5 (19.1)
$\sigma_{4,max}/\sigma_w$ at $0.6*F_{max}$	0.99	0.94	1.04	1.79	0.85	0.91
$\sigma_{4,max}/\sigma_T$ at $0.6*F_{max}$	1.21	1.15	1.27	2.20	1.05	1.12
$\sigma_{4,avg}/\sigma_w$ at $0.6*F_{max}$	0.75	0.59	0.99	0.69	0.57	0.33
$\sigma_{4,avg}/\sigma_T$ at $0.6*F_{max}$	0.55	0.60	1.19	0.41	0.59	0.17
σ_p/σ_w at $0.6*F_{max}$	1.15	1.03	1.81	1.89	0.98	1.66

a) 1 = combination loading (M4+M3+M5), 2 = monotonic loading (M4 only)
b) Initial imperfection includes applied imperfection
c) σ_4 = stress in M4 direction, σ_w = Whitmore stress, σ_T = Modified Thornton stress, F_{max} = Max axial load, σ_p = principle compressive stress at center of Whitmore width

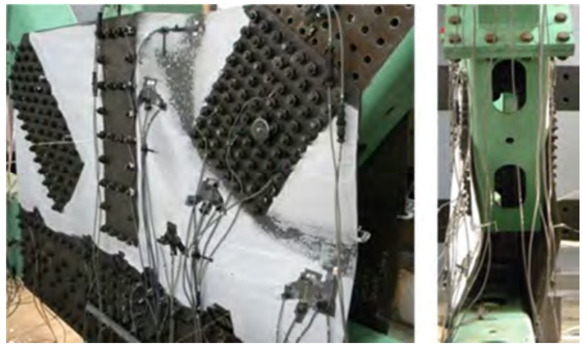

Fig. 2-6: Photographs of buckled shape (front and side views)

2.5.1 Load versus Out-of-Plane Displacement Behavior

The compression member M4 axial load versus out-of-plane displacement of the gusset plate at the free edge behavior is shown in Fig. 2-7 for all six tests. The displacements shown are the average relative out-of-plane displacement of the two gusset plate free edges with the rigid-body motion of the truss removed from the measurement. Since the test setup used an entire truss joint there was rigid-body movement at the work point of the connection that occurred upon loading. To adjust for this motion, the rigid body motion at the gusset free edge was determined from the displacement sensors on the members and work point and projected to the free edge of the gusset plate. This motion was subtracted from the measured displacements at the free edge so that the plate motion relative to the truss members could be captured. There were also non-conservative contact surface deformations present that produced load stiffening at the beginning of the tests. These were removed in post-processing by best-fit of the linear elastic portion of the curve.

Overall responses shown in Fig. 2-7 are not shown over the entirety of the tests of specimens #1 and #3 for clarity. Results for specimens #1 and #3 are provided for the final load cycle only. Specimen #1 is further reported as a backbone curve of the final cycle; however, the full final cycle is detailed in Fig. 2-8 to illustrate the effects of the member combination loading. For specimen #2, which had all the same parameters as specimen #1 with the exception of the loading protocol, the buckling capacity was 17% higher when subjected to only monotonic loading of M4. This is because the combination loading reduced the connection strength due to accumulated lateral deformation of the overall gusset plate at the work point from application of the other member loads. This was because the other actuator loads applied to the truss chord and vertical (which are also compressive) produced lateral displacements of the gusset plate that did not rebound upon unloading (as measured at the work point). In addition, as the chord load is reduced the compressive stress in the plate near member M4 increased but the gusset plate retained the additional lateral displaced shape obtained at the maximum chord load. Thus the gusset plate compressive stresses increased to the previous threshold (when only M4 was loaded) but due to the larger lateral displacement of the overall connection it buckled with a constant load in member M4.

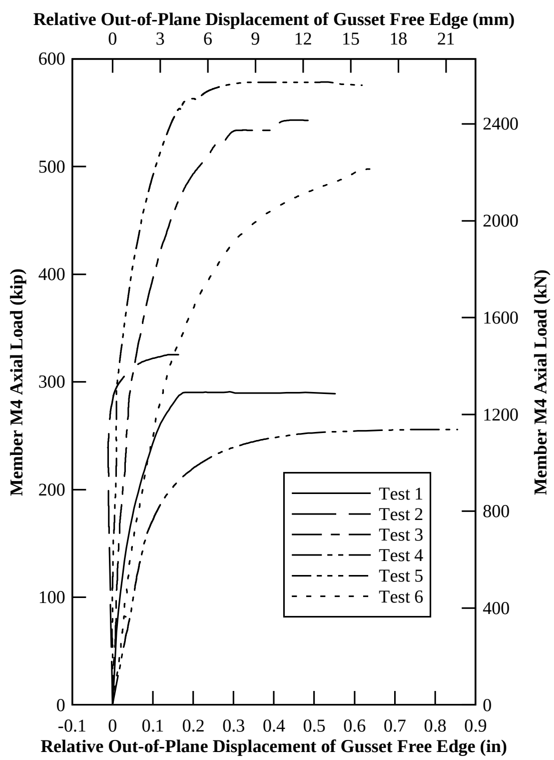

Fig. 2-7: Compression diagonal load (in M4) and corresponding out-of-plane displacement at the free-edge for all tests

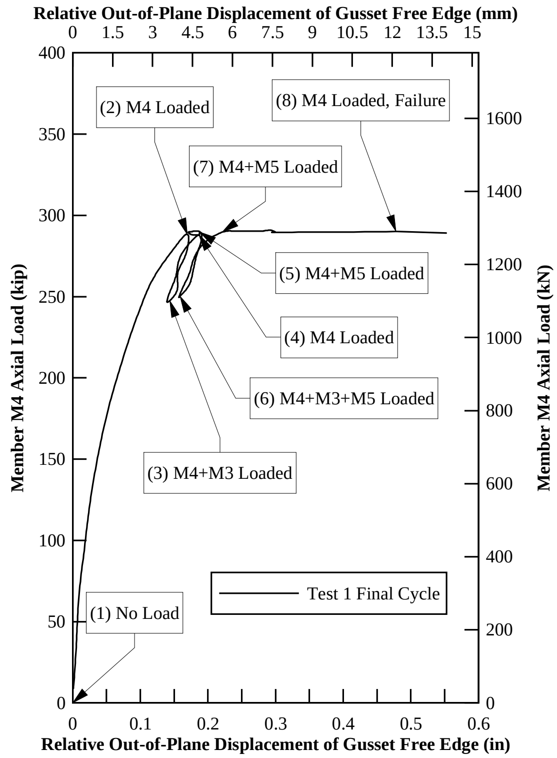

Fig. 2-8: Compression diagonal load and corresponding out-of-plane displacement at the free-edge for Test 1 during final load cycle that produced failure.

To investigate the influence of initial plate imperfections, such as that observed in connection U10 prior to collapse, plate imperfections were imposed on specimen #3. Firstly, specimen #3, with the inherent imperfections described previously, was tested to the capacity of the actuators without failure. Then additional imperfection was applied to approximate the lowest buckling mode shape, using a hydraulic ram positioned at the midpoint of the gusset free edge as shown in Fig. 2-9. The experimental response of this specimen is shown in Fig. 2-5 where the plates with inherent imperfections are seen moving in the opposite direction of the rigid body motion until approximately 1300 kN, when they changed direction. By imposing initial imperfection both plates move in the same direction and the overall member force-plate displacement response showed lateral movements at lower load. Finally, the out-of-plane flexural stiffness of member M4 was seen to significantly alter the behavior and strength of the connection. This is seen by comparing specimens #2 and #4. Both were monotonically loaded 6.4 mm (0.25 in.) thick plates with similar initial plate imperfections. However, specimen #2 contained the stiff brace for M4 while specimen #4 contained the soft brace for M4. Specimen #4 showed a 21% reduction in capacity compared to specimen #2. The out-of-plane displacement of the plates at failure was also significantly different. In specimen #2, the relative displacement of the plates at the free edge was only 4.1 mm (0.16 in.) while in specimen #4 it was 21.6 mm (0.85 in.). A similar change in displacement occurred between specimen #3 and specimen #5 (9.5 mm thickness). Although the final buckling load is higher in specimen #5, soft M4 section, than in specimen #3, stiff M4 section, there is still more out-of-plane displacement at failure in specimen #5, which increased by 2.5 mm over specimen #3. The differences in capacity, 6% reduction from specimen #5 to specimen #3, can also be explained by initial imperfection. In specimen #3, the plates were pushed out-of-plane to 102% of the plate thickness, which decreased the capacity of the connection, while specimen #5 had initial imperfection of only 40% of plate thickness. Comparison of specimen #6 (soft brace with 98% initial plate imperfection imposed) with specimen #3 (stiff brace with 102% initial plate imperfection) showed a 8.6% reduction in load capacity. This is not as significant a reduction due to the brace stiffness as observed for specimens #2 and #4 and shows that significant plate imperfections can dominate the behavior and reduce the influence of brace stiffness on buckling strength.

In addition to the free-edge motions of the plates, the influence of the compression diagonal flexural stiffness was observed in the strain gages placed at the midpoint of member M4. The strain profiles were obtained to assess axial and bending effects in the member. The resulting bending strains were projected to the interface of the member and the gusset plates assuming zero moment at the spherical bearing. The resulting strain profiles are shown in Fig. 2-10 as a combination of axial and bending strain for all six tests. The profiles show very little bending in the stiff tubular M4 (specimen #2), while significantly more bending is observed in the soft back-to-back channel M4 (specimen #4). The lateral bending of the brace provides less restraint to the connection thereby affecting the strength of the connection. This interaction is like that of a column that exhibits lower buckling strength if connection restraints at the ends are reduced, so that similarly, the connection shows reduced buckling strength when the member restraint is reduced. This is an important finding that has not previously been included in connection capacity evaluation. Considering the very long members in some real truss bridges, the resulting low translational and rotational stiffnesses of the compression members could produce significant connection buckling strength reductions compared to the assumed rigid member assumptions.

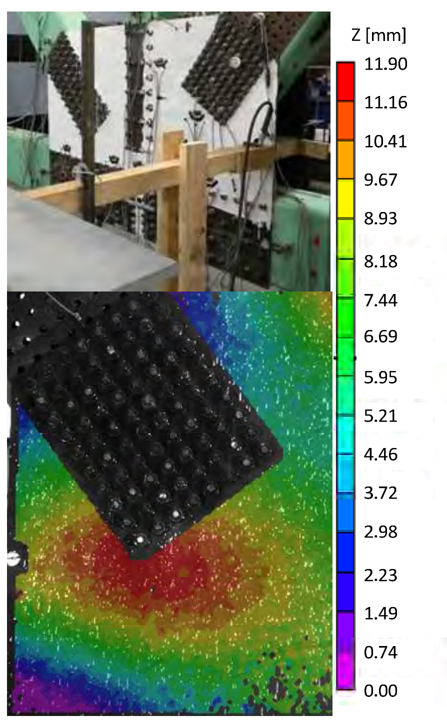

Fig. 2-9: Hydraulic ram setup for imposing out-of-plane imperfections and DIC measured imposed imperfections across plate surface for specimen #6.

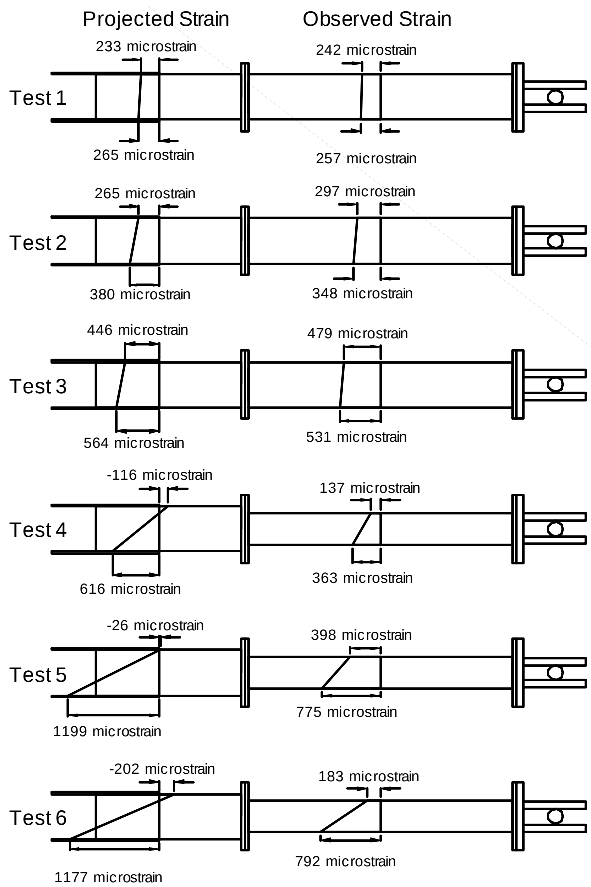

Fig. 2-10: Bending strains measured in compression diagonal M4 (top view), with compression shown as positive.

2.5.2 Plate Stresses

Plate stresses were also measured and are important metrics used in plate evaluations. Three sections were instrumented to obtain plate stress data from the specimens. These sections are labeled A-A, B-B, and C-C on Fig. 2-11d. Plane A-A corresponds to the horizontal plane above the bottom chord of the truss which is commonly used in assessment of shear capacity. Path B-B corresponds to the Whitmore section and is used to assess buckling capacity. Path C-C corresponds to the line of action of member M4 running from the work point of the plate to the midpoint of the Whitmore section which corresponds to Thornton's effective column length. Because strain gage rosettes were placed on only one side of the plate and at larger load magnitudes plate bending was observed due to lateral motion of the gusset plates, the stresses are reported at loads of $0.6F_{max}$ (60% of the failure load) which corresponds to the point just prior to significant introduction of surface bending stresses. Symbols shown on Fig. 2-3 indicate the locations of the strain rosettes on the given paths.

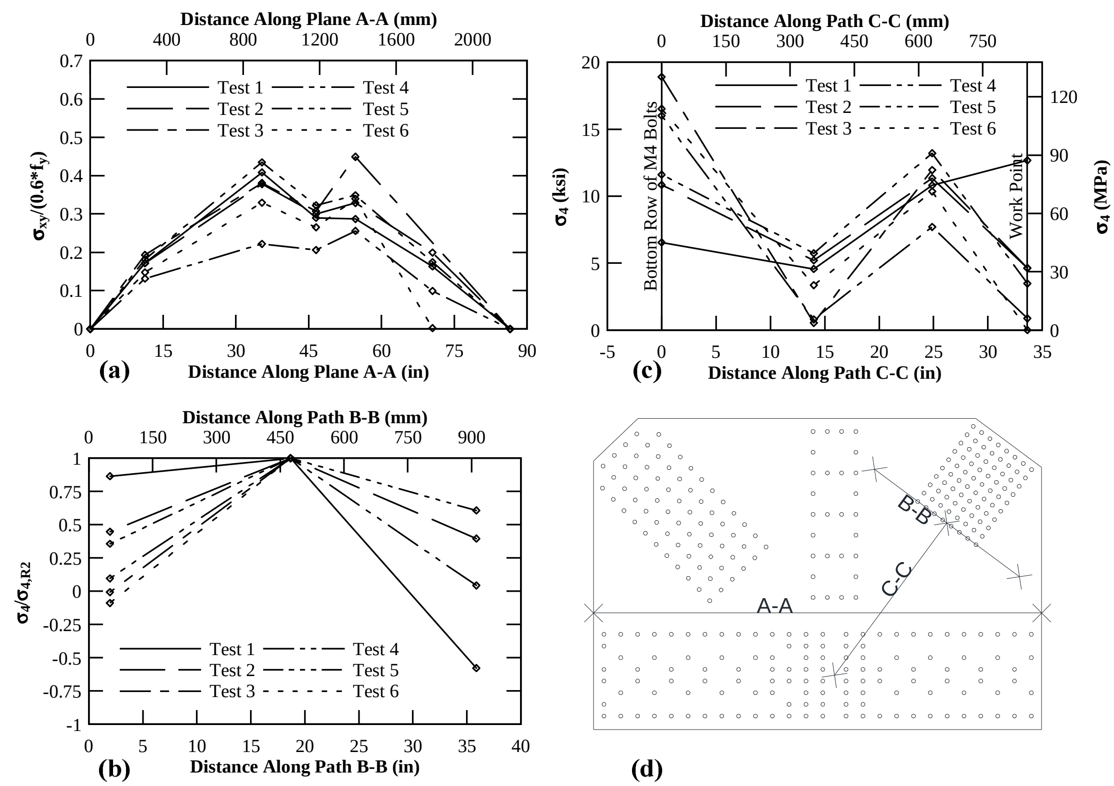

Fig. 2-11: Plate stresses at 0.6Fmax, (a) Normalized shear stress across path A-A, (b) Normalized stress in M4 direction across line B-B, (c) Stress in M4 direction along M4 line of action C-C (positive is compression), (d) Defined stress paths.

Since plane A-A is primarily used for checking shear capacity, the shear stresses in the global xy direction were normalized with respect to shear yielding ($0.6f_y$) and are shown in Fig. 2-11a. The figure shows the stress along the length of the plane and that the shear stresses followed the same pattern for all six tests with the largest stresses occurring over the work point. Notice that the shear stress magnitude along the plane was approximately the same for different plate thickness and diagonal member stiffnesses and the shear stresses were significantly below yielding.

Plate stresses in the M4 direction for path C-C are shown in Fig. 2-11c. The plots show a large decrease in stress only a short distance from the bottom row of bolts on M4; however, DIC measurements show that the location of the second strain gage from the left is typically a location for local bending in the plate and bending of the plate likely influenced these measurements. The overall trend was increasing distribution of stress (reduction in magnitudes) moving away from the end of the member toward the work point.

For path B-B, the plate stresses are shown in the M4 direction normal to the path and were normalized to the center gage to obtain stress distribution in Fig. 2-11b. The far right gages for specimens #3 and #6 are not shown due to bending stresses that were produced by the artificially imposed initial plate imperfections. The stress distribution across the Whitmore effective width was non-uniform with the center gage exhibiting significantly higher stress than the edges. There was also wide dispersion along the edges of the path showing significant variation from specimen to specimen with some specimens even showing tension stress due to bending of the plates at the edge. The magnitude of the maximum measured gusset plate stress at the Whitmore section in the direction of member M4 (located in the middle of the path, very close to the end of the compression diagonal) was compared to the theoretical Whitmore stress (taken as the member force divided by the thickness of the plate and Whitmore length) as seen in Table 2-3 and the mean ratio was 1.14. When the measured stress in the M4 direction along the path was averaged between all three gages and compared with the theoretical Whitmore stress, the mean ratio was 0.65. The Modified Thornton stress (assuming 45 degree dispersion), was less effective in predicting the maximum and average stress in the M4 direction across the Modified-Thornton effective width with mean ratios of 1.40 and 0.54 for maximum and average stress respectively. This indicates for the parameters considered in this program that using Whitmore stress would tend to overestimate the magnitude of the average stress in the plate and underestimate the maximum stress in the gusset plate. Since average stress is typically used in predicting buckling loads, Whitmore would predict lower buckling loads than those observed. The values from specimens #3 and #6 were not used for this assessment due to bending stresses produced by the large imposed out-of-plane deformations for these tests.

2.5.3 Comparison of Results to FHWA Guide

The experimental results were compared with the predicted strengths using the methods provided in the *FHWA Guide.* Only the compression strength of the connection was evaluated relative to member M4. One of the important parameters is selecting the appropriate effective length factor, *K*. With the test data available in this study, *K* values were back-calculated using Eqns. 2-1 – 2-7 as:

$$K = \frac{r_s \pi}{l}\sqrt{\frac{\lambda E}{F_y}} \tag{2-8}$$

The results are shown in Table 2-3 and are compared to the results assuming a *K* value of 1.2 as has been commonly employed by rating engineers based on the example problem provided in the *FHWA Guide*. As seen in Table 2-4, using an assumed *K* of 1.2 greatly underestimated the observed buckling capacity of the connections for all cases. Even as all tests exhibited sway buckling with relatively large stand-off distance of the compression diagonal from the work point. The 6.4 mm (0.25 in.) thick plates had capacities 4 times and the 9.5 mm (0.375 in.) thick plates had capacities 2.5 times greater than the predicted values. The back-calculated values of *K* show that the effective length ranged from 0.54 to 0.61 for the 6.4 mm plates and 0.73 to 0.80 for the 9.5 mm plates. While these values seem illogical for sway buckling, it is important to remember that the analytical model assumes an equivalent column with the Whitmore section and does not properly account for plate behavior. The influence of the member stiffness is also apparent in the computed effective length factors with the *K* value increasing 0.06 from specimen #2 to specimen #4 and 0.04 from specimen #3 to specimen #6 when only the M4 stiffness was varied.

Table 2-4: Comparison of experiment to FHWA Design Guide

	Test 1	Test 2	Test 3	Test 4	Test 5	Test 6
t, mm (in)	6.4 (0.25)	6.4 (0.25)	9.5 (0.375)	6.4 (0.25)	9.5 (0.375)	9.5 (0.375)
L, mm (in)	394 (15.53)	394 (15.53)	394 (15.53)	394 (15.53)	394 (15.53)	394 (15.53)
w, mm (in)	884 (34.78)	884 (34.78)	884 (34.78)	884 (34.78)	884 (34.78)	884 (34.78)
r_s, mm (in)	1.8 (0.072)	1.8 (0.072)	2.7 (0.108)	1.8 (0.072)	2.7 (0.108)	2.7 (0.108)
F_y, MPa (ksi)	324 (47)	311 (45)	317 (46)	311 (45)	318 (46)	319 (46)
E, MPa (ksi)	199,810 (29,000)	199,810 (29,000)	199,810 (29,000)	199,810 (29,000)	199,810 (29,000)	199,810 (29,000)
K_{FHWA}	1.2	1.2	1.2	1.2	1.2	1.2
λ_{FHWA}	10.96	10.52	4.76	10.51	4.78	4.79
P_{FHWA}, kN (kip)	292 (66)	292 (66)	986 (222)	292 (66)	986 (222)	986 (222)
$P_{experiment}$, kN (kip)	1294 (291)	1446 (325)	2424 (545)	1139 (256)	2575 (579)	2215 (498)
$\lambda_{experiment}$	2.47	2.12	1.90	2.70	1.76	2.13
$K_{experiment}$	0.57	0.54	0.76	0.61	0.73	0.80
P_{exp} /P_{FHWA}	4.43	4.95	2.46	3.90	2.61	2.25
% Difference	343%	395%	146%	290%	161%	125%

An analytical model that demonstrates the systems' interactions between the brace and connection is a stepped column as illustrated in Fig. 2-12. The buckled shape of the system is influenced by the relative bending stiffness of the connection and member and solution of this class of problem is well documented (Galambos and Surovek 2008). Assuming sway failure modes, as observed in the test program, the extreme bounds of compression member stiffness are shown in the figure. As seen here, depending on the member stiffness the effective K value for the plate can vary from 2.0 (very soft member) to less than 1.0 (very stiff member) and clearly shows the influence of the member stiffness on the bucking behavior of the system. Numerically this is seen in Fig. 2-13 which is derived from the eigenvalue buckling load for a stepped column. This formulation suffers from the limitations associated with using a column analogy, but serves to highlight the observed experimental system interactions. A more representative model that incorporates plate-member interactions is under development as are detailed non-linear finite element studies of the test specimens which will be reported in the future.

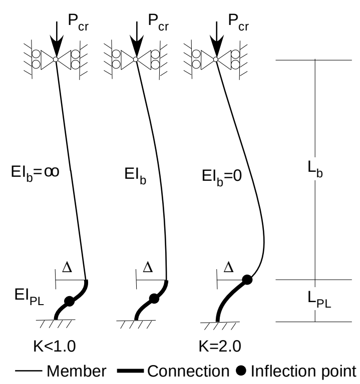

Fig. 2-12: Stepped column analogy for brace-member system interaction.

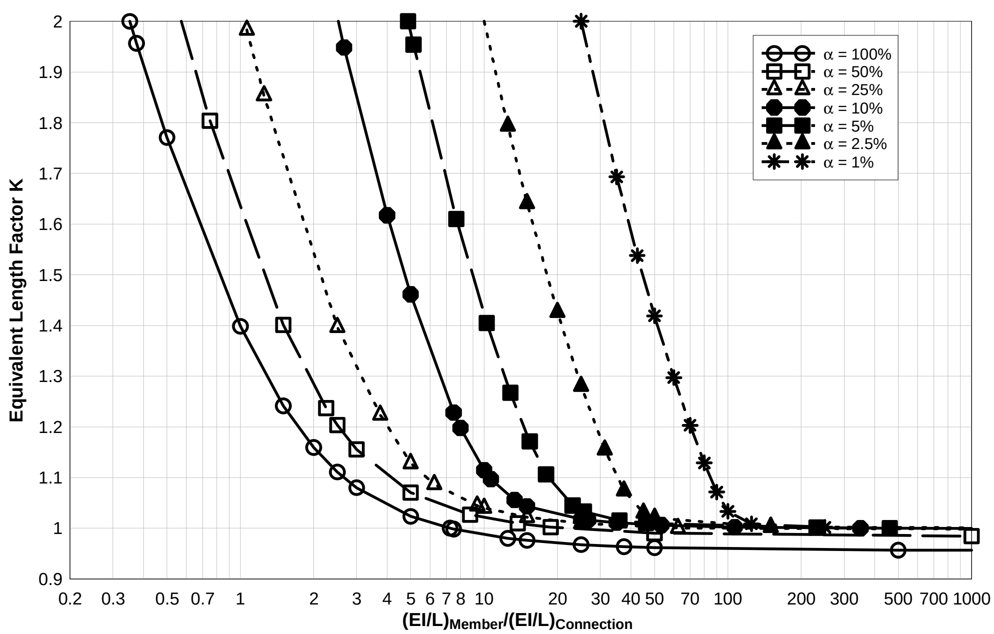

Fig. 2-13: System interactions for buckling of stepped column showing member interaction on connection equivalent length factor, $\alpha = L_{connection}/L_{member}$.

2.6 Conclusions

Six large-scale gusset plate specimens were tested to produce new data on behavior and capacity of gusset plate connections with lateral sway-buckling response. The parameters included in this study were: plate thickness, initial out-of-plane imperfection, compression member stiffness, and member load combinations. Variation of the diagonal compression member out-of-plane flexural stiffness was unique to the testing program. The program evaluated the effectiveness of Whitmore, Modified Thornton, and the *FHWA Guide* to predict the buckling load and stress distribution of gusset plate connections. All six specimens exhibited sway-buckling behavior and the key findings are summarized below.

- Interaction of member and plate stiffness influenced the gusset plate buckling capacity, with reduced buckling strength of the plates when the compression member stiffness was reduced. Such interactions of the member and plate relative stiffnesses on sway buckling were also shown analytically.
- Member-connection interactions may need to be considered to predict connection sway-buckling capacity. Such connections include those with very long truss compression diagonals.
- Initial imperfections on the order of the plate thickness decreased buckling capacity of the gusset plates. Relatively large initial imperfections in the plate lessened the influence of the member stiffness on the plate buckling capacity.
- Combination loading reduced buckling capacity of a specimen due to incremental out-of-plane deformations produced from the individual member loads that were not recovered upon unloading the individual members.

- Whitmore was more effective than Modified-Thornton at predicting gusset plate stresses with both methods overestimating the average measured stress in the direction of M4 and underestimating the maximum measured stress in the direction of M4.
- Back-calculated *K* values based on the *FHWA Guide* methodology were much lower than those shown in the *FHWA Guide*. This is an artifact of the column analogy used to describe plate behavior.
- Using the example *K* value (1.2) shown in the *FHWA Guide* under-predicted all the specimen capacities by more than a factor of 2. Even for the case of large initial plate imperfections (100% plate thickness) the largest experimental K value was 0.8. These findings show that K values less than unity can be used to analyze sway dominated gusset plates.

2.7 Acknowledgements

This research was funded by the Oregon Transportation Research Consortium with match funding provided by the Oregon Department of Transportation. The authors would like to recognize collaborative research performed at Portland State University by Dr. Peter Dusicka and Mr. Thomas Kay in developing detailed finite element models of the experimental specimens. These findings will be reported in future works. The findings, conclusions, and recommendations presented are those of the authors and do not necessarily reflect the views of the project sponsors or individuals acknowledged.

2.8 References

AISC. *Steel Construction Manual.* 13th, Fourth Printing. American Institute of Steel Construction (AISC), 2008.

ASTM. "Standard Test Methods and Definitions for Mechanical Testing of Steel Products." *A 370-97a.* American Society for Testing and Materials, 1997.

FHWA. "Load Rating Guidance and Examples For Bolted and Riveted Gusset Plates In Truss Bridges." *FHWA-IF-09-014.* U.S. Department of Transportation, Federal Highway Administration, February 2009.

Galambos, T. V., and A. E. Surovek. *Structural Stability of Steel: Concepts and Applications for Structural Engineers.* 1st. Wiley, 2008.

Gross, John L. "Experimental Study of Gusseted Connections." *Engineering Journal* (American Institute of Steel Construction), Third Quarter 1990: 89-97.

Hardin, B. O. "Experimental Investigation of the Primary Stress Distribution in the Gusset Plates of a Double-Plane Pratt Truss with Chord Splice at the Joint." *Bulletin No. 49* (University of Kentucky, Engineering Experiment Station), September 1958.

Irvan, W. G. "Experimental Study of Primary Stresses in Gusset Plates of a Double Plane Pratt Truss." *Bulletin Vol. 12* (University of Kentucky, Engineering Experiment Station), no. 2 (1957).

NTSB. *Collapse of I-35W Highway Bridge, Minneapolis, Minnesota, August 1, 2007.* Highway Accident Report NTSB/HAR-08/03, Washington, DC: National Transportation Safety Board (NTSB), 2008.

Thornton, W.A. "Bracing Connection for heavy Construction." *Engineering Journal* (American Institute of Steel Construction (AISC)), 1984: 139-148.

Vasarhelyi, Desi D. "Tests of Gusset Plate Models." *Journal of the Proceedings of the American Society of Civil Engineers Structural Division*, February 1971: 665-678.

Whitmore, R. E. "Experimental Investigation of Stresses in Gusset Plates." *Engineering Experiment Station*, *The University of Tennessee*, no. Bulletin No. 16 (May 1952): 1-33.

Yam, M C H, and J J R Cheng. *Analytical Investigation of the Compressive Behavior and Strength of Steel Gusset Plate Connections.* Structural Engineering Report No. 207, University of Alberta, 1994.

EFFECTS OF CORROSION AND RETROFITS ON SWAY-BUCKLING RESOPONSE OF GUSSET PLATE CONNECTIONS

Anthony G. Hafner and Christopher Higgins

Journal of Bridge Engineering, ASCE

1801 Alexander Bell Dr.

Reston, VA 20191-4400

Issue not yet determined

3 EFFECTS OF CORROSION AND RETROFITS ON SWAY-BUCKLING RESPONSE OF GUSSET PLATE CONNECTIONS

Anthony Hafner[5] S.M.ASCE and Christopher Higgins[6] P.E. M.ASCE

3.1 Abstract

Following the collapse of the I-35W Bridge in Minnesota in 2007, the evaluation and rehabilitation of gusset plate connections has become of interest nationally. Key issues are the influence of corrosion on behavior and buckling capacity and how to effectively strengthen connections. This research addresses the effects of commonly observed corrosion on sway-buckling capacity and proposes new retrofit approaches based on experimental tests of large-scale steel gusset plate connections. A parametric finite element model was developed to determine lateral-stiffness of gusset plates. Experimental results showed that the corrosion considered had a minor impact on sway-buckling capacity. The two retrofit options considered significantly increased sway-buckling capacity and lateral stiffness of gusset plate connections. The key response parameters were load versus out-of-plane displacement of the gusset free edge, stress distribution along critical paths, buckled shapes, and translational stiffness. An economic comparison is also included showing the advantages of the proposed retrofits over other conventional retrofit options.

3.2 Introduction

The condition of gusset plate connections in existing steel truss bridges throughout the United States is currently of interest to transportation agencies following the collapse of the I-35W Bridge in Minneapolis, MN in 2007. As of 2010, there were 11,424 truss bridges in the national bridge inventory with 6,445 considered structurally deficient (FHWA 2010).

---

[5] Graduate Research Assistant at Oregon State University
[6] Professor and Slayden Construction Faculty Fellow, School of Civil and Construction Engineering, Oregon State University

Corrosion of gusset plates is the main cause of deterioration and when significant section loss occurs it can impact the strength of the connection and thereby influence the overall structurally deficiency. In addition, efficient and cost effective rehabilitation methods are needed to ensure safety and freight mobility. To address these issues, an experimental research program was undertaken to investigate corrosion effects and retrofit methods on gusset plate connection performance and strength. This research is the second phase of a study which focuses on the behavior of large-scale gusset plate connections under sway-buckling conditions. The corrosion and retrofit solutions considered in the present study were based on results from an initial phase of testing that is reported by Higgins, et al. (2012). Key variables considered in the present research were: the overall buckling capacity, out-of-plane deformation of the free edges of the gusset plates, and distribution of gusset plate stresses. Additionally, finite element analyses (FEA) were used to assess the lateral stiffness of the gusset plates from different retrofit options. This paper discusses the experimental design and setup, significant findings and interpretation of the results, and provides guidelines for retrofit of gusset plate connections susceptible to sway-buckling behavior.

3.3 Background

Corrosion is widely recognized as a significant contributor to deterioration of existing steel bridges. Currently, bridge inspectors look for loss of steel areas caused by corrosion and have observed that corrosion is typically observed in areas that trap debris and/or water, such as along the top edge of a bottom chord (Medwick 2010). Current practice is to apply a reduction factor equivalent to the measured section loss observed in field inspections (Anderson 2010) or to rework the analysis using the minimum remaining thickness (Curtis 2009). However, the actual effect of corrosion on buckling capacity of gusset plates has not previously been investigated.

Current retrofit options for bridges with structurally deficient gusset plates are limited and have not been validated experimentally. Often, old gusset plates are replaced with new thicker plates or a shingle plate is added over the existing plate to increase capacity (Curtis 2009; Anderson 2010). Another option is to add angles to the free edge of the gusset plate to increase lateral stiffness; however, design guidelines for these options are not documented.

To address these needs, experimental tests were performed to characterize the effects of corrosion and alternative retrofit strategies on sway-buckling behavior of bridge gusset plate connections. Results of these tests are reported here and design guidance is provided for application of the rehabilitation strategies.

3.4 Experimental Design, Setup and Testing Methods

Based on the identified cause of failure for the I-35W Bridge, the experimental program focused on the sway buckling response of double-sided gusset plates typical of truss bridges. The actual size and strength of connection U10 in the I35-W Bridge makes full-size testing difficult and costly. While it was not the intent of this study to test a reduced-scale replica of the original connection, the selected laboratory gusset plate configuration and proportions were inspired by the original U10 connection in the I-35W Bridge which produced buckling failure. Modifications to fastener patterns, member framing angles, and member lengths were made to allow it to fit within the laboratory capability. An elevation view of the overall test setup is shown in Fig. 3-1. The connection consisted of double-sided gusset plates joined to tubular truss members using high-strength bolts. The truss members were attached to a test frame that reacted against the applied forces and the generated member forces. The setup allowed over 4448 kN (1 million pounds) of force to be generated within the setup. A lateral brace was positioned on the west gusset plate at the work point. The brace allowed vertical motion but restricted out-of-plane displacement of the truss and represents the lateral support available to a real truss gusset connection due to floor beams or wind bracing. Slotted holes in the connection angles used to join the brace to the gusset ensured that significant forces cannot flow through the connection angles.

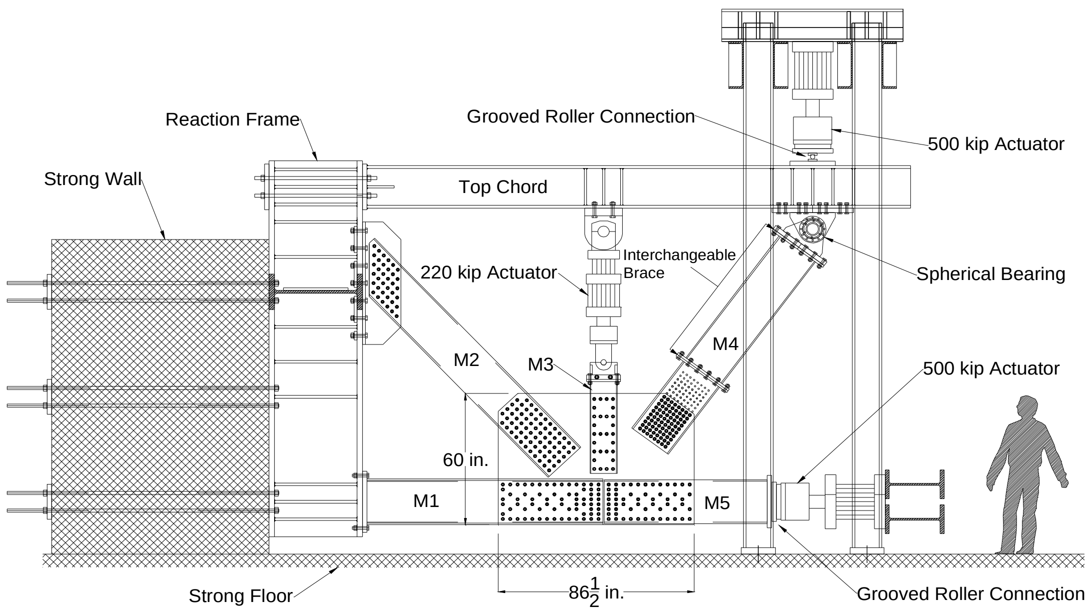

Fig. 3-1: Overall elevation view of experimental setup

Five truss members were joined by the gusset plates in the setup: members M1 and M5 represented top or bottom chord members, M2 a tension diagonal, M3 a vertical member, and M4 a compression diagonal (Fig. 3-1). The gusset plates were designed so that sway buckling failures could occur at the M4 connection. The dimensions and bolt patterns are detailed in Fig. 3-2. Member M1 was a built-up box member made of four 31.75 mm (1.25 in.) thick A36 steel plates with overall member dimensions of 533.4 mm x 304.8 mm (21 in. x12 in.). The strong bending axis was oriented in the plane of the truss. Members M2 and M5 were HSS508x304.8x15.9 (HSS20x12x5/8) rectangular tubes with the strong axis oriented in the plane of the truss. Member M3 was an HSS304.8x304.8x9.5 (HSS12x12x3/8) square tube. Member M4 was a built-up member composed of back-to-back MC408x86 (MC18x58) A36 steel channel sections. The tube sections were A500 steel and all members were designed to remain elastic at the full capacity of the available hydraulic actuators. The reason for using a nonstandard section for the compression diagonal originated from results of the initial of the research program which showed plate buckling capacity was reduced as the diagonal compression member out-of-plane flexural stiffness was reduced. The stiffness of the compression diagonal is comparable with the translational stiffness of in-service truss bridges (Higgins *et al*. 2012). All of the connections were bolted with 19 mm (3/4 in.) diameter A325 bolts and tightened with a pneumatic impact wrench except for the M4 connection, which was hand-torqued to a relatively low 0.136 kN-m (100 ft-lbs) to allow fastener bearing rather than slip-critical behavior. The M4 stand-off distance from the work point was specifically designed to allow the entire Whitmore section to be effective in the plate without interference with adjacent bolt patterns and facilitated buckling of the connection. All the gusset plates tested were grade A36 steel and two thicknesses were tested: 6.4 mm (0.25 in.) for retrofits and 9.5 mm (0.375 in.) for corrosion. The mechanical properties of the plates were determined according to ASTM A370 (1997) and are shown in Table 3-1.

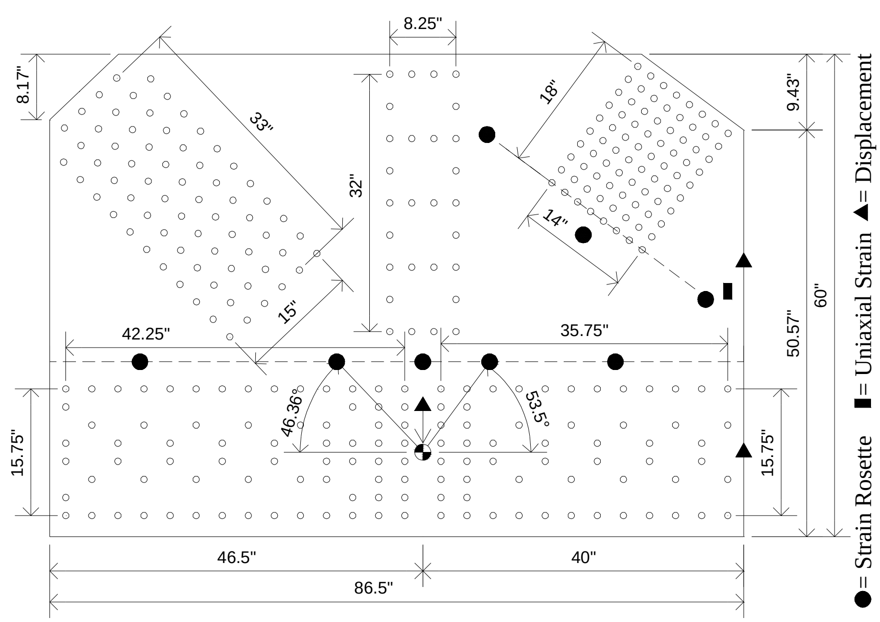

Fig. 3-2: Gusset plate details with relevant strain gage and displacement sensor locations

Table 3-1: Mechanical properties of test specimens

Specimen	Average F_y, MPa (ksi)	Std. Dev.	Average F_u, MPa (ksi)	Std. Dev.
Retrofit Control	310.7 (45.10)	1.55	482.0 (69.96)	0.31
Corrosion Control	317.9 (46.13)	0.66	467.3 (67.83)	0.34
Corrosion	341.4 (49.55)	0.82	474.5 (68.87)	0.25
Retrofit 1	357.9 (51.95)	1.02	495.1 (71.86)	0.49
Retrofit 2	350.4 (50.85)	0.40	483.9 (70.23)	0.33

3.4.1 Instrumentation Plan

The instrumentation plan was developed to acquire data for the plate stresses, plate and member displacements, and member forces and interactions. The plate was instrumented with uniaxial and 45 degree rosette strain gages. The uniaxial gages were placed along the free edges of the plate and within the bolt pattern of member M4. Uniaxial strain gages were placed on all truss members except M3 to capture strains near the midpoint of the member to measure member axial force and bending. Member M3 was not instrumented since the hydraulic actuator and attached load cell effectively act as the member and the member force transducer. To measure out-of-plane displacement of the plate, displacement sensors were positioned along the free edges of the gussets. Rigid body motion was captured by displacement sensors at the work point, the edge of the gusset at the M5 connection, and the base of the gusset plates. There were also displacement sensors positioned between the members and gusset plates to measure relative slip and between the member and gusset plate at the work point to measure overall member deformations. The sensors used in reporting plate stresses, strains, and displacements are shown in Fig. 3-2. In addition to the discrete displacement measurements, a digital image correlation system monitored plate deformations on the west side of the connection and was also used to determine initial imperfection.

3.4.2 Loading Protocol

A 2240 kN (500 kip) actuator placed vertically over the compression diagonal M4 was used to load the member and generate stresses in the gusset plate. To minimize bending in member M4, a special high-force spherical bearing was fabricated to connect the end of the member to the loading frame as seen in Fig. 3-1. The spherical bearing provided no rotational restraint. All the specimens were loaded monotonically using the M4 actuator at a rate of 4.4 kN/sec (1 kip/sec).

3.4.3 Control Specimens

Two specimens were used as control specimens for the corrosion and retrofit specimens. The Retrofit Control specimen used 6.4 mm (0.25 in) thick gusset plates for comparison with the subsequent alternative retrofit specimens, and the Corrosion Control specimen used 9.5 mm (0.375 in) thick gusset plates for comparison with the simulated corrosion specimen.

3.4.4 Simulated Corrosion Specimen

In order to assess the effects of corrosion on gusset plate strength and performance, 9.5 mm (0.375 in.) thick plates were used as they permitted significant material to be removed and data from previous tests could be used for comparison. Natural corrosion of the plates could not be pursued due to time constraints and accelerated electro-chemical corrosion was not economical and could not produce a well-defined corrosion profile in the large plates used in this study. Therefore, corrosion was simulated by removing material in the plate along the length of member M5. This was achieved by milling a channel on the inside of the plates and the amount of section loss was identical on both east and west plates. The depth of the channel was 6.4 mm (0.25 in.) and height was 50.8 mm (2 in.). A 25.4 mm (1 in.) diameter ball-in mill was used to remove the material which provided a 12.7 mm (0.5 in.) radius at the edges of the channel. The depth of the cut produced 67% section loss at the corroded section. Photographs of the milling are shown in Fig. 3-3. The location of the corrosion section loss is typical for existing steel truss bridges where water and debris can accumulate along the top side of a bottom chord against the gusset plate. Unlike most corrosion observed in the field, the artificial corrosion did not extend the entire length of the gusset. This was to prevent the possibility of a shear failure along the corroded section.

Fig. 3-3: Photographs of milled plate to simulate corrosion above the chord

3.4.5 Retrofit Specimens

Two alternative retrofit approaches were investigated in this study to increase the sway-buckling capacity of gusset plates. The first retrofit approach was to stiffen the free edges of the plates and prevent them from moving independently. This is analogous to lean-on bracing systems widely used in structural engineering practice. Since failure loads were anticipated to increase significantly, the thickness of the gusset plates was chosen as 6.4 mm (0.25 in.) to ensure that the available actuator capacity was sufficient to fail the connection. To stiffen the free edges, a 76x76x6.4 mm (3x3x1/4 in) angle was bolted to the inside of each plate at the edge with the out-standing leg flush with the free edge (Fig. 3-4). Detailed drawings of the retrofit plate are shown in Fig. 3-5. After fastening the angles with bolts to the gusset plates, a 6.4 mm (0.25 in) grade A36 steel plate was bolted to the out-standing leg of each angle (Fig. 3-4). All fasteners were 19 mm (3/4 in.) diameter A325 high-strength bolts. The bolts were tightened with a pneumatic impact wrench. It is important to note that the stiffener plate was designed to be installed in a field setting and does not extend all the way to the bottom chord or to contact with the compression diagonal. The construction tolerances allow for irregularities present in existing connections. There are also cutouts at both the top and bottom of the plate to allow for assembly and inspection.

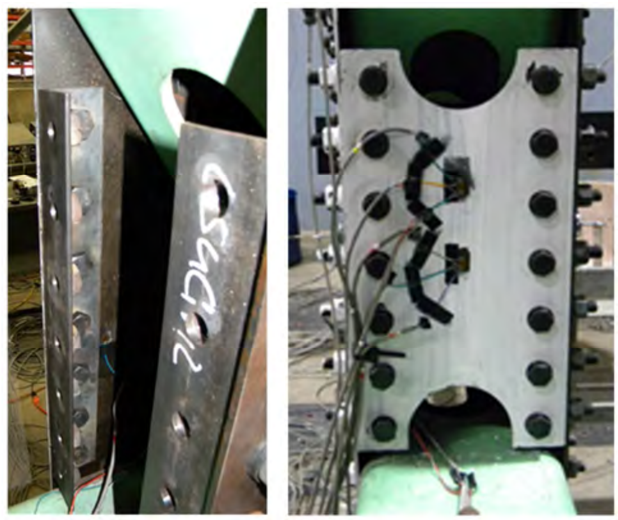

Fig. 3-4: Photographs of retrofit #1

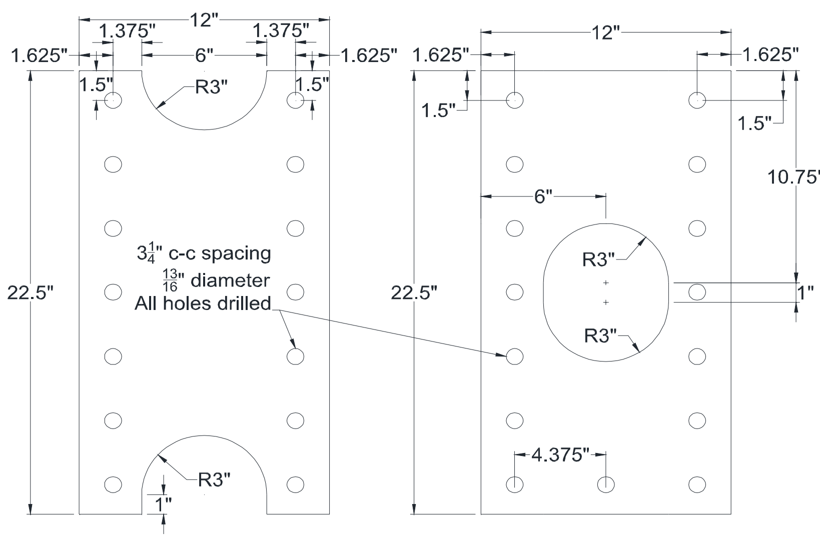

Fig. 3-5: Plate details for retrofit #1 (left) and retrofit #2 (right)

The design of retrofit #2 was based on the results of the retrofit #1. This specimen was nearly identical, again using 6.4 mm (0.25 in.) thick gusset plates; however, there was an addition of a base angle at the bottom of the stiffener plate that was connected to the chord member. Detailed drawings of the retrofit plate are shown in Fig. 3-5. Again 76x76x6.4 mm (3x3x1/4 in) A36 steel angles were used to stiffen the free edge and a 6.4 mm (0.25 in.) A36 steel plate was bolted to the out -standing leg of the angles. The base angle was a 102x102x12.7mm (4x4x1/2 in) A36 steel angle connected to the bottom of the stiffener plate and connected to the chord member M5 (Fig. 3-6). The stiffener plate was also modified from retrofit #1 by changing the location of the cut-out. The same total area of material was removed; however, one large cut-out was made in the center of the plate rather than at the top and bottom of the plate. All fasteners were 19 mm (3/4 in.) diameter A325 high-strength bolts except for the bottom angle-to-chord connection which used 22.2 mm (7/8 in) diameter A325 bolts. The addition of the base angle at the base of the stiffener plate prevents relative out-of-plane displacement between the free edge and chord member. Restricting the movement of the gusset plates relative to the chord increased the lateral stiffness and thereby should increase buckling capacity of the connection.

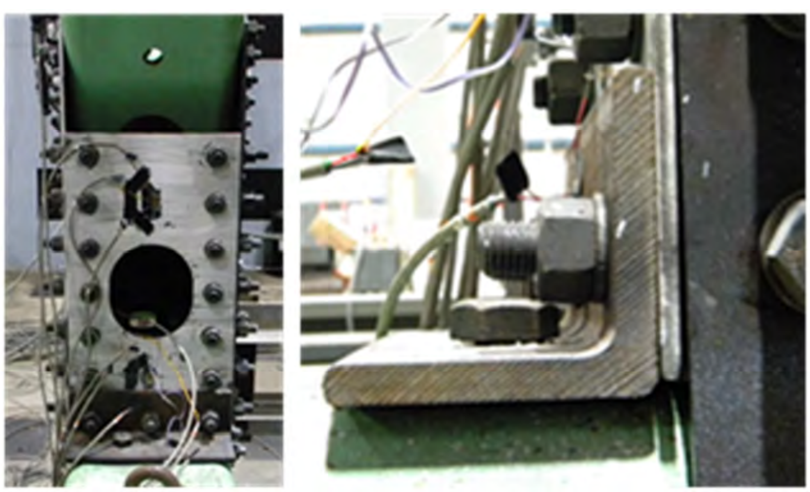

Fig. 3-6: Photographs of retrofit #2

3.5 Experimental Results

Five specimens were tested to failure in this study. Two specimens were control specimens, two were retrofitted specimens, and one contained simulated corrosion. Table 3-2 summarizes key properties and results for each specimen including: the axial load at failure in member M4, magnitude of the initial imperfection of the gusset plate free edge, and out-of-plane displacement at failure. All specimens failed due to sway-buckling at the M4 connection in the direction of the floor brace. The key experimental observations are described subsequently.

Table 3-2: Testing matrix with results

	Retrofit Control	Corrosion Control	Corrosion	Retrofit #1	Retrofit #2
Plate Thickness, mm (in)	6.4 (0.25)	9.5 (0.375)	9.5 (0.375)	6.4 (0.25)	6.4 (0.25)
Initial Plate Imperfection, % plate thickness	43%	40%	34%	43%	40%
Gusset Free Edge Out-of-Plane Displacement at Failure, mm (in)	21.1 (0.83)	15.2 (0.60)	22.4 (0.88)	10.2 (0.40)	-0.8 (-0.03)
M4 Axial Load at Failure, kN (kip)	1139 (256)	2575 (579)	2504 (563)	1624 (365)	2126 (478)

3.5.1 Load versus Out-of-Plane Displacement Behavior

The axial compressive load for member M4 versus out-of-plane displacement of the free edge is shown in Fig. 3-7 for all specimens. The displacement is at the midpoint of the gusset plate free edge with rigid body motion of the truss removed. Rigid body motion of the truss was captured at both the work point of the gusset plate and the edge of the gusset plate at the M5 connection. The control specimens did not have measurements for the edge of the gusset plate at the M5 connection, so linear projections were made from the work point of the gusset to determine the rigid body motion at the edge of the gusset plate. There were also non-conservative contact surface deformations present that produced load stiffening at the beginning of each test. These were removed in post-processing by best-fit of the linear elastic portion of the curve.

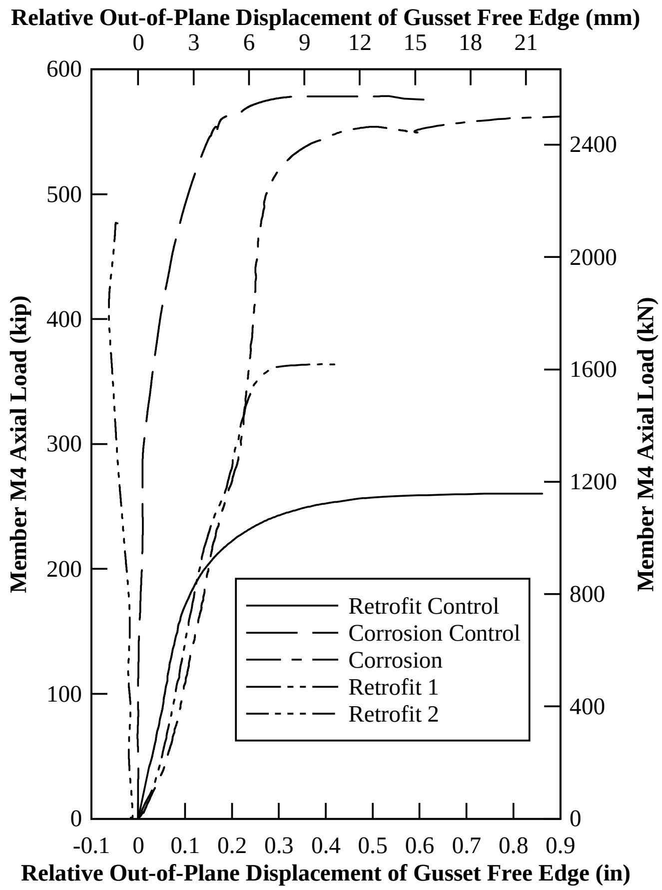

Fig. 3-7: Compressive M4 axial load versus out-of-plane displacement of the gusset free edge for all specimens

The simulated corrosion specimen showed less stiffness during loading and had much larger out-of-plane deformation, 22.4 mm (0.88 in.), than the corrosion control specimen, 15.2 mm (0.60 in.); however, the failure load was only slightly lower at 2504 kN (563 kip) than the control specimen at 2575 kN (579 kip). This behavior suggests that the reduced section provided less fixity above the bottom chord enabling larger out-of-plane deformations even though the buckling capacity reduced by only 2.8% compared to the corrosion control specimen. The results showed that large section loss along the chord, for the plate sizes, thicknesses, and member stiffnesses considered here did not produce a proportionally large reduction in sway-buckling capacity.

For retrofit #1, the load versus displacement behavior showed significant increases in capacity and decreases in the out-of-plane displacement of the free edge. The stiffness of the curve in the linear elastic region showed that the plates initially moved out-of-plane at the same rate as the retrofit control specimen. However, the control specimen exhibited softening as retrofit #1 continued loading elastically. This was attributed to the edge stiffening and enforcing plate compatibility. The final out-of-plane displacement dropped from 21.1 mm (0.83 in.) for the control specimen to 10.2 mm (0.40 in.) for retrofit #1, a 52% reduction in displacement at failure. Correspondingly the compression diagonal load at failure increased from 1139 kN (256 kip) for the control to 1624 kN (365 kip) for retrofit #1, a 40% increase.

Retrofit #2 showed even greater effects than retrofit #1and the plate behavior was very different from that previously observed for the control specimen. The free edge out-of-plane displacement was nearly eliminated and the final displacement was just -0.8 mm (-0.03 in.) compared to 10.2 mm (0.4 in.) for retrofit #1 and 21.1 mm (0.83 in.) for the retrofit control. There was also a significant increase in sway-buckling capacity, increasing 87% from 1139 kN (256 kip) for the retrofit control to 2126 kN (478 kip) for retrofit #2. By fastening the base angle to the stiffener plate and bottom chord, the gusset plate free edges were effectively restrained to each other and the chord thereby preventing relative out-of-plane displacement. The performance of retrofit #2 was better than retrofit #1 with only the base angle addition.

3.5.2 Plate Stresses

Stresses on the gusset plate surface, and also the stiffener plate surface in the retrofits, were captured throughout the tests. Two paths of interest were plane A-A, the shear plane that runs across the gusset plate just above the bottom chord, and path B-B which corresponds to the Whitmore width (Fig. 3-8(c)). Comparisons were made between the simulated corrosion specimen and corrosion control specimen and the two retrofit specimens and retrofit control specimen. Stresses on the stiffener plate were obtained at two locations along the vertical centerline of the plate for each specimen. All stresses were compared at $0.6F_{max}$ (60% of maximum axial load) to prevent contamination of the intended membrane strain measurements from bending strains induced in the plates as large lateral motions occurred late in the experiments.

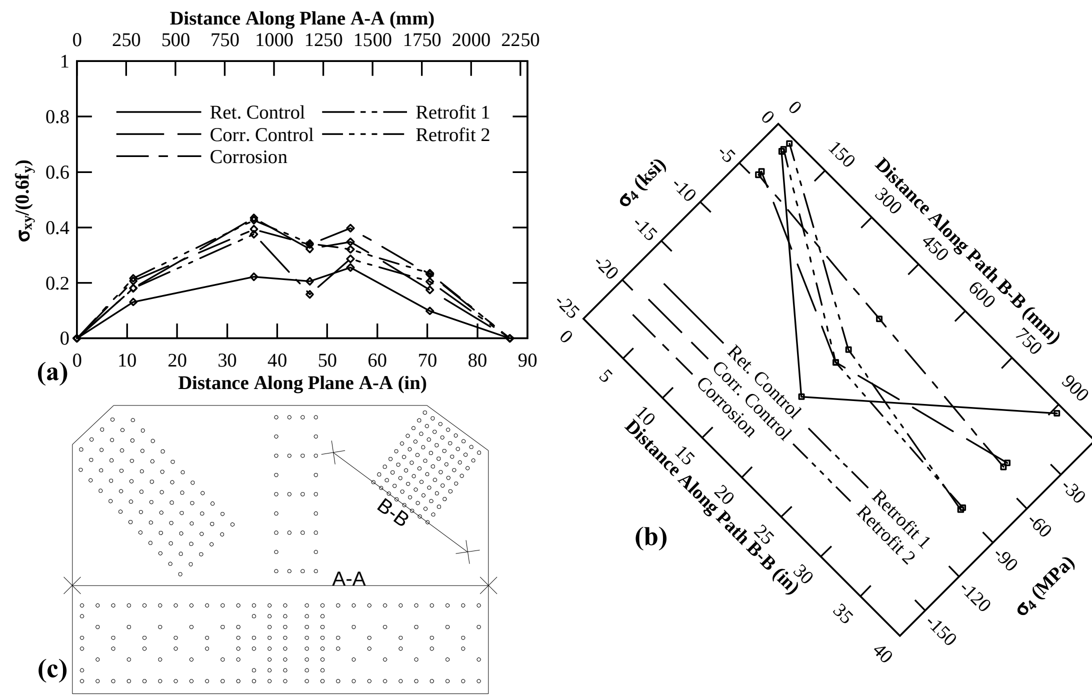

Fig. 3-8: Plate stresses at 0.6Fmax, (a) Shear stress in global xy direction normalized to shear yielding, (b) Stress in M4 direction, (c) Defined stress paths

The stresses along plane A-A were of particular interest for the simulated corrosion specimen since this plane is located along the section with significant section loss. Fig. 3-8(a) shows the shear stresses for all specimens normalized to shear yielding (taken as $0.6f_y$). The corrosion specimen exhibited little change in behavior which is somewhat unexpected.

However, the stress in the retrofitted specimens increased dramatically from the retrofit control specimen, with behavior corresponding more closely to that of the thicker plates of the corrosion control specimen. This increase in stress stems from the added lateral stiffness provided by the retrofits that allowed larger forces to be carried and thereby larger stresses achieved in the plate.

The gusset plate stresses along path B-B are shown in Fig. 3-8(b) and indicated the relative stress distribution along the Whitmore width for the different specimens. The stresses in Fig. 3-8(b) are shown in the direction of the applied force from compression diagonal member M4. In general, the distributions were similar for all specimens. However, the right side of the path in both of the retrofit specimens exhibited higher stresses than the retrofit specimen and the simulated corrosion specimen showed lower less stress at the midpoint than the corrosion control specimen.

The stresses in the supplemental stiffener plates were measured to monitor stress levels to determine if excessive stress was being carried by the plate. The maximum principle compressive stress observed throughout the tests in either retrofit was 81 MPa (11.8 ksi) and the maximum principle tensile stress was 37 MPa (5.6 ksi), both of which were well below any yield criterion.

3.5.3 Buckled Shapes

The buckled shapes show how different restrictions to the gusset plates changed the buckling mode of the connection. Fig. 3-9 shows the buckled shapes for all specimens and Digital Image Correlation measurements of the buckled shapes for the retrofit control specimen and both alternative retrofit specimens are shown in Fig. 3-10 to illustrate the plate deformations at failure. For the control specimens the buckled zone ran from the midpoints of the free edges to just below the last row of bolts on M4. This was also the case for the simulated corrosion specimen even as yielding was observed along the reduced section above the chord near failure (visible due to the whitewash flaking). Upon buckling, the reduced section of the simulated corrosion specimen fractured due to highly localized bending at the reduced section thickness.

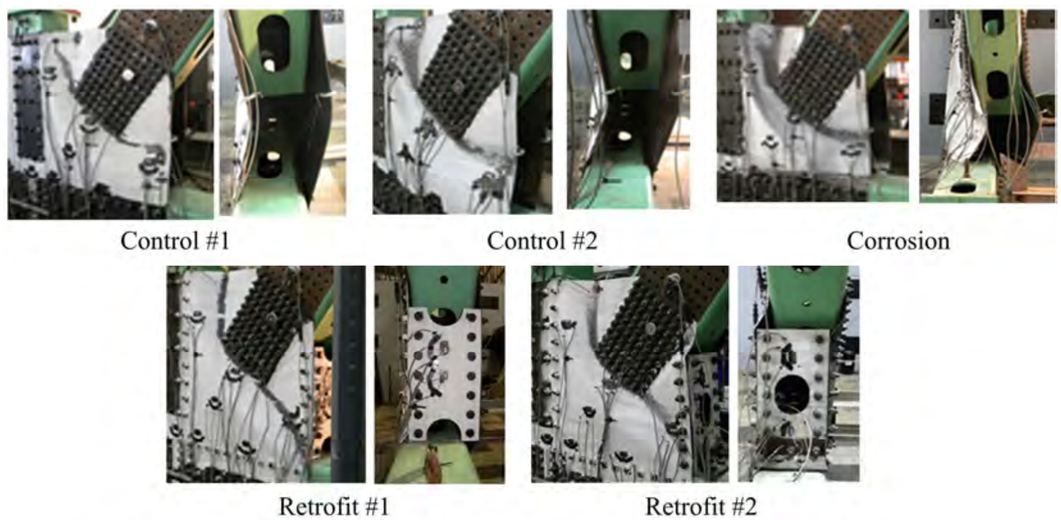

Fig. 3-9: Photographs of buckled shapes for all specimens (front and side views)

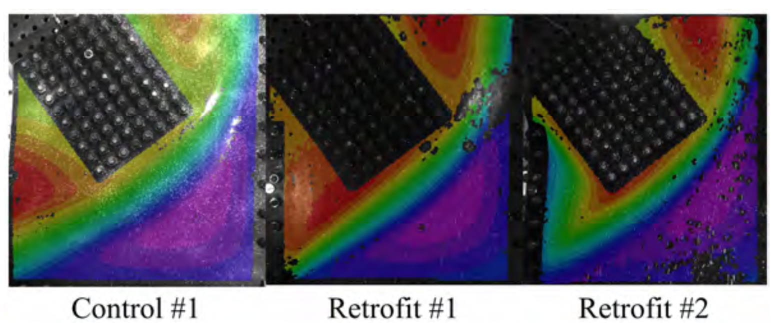

Fig. 3-10: DIC buckled shapes shown without magnitudes (purple = farthest, red = closest)

The retrofitted specimens each had different buckled shapes caused by the different restrictions imposed at the free edge. In retrofit #1, the buckled zone extended from the base of the M4 connection to the gap between the stiffener plate and the chord. This was caused by the majority of the free edge being stiffened and the path of least resistance became the unstiffened zone just above the chord. Retrofit #2 could not buckle in the same manner as retrofit #1 due to the base angle preventing movement of the free edge at the chord. Therefore the path of least resistance became the upper portion of the plate at the gap between the top of the stiffener plate and member M4. The buckled shapes achieved by the retrofits are higher mode shapes not achievable by the unstiffened control specimen.

3.6 FEA Modeling of Lateral Stiffness

In order to determine how the different retrofit options can increase the lateral stiffness of the gusset plates, finite element models were developed using the software package Abaqus (Dasault Systèmes 2011). The analysis considered the relative translational stiffness (out-of-plane stiffness) of the gusset plates. Based on laboratory observed results, the gusset plate connection was idealized by considering only the section of the gusset plate exhibiting buckling. The section considered was the region containing the M4 connection and bounded by the vertical member M3 and bottom chord M5 (Fig. 3-11). The plates were modeled with S3R shell elements assuming linear elastic behavior. The gusset plates were spaced apart by the dimension of the M4 diagonal and the same bolt pattern was used as that for the M4 connection. To avoid modeling the members explicitly, the plate boundaries were taken to correspond to the first row of bolts for members M3 and M5 and fixed boundary conditions were applied along these two edges. To ensure that the two plates moved together at the M4 connection, very stiff springs were used to join the plates together at the bolt locations on the M4 member.

The supplemental stiffener plate and edge connection angles used in the retrofit designs were modeled using shell elements. The angles were attached to the free edge of the gusset plate and to the supplemental stiffener plate using rigid multi-point constraint (MPC) fasteners at the discrete bolt locations. Contact surfaces were defined to account for interaction between angles and plates. Retrofit #1 did not use a base angle to connect the supplemental stiffener plate to the chord. For retrofit #2, the base angle was used but was not explicitly modeled. Instead a fixed boundary condition was applied to the bottom of the supplemental stiffener plate and this fixity was reflective of the observed experimental response.

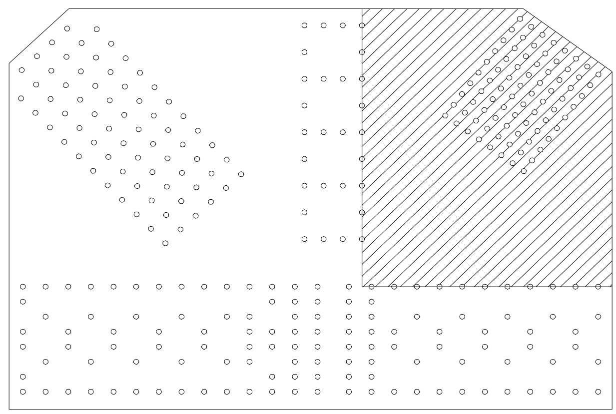

Fig. 3-11: Gusset plate section used in FEA model represented by hatched region

The stiffness of the connection was determined by applying a unit displacement to the entire M4 bolt group and summing the reaction forces along the constrained edges of the gusset plate in the out-of-plane direction. The lateral stiffness is expressed as force per unit displacement. The predicted deformed shapes for the unstiffened control gusset plates and both retrofits #1 and #2 are shown in Fig. 3-12. The stiffness of the control specimen was 1.98 kN/mm (11.3 kip/in), and is designated as the initial stiffness hereafter. The lateral stiffness for retrofit #1 was 4.62 kN/mm (26.4 kip/in) or 2.33 times the initial stiffness, and the lateral stiffness for retrofit #2 was 5.64 kN/mm (32.2 kip/in) or 2.95 times the initial stiffness. Based on the performance of retrofit #2, considering the marginal extra cost of the base angle, this approach was considered to be the better alternative. Increasing the gusset plate connection lateral stiffness effectively allows higher compression forces to be carried by the connection.

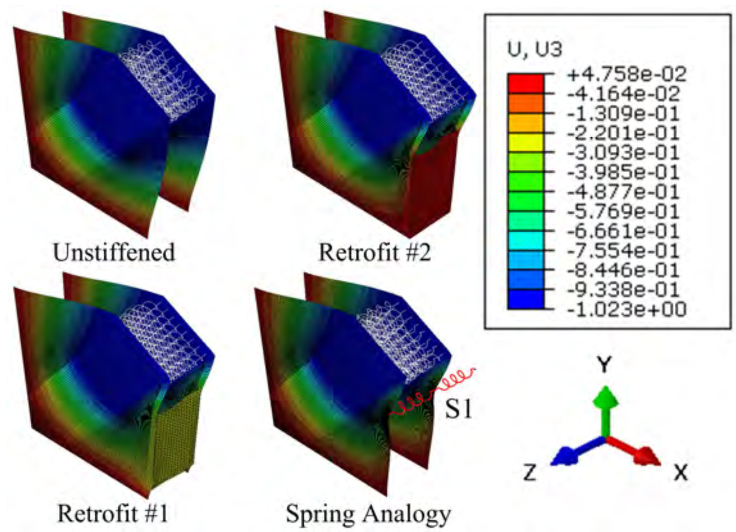

Fig. 3-12: Deformed shapes from Abaqus showing out-of-plane displacement, spring S1 resists translation and rotation

The effects of the supplemental stiffener plate were evaluated by idealizing the lateral and rotational stiffness of the plate as a set of springs located only at the top level of the supplemental stiffener plate. Three separate springs were used to represent the restraint provided by the supplemental stiffener plate which restrained translation in the z direction and rotation about the x and y axes as shown in Fig. 3-12. The rotational spring stiffnesses were determined from the translational stiffness by:

$$k_T = \frac{AG}{h} \tag{3-1}$$

$$k_{Rx} = \frac{3EI}{h} \tag{3-2}$$

$$k_{Ry} = \frac{6EI}{b} \tag{3-3}$$

where k_T is the translational stiffness, k_{Rx} is the rotational stiffness about the x axis, and k_{Ry} is the rotational stiffness about the y axis. All variables were held constant with the exception of stiffener plate thickness which was used in *A* and *I*. The results were compared to models where pinned and fixed boundary conditions were applied at the spring connection points and the results are shown in Fig. 3-13. As seen here, when the supplemental stiffener plate was sufficiently stout (defined by width to thickness ratio) then the gusset plate was effectively restrained against translation and the stiffening effect on the gusset plates was closely approximated as a pin support at the top of the supplemental stiffener plate. If the thickness of the supplemental stiffener plate was increased further, the additional rotational restraint provided by the thick plate was closely approximated as a fixed support at the top of the supplemental stiffener plate. The lateral stiffness provided by the supplemental stiffener plate was estimated considering both shear and bending stiffness contributions as:

$$k = \frac{1}{\frac{h^3}{3EI} + \frac{h}{AG}} \tag{3-4}$$

where *h* was the height from the top of the stiffener plate to the first row of bolts on the bottom chord connection , *A* was the cross-sectional area of the stiffener plate, *G* was the shear modulus, *E* was the modulus of elasticity, and *I* was the second moment of area of the cross section. For the given connection geometry (h= 632 mm (24.875 in.), E=199,810 MPa (29,000 ksi), I=1.498x10^7 mm^4 (36 in.^{4}), A=1935 mm (3 in.^{2}), and G=78,918 MPa (11,154 ksi)) , the lateral stiffness of the plate was computed as 30.8 kN/mm (176 kip/in) with a 6.4 mm (0.25 in.) thick supplemental stiffener plate. This is shown as a vertical reference line in Fig. 3-13. For design purposes, the stiffness contribution of the supplemental stiffener plate is considered to be the idealized pin supported condition and details of the design approach are described subsequently.

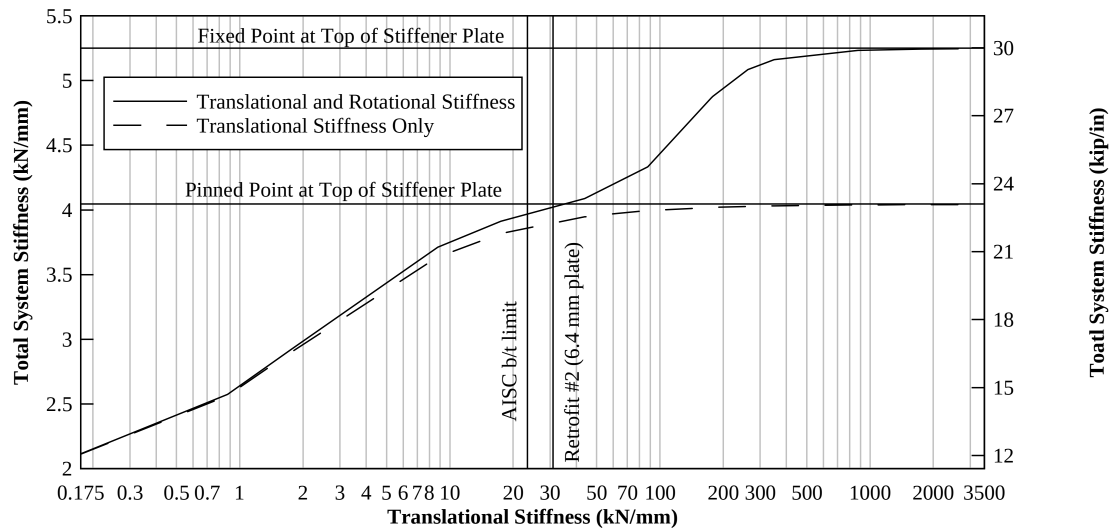

Fig. 3-13: Relationship between stiffener plate stiffness and total system stiffness

3.7 Proposed Design Guidelines for Retrofitting Gusset Plates to Resist Sway Buckling

In order to detail the supplemental plate and connection, a design procedure was developed. The first step is to establish the buckling capacity of the existing connection. The approach developed relies on the established methods reported in the *FHWA Guide* (2009). An equivalent column is determined for the gusset plate using the Whitmore section and an average column length extending from the Whitmore section to the intersections of the adjacent members. To account for connection-member interaction, a stepped column analogy is used to model both the member and connection. The length, elastic modulus, and second moment of area of the compression diagonal and the gusset plate equivalent column are used to determine the effective length factor (K) for the gusset plates. This is then used in the FHWA Guide to establish the connection buckling strength of the unretrofitted connection. To strengthen the connection against sway buckling, the lateral stiffness of the gusset plates needs to be increased. This is done by adding a supplemental stiffener plate (as described in the experimental results) with connection angles used to join this new plate to the existing gusset plates and chord. The supplemental stiffening plates act to restrain both the lateral translation and rotation of the free edge of the gusset plate. The lateral stiffness of the unretrofitted gusset plate is needed to compare with the retrofitted stiffness to determine the resulting strength increase. Closed-form solutions are not available to determine the lateral stiffness of gusset plates and the simplified finite element analysis described previously (see Fig. 3-13) were used to establish unretrofitted lateral stiffness (k_o). The retrofitted lateral stiffness of the strengthened gusset plates is then determined. As described previously, the influence of the supplemental stiffener plate is idealized as a pin connection at the free edge of the gusset plate at the top level of the supplemental stiffener plate. The lateral stiffness of the gusset plates with the idealized restraint from the supplemental stiffener plate is determined from the FEA as k_{retro}. The ratio of k_{retro}/k_o is taken as the amount of stiffness increase available to the Whitmore effective column analogy. To include the influence of the increased connection stiffness relative to the compression diagonal stiffness the stepped column analysis is repeated to establish the effective length factor (K will be larger) and the *FHWA Guide* procedure repeated to determine the retrofitted gusset plate connection capacity.

Detailing the plate and connection angles requires both adequate strength and stiffness of the components. In order for the supplemental stiffener plate to provide sufficient lateral stiffness, the plate must be sufficiently stout to prevent tension field action. This limit is defined by AISC Section G (2008) as:

$$\frac{b}{t} \leq 1.10\sqrt{\frac{5E}{F_y}} \quad for \quad \frac{b}{t} < 260 \tag{3-5}$$

where *b* is the width and *t* is the thickness of the supplemental stiffener plate. In this case, the width is the spacing between the gusset plates. For the retrofit plates considered in the present experimental study, the above slenderness criteria provided an effective lateral stiffness (as calculated by Eqn. 3-5) of 23.40 kN/mm (133.6 kip/in.). The resulting gusset plate system stiffness was at that of the idealized pin support at the free edge location as seen in Fig. 3-13. As a practical minimum, the supplemental stiffener plate should be at least the thickness of the gusset plates.

The side bracket angles should be designed so that the thickness of the angle must be greater than or at least equal to that of the supplemental stiffener plate. Minimum fastener spacing and edge distances should follow the guidelines of AISC Section J3 (2008) and the total force resisted by the fasteners should be adequate to transfer the forces from a fully plasticized supplemental stiffener plate to the supporting angles. The base angle at the bottom of the supplemental stiffener plate should be sized to resist the fully develop shear yielding strength of the supplemental stiffener plate.

3.8 Economic Comparison

The goal of any retrofit is to increase or restore the capacity of an existing structure through means that are cost effective and enduring. To this end, the retrofits used in this study were designed to be simple additions that minimize materials and installation labor. Table 3-3 includes a breakdown of the direct cost of the two different retrofit options considered compared to the cost of a shingle plate over the existing gusset. The reported costs are the material and fabrication costs incurred in this experimental program. As seen in this table, retrofit #2 produced the largest percentage increase per dollar expended. It is also important to note that labor requirements for the proposed retrofits would be modest as they can be installed with limited field fabrication requiring only hole drilling of the gusset plate edges and chord with a magnetic-based drill.

Table 3-3: Cost comparison of retrofit options per connection

	Retrofit 1	Retrofit 2	Shingle Plate
Material cost	$59.21	$142.19	$1,130.27
Manufacturing cost	$433.00	$455.00	$3,750.00
Total Cost	$492.21	$597.19	$4,880.27

3.9 Conclusions

Five large-scale gusset plate specimens were tested to produce new data on the effects of gusset plate section loss from simulated corrosion on sway-buckling capacity and two retrofit design alternatives to increase the sway-buckling capacity of existing gusset plate connections. Results from the simulated corrosion and retrofit specimens were compared to otherwise similar control specimens. The simulated corrosion specimen exhibited larger out-of-plane deformation but only a small loss of strength compared to the similar control specimen. The retrofitted specimens showed increased stiffness and strength compared to the similar control specimen. Design principles were established for proportioning the supplemental stiffening plates and connection angles. The key findings of the research are summarized below.

- The simulated corrosion produced 66% loss of gusset plate thickness above the chord but reduced the sway-buckling capacity by only 2.8% compared to the similar control specimen.
- The relationship between sway-buckling capacity and local plate thickness reduction above the chord was not directly linked. To estimate sway buckling capacity for gusset plates with localized cross section loss along the chord, the degree of restraint at the boundary should be modeled as simply supported rather than fixed.

- The effect of localized cross section loss on the gusset plates could cause other modes of failure to control connection performance and these must also be considered for evaluation of in-service gusset plate connections.
- Retrofitting existing gusset plates with a supplemental stiffener plate increased the lateral stiffness of gusset plate connections. Both retrofit details produced large increases in sway buckling capacity.
- The preferred retrofit alternative uses a supplemental stiffener plate that is connected to the bottom chord with a base angle at the bottom of the stiffener plate. This detail produced the greatest increase in sway buckling strength (1.94 times the control specimen).
- A design approach was presented that includes member-connection interaction for determining connection strength and detailing requirements for proportioning the stiffener plate, angles, and fasteners. The approach relies on simplified and idealized finite element modeling to establish gusset plate lateral stiffness.
- Current retrofit options, such as replacement or shingling of gusset plates, are very expensive and the proposed retrofit alternatives provide a cost effective solution for rehabilitating gusset plate connections susceptible to sway-buckling.

3.10 Acknowledgements

This research was funded by the Oregon Transportation Research Consortium with match funding provided by the Oregon Department of Transportation. The findings, conclusions, and recommendations presented are those of the authors and do not necessarily reflect the views of the project sponsors or individuals acknowledged.

3.11 References

AISC. *Steel Construction Manual.* 13th, Fourth Printing. American Institute of Steel Construction (AISC), 2008.

Anderson, Ralph E. "Gusset Plate Retrofit in Illinois." Illinois Department of Transportation, May 2010.

ASTM. "Standard Test Methods and Definitions for Mechanical Testing of Steel Products." *A 370-97a.* American Society for Testing and Materials, 1997.

Curtis, Rebecca. "Load Rating Gusset Plates on Non-Load-Path-Redundant Steel Truss Bridges." *Bridge Advisory Number: BA-2009-01.* Michigan: Michigan Department of Transportation, January 15, 2009.

Dasault Systèmes. "Abaqus 6.11." *User Manual.* Providence, RI: Dassault Systèmes, 2011.

FHWA. "Bridge Technology: National Bridge Inventory." *Federal Highway Administration.* December 2010. http://www.fhwa.dot.gov/bridge/struct.cfm.

FHWA. "Load Rating Guidance and Examples For Bolted and Riveted Gusset Plates In Truss Bridges." *FHWA-IF-09-014.* U.S. Department of Transportation, Federal Highway Administration, February 2009.

Higgins, Christopher, Anthony Hafner, O. Tugrul Turan, and Thomas Schumacher. "Experimental Tests of Gusset Plate Connections with Sway-Buckling Response." *Journal of Bridge Engineering* (ASCE), 2012.

Medwick, Seth. "Truss bridges: Inspection and load rating, post I-35W Bridge collapse." *Rebuilding America's Infrastructure,* March 2010.

NTSB. *Collapse of I-35W Highway Bridge, Minneapolis, Minnesota, August 1, 2007.* Highway Accident Report NTSB/HAR-08/03, Washington, DC: National Transportation Safety Board (NTSB), 2008.

4 GENERAL CONCLUSION

Throughout the experimental testing program a total of nine large-scale gusset plate specimens were tested to failure. Variables examined throughout each test include: plate thickness, member combination loading, initial out-of-plane imperfection of the gusset free edge, out-of-plane stiffness of the diagonal compression member, corrosion, and two retrofit designs. The data produced from these experiments has helped to develop a better understanding of how gusset plate connections in steel truss bridges behave in sway-buckling conditions.

The most unique finding was the discovery of interaction between the diagonal compression member and the gusset plates in governing buckling capacity. While the conventional design assumptions assumed that truss members were rigid in relation to the gusset plates, the specimens tested in the first manuscript showed this assumption to be invalid. It also showed the FHWA Design Guide (2009) to be highly conservative since the methodology rests in buckling stress (Whitmore 1952) and column theory (Thornton 1984) which is different from plate behavior. This is particularly evident when choosing an effective length factor, *K*. The FHWA Guide recommends values between 1.2 and 2.0 for sway buckling, but experimental results suggest values less than 1.0 are acceptable for sway-buckling conditions. The interaction curves developed for the first manuscript should help to give better estimates of buckling capacity in the future.

Another key purpose of this research was to find a cost-effective retrofit method to strengthen gusset plate connections susceptible to sway-buckling failures. The retrofit models used in the second manuscript both increased the buckling capacity of the connection with retrofit #2 being the most effective. The lateral stiffness of the gusset plates increased dramatically with the addition of the supplemental stiffener plate placed between the gusset plates and in turn increased the sway-buckling capacity of the connection by up to 87%. The retrofits were also extremely easy to install and would require much less work to install on existing steel truss bridges than current retrofits, such as replacing the existing gusset plates or adding a second gusset plate.

Finally, the parametric finite element model provided important information on how the retrofits affect the lateral stiffness of the gusset plates. With sufficient supplemental stiffener plate stiffness, the free edge of the gusset plate can be idealized as a pinned support at the top of the supplemental stiffener plate. Using this analogy a general set of design guidelines was proposed based on an equivalent spring system. Other variables that contribute to gusset plate stiffness include: height of the retrofit plate, percent of the gusset free edge that remains unstiffened, aspect ratio of the gusset plate section, and thickness of the gusset plate.

In conclusion, the results from this experimental program will help to better define how gusset plate connections are treated in the design of new truss bridges and rehabilitation of existing bridges. It is imperative to remember that by better understanding how structural elements behave and interact, we can prevent the types of engineering failures, such as the I-35W bridge collapse, which result in catastrophic loss of human life.

BIBLIOGRAPHY

AISC. *Steel Construction Manual.* 13th, Fourth Printing. American Institute of Steel Construction (AISC), 2008.

Anderson, Ralph E. "Gusset Plate Retrofit in Illinois." Illinois Department of Transportation, May 2010.

ASTM. "Standard Test Methods and Definitions for Mechanical Testing of Steel Products." *A 370-97a.* American Society for Testing and Materials, 1997.

Curtis, Rebecca. "Load Rating Gusset Plates on Non-Load-Path-Redundant Steel Truss Bridges." *Bridge Advisory Number: BA-2009-01.* Michigan: Michigan Department of Transportation, January 15, 2009.

Dasault Systèmes. "Abaqus 6.11." *User Manual.* Providence, RI: Dassault Systèmes, 2011.

FHWA. "Bridge Technology: National Bridge Inventory." *Federal Highway Administration.* December 2010. http://www.fhwa.dot.gov/bridge/struct.cfm.

FHWA. "Load Rating Guidance and Examples For Bolted and Riveted Gusset Plates In Truss Bridges." *FHWA-IF-09-014.* U.S. Department of Transportation, Federal Highway Administration, February 2009.

Galambos, T. V., and A. E. Surovek. *Structural Stability of Steel: Concepts and Applications for Structural Engineers.* 1st. Wiley, 2008.

Gross, John L. "Experimental Study of Gusseted Connections." *Engineering Journal* (American Institute of Steel Construction), Third Quarter 1990: 89-97.

Hardin, B. O. "Experimental Investigation of the Primary Stress Distribution in the Gusset Plates of a Double-Plane Pratt Truss with Chord Splice at the Joint." *Bulletin No. 49* (University of Kentucky, Engineering Experiment Station), September 1958.

Higgins, Christopher, Anthony Hafner, O. Tugrul Turan, and Thomas Schumacher. "Experimental Tests of Gusset Plate Connections with Sway-Buckling Response." *Journal of Bridge Engineering* (ASCE), 2012.

Irvan, W. G. "Experimental Study of Primary Stresses in Gusset Plates of a Double Plane Pratt Truss." *Bulletin Vol. 12* (University of Kentucky, Engineering Experiment Station), no. 2 (1957).

Medwick, Seth. "Truss bridges: Inspection and load rating, post I-35W Bridge collapse." *Rebuilding America's Infrastructure,* March 2010.

NTSB. *Collapse of I-35W Highway Bridge, Minneapolis, Minnesota, August 1, 2007.* Highway Accident Report NTSB/HAR-08/03, Washington, DC: National Transportation Safety Board (NTSB), 2008.

Thornton, W.A. "Bracing Connection for heavy Construction." *Engineering Journal* (American Institute of Steel Construction (AISC)), 1984: 139-148.

Vasarhelyi, Desi D. "Tests of Gusset Plate Models." *Journal of the Proceedings of the American Society of Civil Engineers Structural Division*, February 1971: 665-678.

Whitmore, R. E. "Experimental Investigation of Stresses in Gusset Plates." *Engineering Experiment Station, The University of Tennessee*, no. Bulletin No. 16 (May 1952): 1-33.

Yam, M C H, and J J R Cheng. *Analytical Investigation of the Compressive Behavior and Strength of Steel Gusset Plate Connections.* Structural Engineering Report No. 207, University of Alberta, 1994.

APPENDICES

APPENDIX A. SPECIMEN #1 ADDITIONAL DATA

Specimen #1 was a ¼” thick set of gusset plates and is described in the first manuscript.

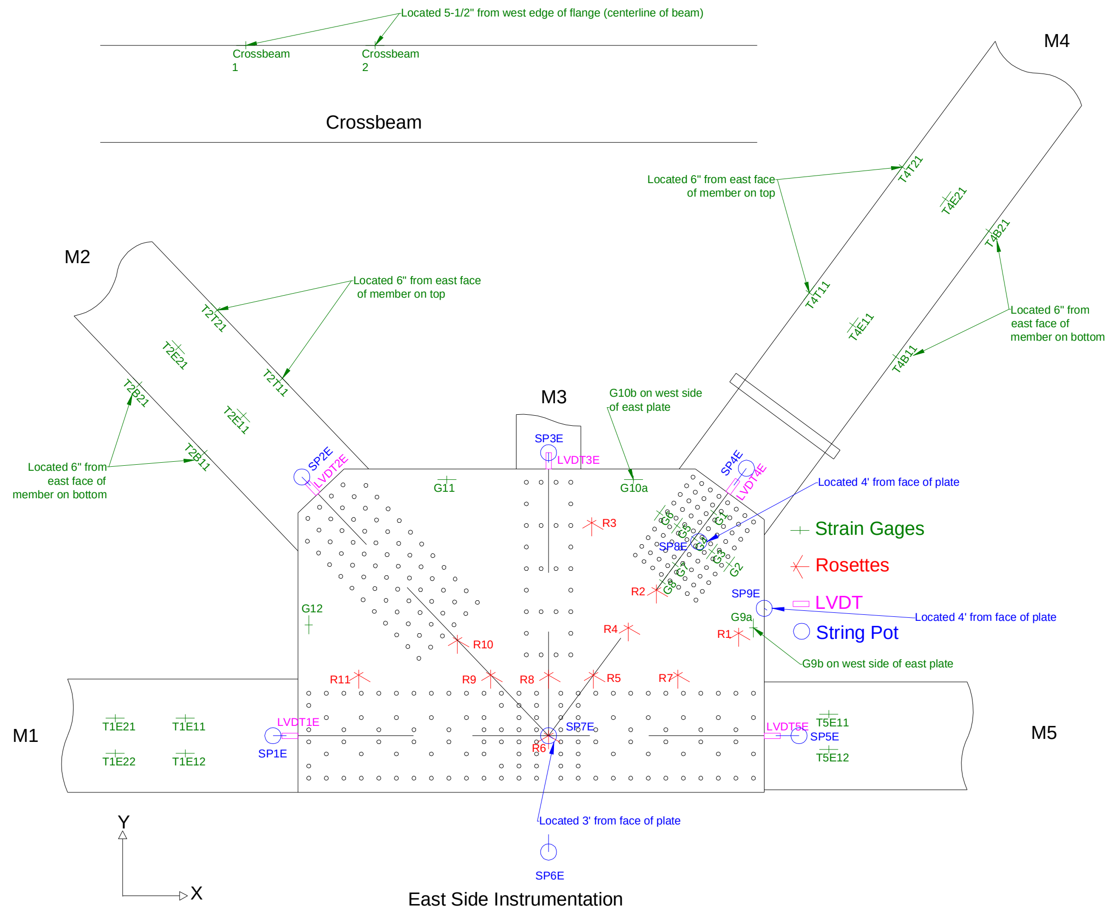

Fig. A-1: Full instrumentation plan east plate specimen #1

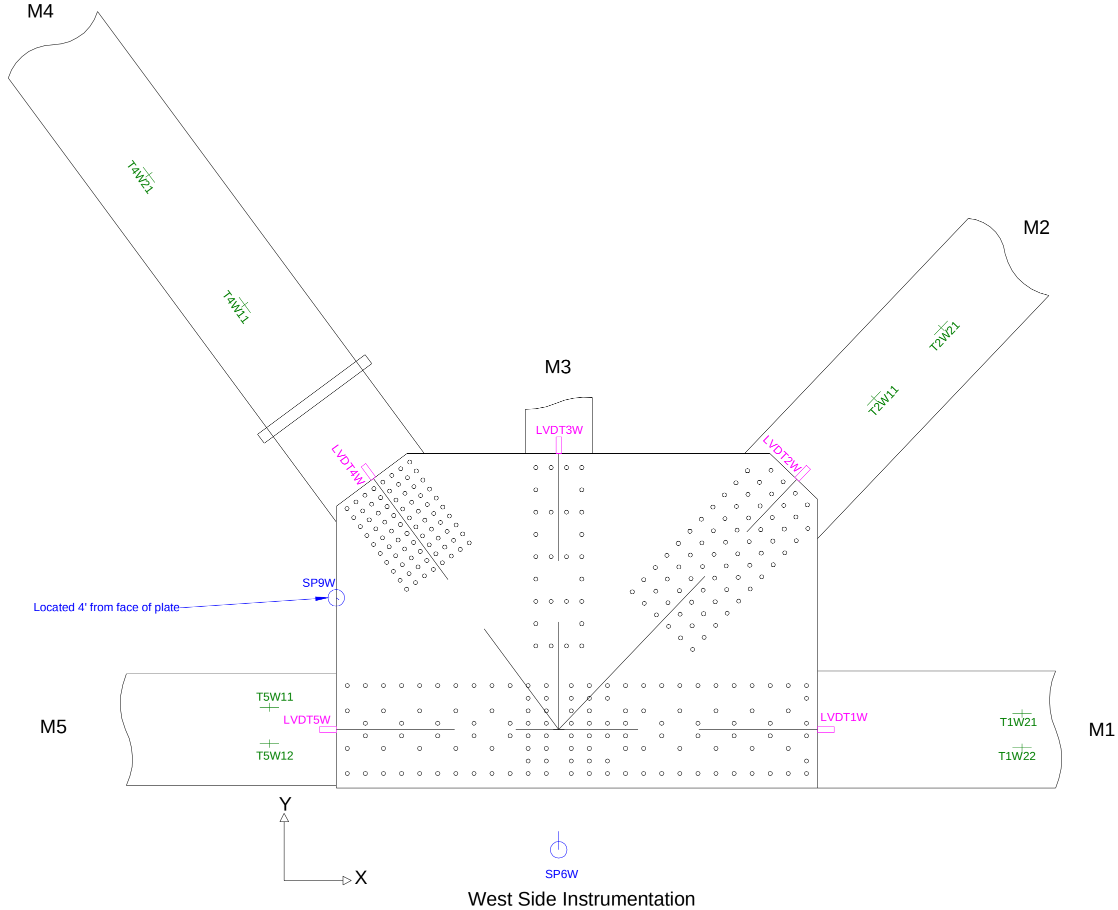

Fig. A-2: Full instrumentation plan west plate specimen #1

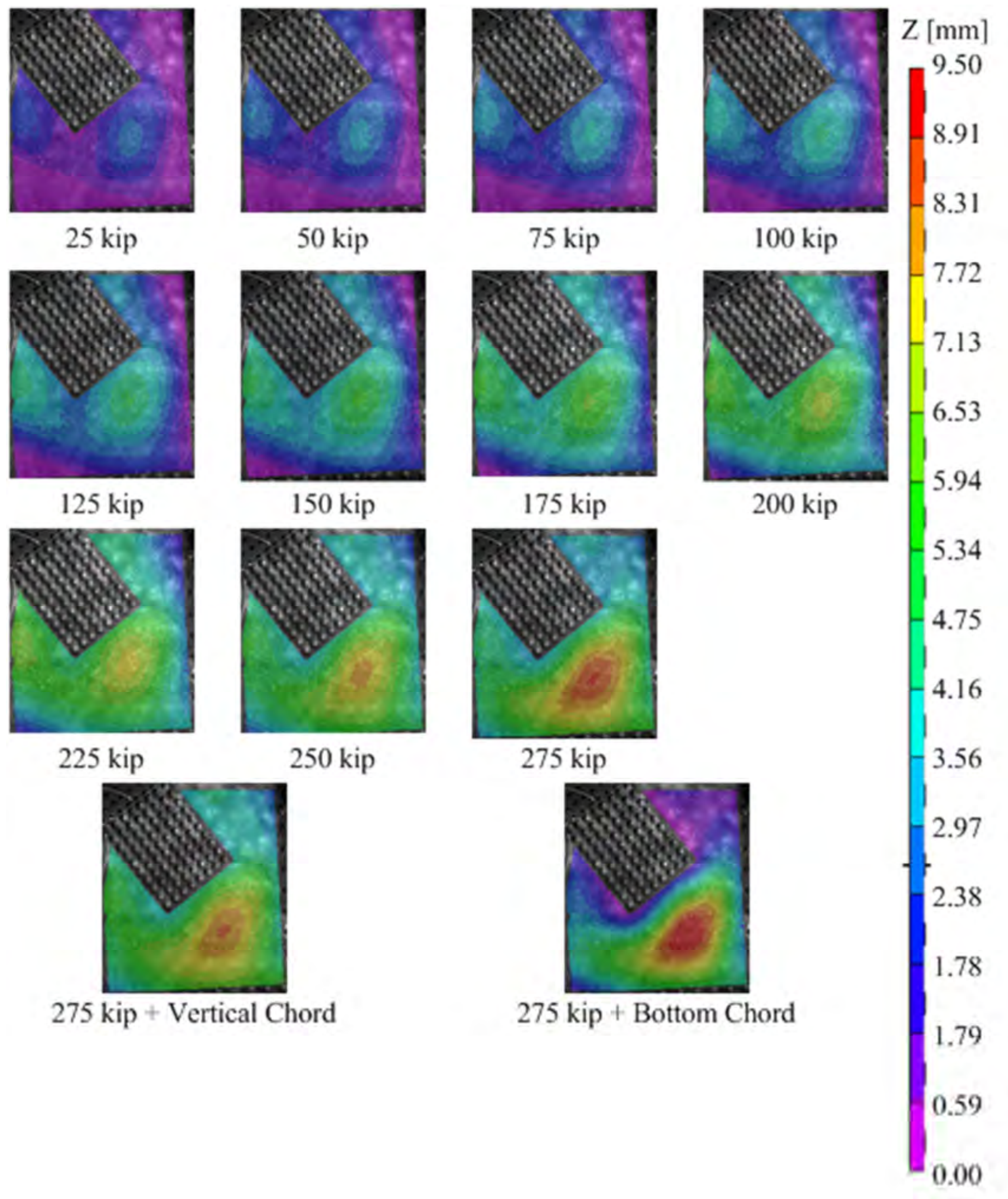

Fig. A-3: DIC measured out-of-plane deformation during final load cycle (loads are M4 actuator loads)

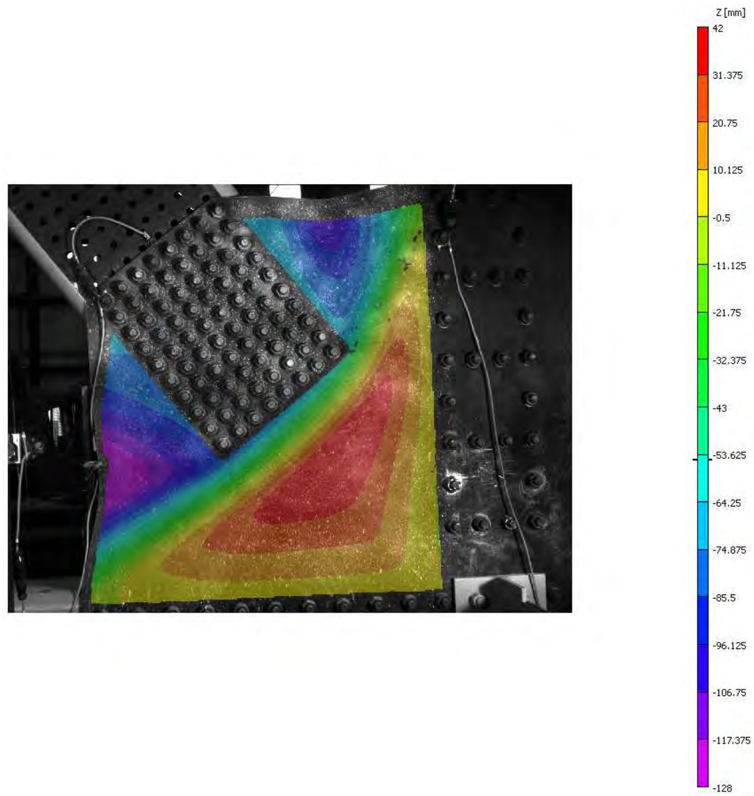

Fig. A-4: DIC measured out-of-plane deformation at failure

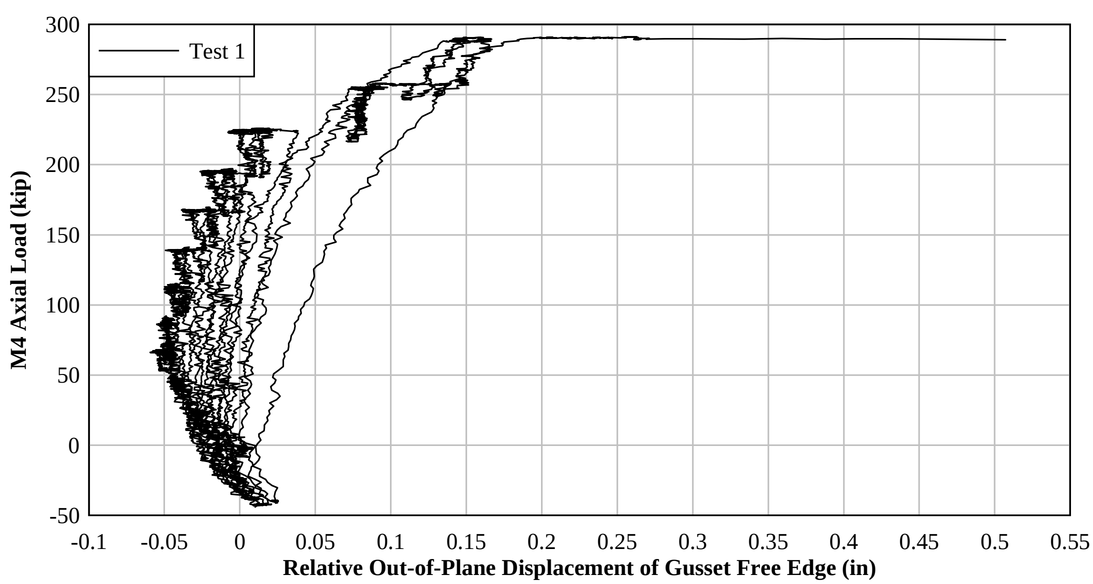

Fig. A-5: Specimen #1 M4 axial load versus out-of-plane displacement behavior for all cycles

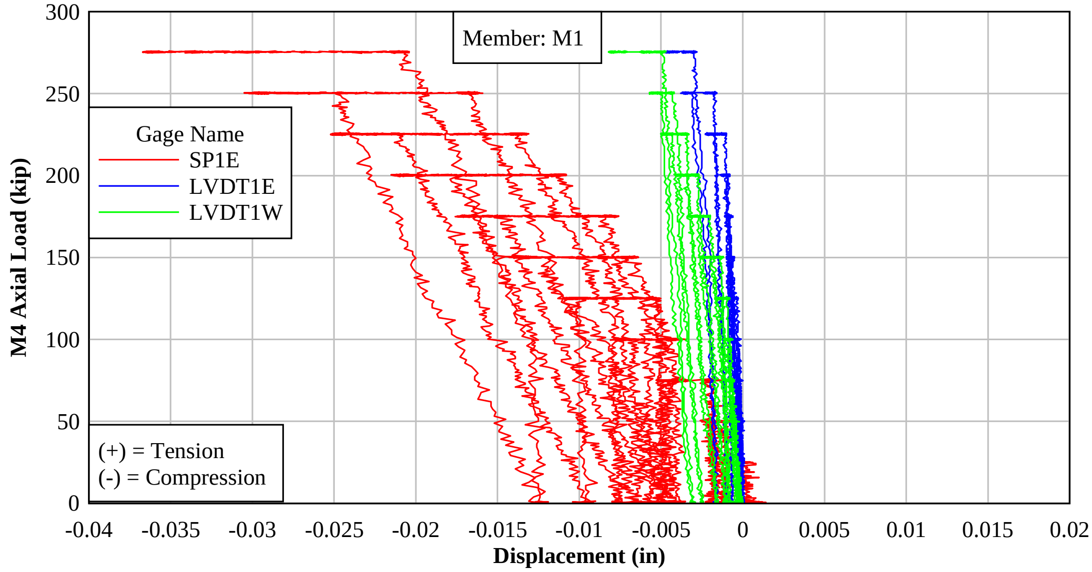

Fig. A-6: Member M1 bolt slip and relative member-to-work point displacement

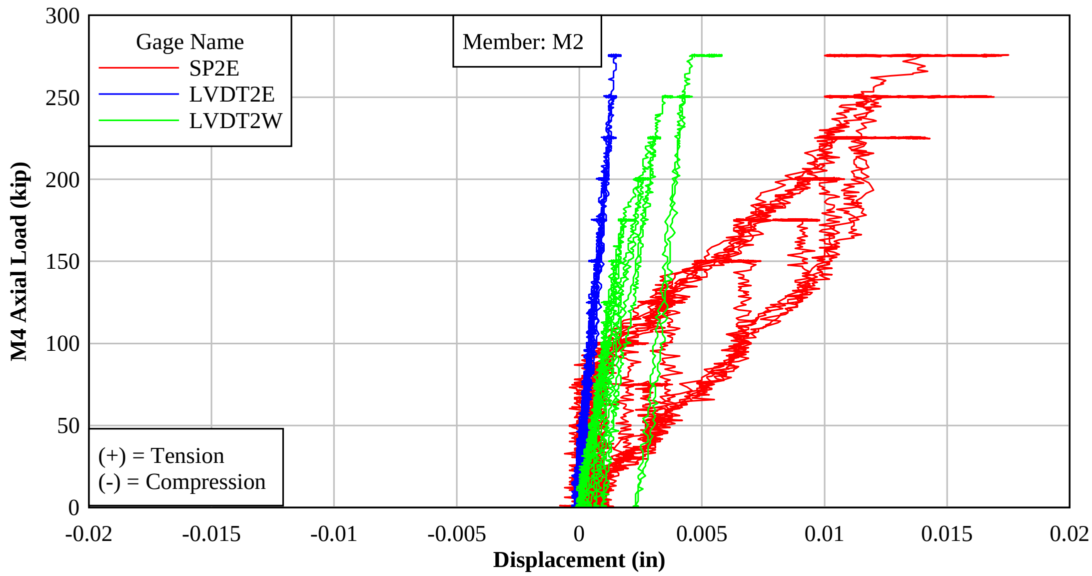

Fig. A-7: Member M2 bolt slip and relative member-to-work point displacement

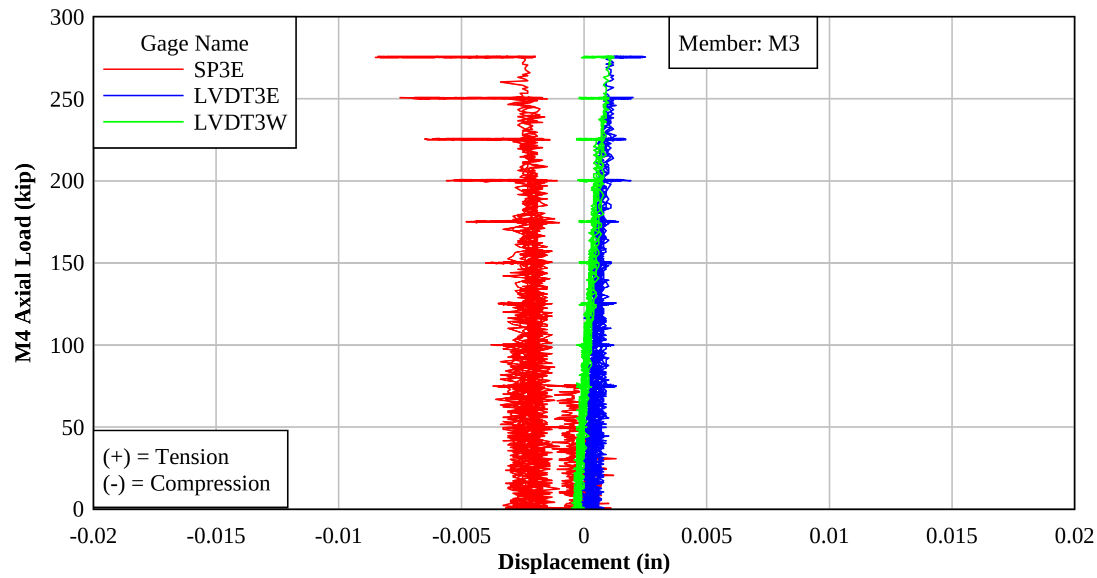

Fig. A-8: Member M3 bolt slip and relative member-to-work point displacement

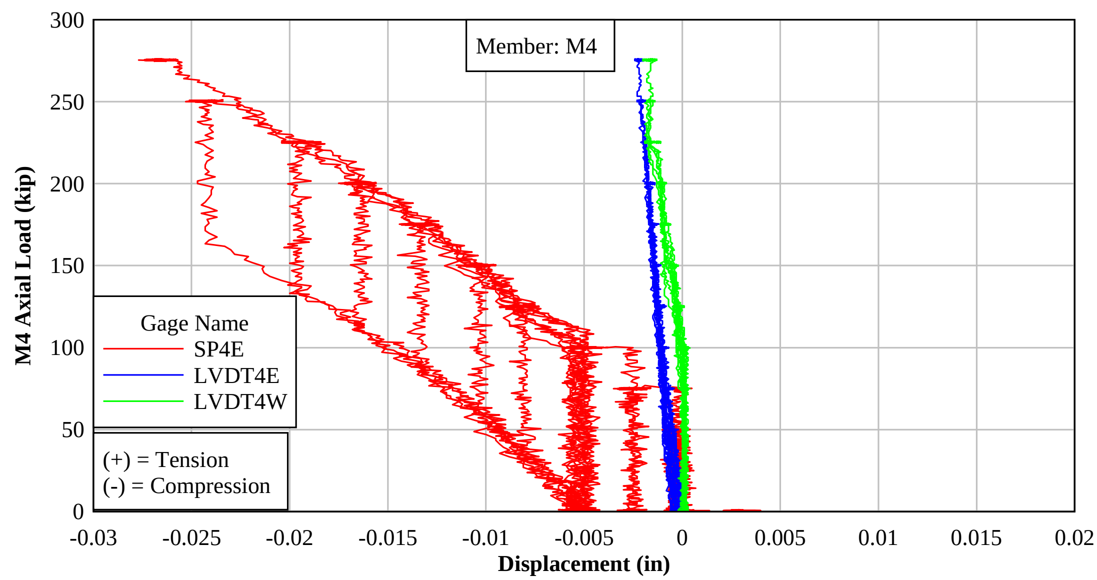

Fig. A-9: Member M4 bolt slip and relative member-to-work point displacement

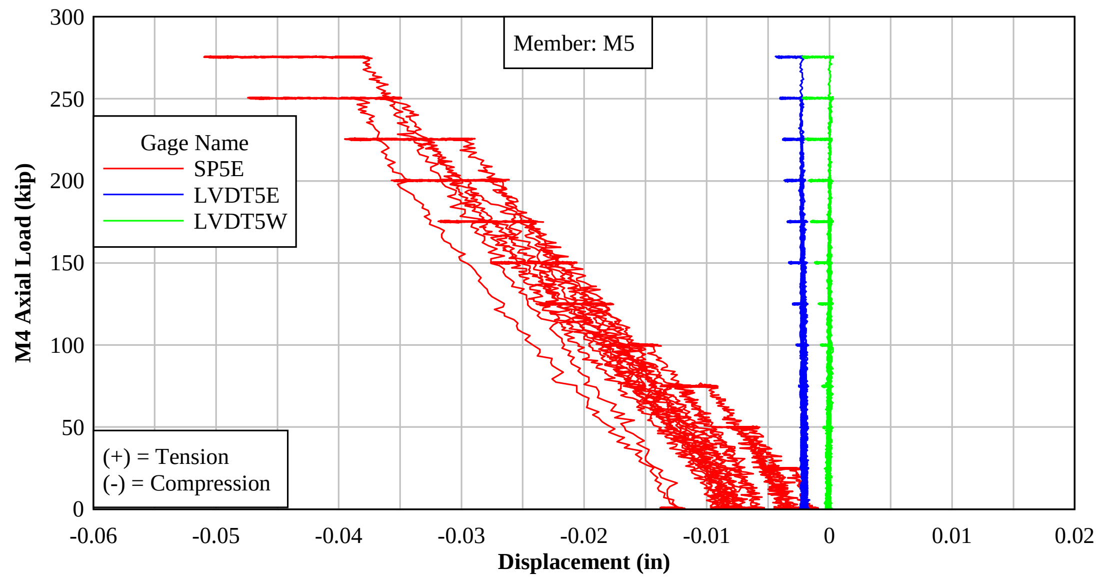

Fig. A-10: Member M5 bolt slip and relative member-to-work point displacement

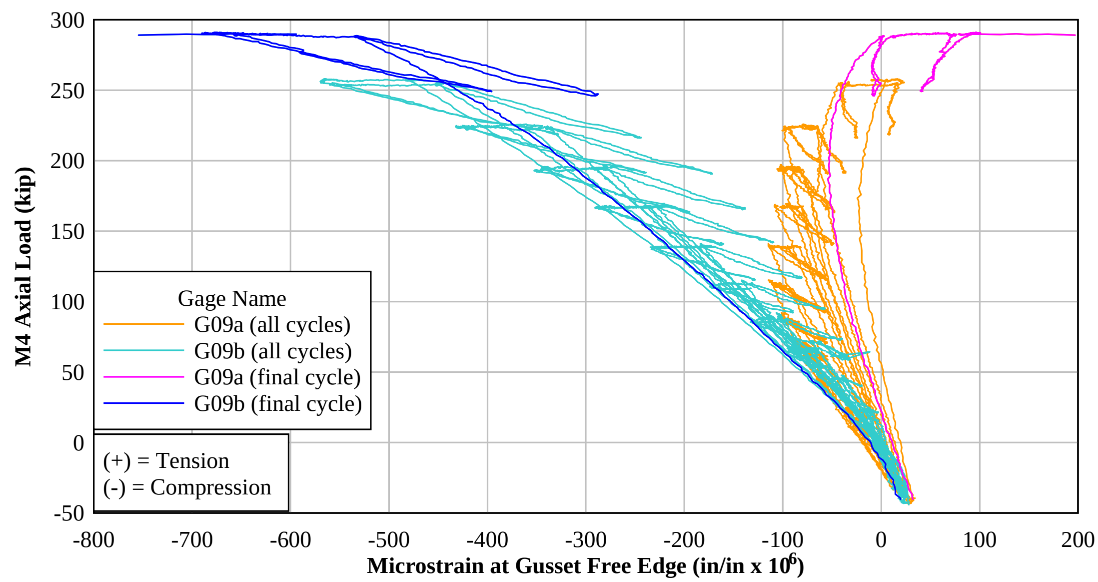

Fig. A-11: Gusset plate free edge strain versus M4 axial load

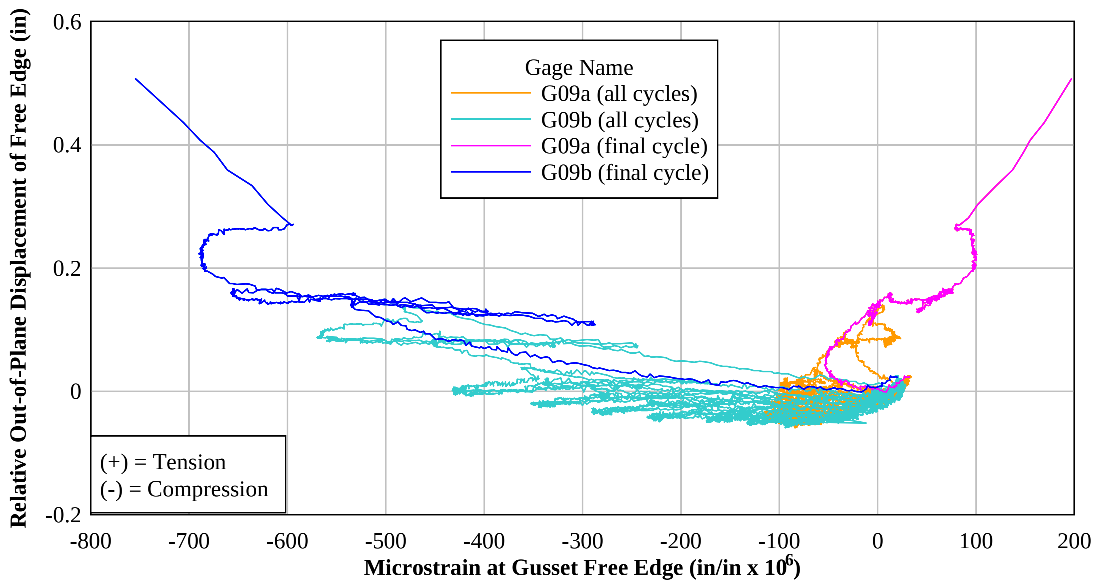

Fig. A-12: Gusset plate free edge strain versus out-of-plane displacement

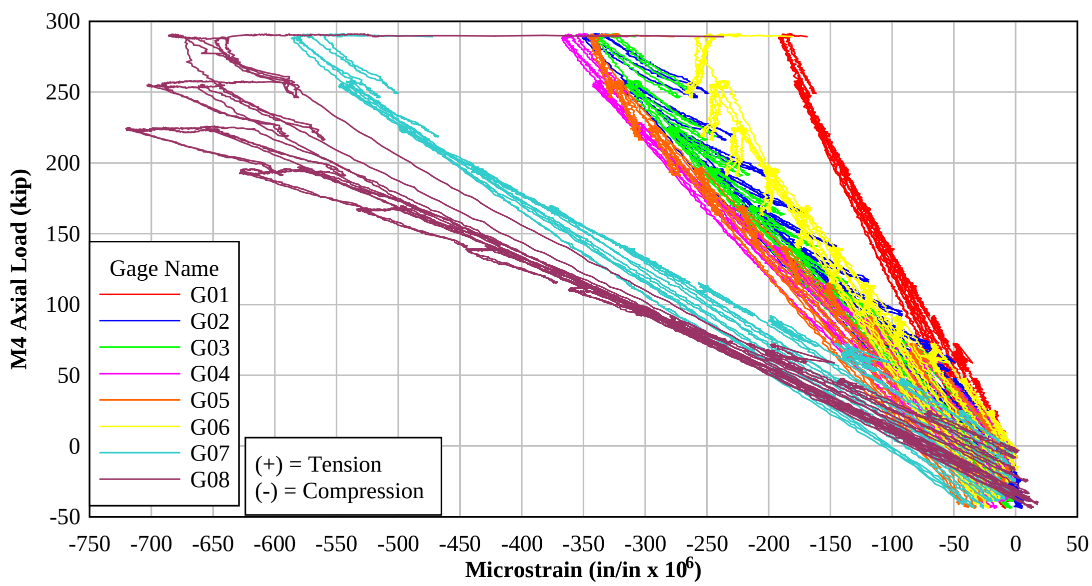

Fig. A-13: Strain in M4 connection versus M4 axial load

APPENDIX B. SPECIMEN #2 ADDITIONAL DATA

Specimen #2 was a ¼” thick set of gusset plates and is described in the first manuscript.

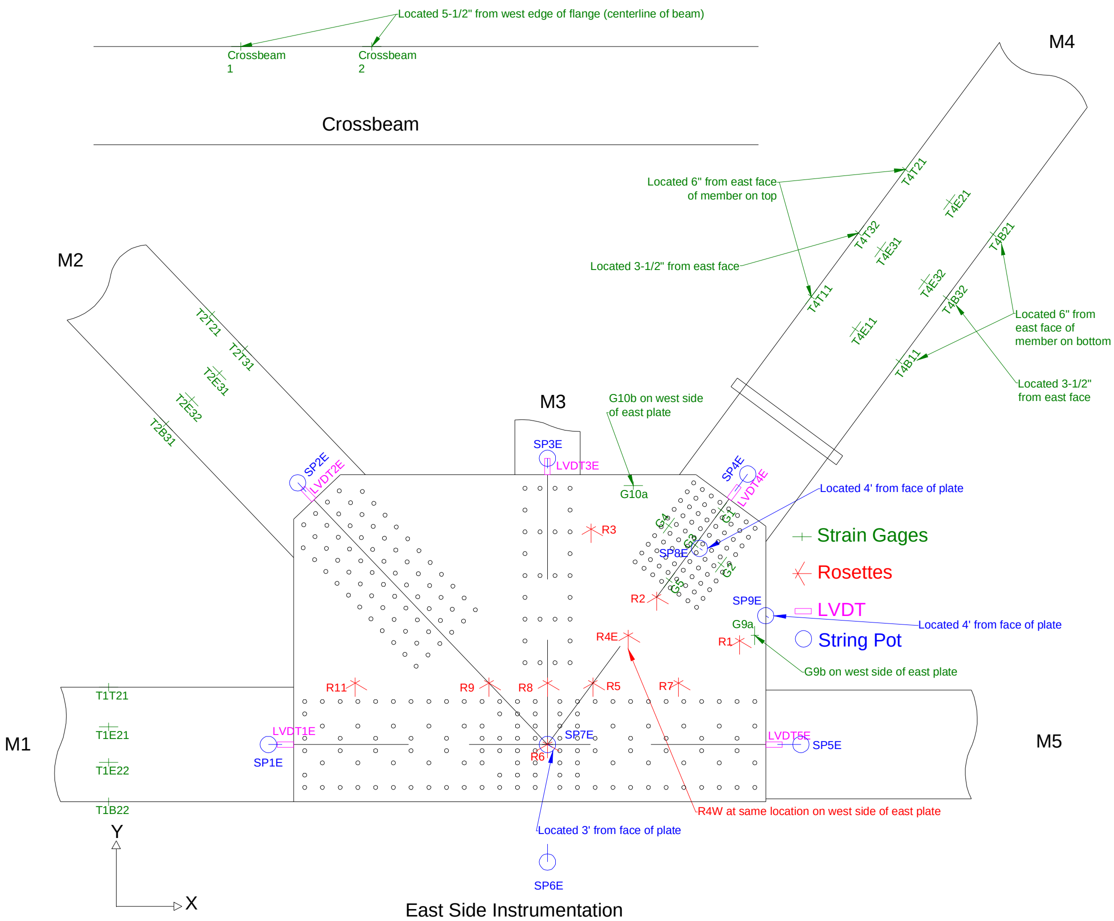

Fig. B-1: Full instrumentation plan east plate specimens #2 and #3

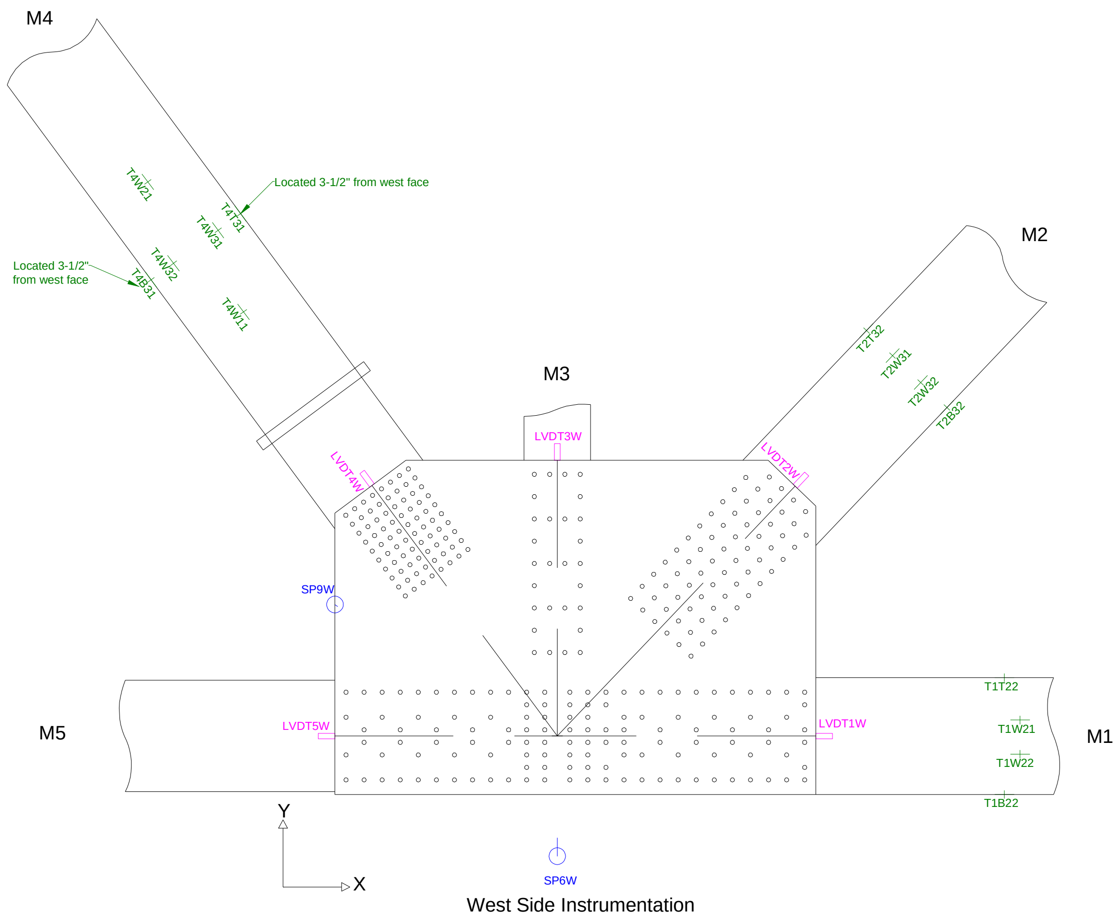

Fig. B-2: Full instrumentation plan west plate specimens #2 and #3

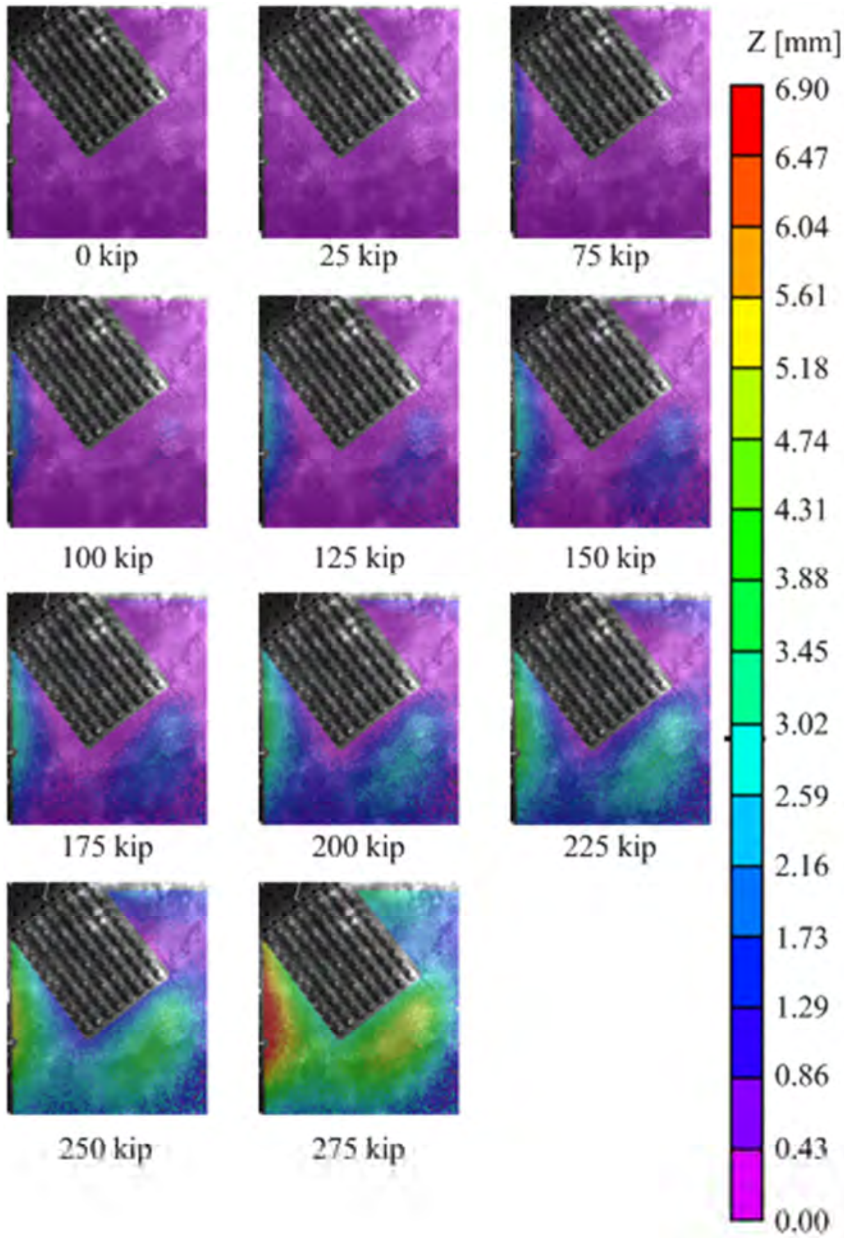

Fig. B-3: DIC measured out-of-plane deformation during loading (loads are M4 actuator loads)

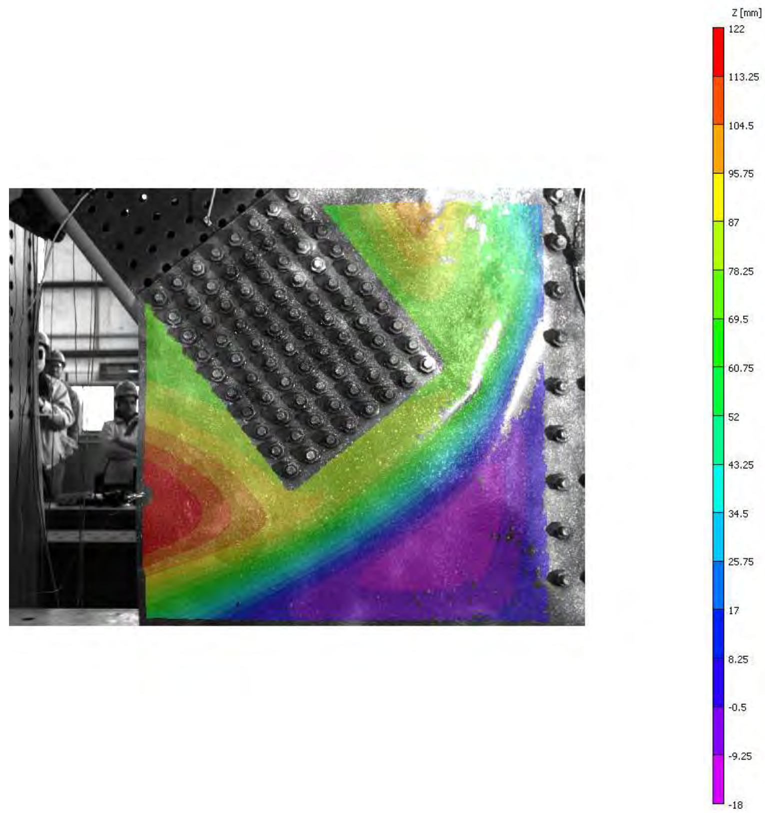

Fig. B-4: DIC measured out-of-plane deformation at failure

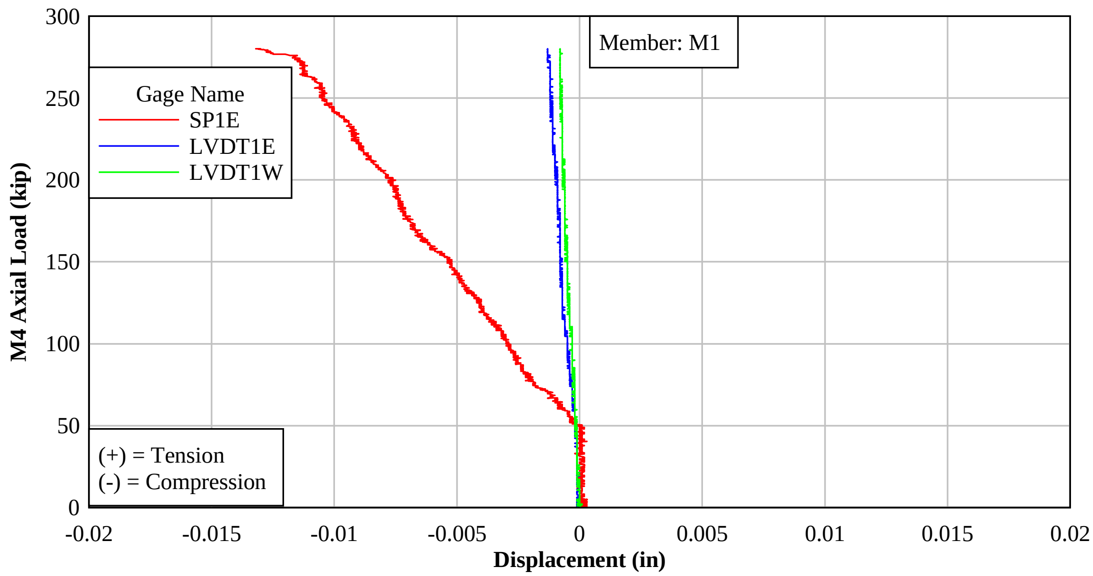

Fig. B-5: Member M1 bolt slip and relative member-to-work point displacement

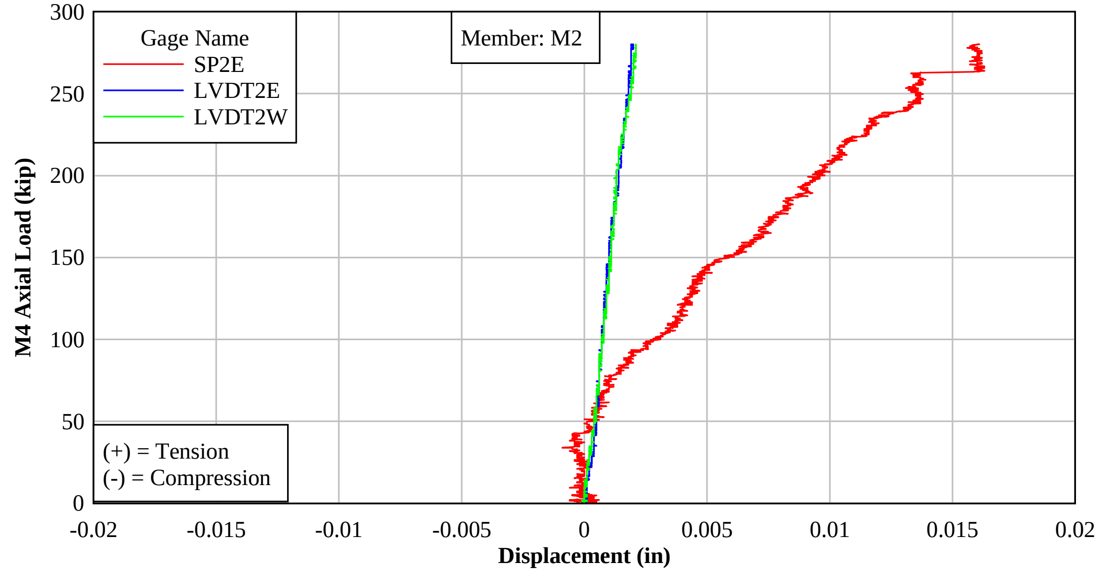

Fig. B-6: Member M2 bolt slip and relative member-to-work point displacement

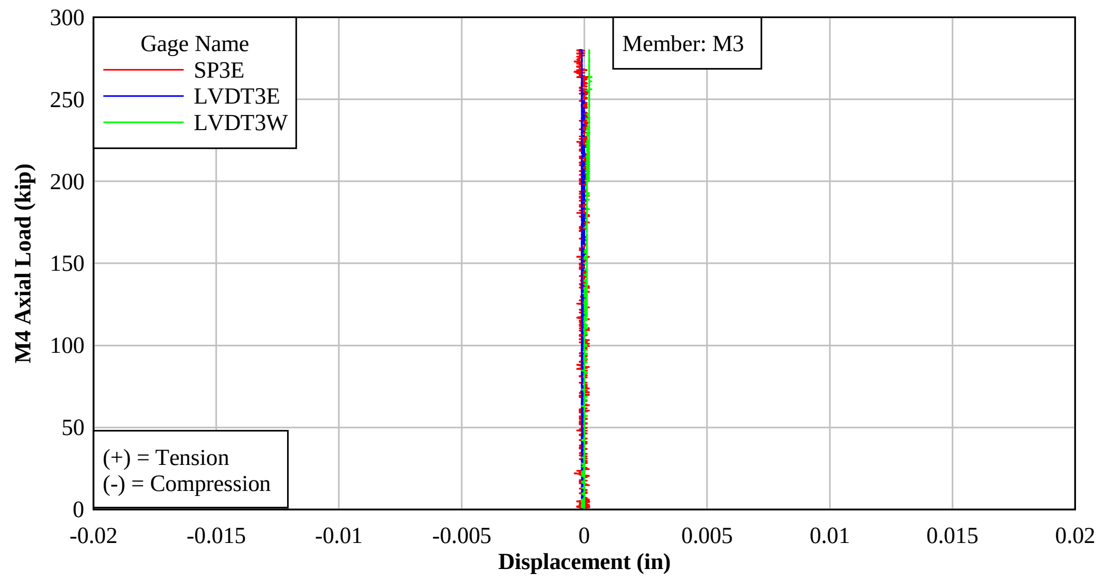

Fig. B-7: Member M3 bolt slip and relative member-to-work point displacement

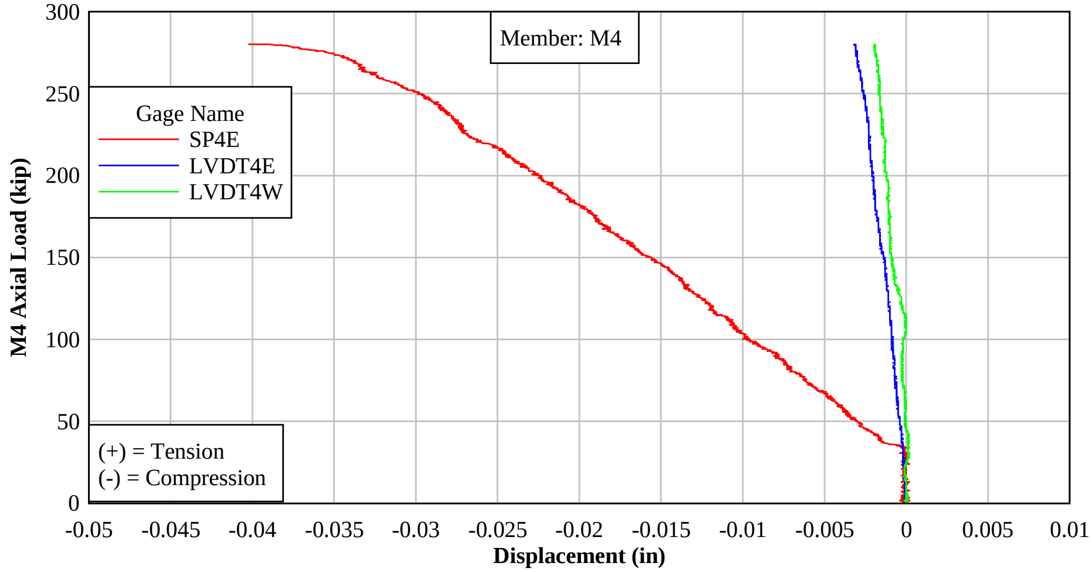

Fig. B-8: Member M4 bolt slip and relative member-to-work point displacement

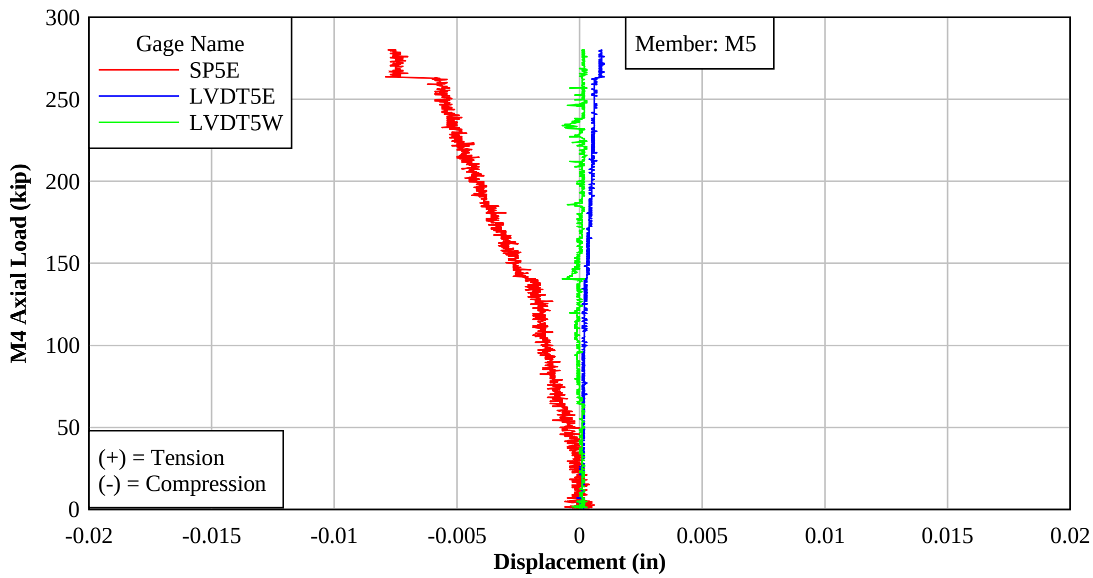

Fig. B-9: Member M5 bolt slip and relative member-to-work point displacement

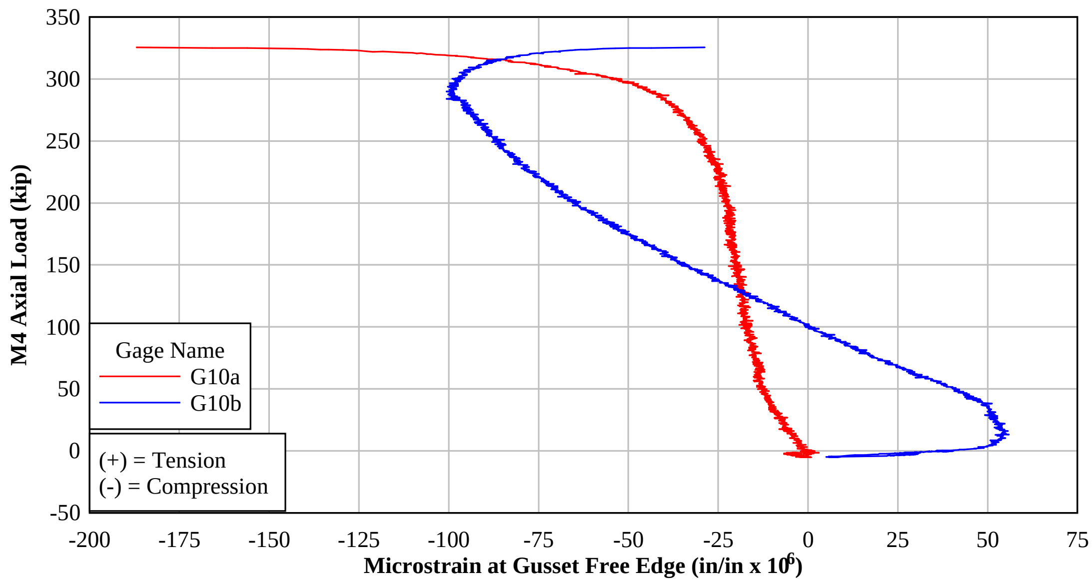

Fig. B-10: Gusset plate free edge strain versus M4 axial load

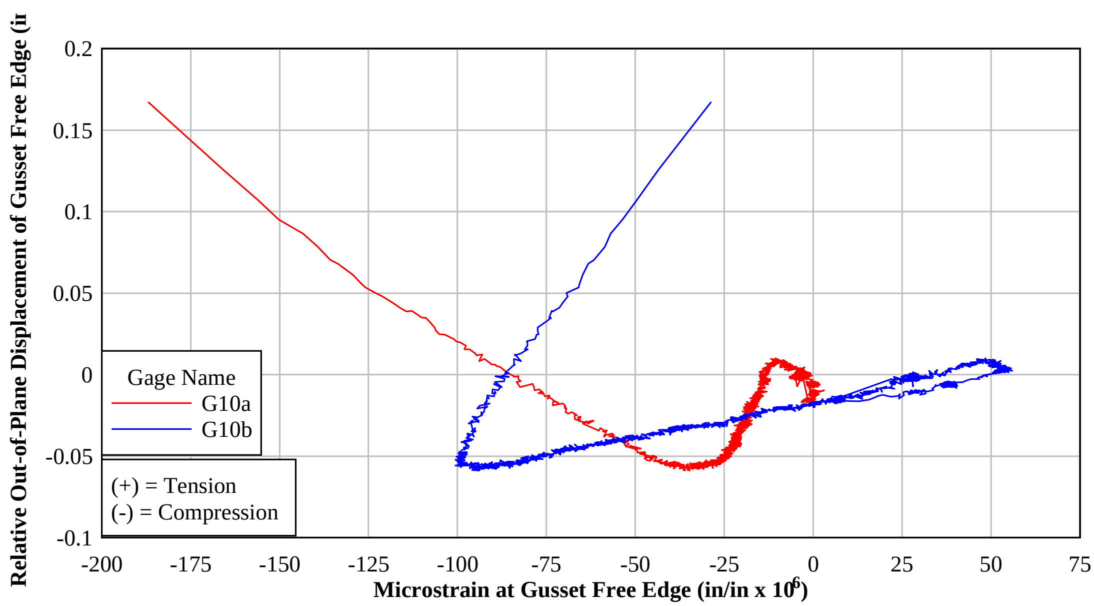

Fig. B-11: Gusset plate free edge strain versus out-of-plane displacement

APPENDIX C. SPECIMEN #3 ADDITIONAL DATA

Specimen #3 was a 3/8" thick set of gusset plates and is described in the first manuscript.

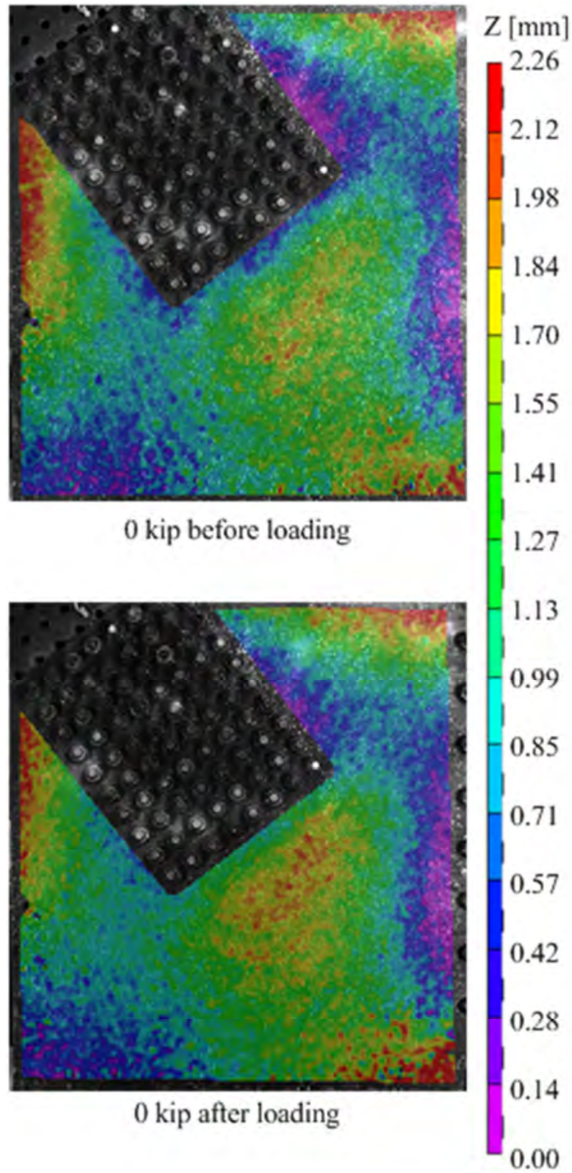

Fig. C-1: DIC measured out-of-plane deformation pre and post loading with no additional imperfection applied

(No DIC data exists for loading or for cycles with artificially imposed initial imperfections)

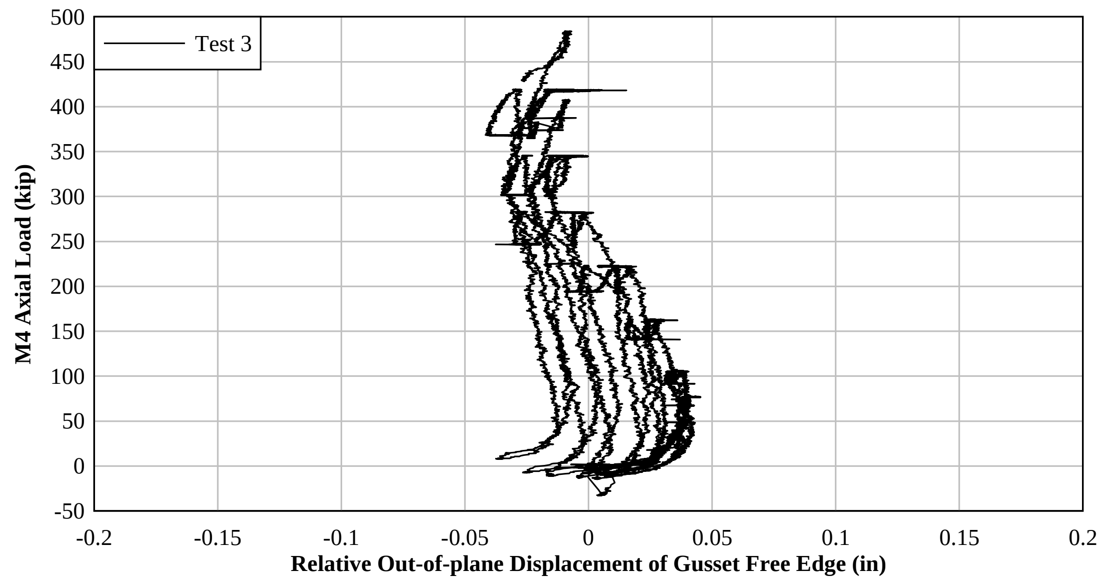

Fig. C-2: Specimen #3 M4 axial load versus out-of-plane displacement of free edge for all load cycles prior to any applied imperfection

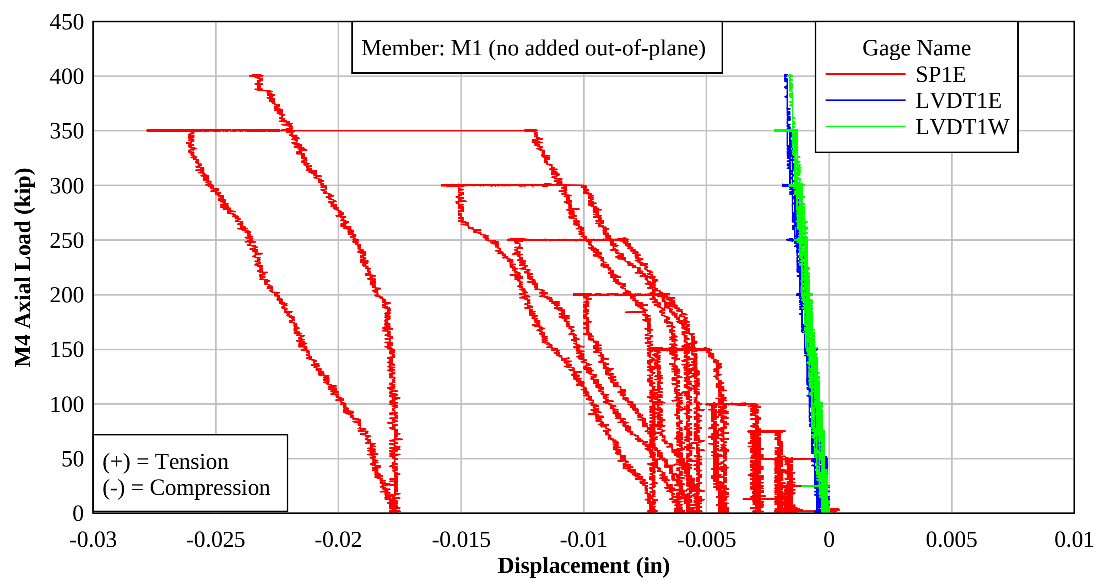

Fig. C-3: Member M1 bolt slip and relative member-to-work point displacement (no additional out-of-plane imperfection)

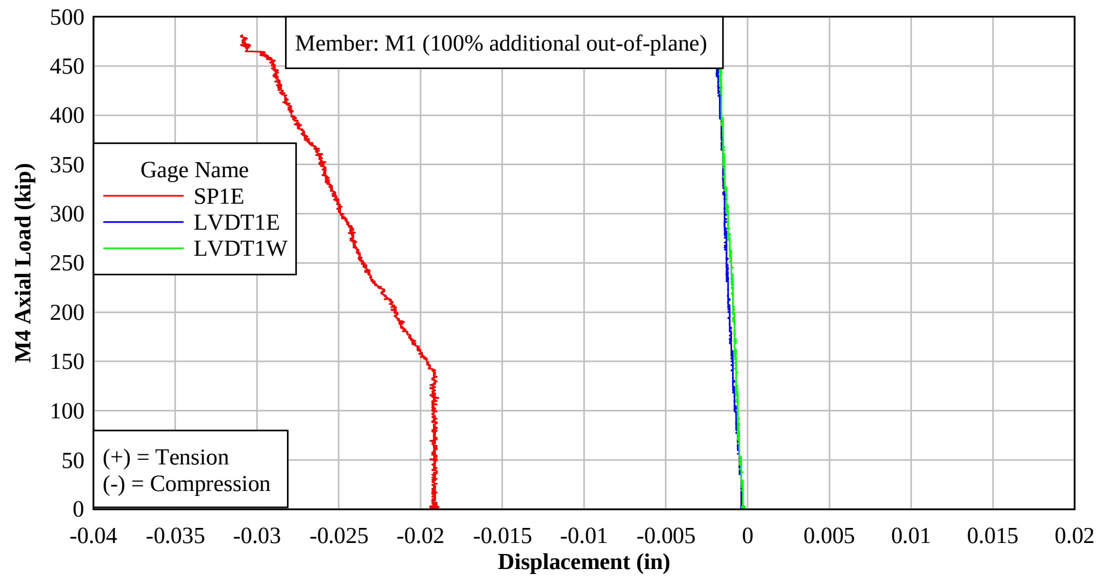

Fig. C-4: Member M1 bolt slip and relative member-to-work point displacement (100% additional out-of-plane imperfection)

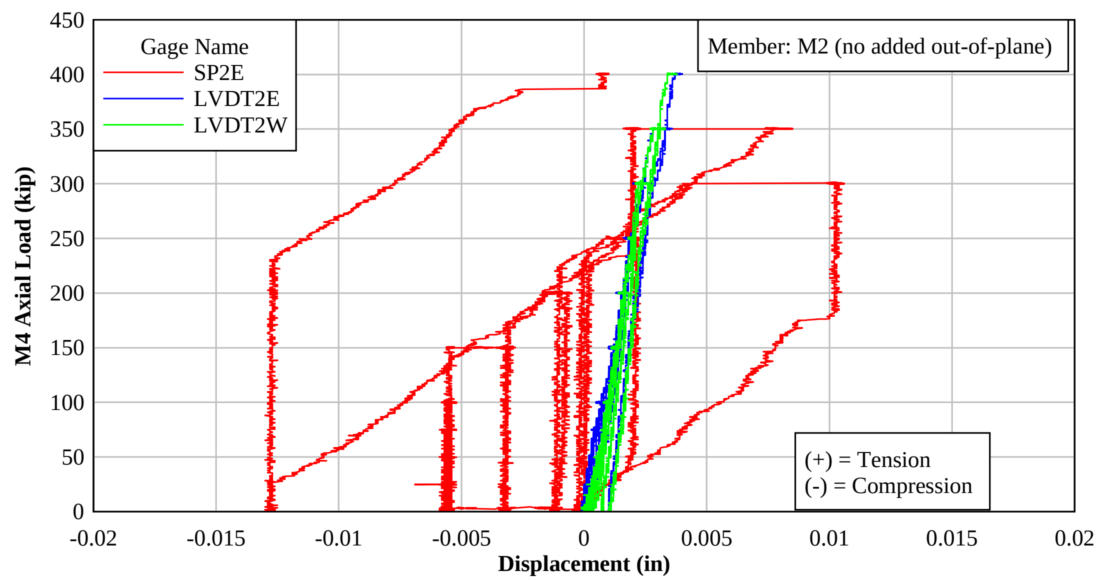

Fig. C-5: Member M2 bolt slip and relative member-to-work point displacement (no additional out-of-plane imperfection)

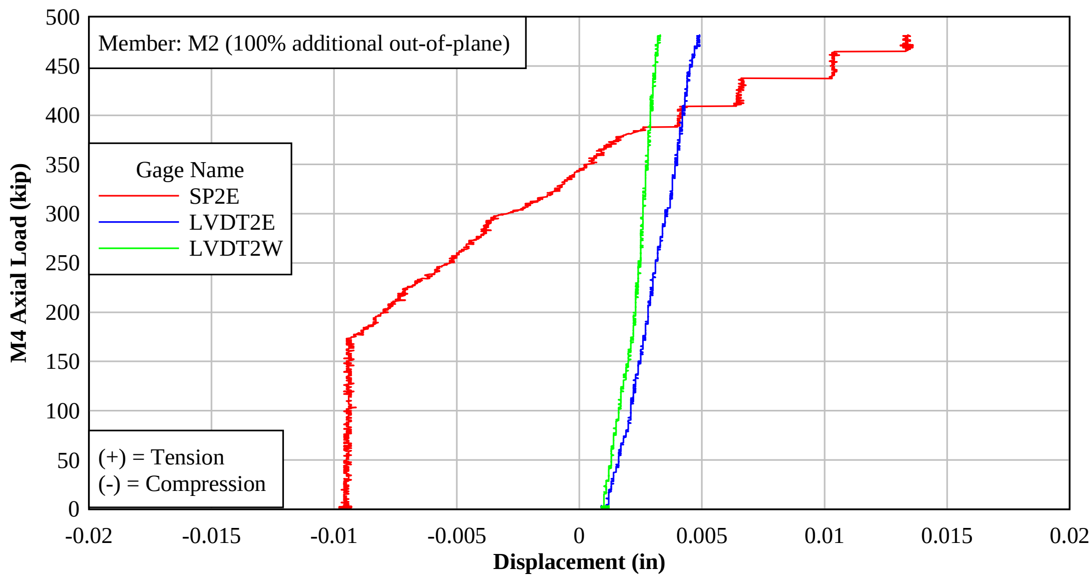

Fig. C-6: Member M2 bolt slip and relative member-to-work point displacement (100% additional out-of-plane imperfection)

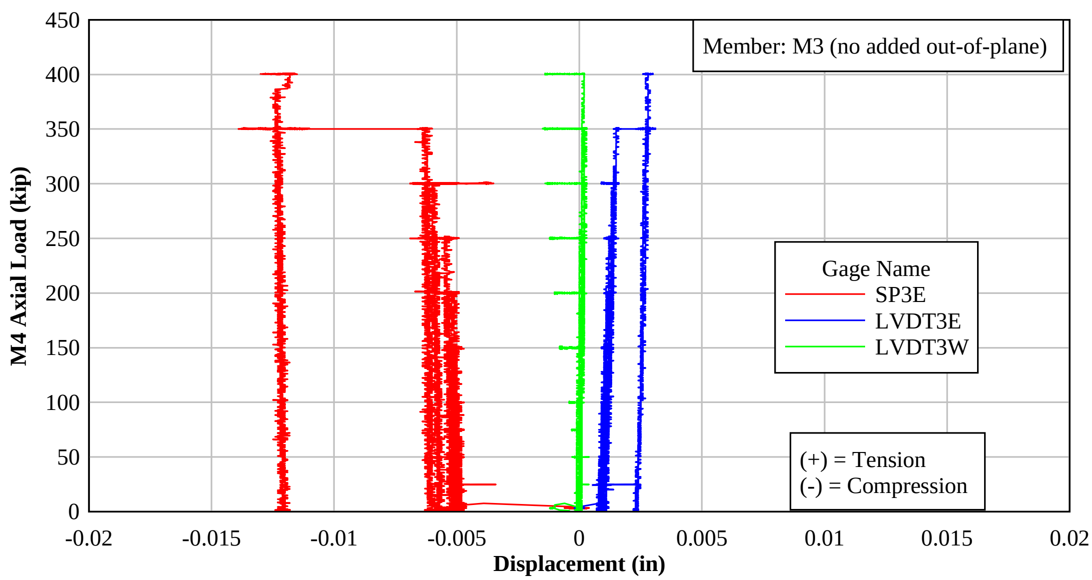

Fig. C-7: Member M3 bolt slip and relative member-to-work point displacement (no additional out-of-plane imperfection)

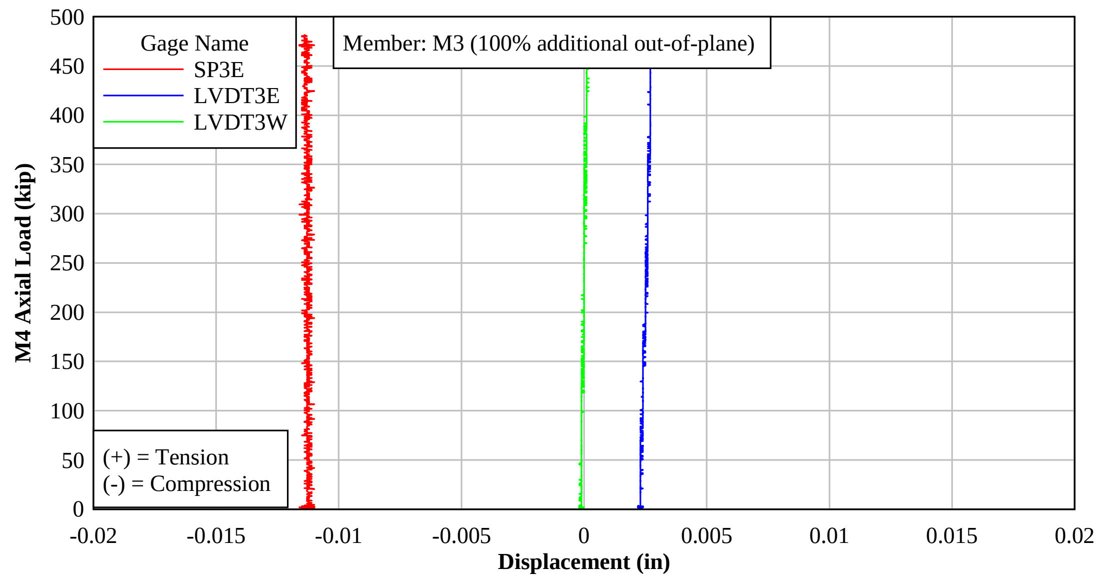

Fig. C-8: Member M3 bolt slip and relative member-to-work point displacement (100% additional out-of-plane imperfection)

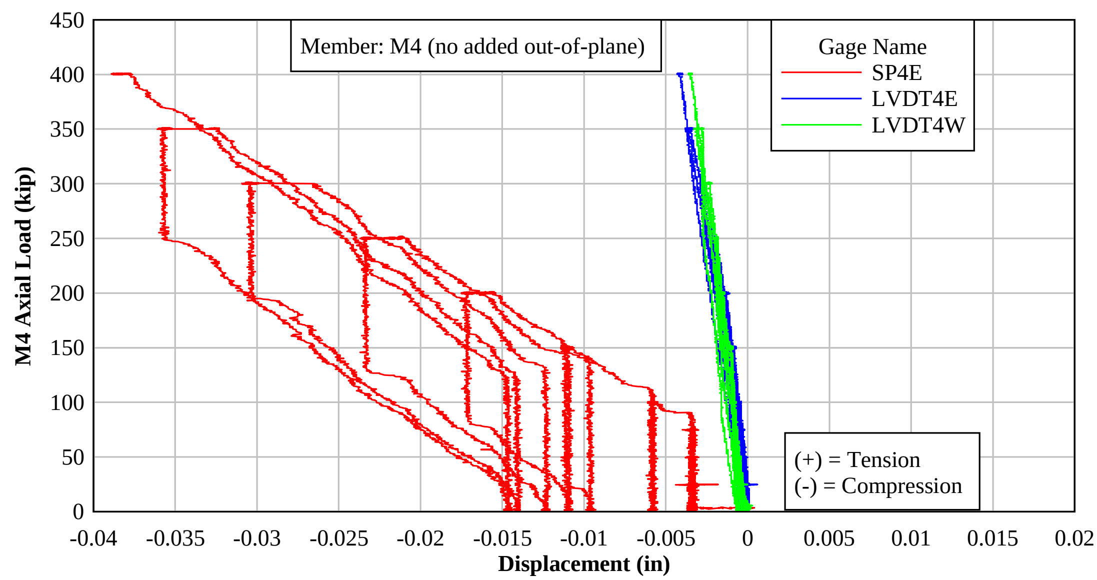

Fig. C-9: Member M4 bolt slip and relative member-to-work point displacement (no additional out-of-plane imperfection)

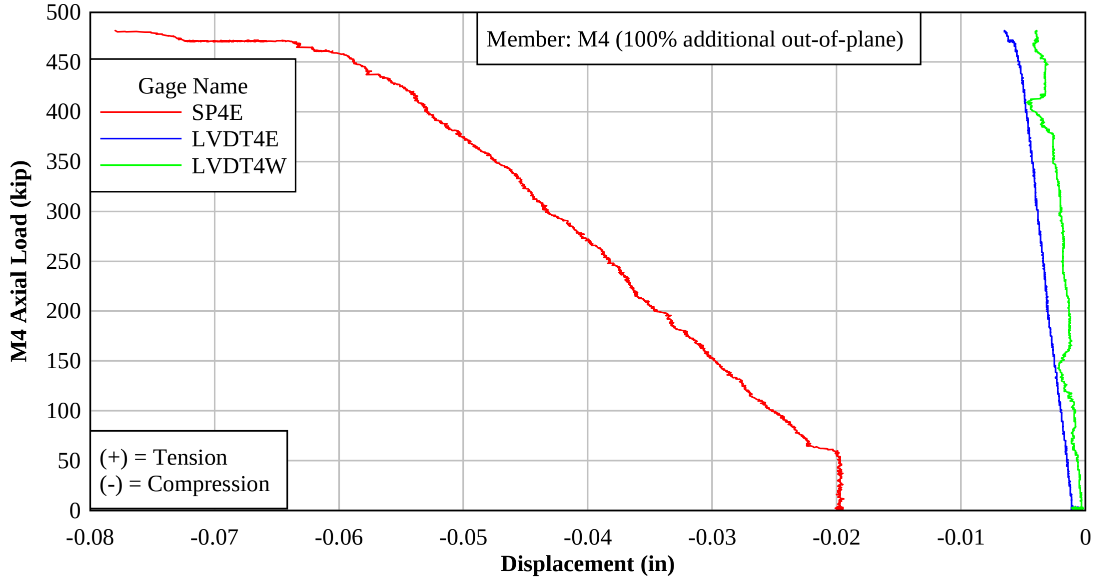

Fig. C-10: Member M4 bolt slip and relative member-to-work point displacement (100% additional out-of-plane imperfection)

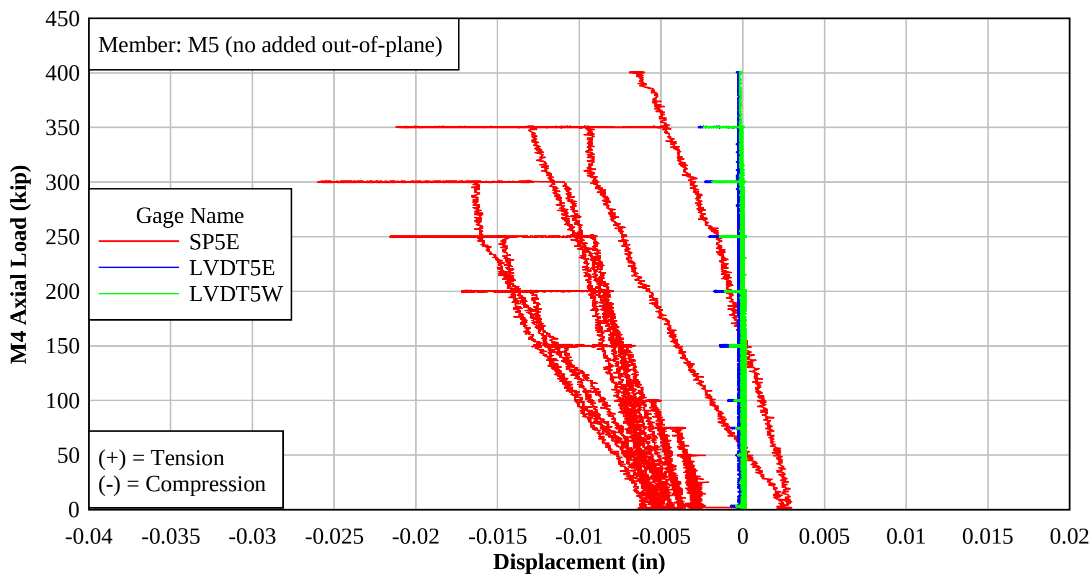

Fig. C-11: Member M5 bolt slip and relative member-to-work point displacement (no additional out-of-plane imperfection)

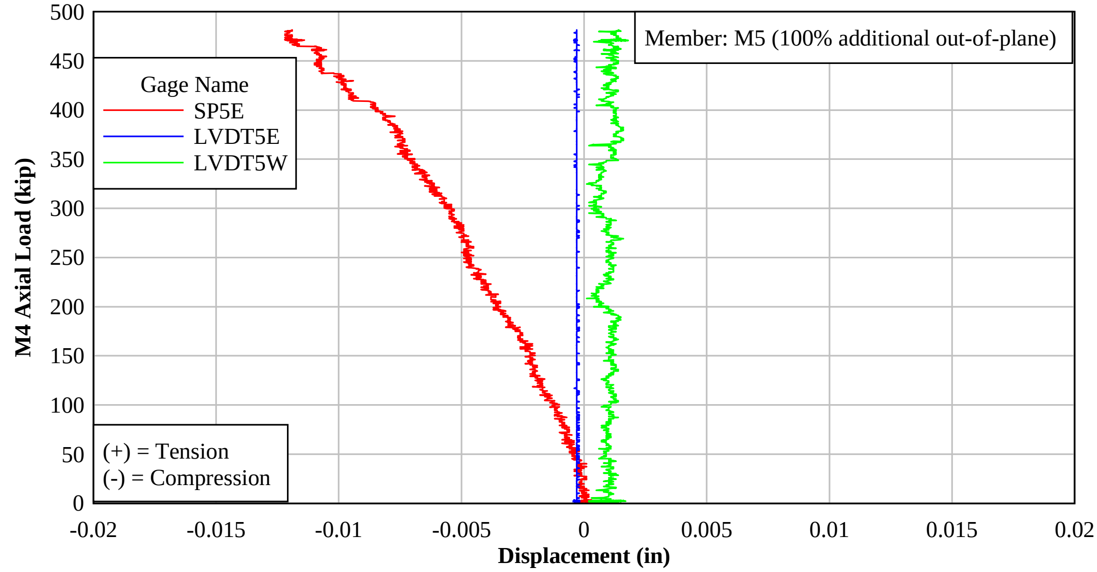

Fig. C-12: Member M5 bolt slip and relative member-to-work point displacement (100% additional out-of-plane imperfection)

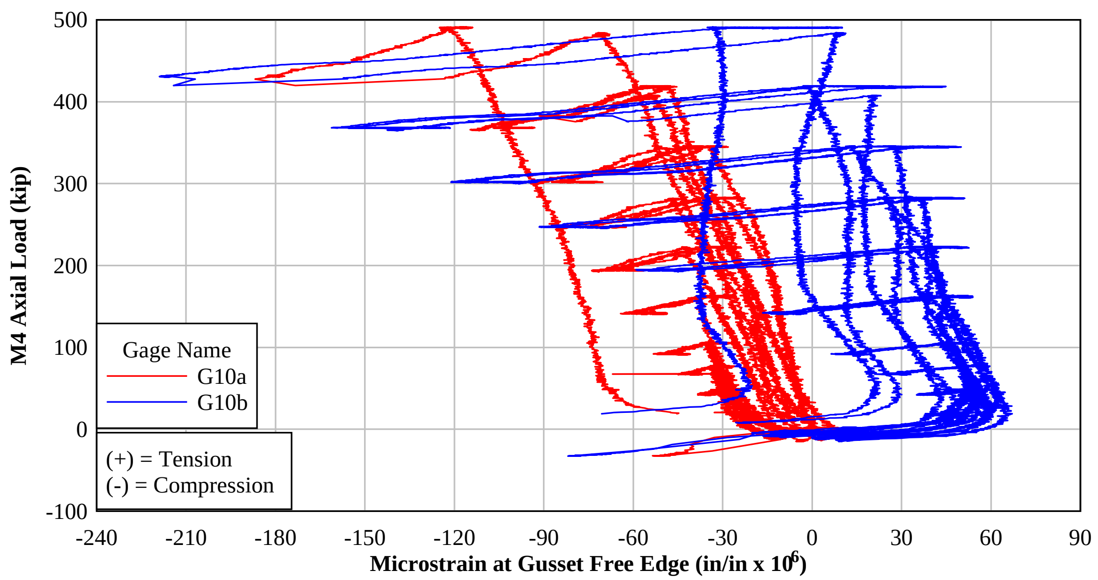

Fig. C-13: Gusset plate free edge strain versus M4 axial load (no additional out-of-plane imperfection)

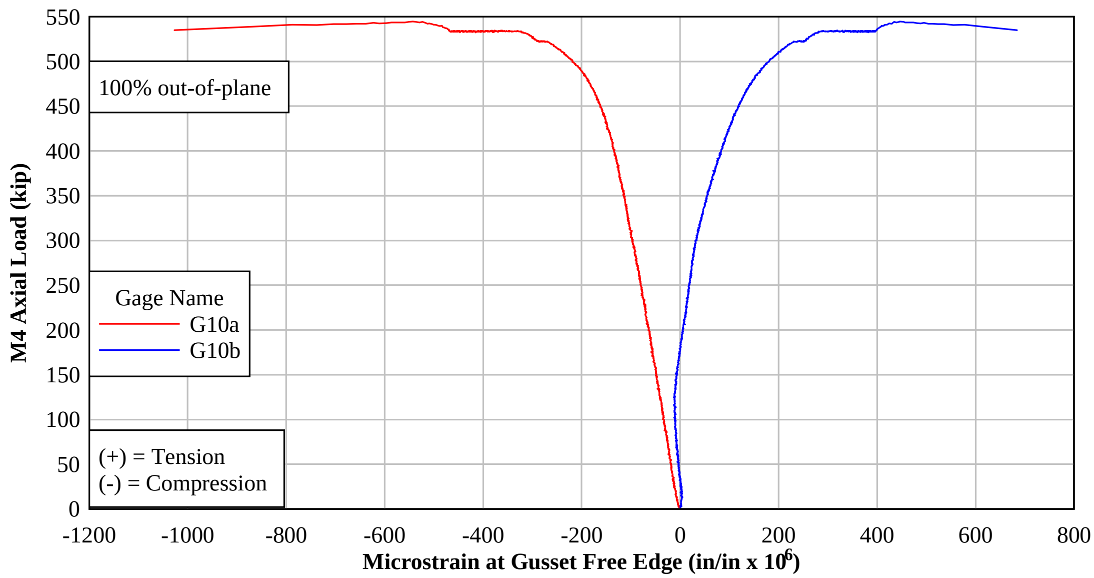

Fig. C-14: Gusset plate free edge strain versus M4 axial load (100% additional out-of-plane imperfection)

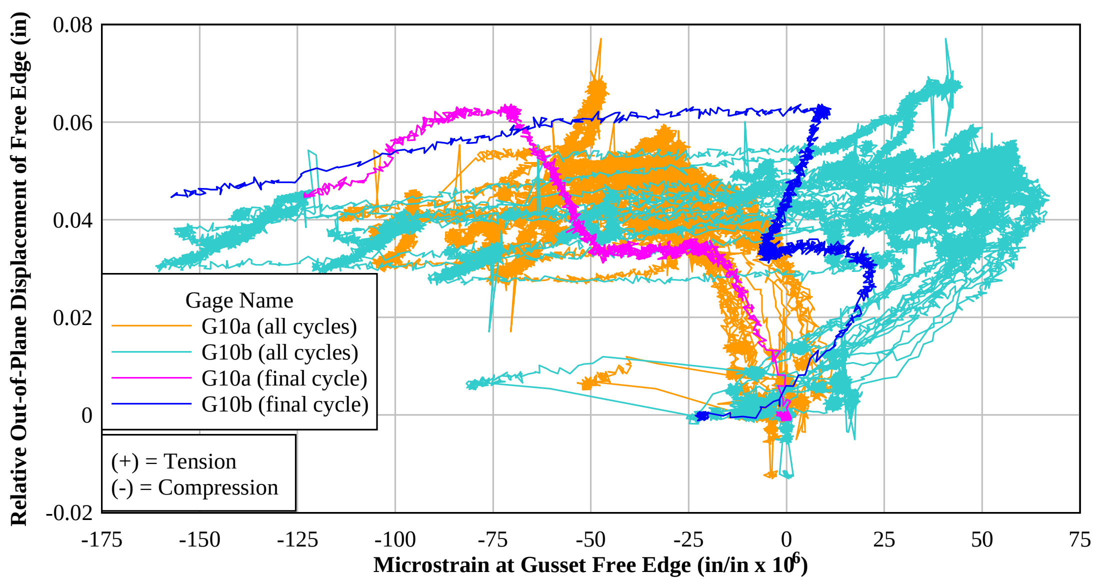

Fig. C-15: Gusset plate free edge strain versus out-of-plane displacement (no additional out-of-plane displacement)

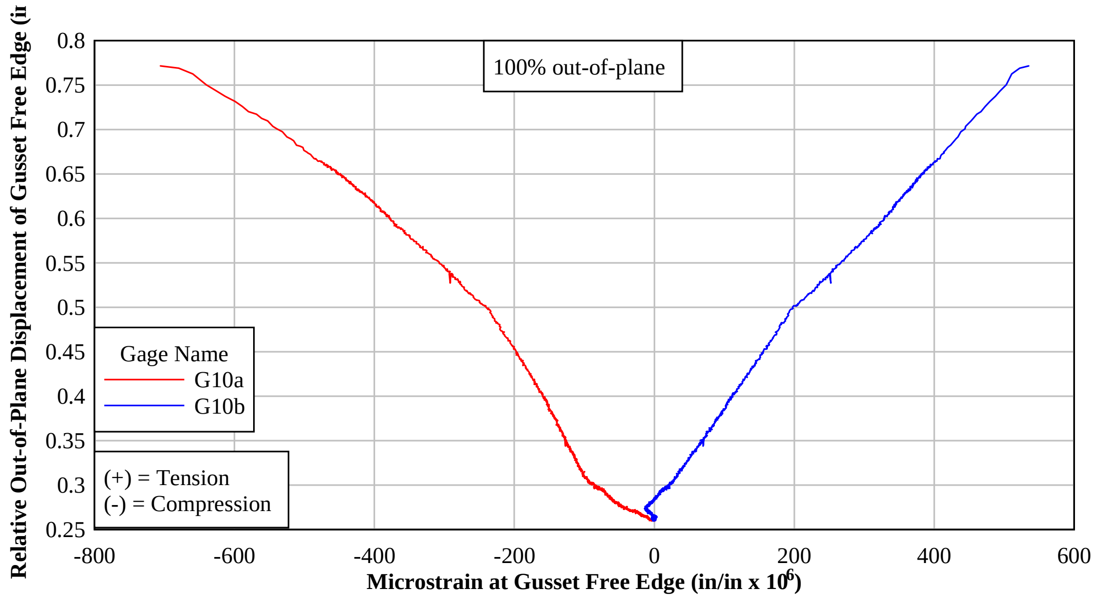

Fig. C-16: Gusset plate free edge strain versus out-of-plane displacement (100% additional out-of-plane imperfection)

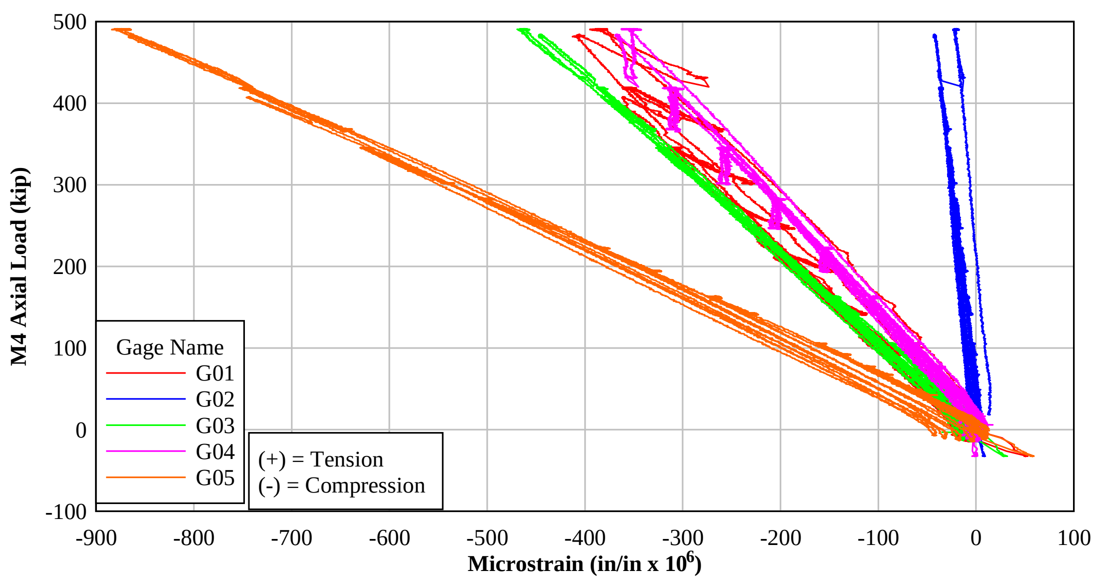

Fig. C-17: Strain in M4 connection versus M4 axial load (no additional out-of-plane imperfection)

APPENDIX D. SPECIMEN #4 ADDITIONAL DATA

Specimen #4 was a ¼" thick set of gusset plates and is described in the first manuscript.

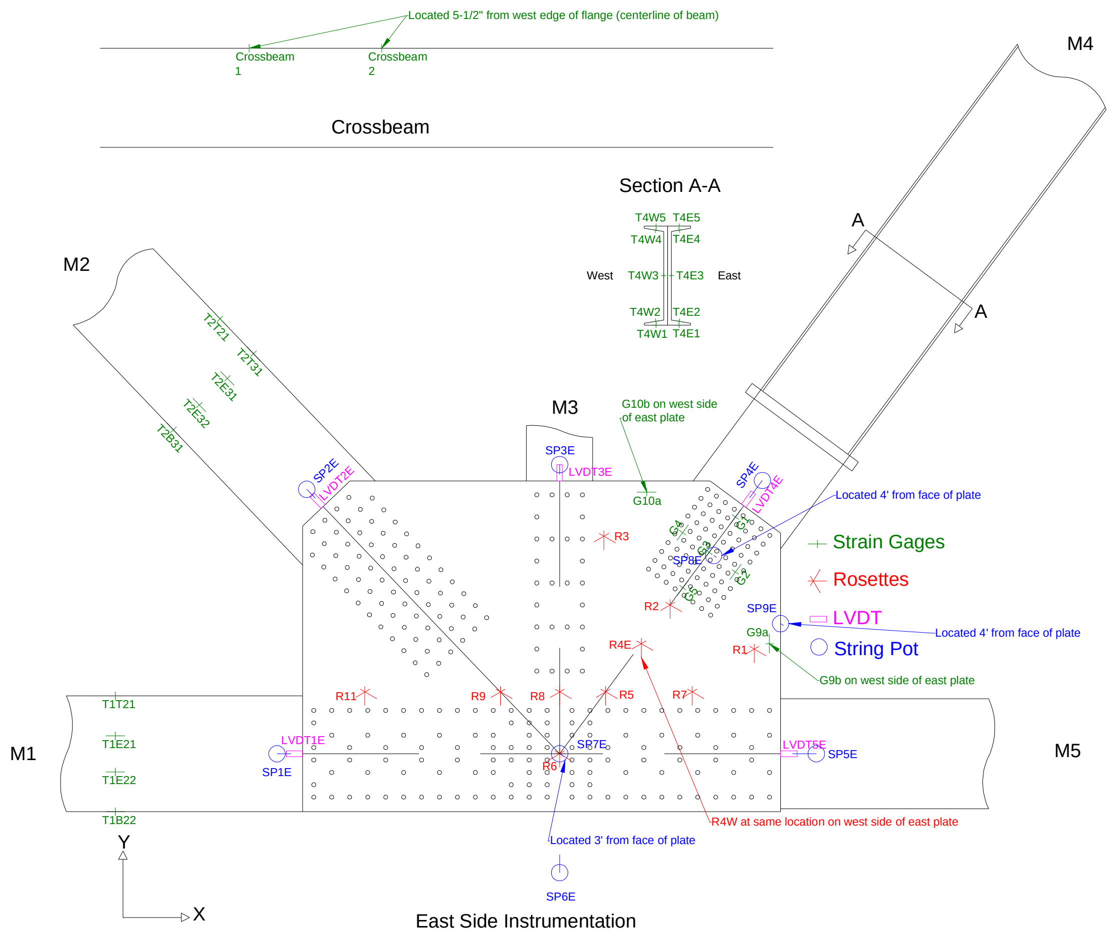

Fig. D-1: Full instrumentation plan east plate specimens #4, #5, and #6

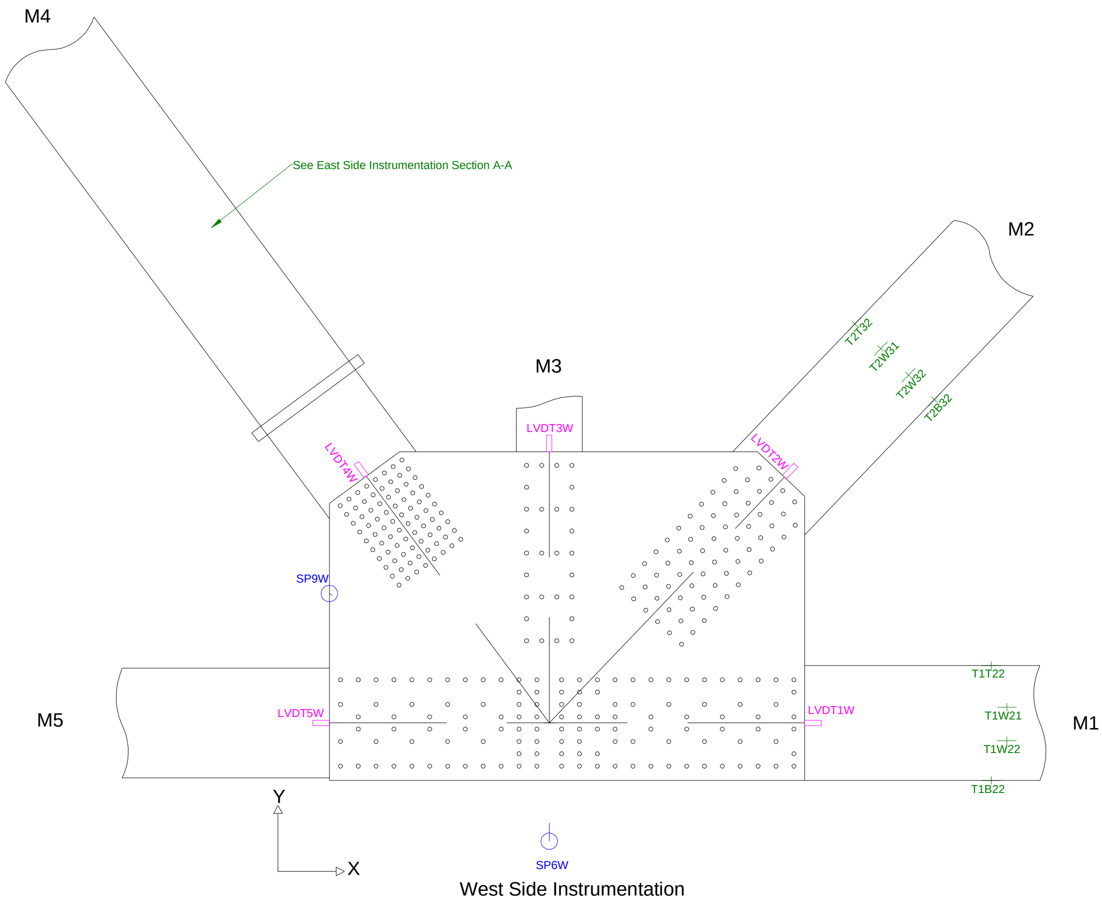

Fig. D-2: Full instrumentation plan west plate specimens #4, #5, and #6

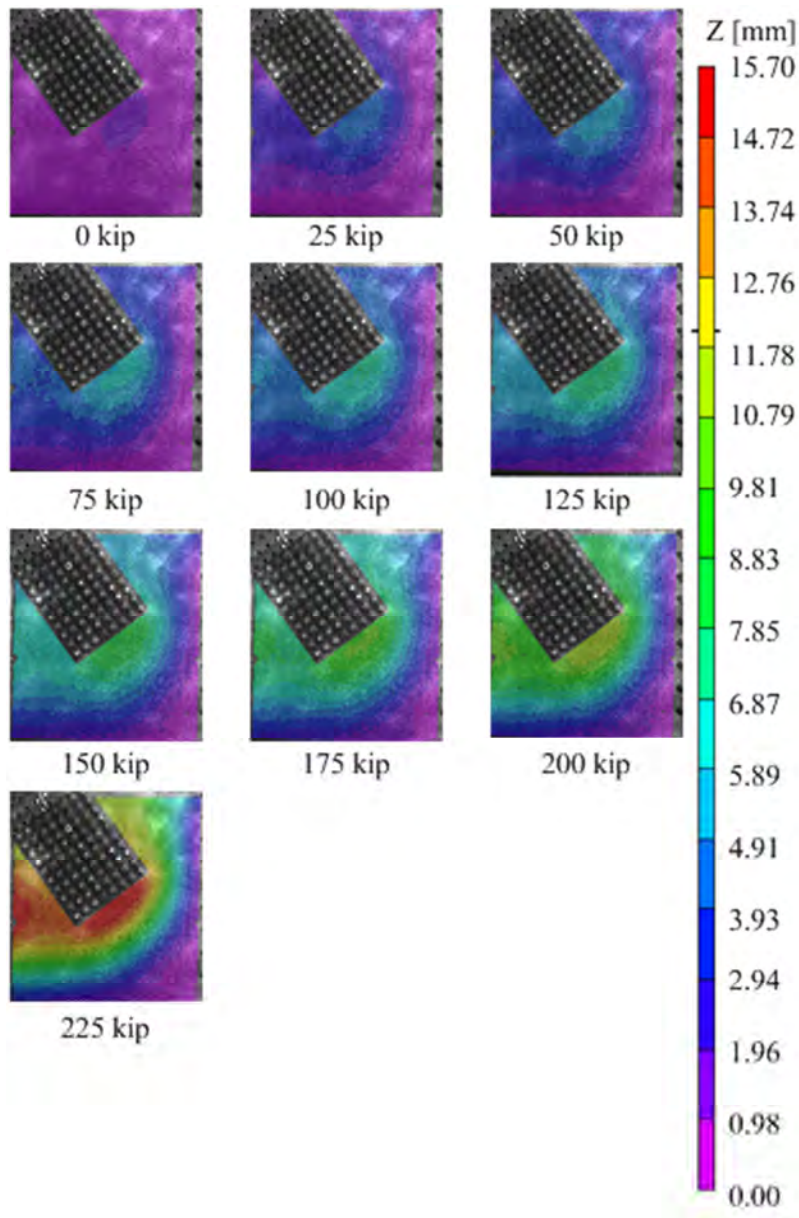

Fig. D-3: DIC measured out-of-plane deformation during loading (loads are M4 actuator loads)

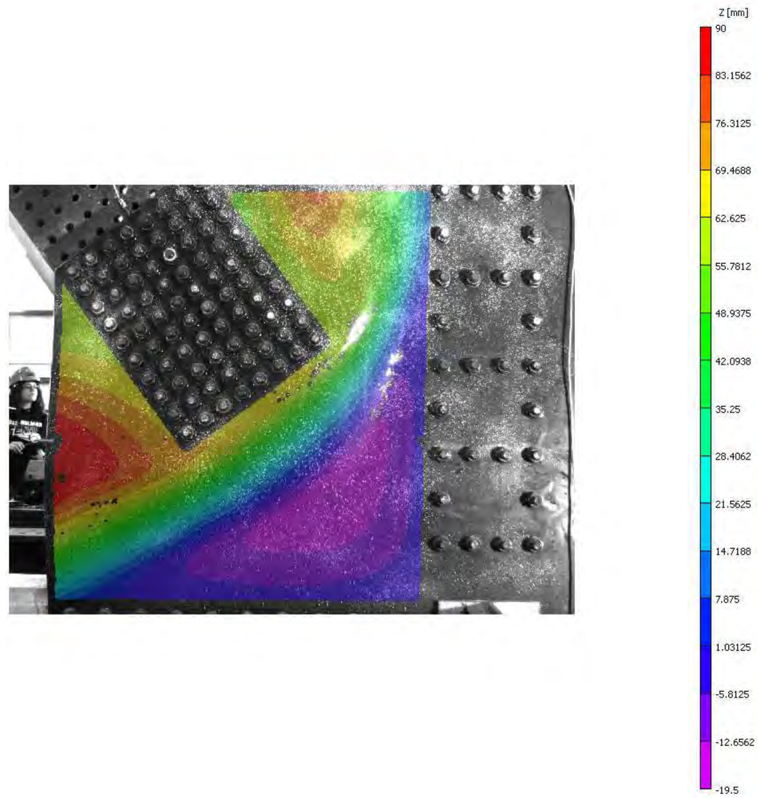

Fig. D-4: DIC measured out-of-plane deformation at failure

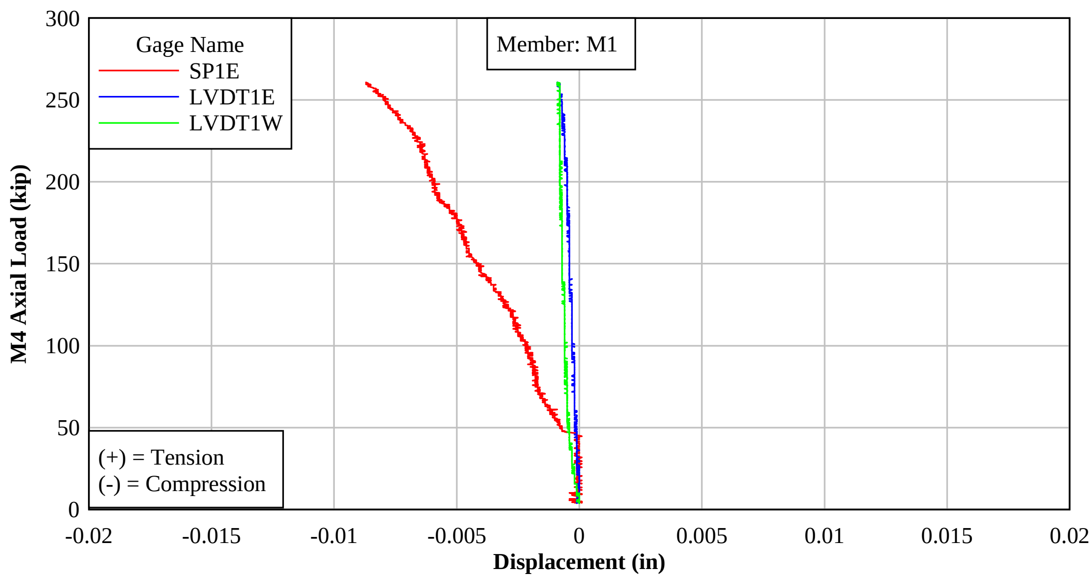

Fig. D-5: Member M1 bolt slip and relative member-to-work point displacement

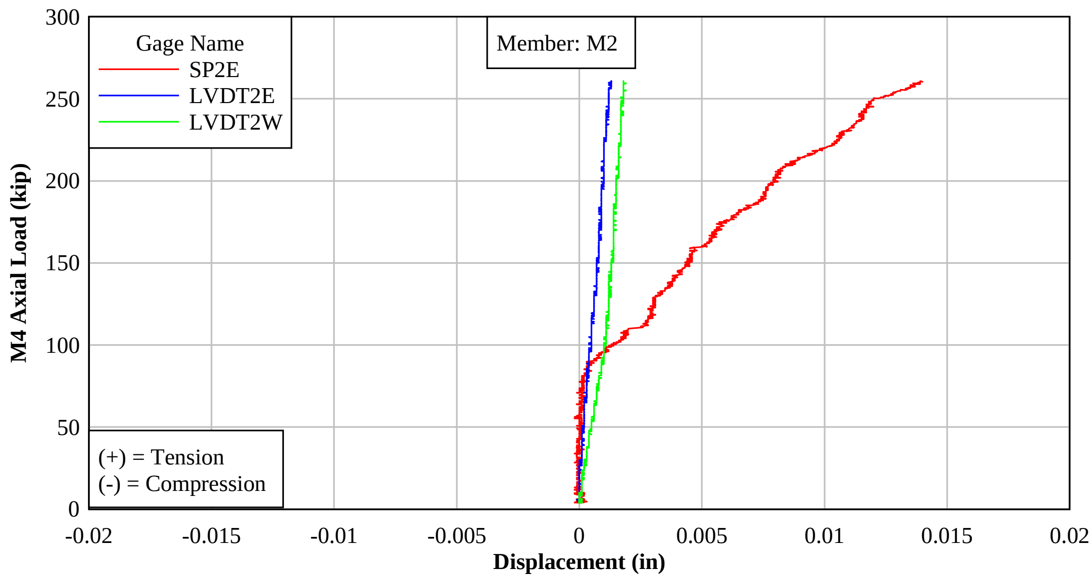

Fig. D-6: Member M2 bolt slip and relative member-to-work point displacement

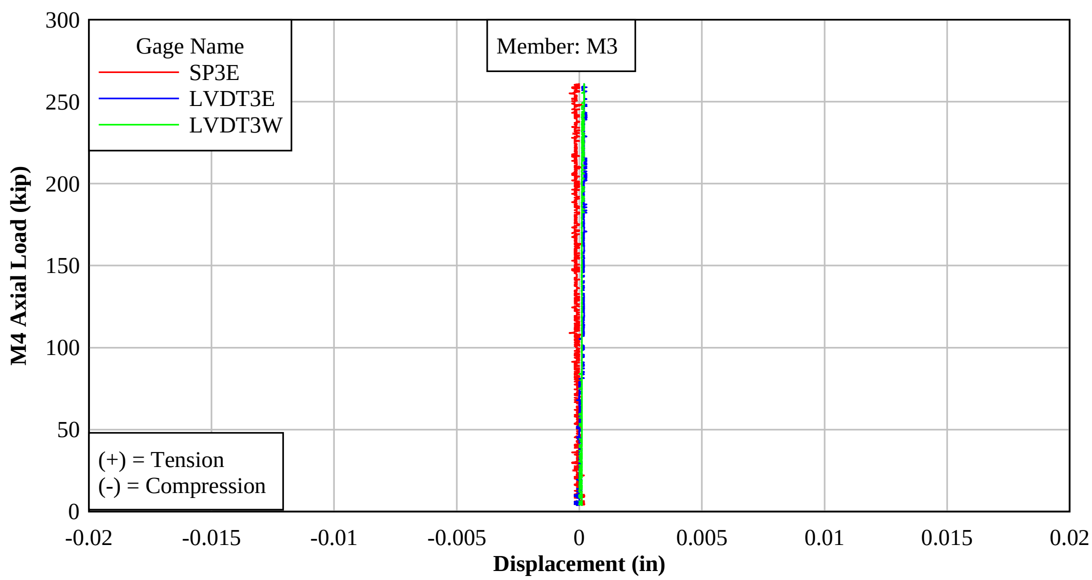

Fig. D-7: Member M3 bolt slip and relative member-to-work point displacement

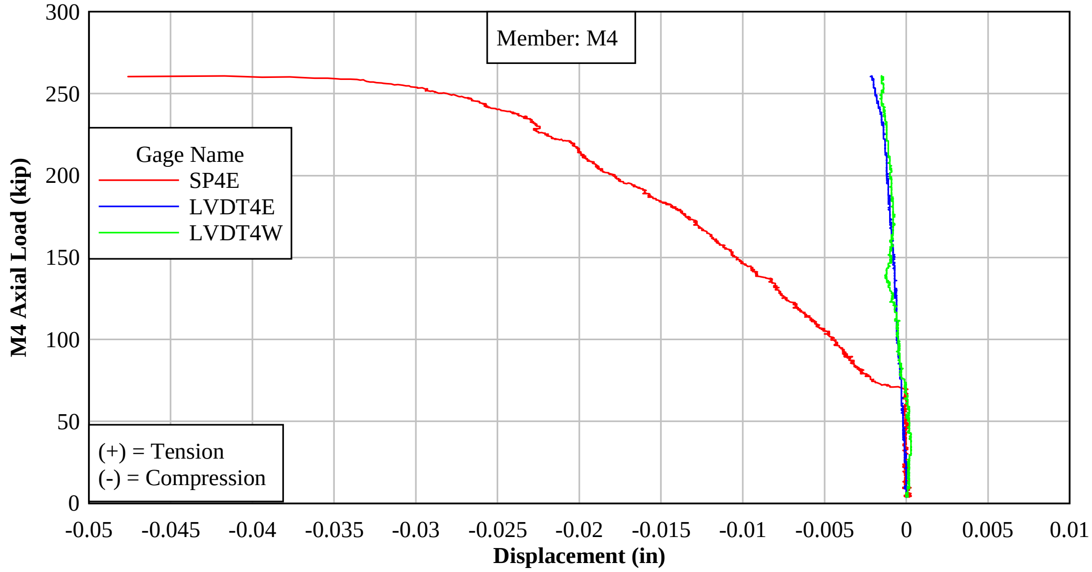

Fig. D-8: Member M4 bolt slip and relative member-to-work point displacement

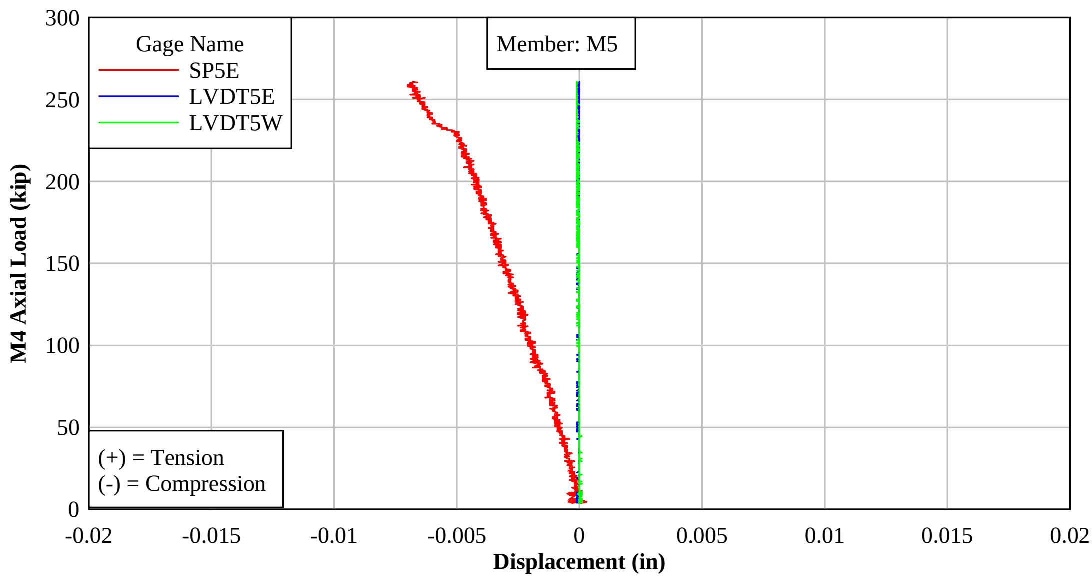

Fig. D-9: Member M5 bolt slip and relative member-to-work point displacement

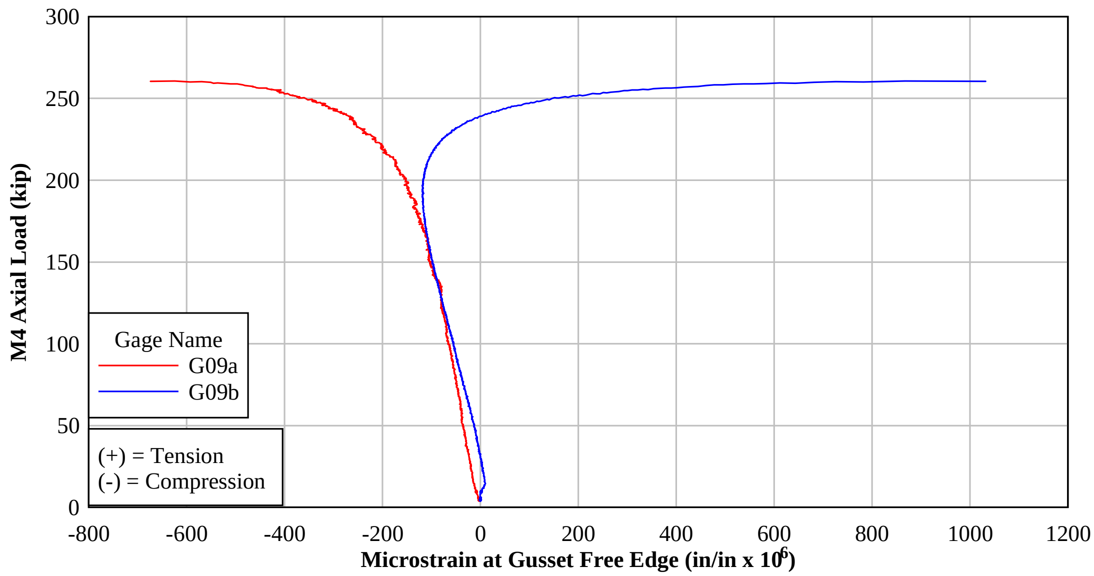

Fig. D-10: Gusset plate free edge strain versus M4 axial load

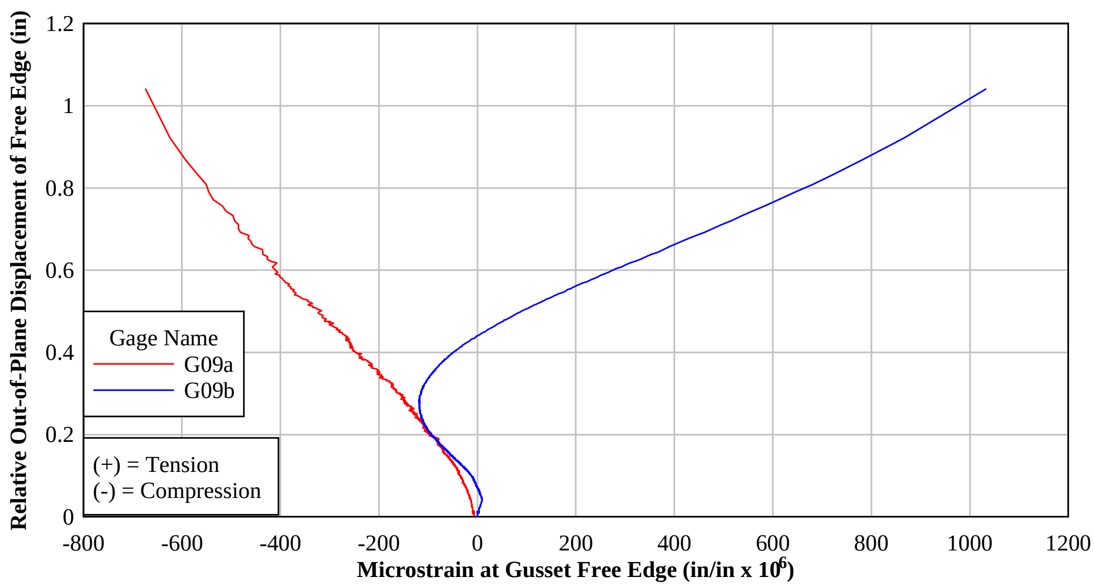

Fig. D-11: Gusset plate free edge strain versus out-of-plane displacement

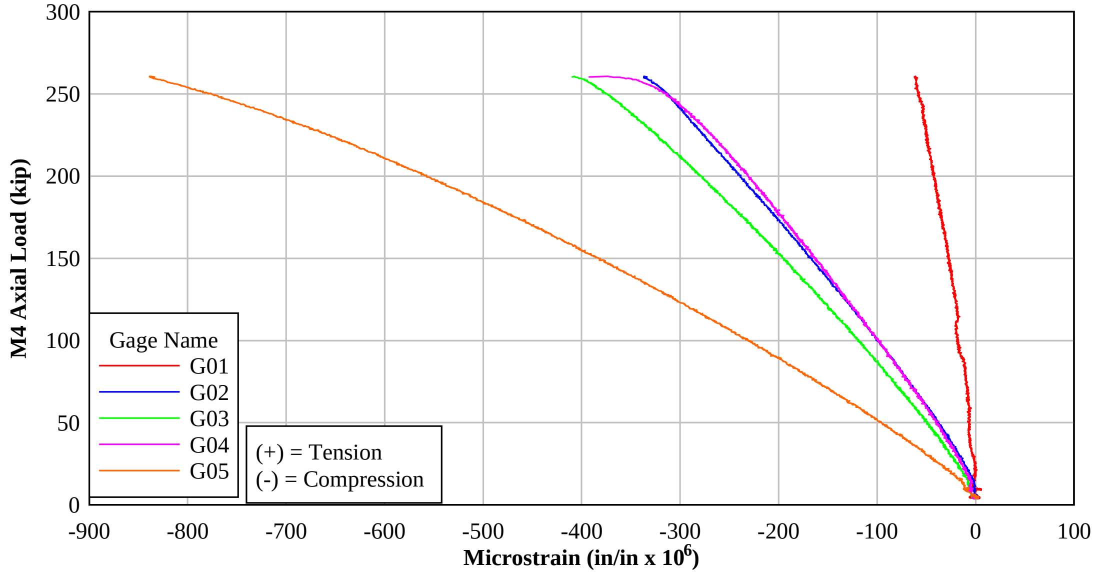

Fig. D-12: Strain in M4 connection versus M4 axial load

APPENDIX E. SPECIMEN #5 ADDITIONAL DATA

Specimen #5 was a 3/8” thick set of gusset plates and is described in the first manuscript.

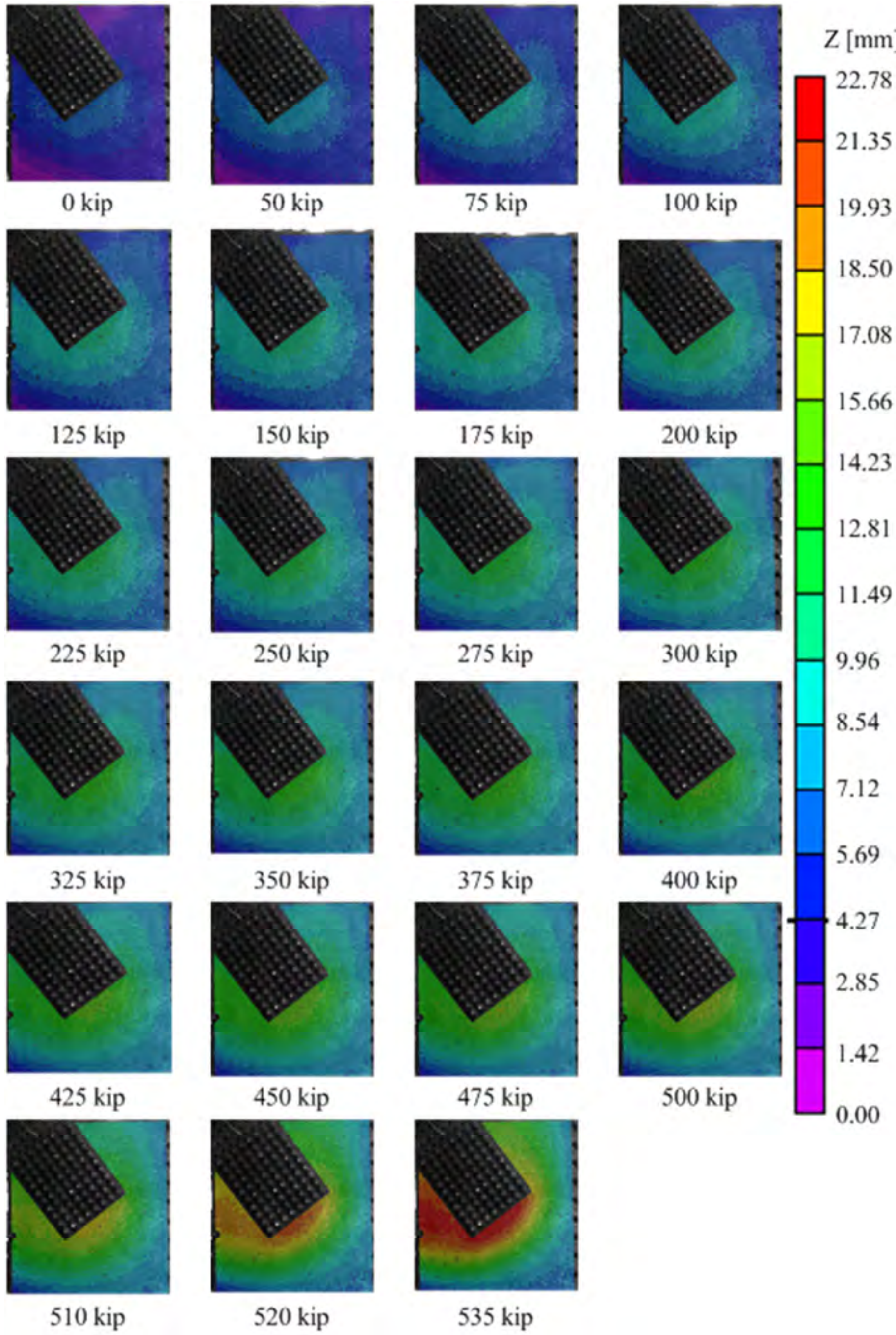

Fig. E-1: DIC measured out-of-plane deformation during loading (loads are M4 actuator loads)

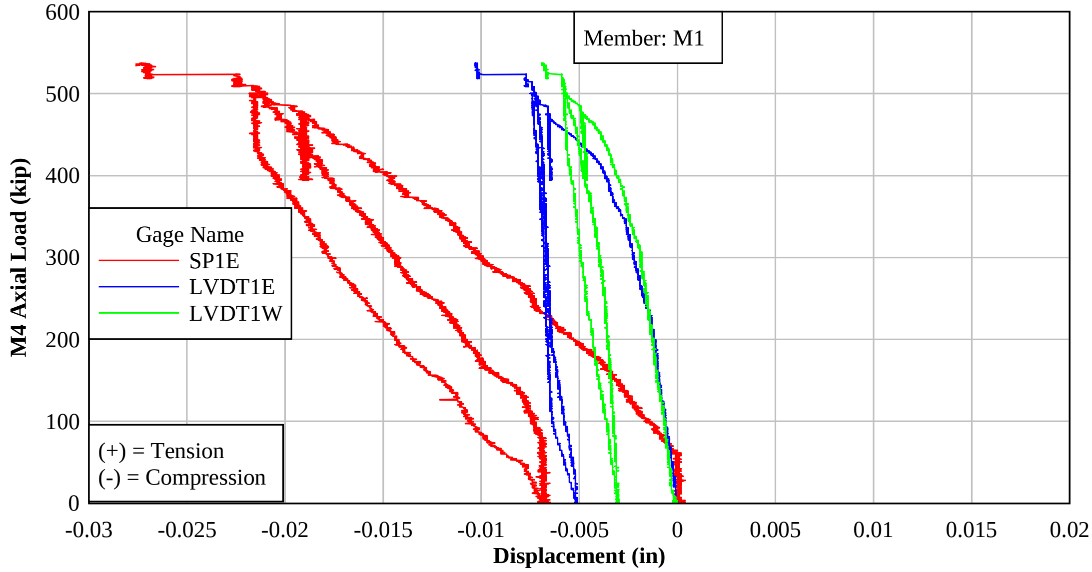

Fig. E-2: Member M1 bolt slip and relative member-to-work point displacement

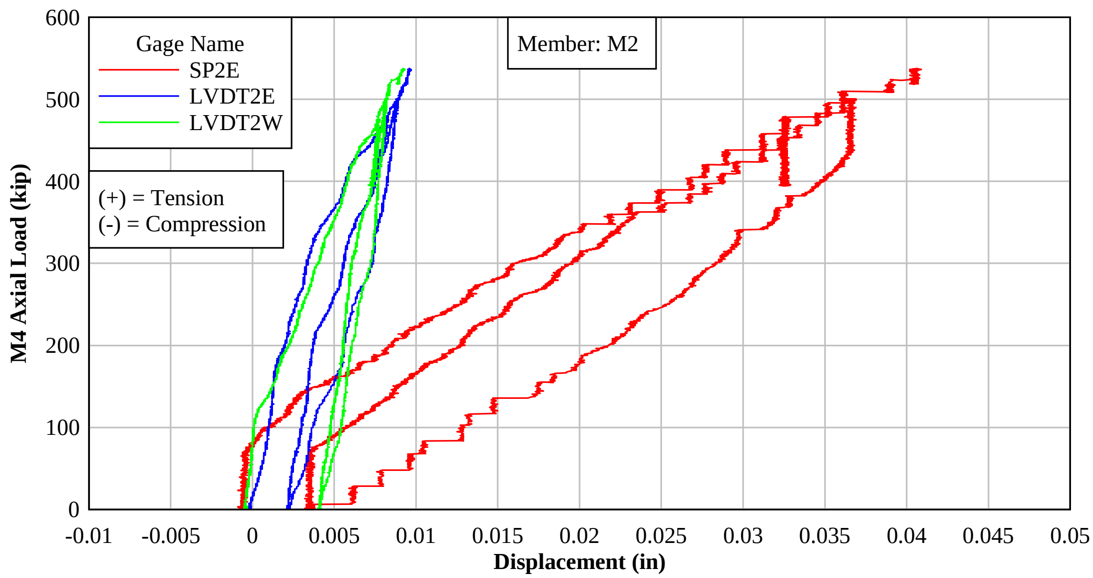

Fig. E-3: Member M2 bolt slip and relative member-to-work point displacement

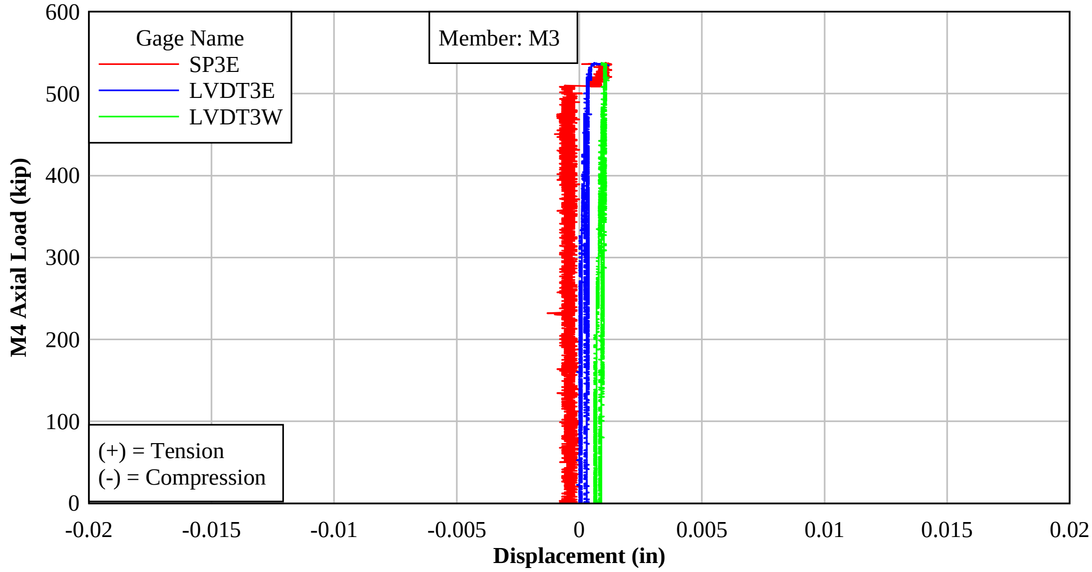

Fig. E-4: Member M3 bolt slip and relative member-to-gusset displacement

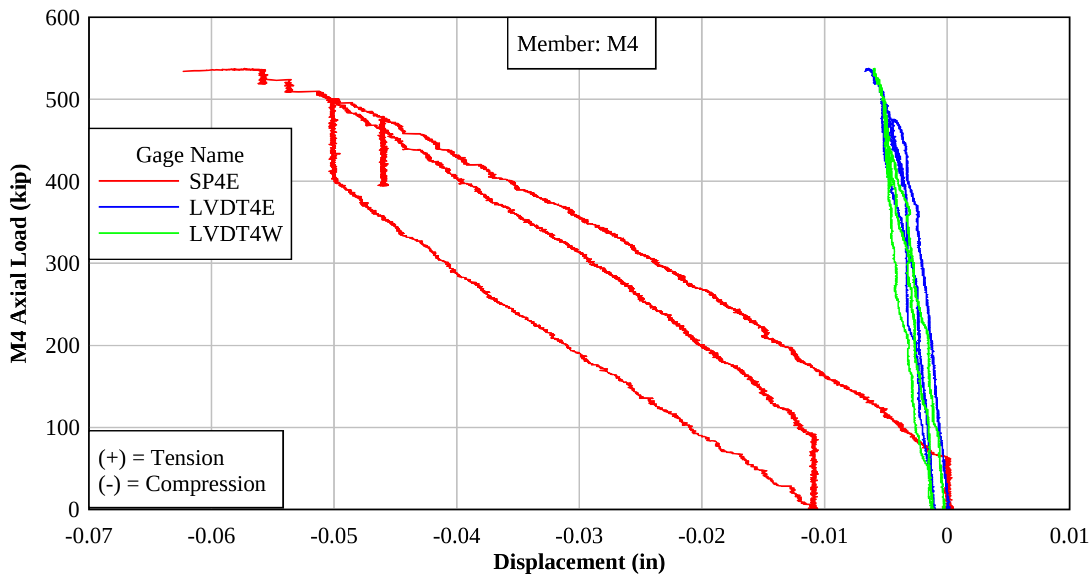

Fig. E-5: Member M4 bolt slip and relative member-to-gusset displacement

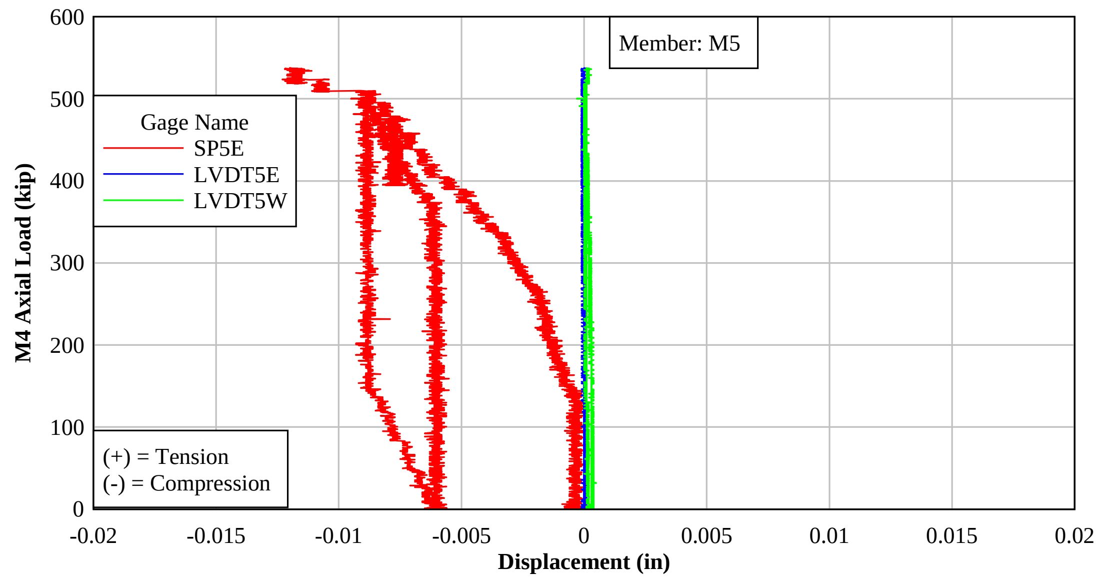

Fig. E-6: Member M5 bolt slip and relative member-to-work point displacement

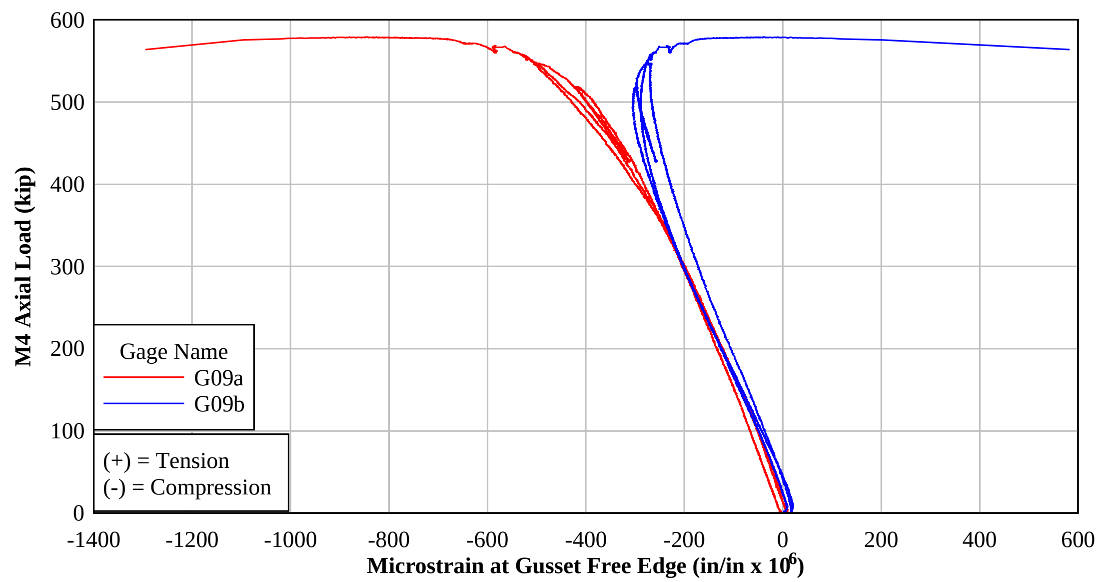

Fig. E-7: Gusset plate free edge strain versus M4 axial load

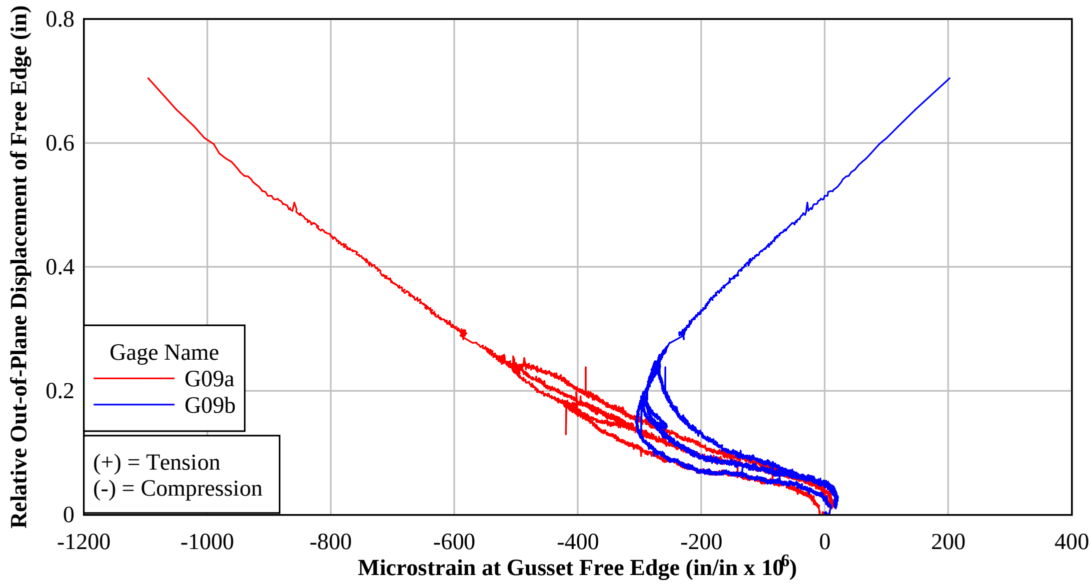

Fig. E-8: Gusset plate free edge strain versus out-of-plane displacement

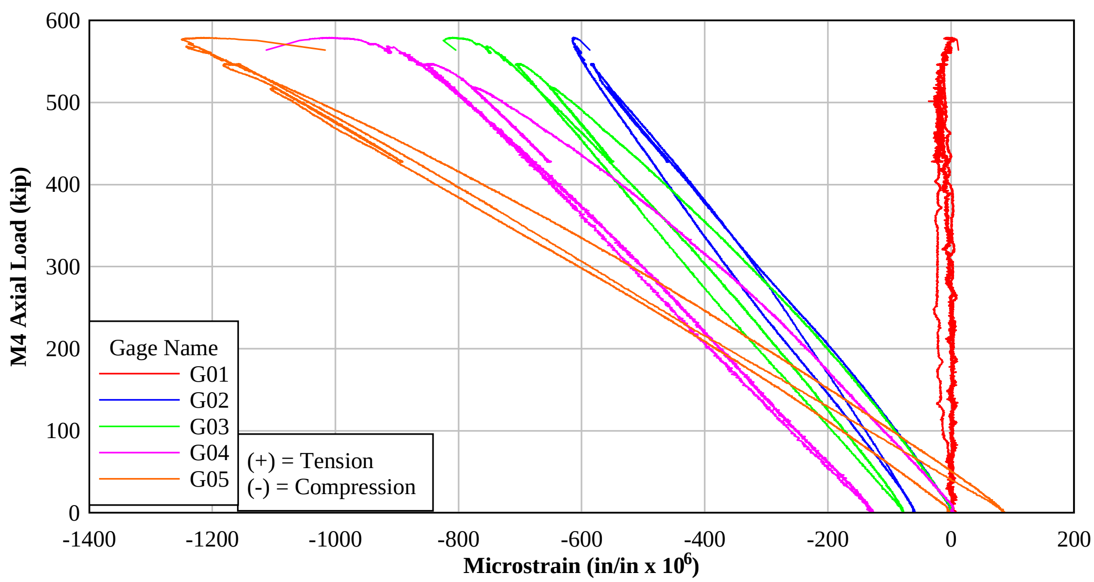

Fig. E-9: Strain in M4 connection versus M4 axial load

APPENDIX F. SPECIMEN #6 ADDITIONAL DATA

Specimen #6 was a ¼” thick set of gusset plates and is described in the first manuscript.

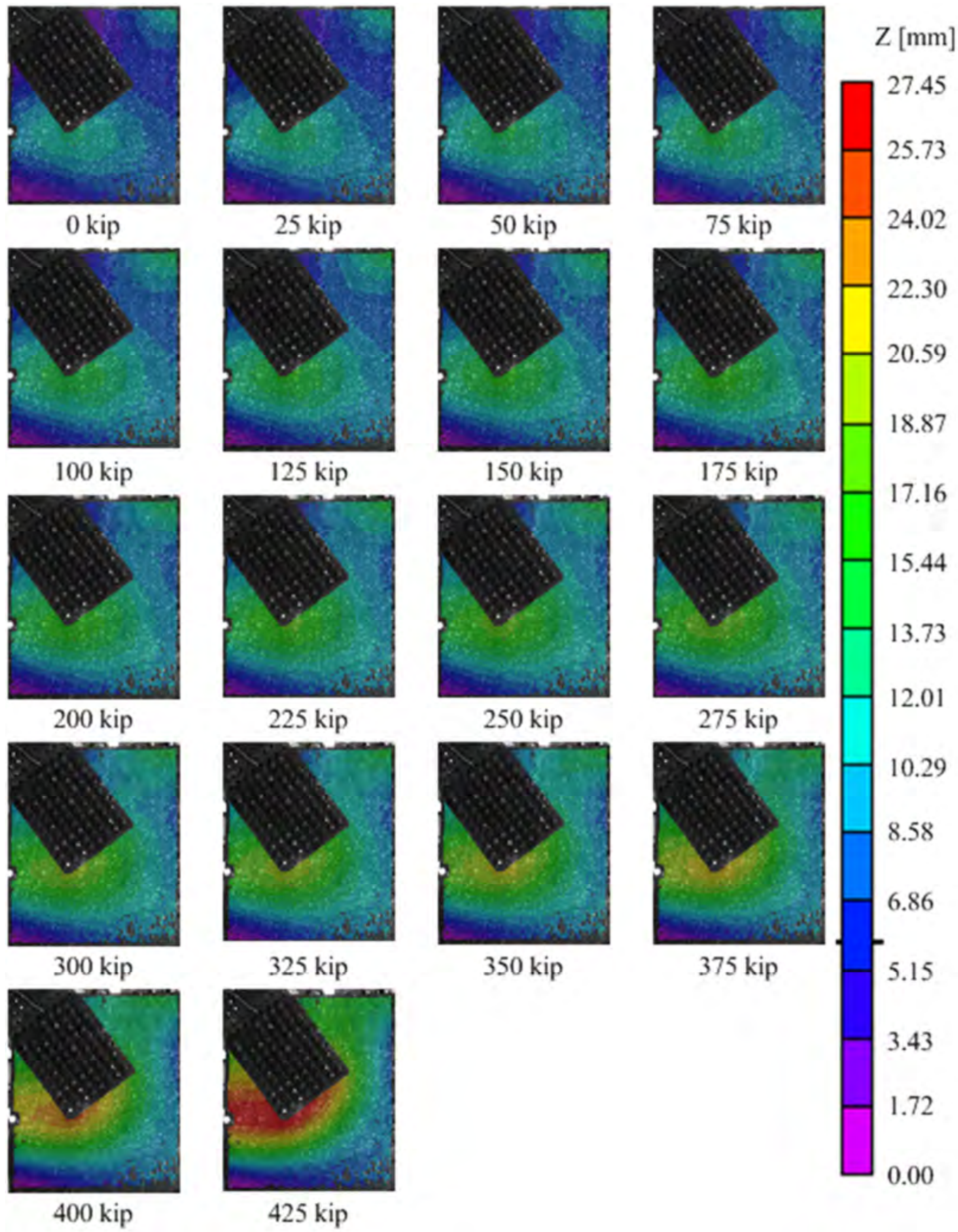

Fig. F-1: DIC measured out-of-plane deformation during loading (loads are M4 actuator loads)

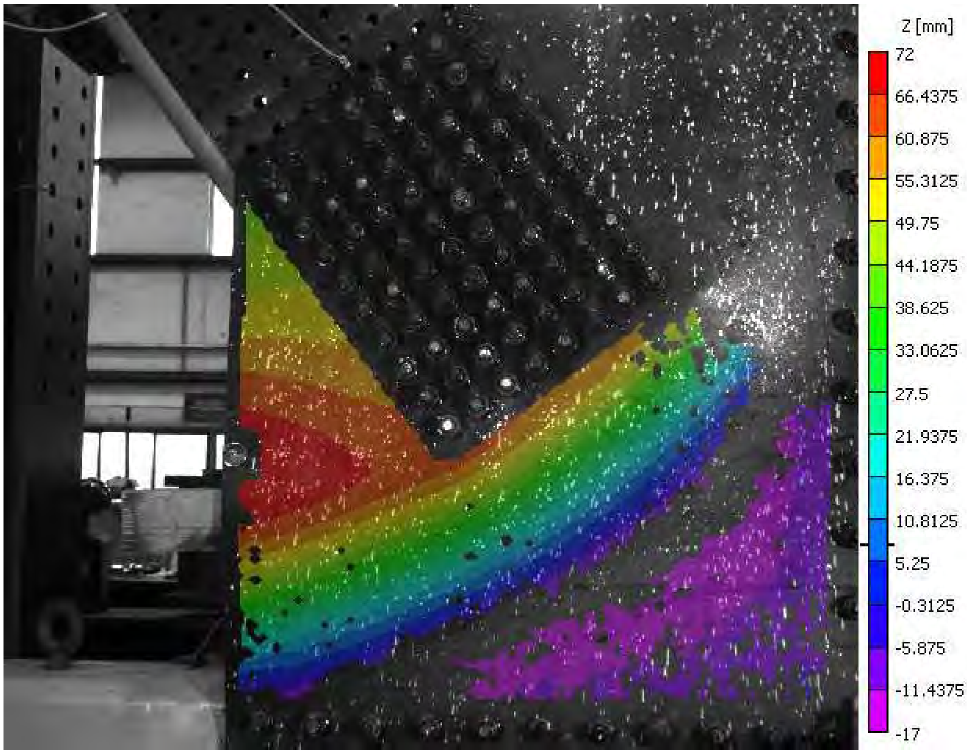

Fig. F-2: DIC measured out-of-plane deformation at failure

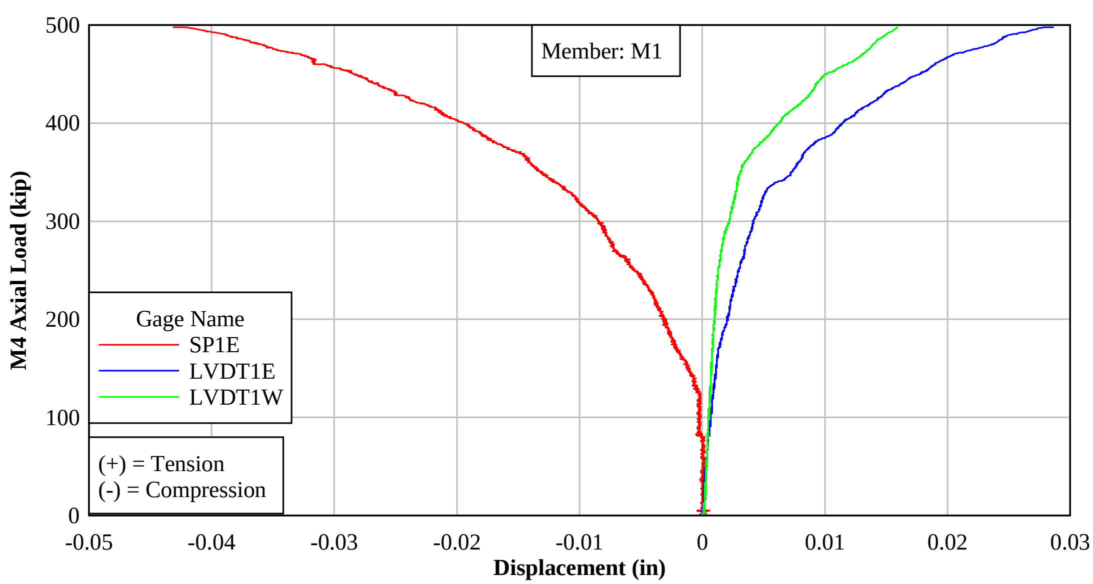

Fig. F-3: Member M1 bolt slip and relative member-to-work point displacement

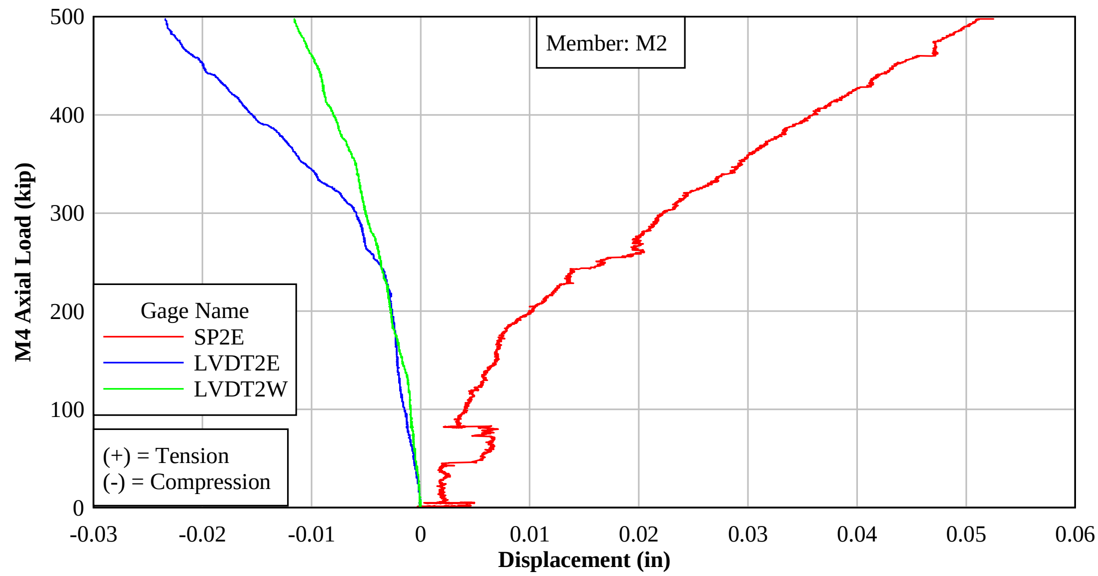

Fig. F-4: Member M2 bolt slip and relative member-to-work point displacement

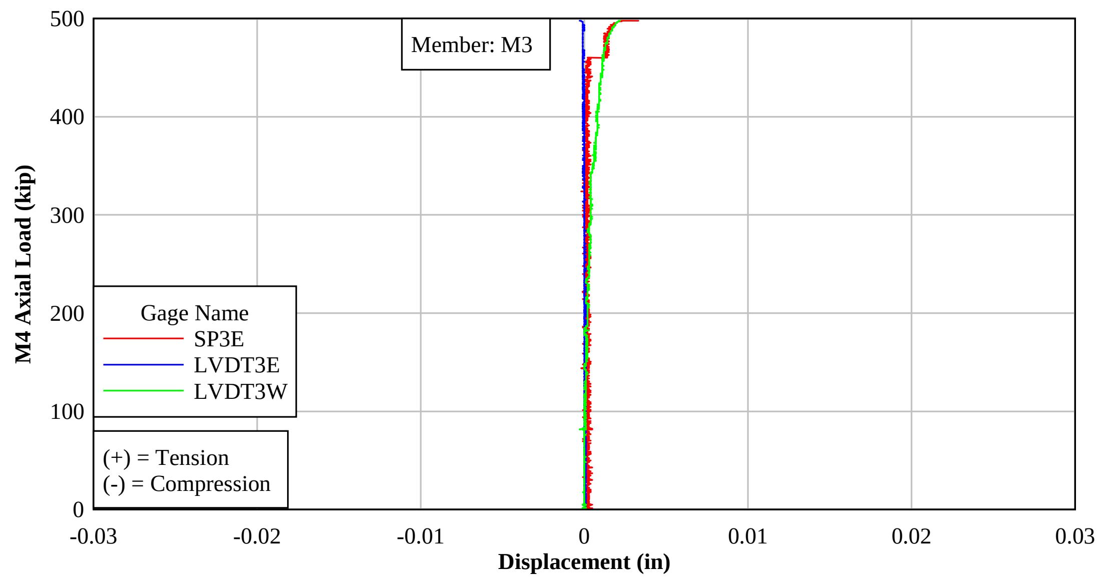

Fig. F-5: Member M3 bolt slip and relative member-to-work point displacement

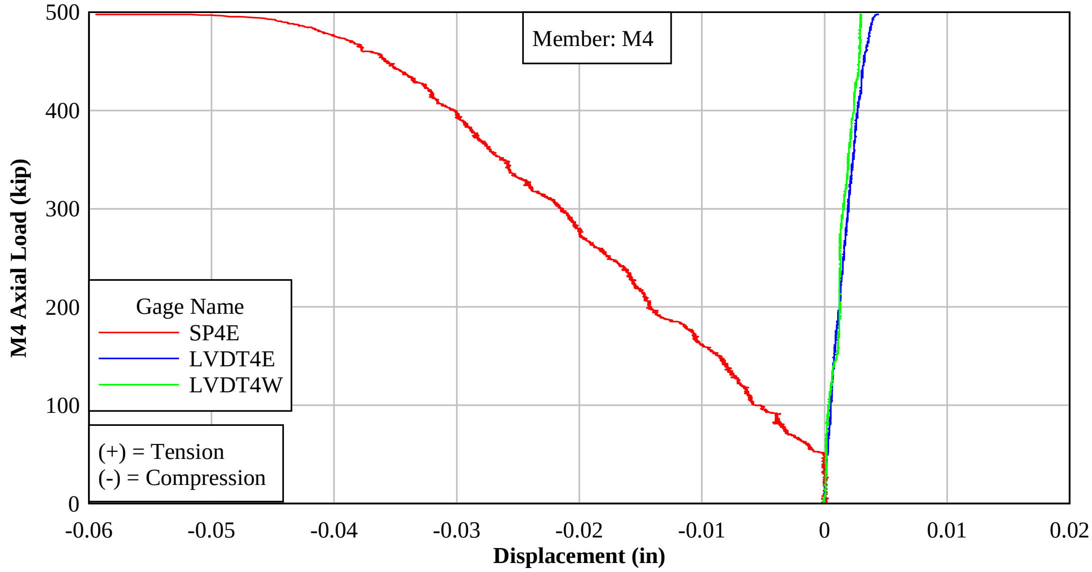

Fig. F-6: Member M4 bolt slip and relative member-to-work point displacement

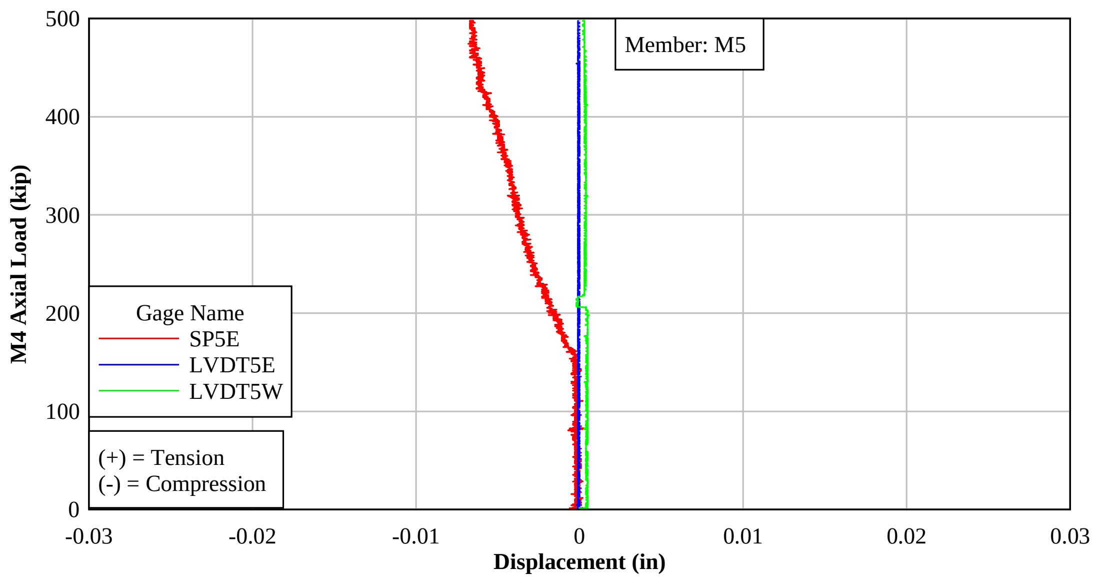

Fig. F-7: Member M5 bolt slip and relative member-to-work point displacement

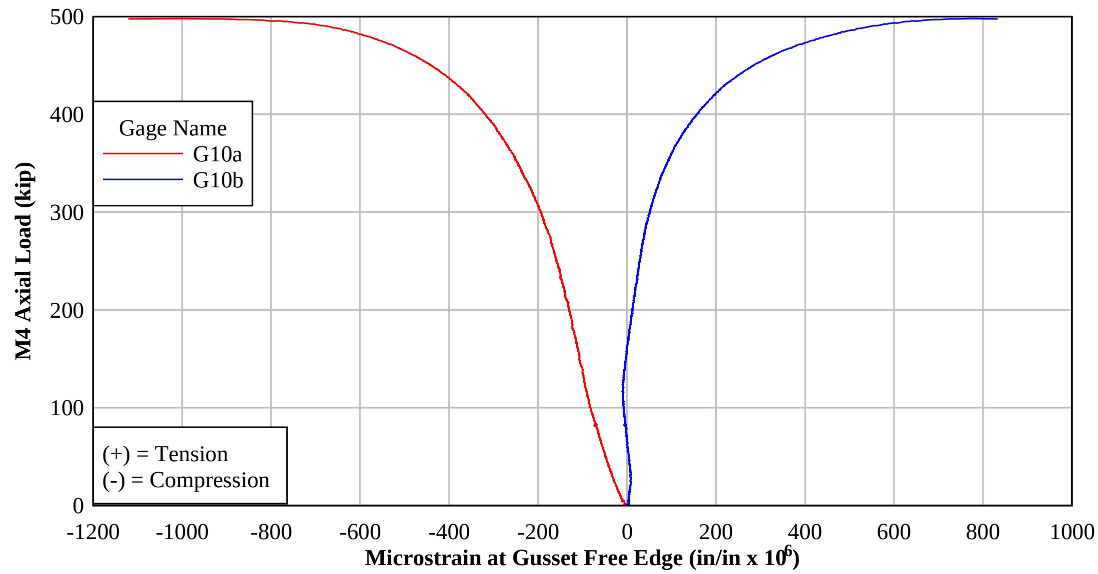

Fig. F-8: Gusset plate free edge strain versus M4 axial load

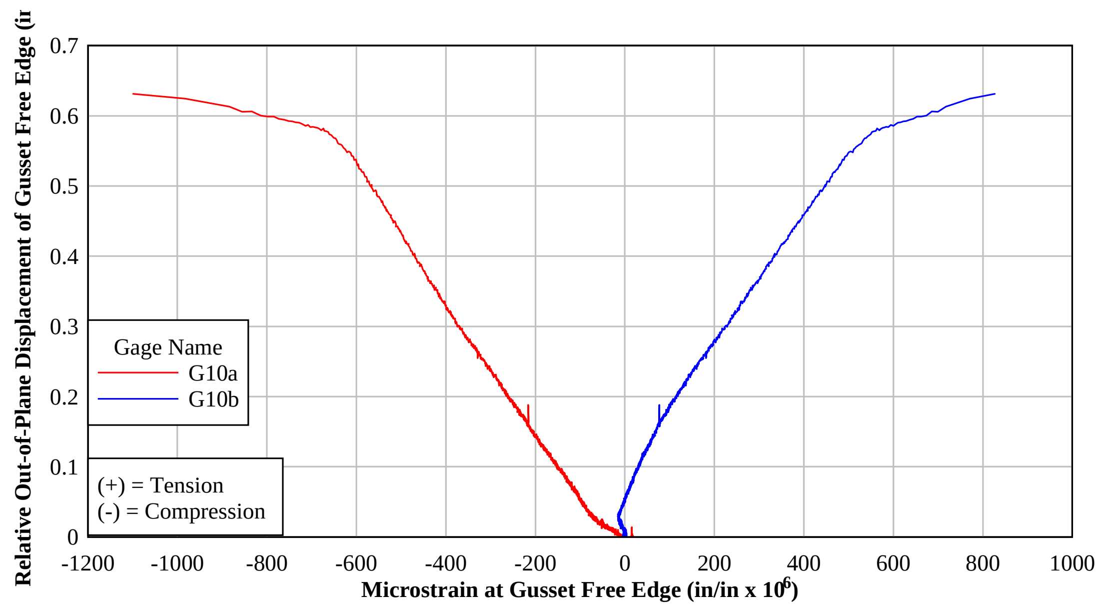

Fig. F-9: Gusset plate free edge strain versus out-of-plane displacement

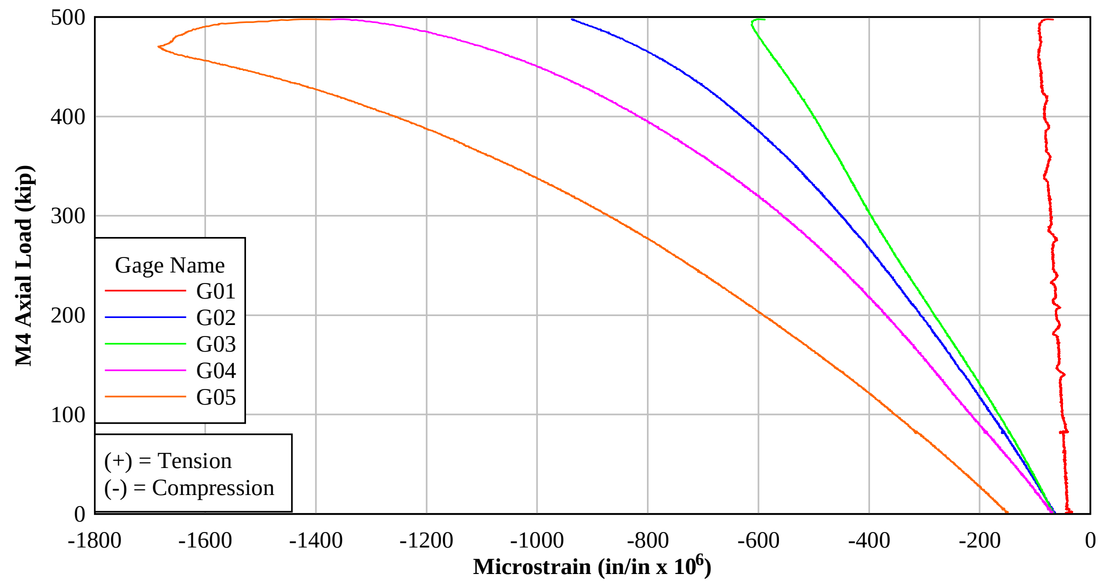

Fig. F-10: Strain in M4 connection versus M4 axial load

APPENDIX G. SPECIMEN #7 (CORROSION) ADDITIONAL DATA

Specimen #7 was a 3/8” thick set of gusset plates and is described in the second manuscript.

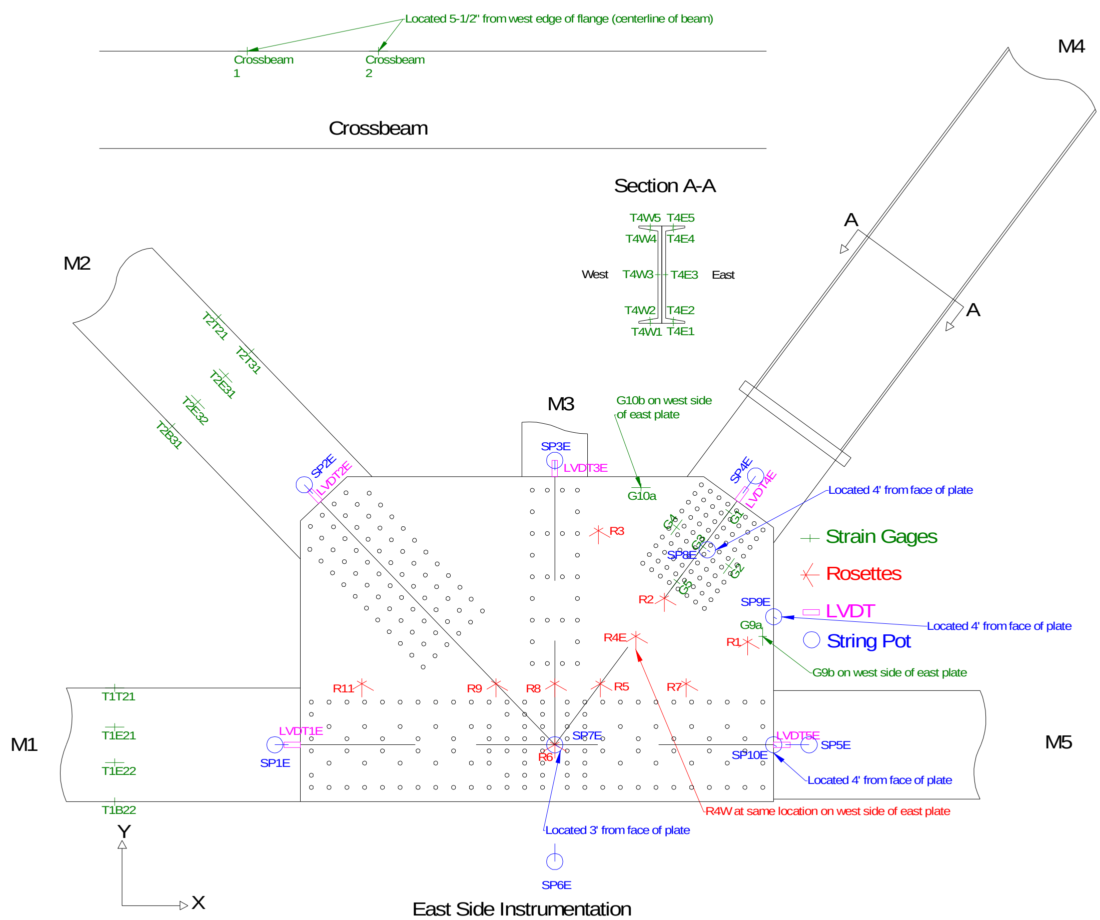

Fig. G-1: Full instrumentation plan east plate specimens #7, #8, and #9

(West plate instrumentation is the same as specimens #4, #5, and #6.)

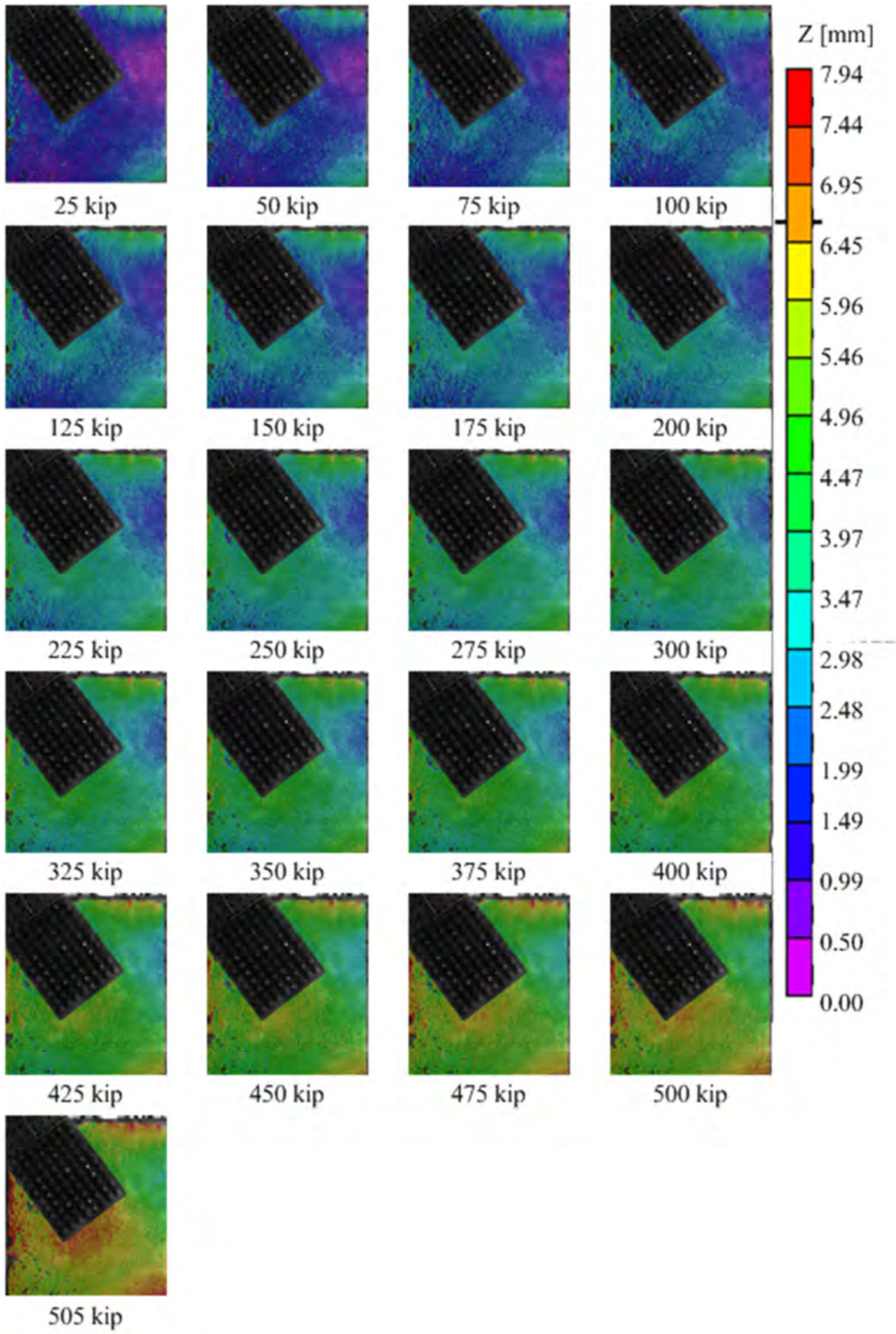

Fig. G-2: DIC measured out-of-plane deformation during loading (loads are M4 actuator loads)

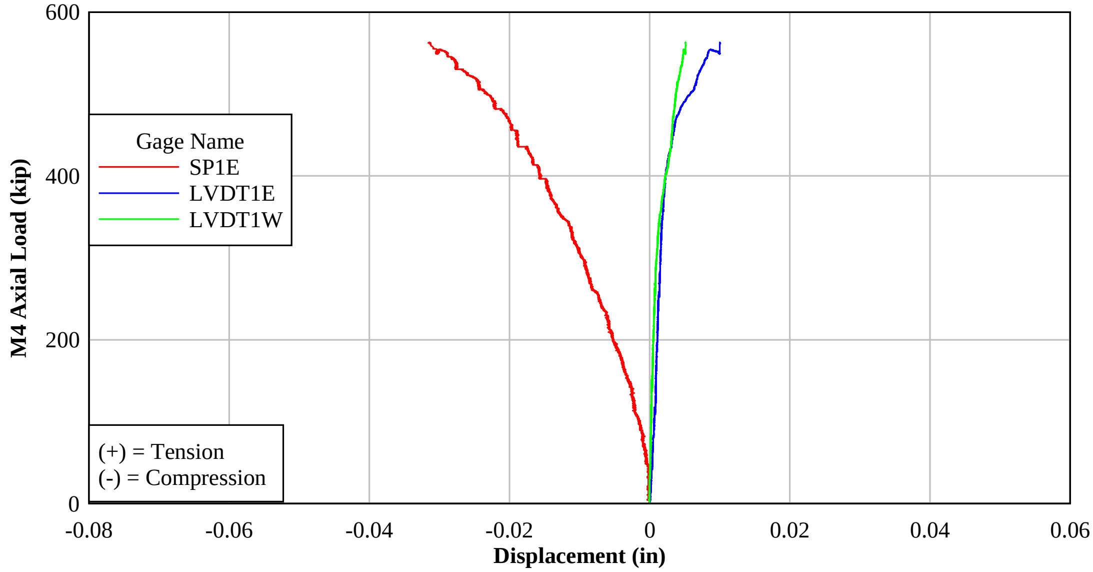

Fig. G-3: Member M1 bolt slip and relative member-to-work point displacement

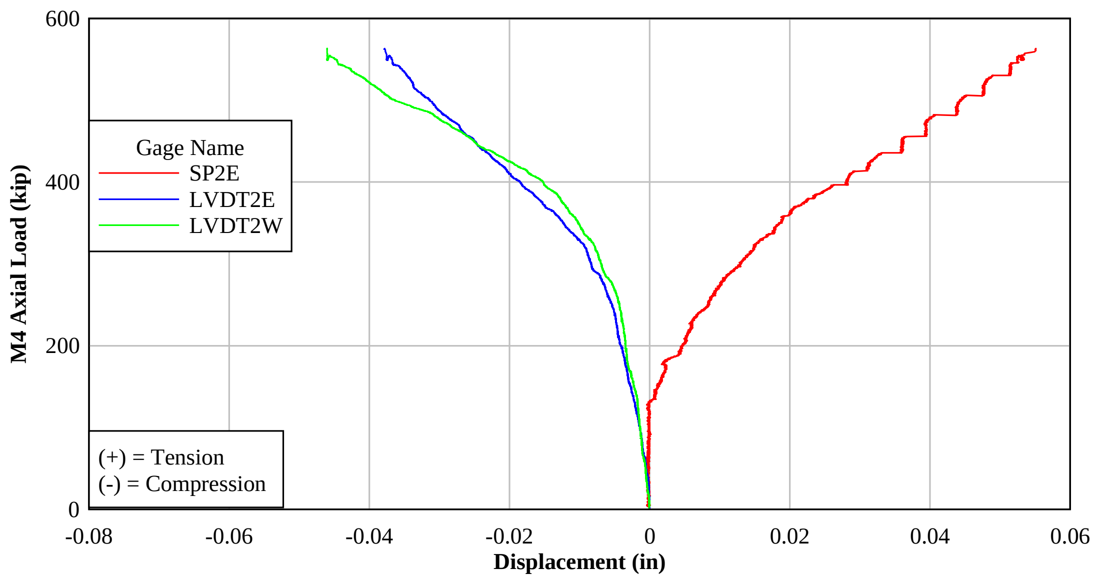

Fig. G-4: Member M2 bolt slip and relative member-to-work point displacement

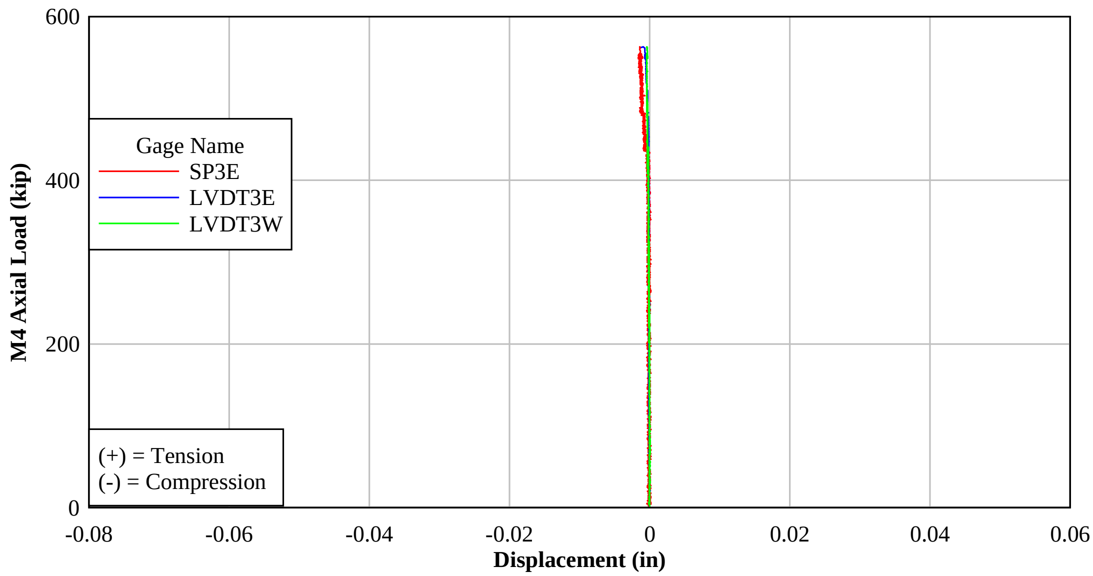

Fig. G-5: Member M3 bolt slip and relative member-to-work point displacement

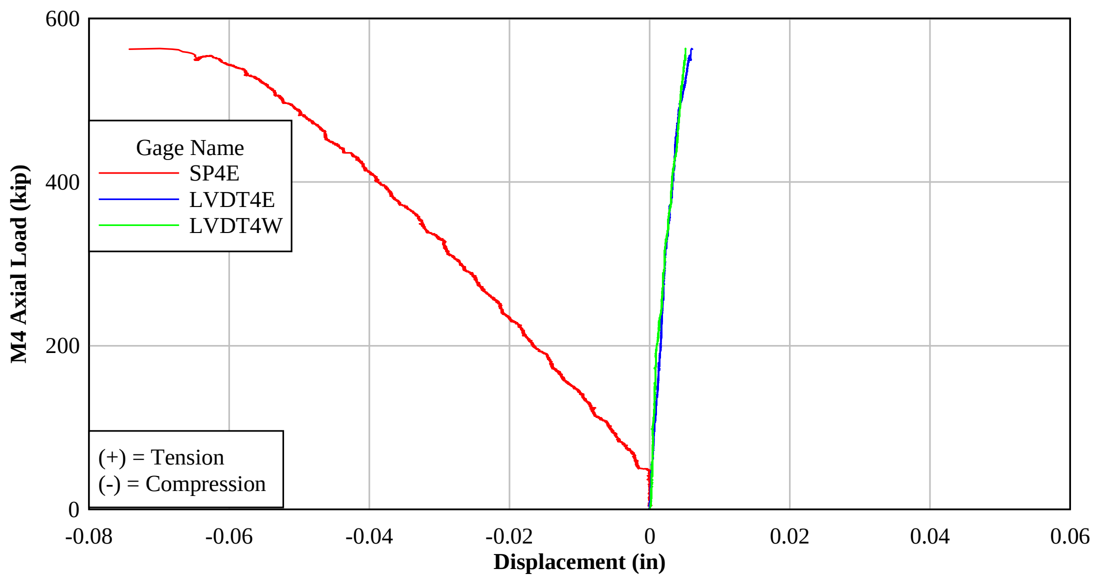

Fig. G-6: Member M4 bolt slip and relative member-to-work point displacement

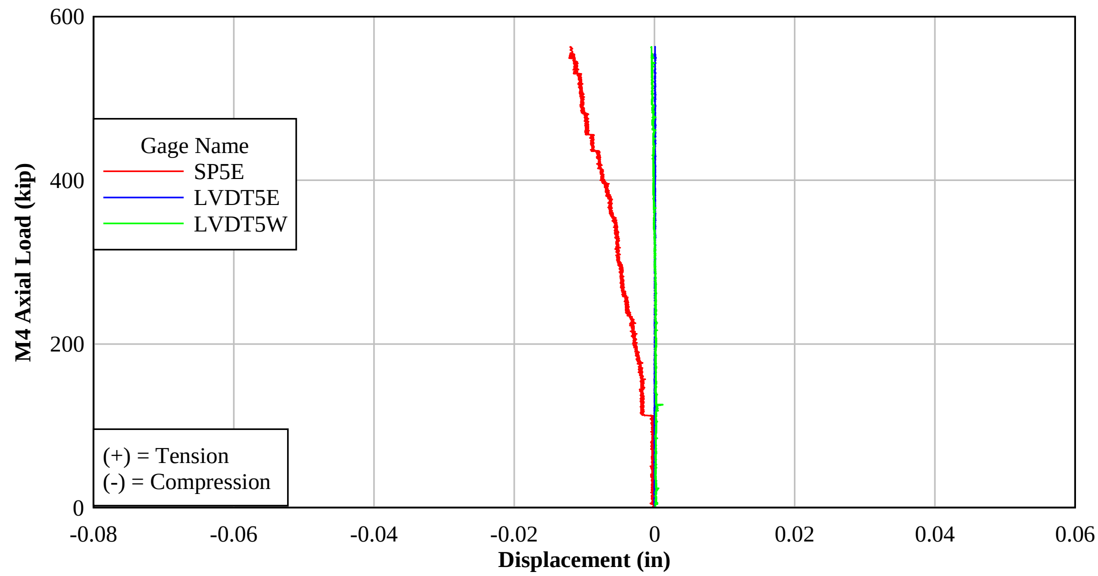

Fig. G-7: Member M5 bolt slip and relative member-to-work point displacement

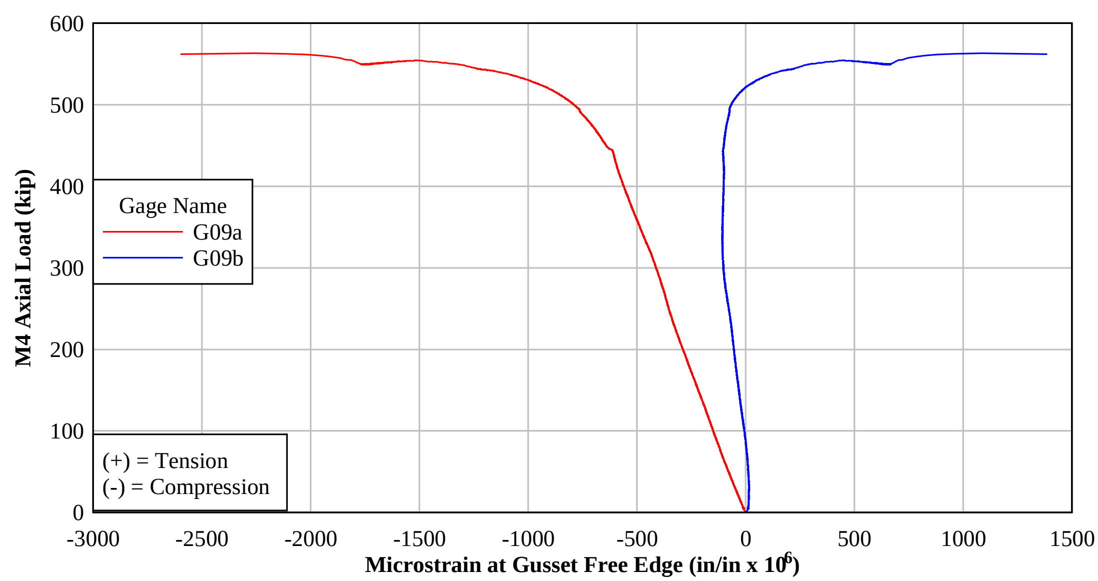

Fig. G-8: Gusset plate free edge strain versus M4 axial load

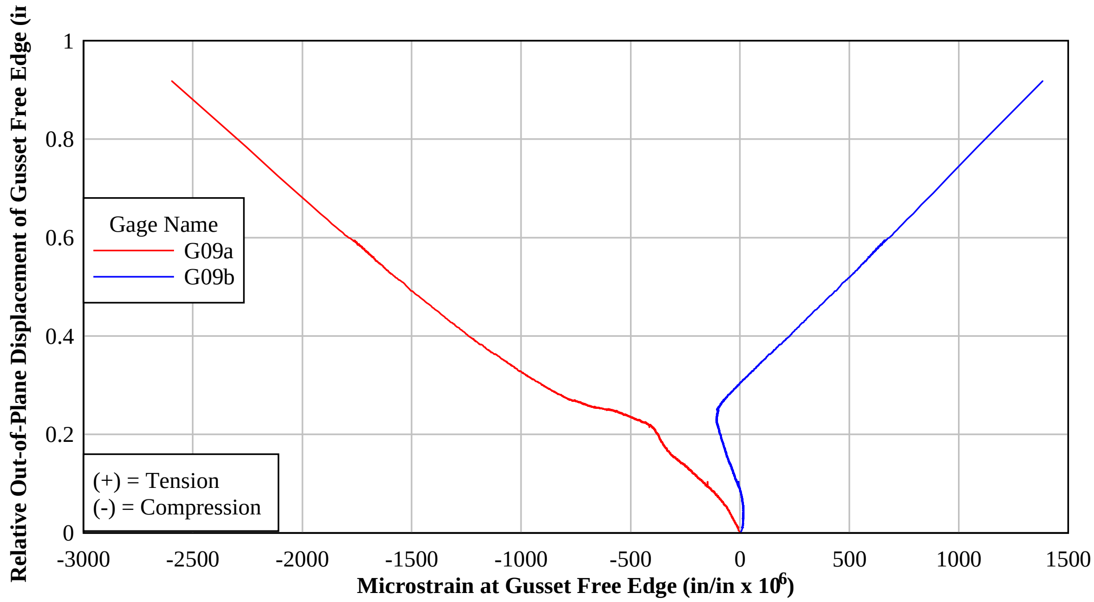

Fig. G-9: Gusset plate free edge strain versus out-of-plane displacement

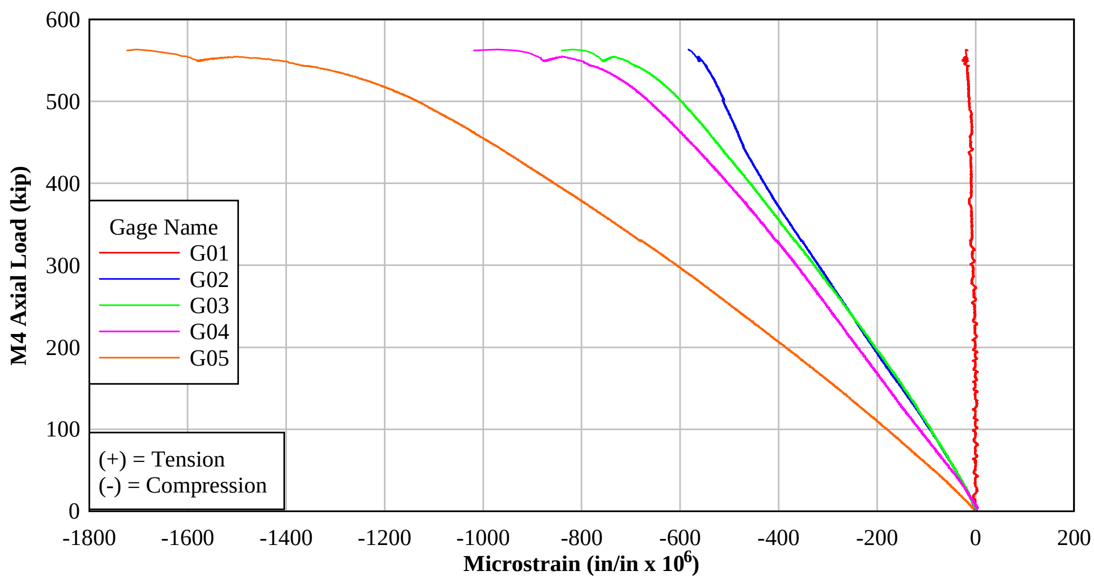

Fig. G-10: M4 connection strain versus M4 axial load

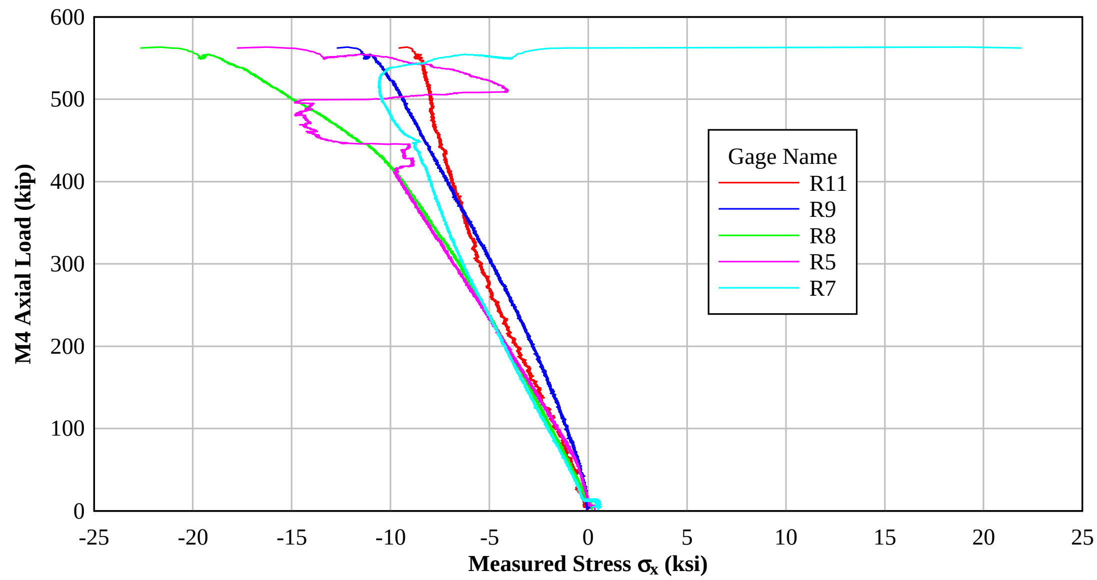

Fig. G-11: Stress in global x direction for all gages along Plane A-A

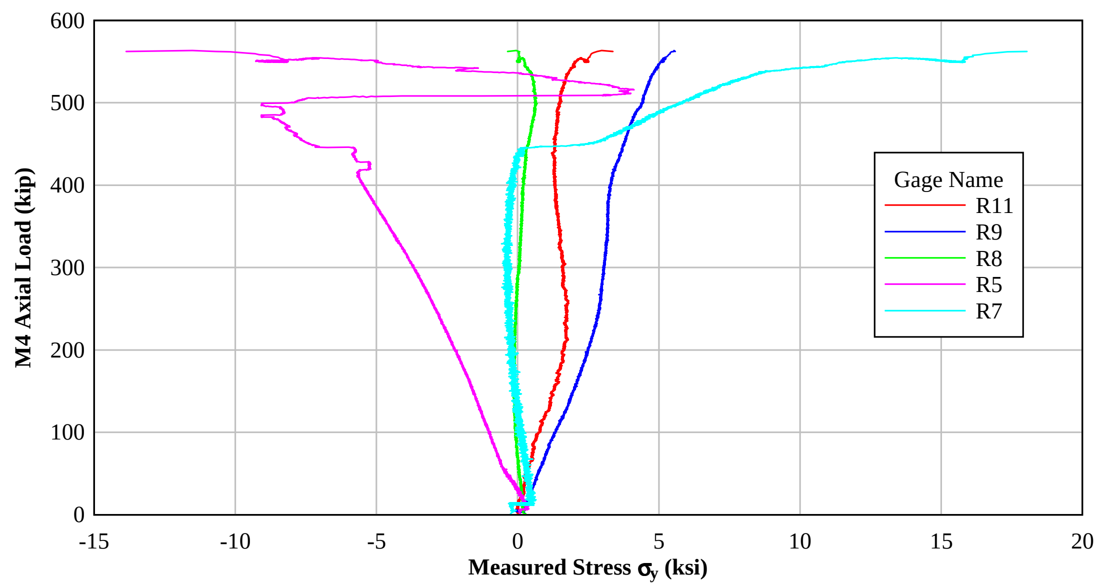

Fig. G-12: Stress in global y direction for all gages along Plane A-A

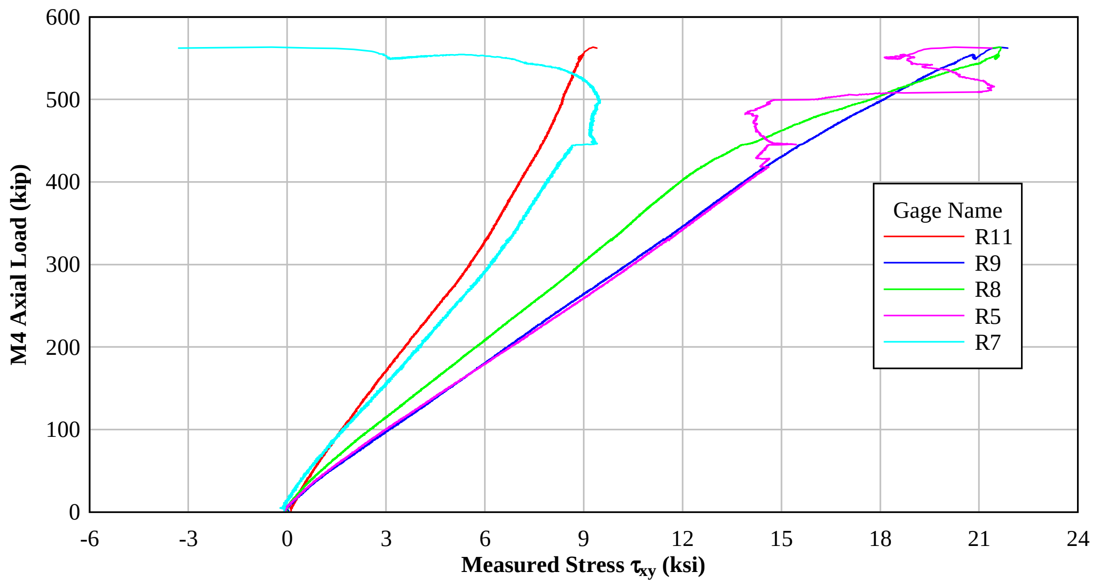

Fig. G-13: Shear stress in global xy direction for all gages along Plane A-A

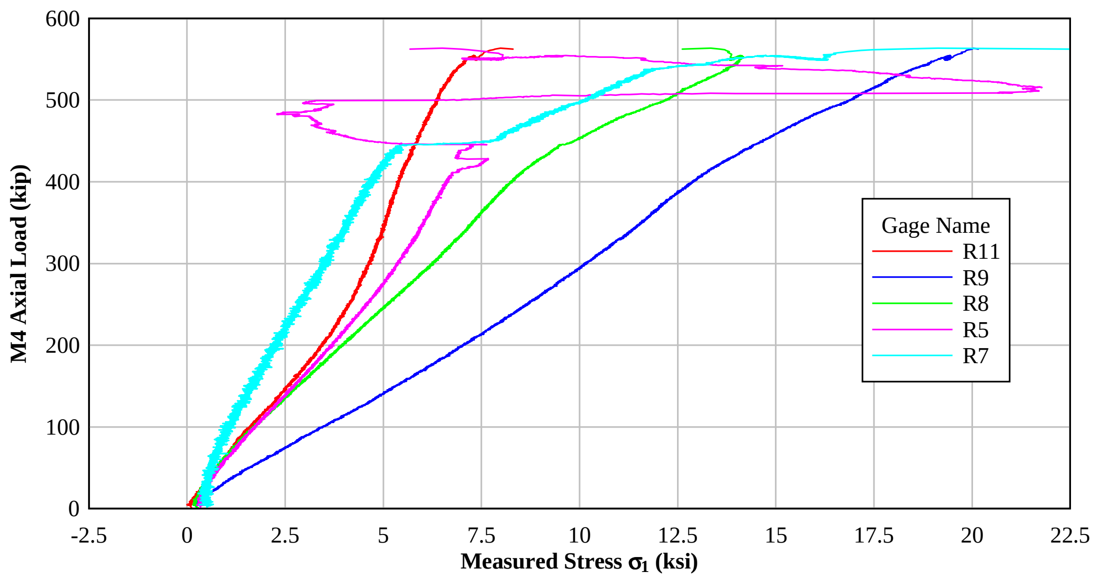

Fig. G-14: 1st principle stress for all gages along Plane A-A

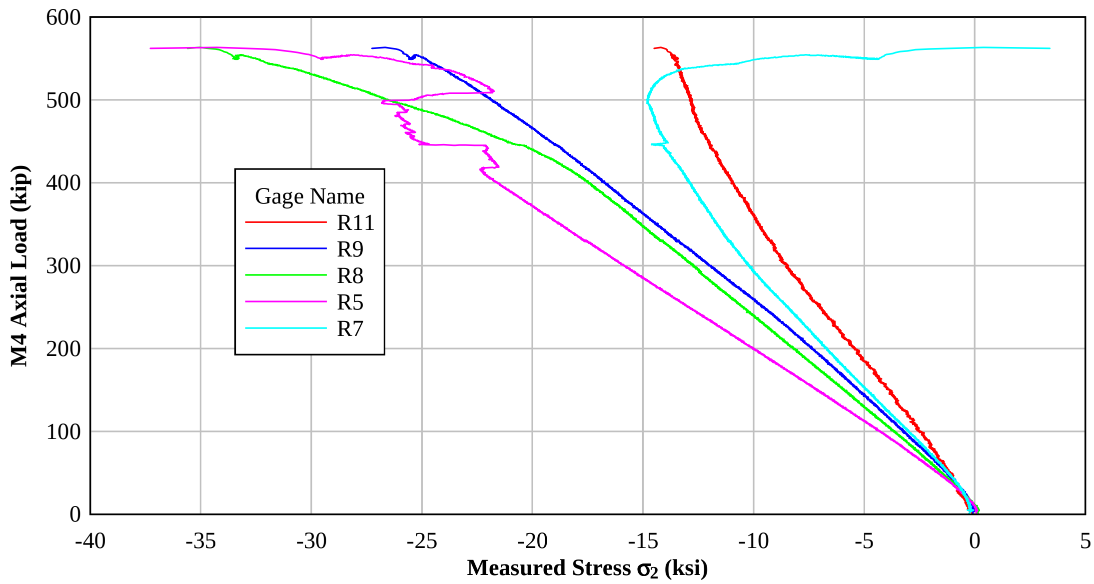

Fig. G-15: 2nd principle stress for all gages along Plane A-A

APPENDIX H. SPECIMEN #8 (RETROFIT #1) ADDITIONAL DATA

Specimen #8 was a ¼” thick set of gusset plates and is described in the second manuscript.

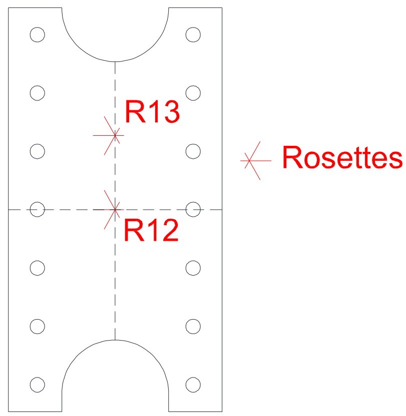

Fig. H-1: Instrumentation for retrofit plate

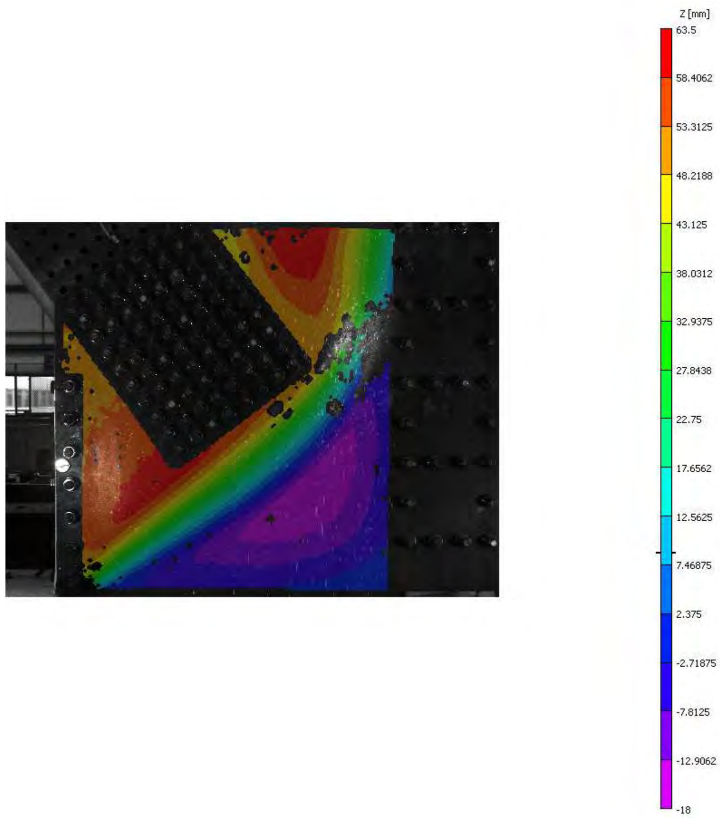

Fig. H-2: DIC measured out-of-plane deformation at failure

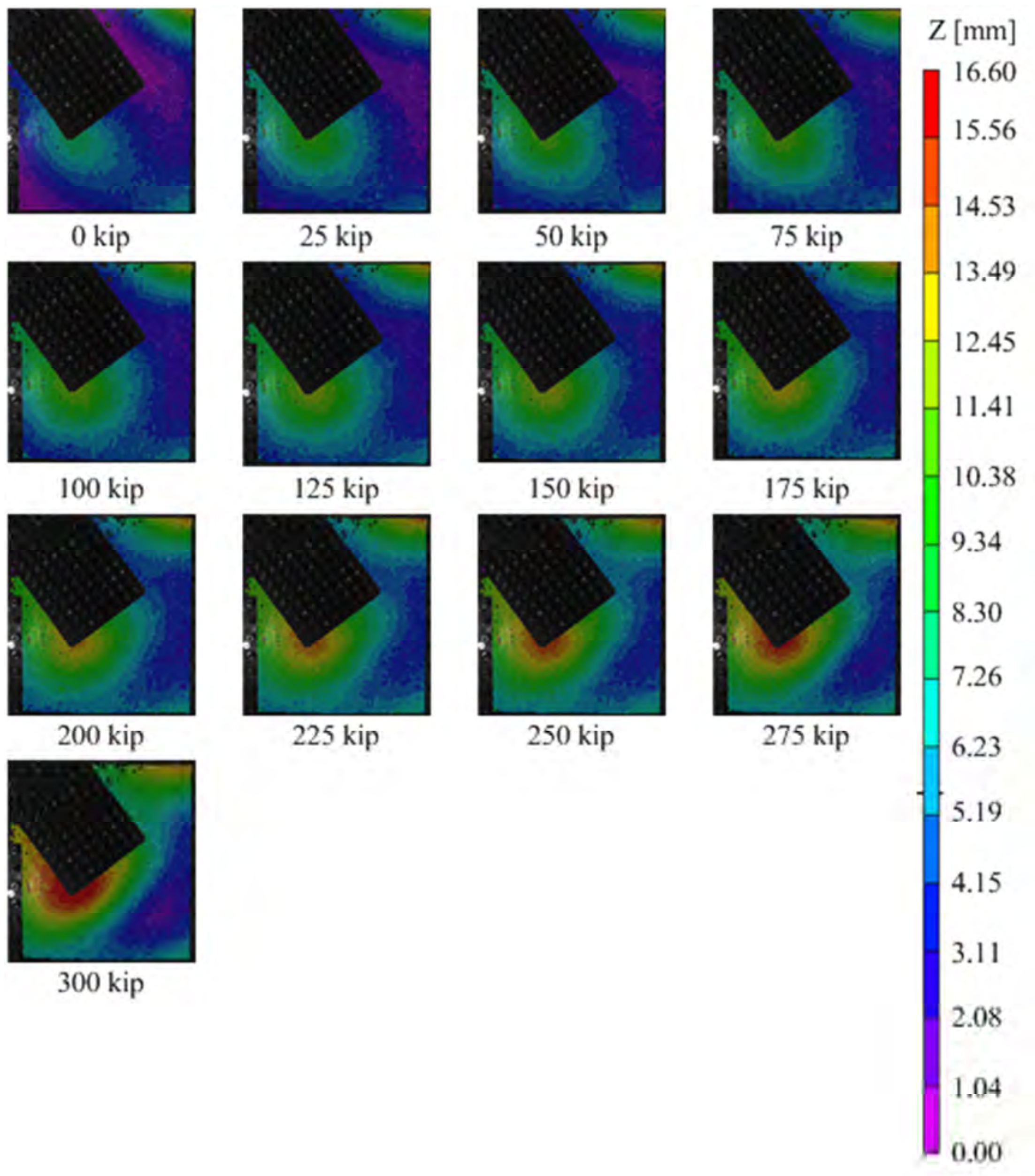

Fig. H-3: DIC measured out-of-plane deformation during loading (loads are M4 actuator loads)

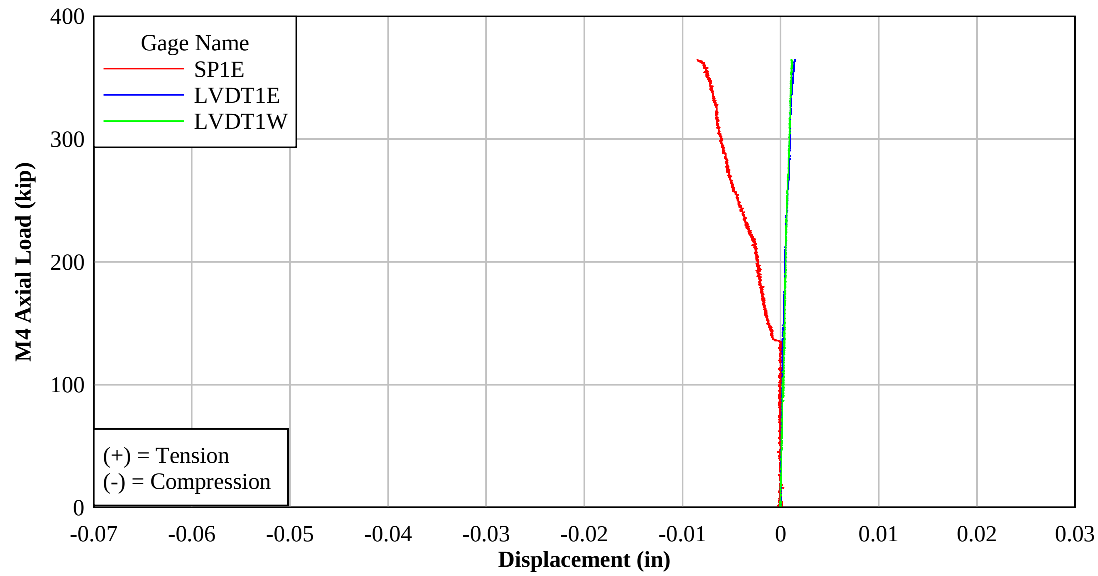

Fig. H-4: Member M1 bolt slip and relative member-to-work point displacement

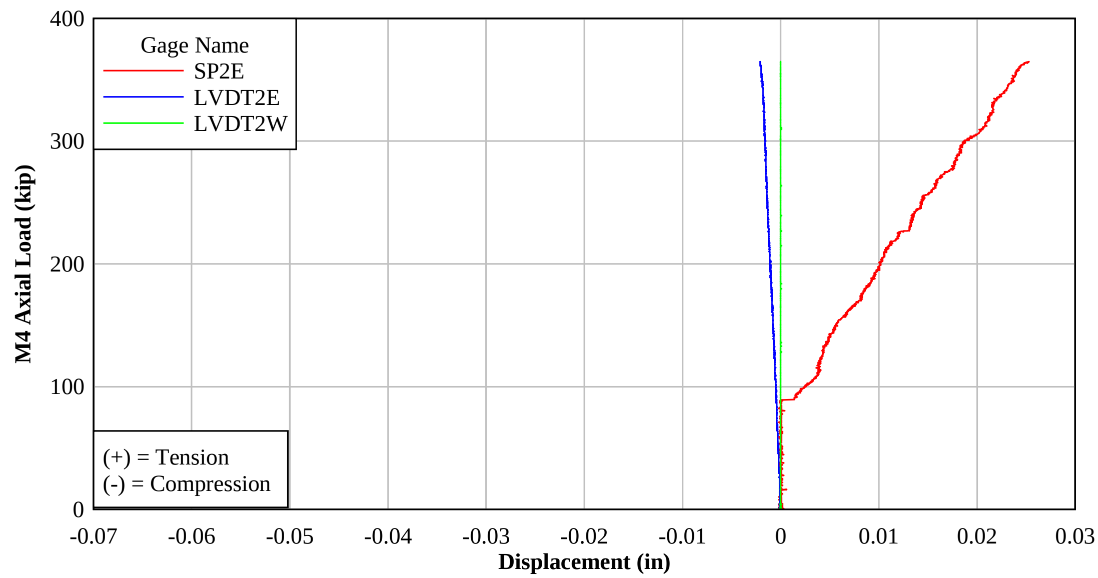

Fig. H-5: Member M2 bolt slip and relative member-to-work point displacement

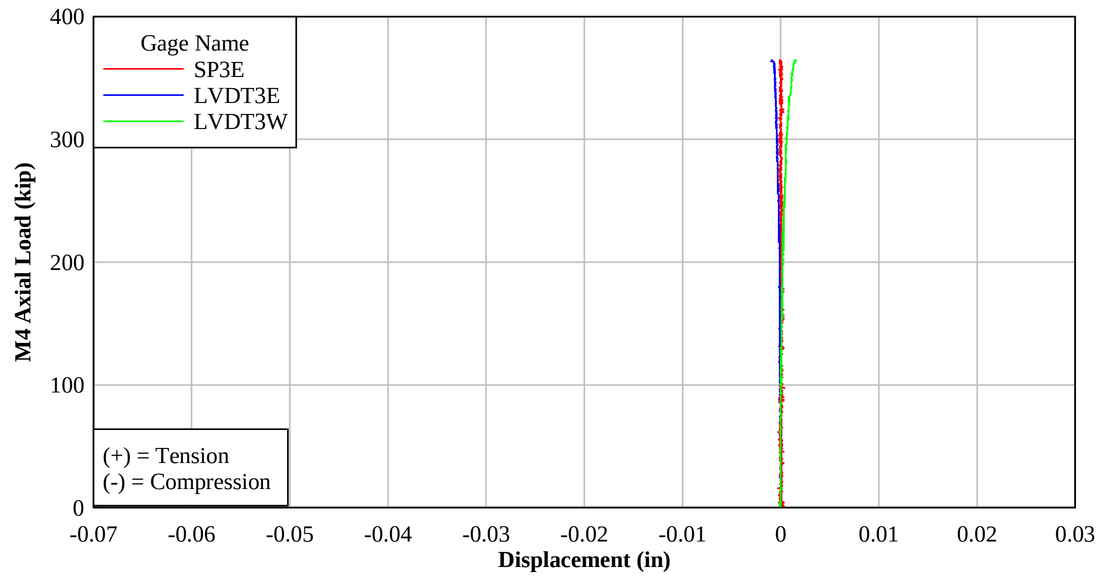

Fig. H-6: Member M3 bolt slip and relative member-to-work point displacement

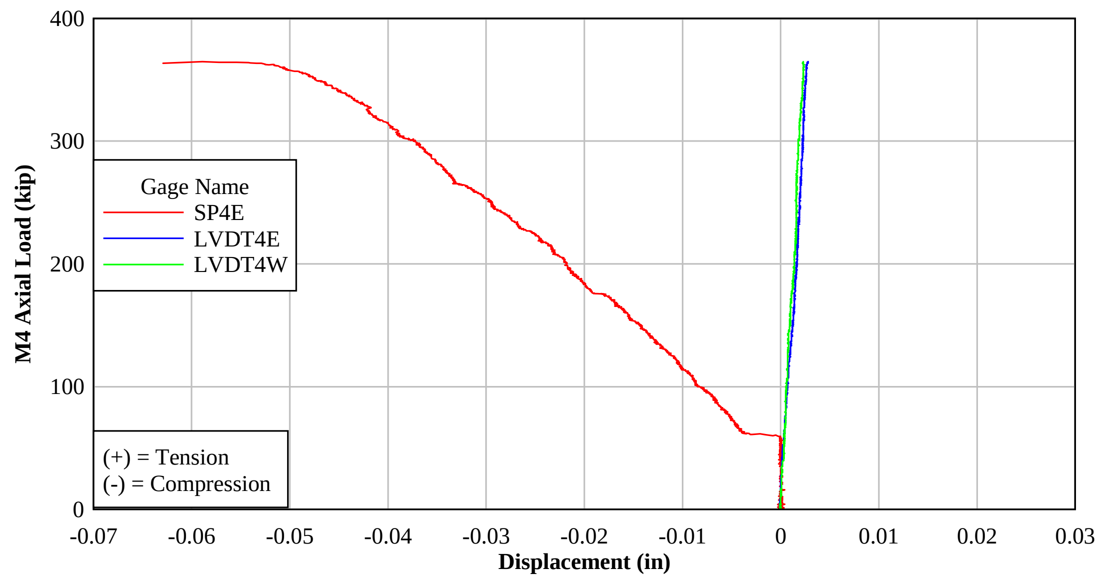

Fig. H-7: Member M4 bolt slip and relative member-to-work point displacement

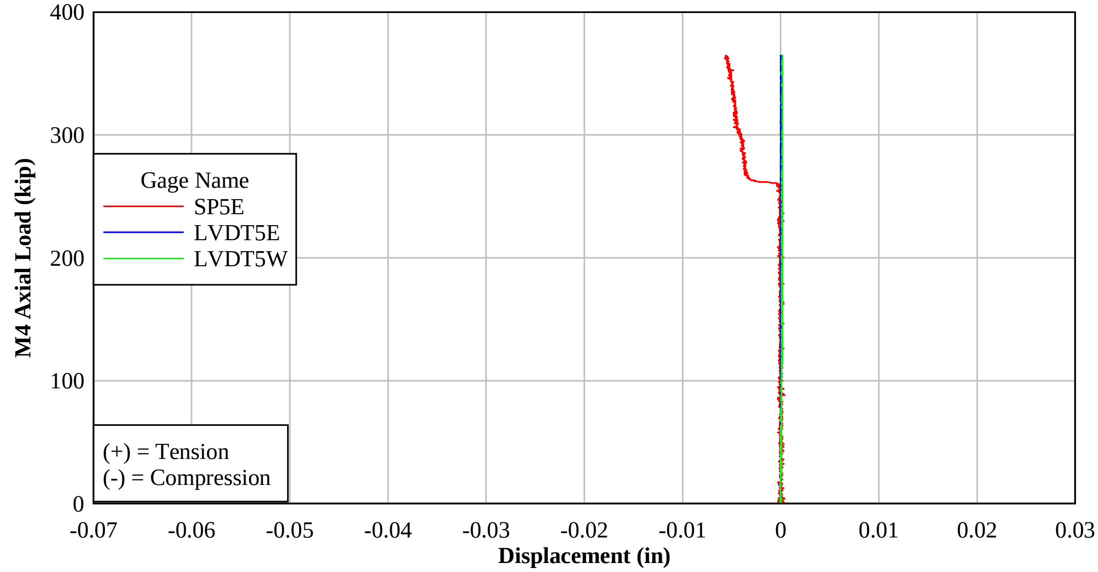

Fig. H-8: Member M5 bolt slip and relative member-to-work point displacement

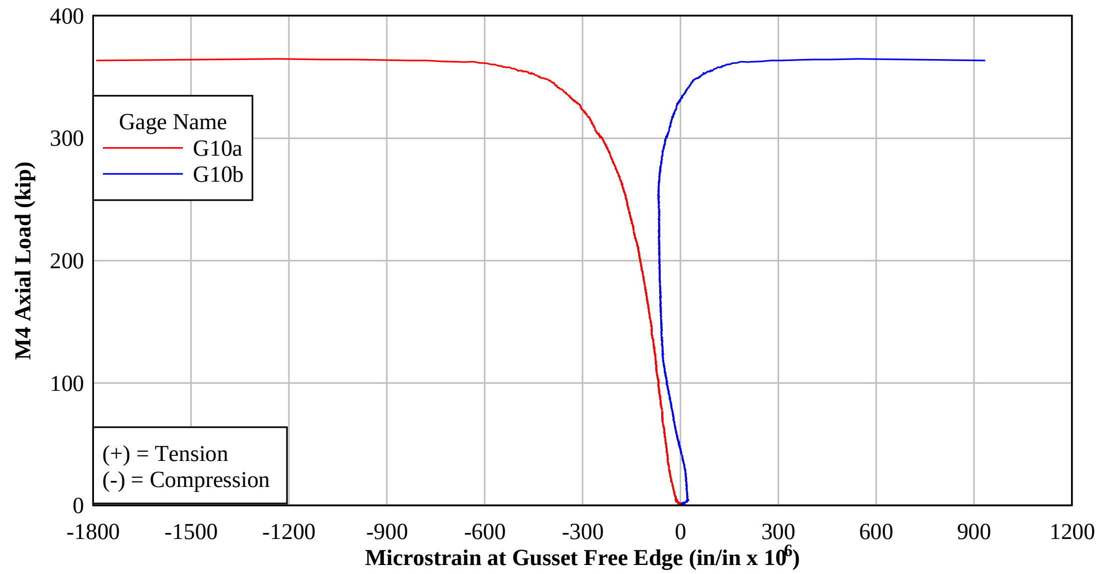

Fig. H-9: Gusset plate free edge strain versus M4 axial load

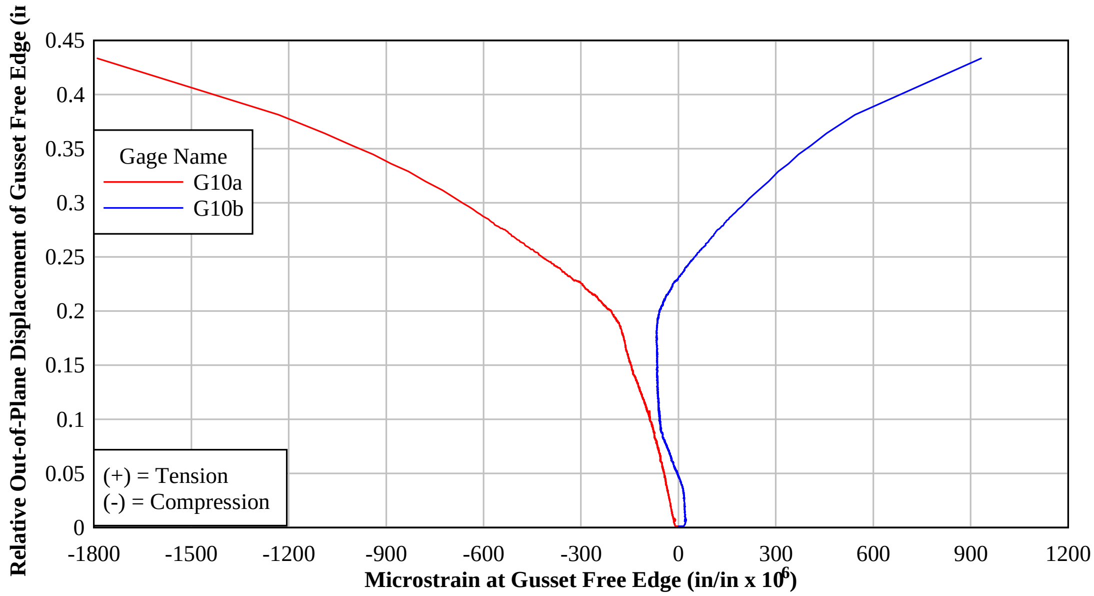

Fig. H-10: Gusset plate free edge strain versus out-of-plane displacement

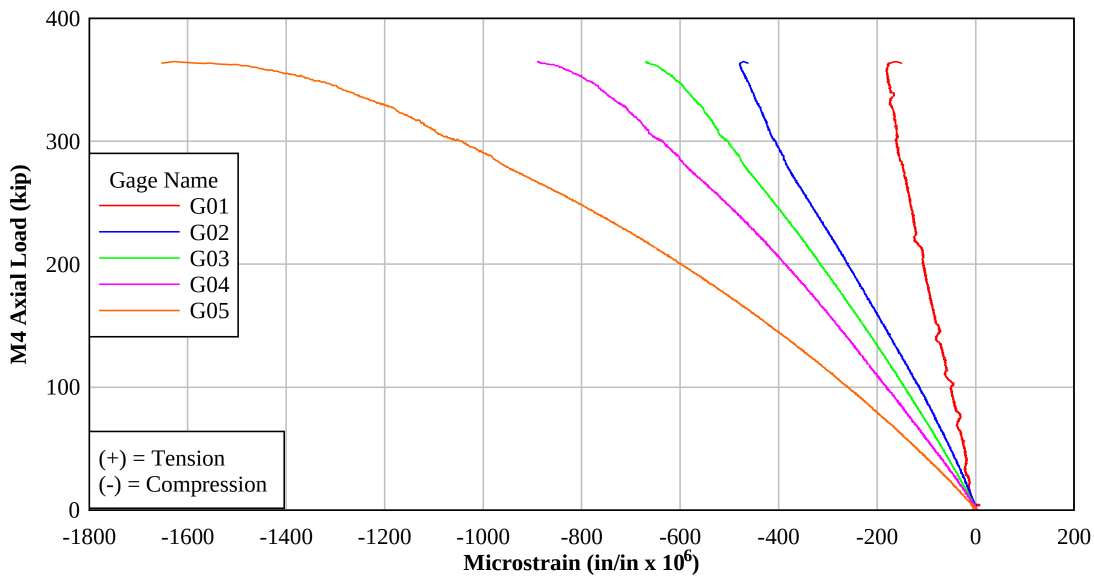

Fig. H-11: Strain in M4 connection versus M4 axial load

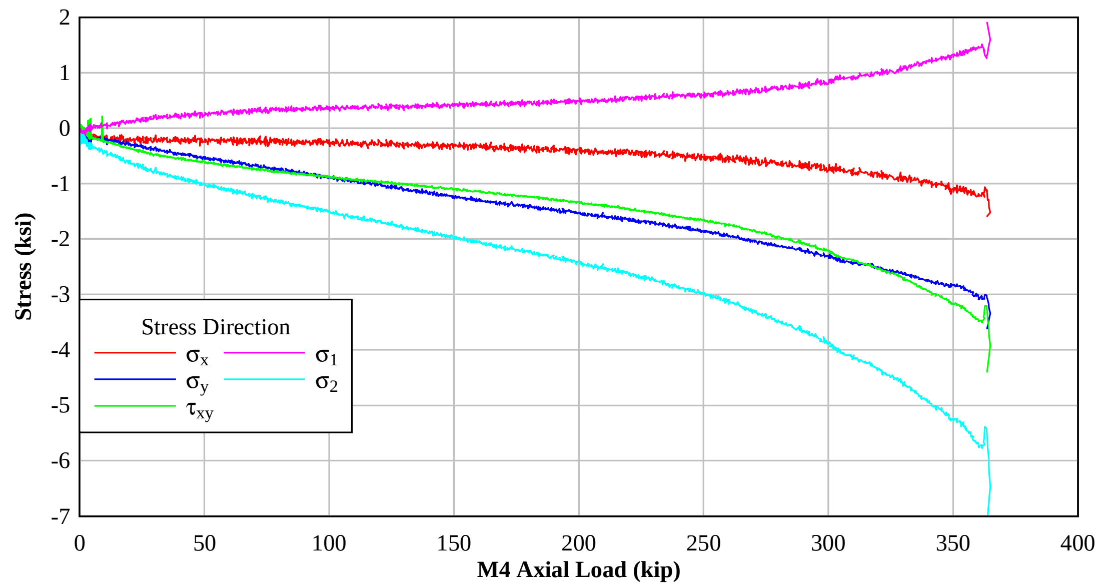

Fig. H-12: Retrofit plate stress at Gage R12 versus M4 axial load

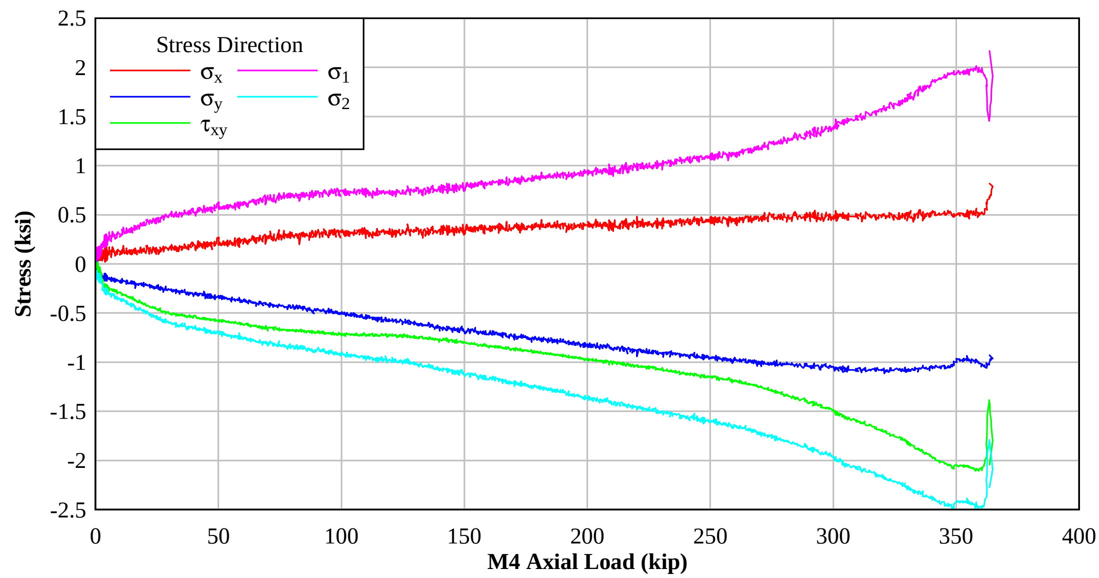

Fig. H-13: Retrofit plate stress at Gage R13 versus M4 axial load

APPENDIX I. SPECIMEN #9 (RETROFIT #2) ADDITIONAL DATA

Specimen #9 was a ¼” thick set of gusset plates and is described in the second manuscript.

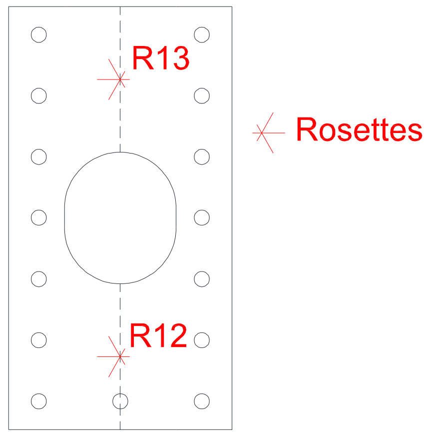

Fig. I-1: Instrumentation for retrofit plate

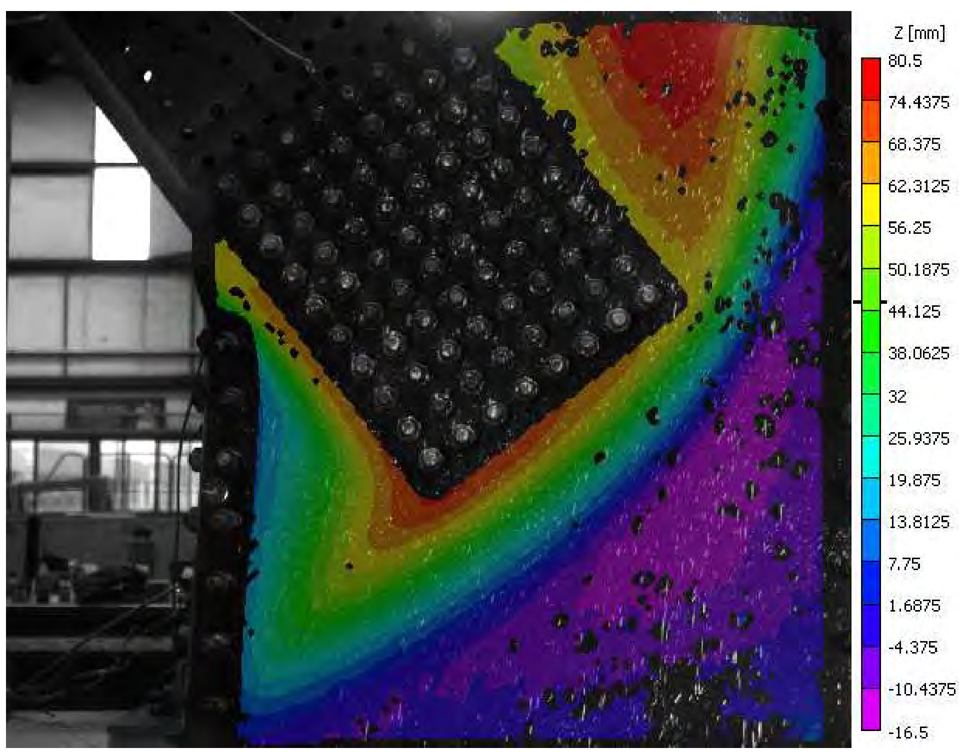

Fig. I-2: DIC measured out-of-plane deformation at failure

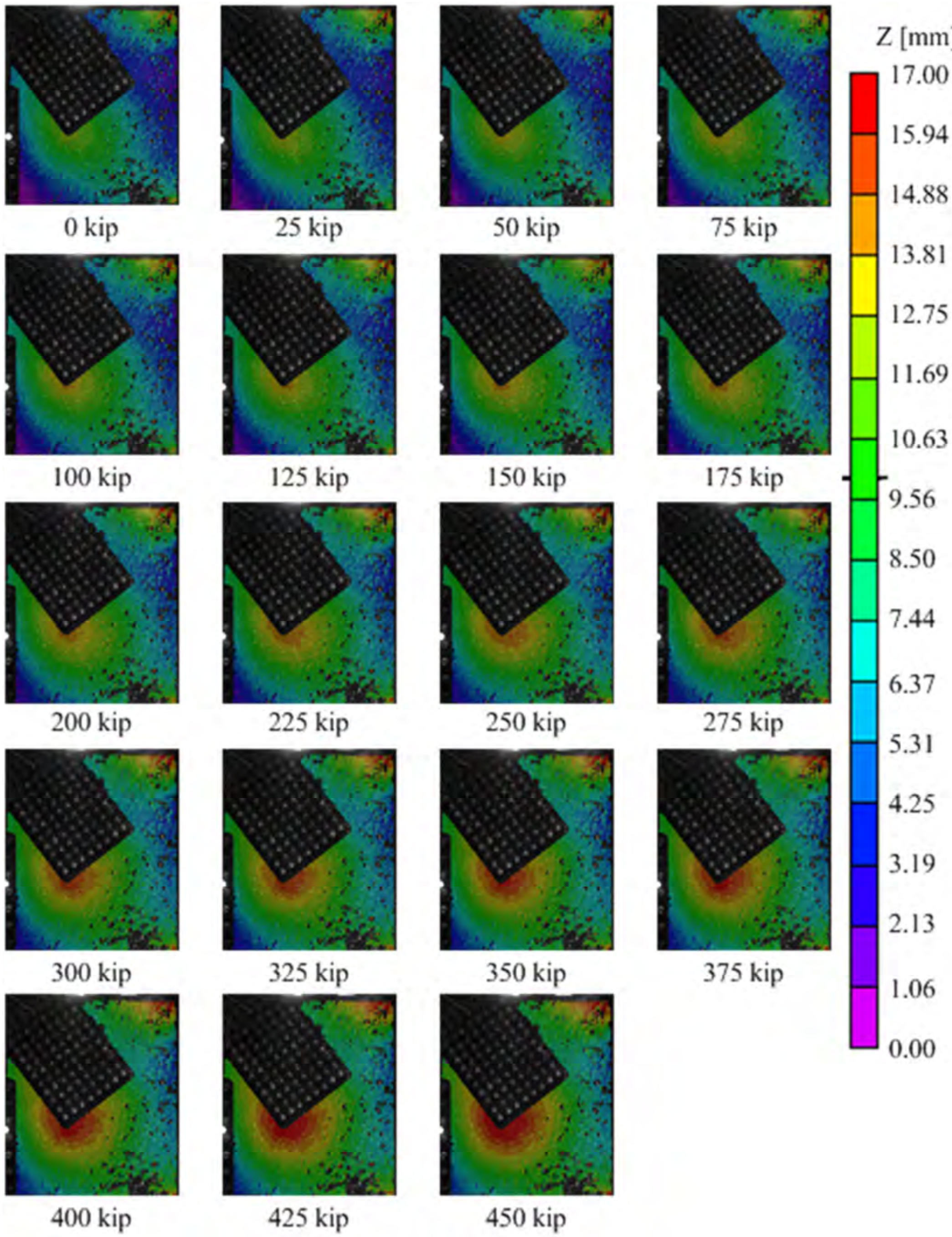

Fig. I-3: DIC measured out-of-plane deformation during loading (loads are M4 actuator loads)

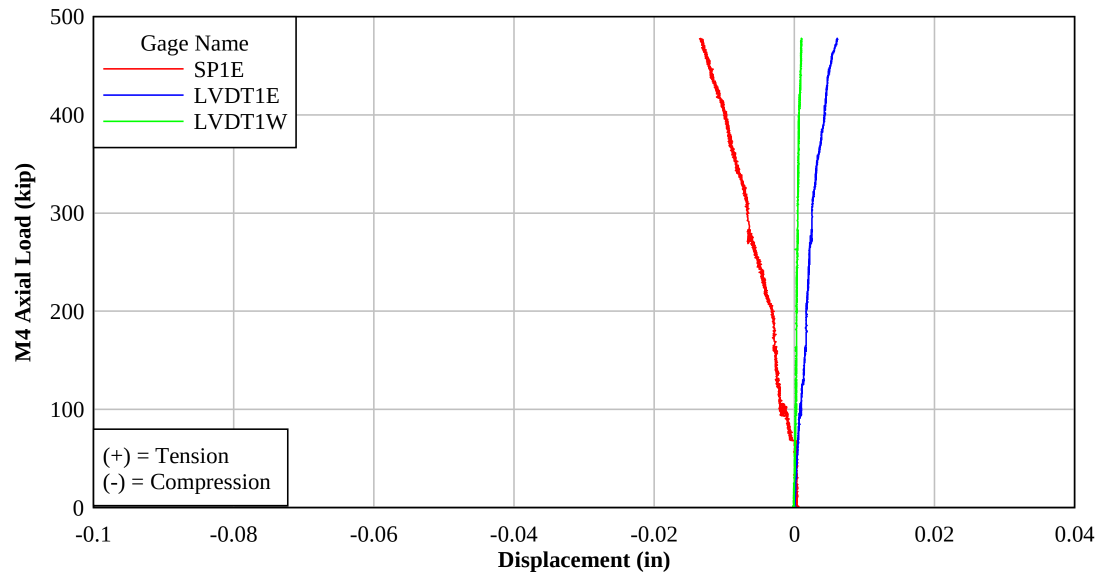

Fig. I-4: Member M1 bolt slip and relative member-to-work point displacement

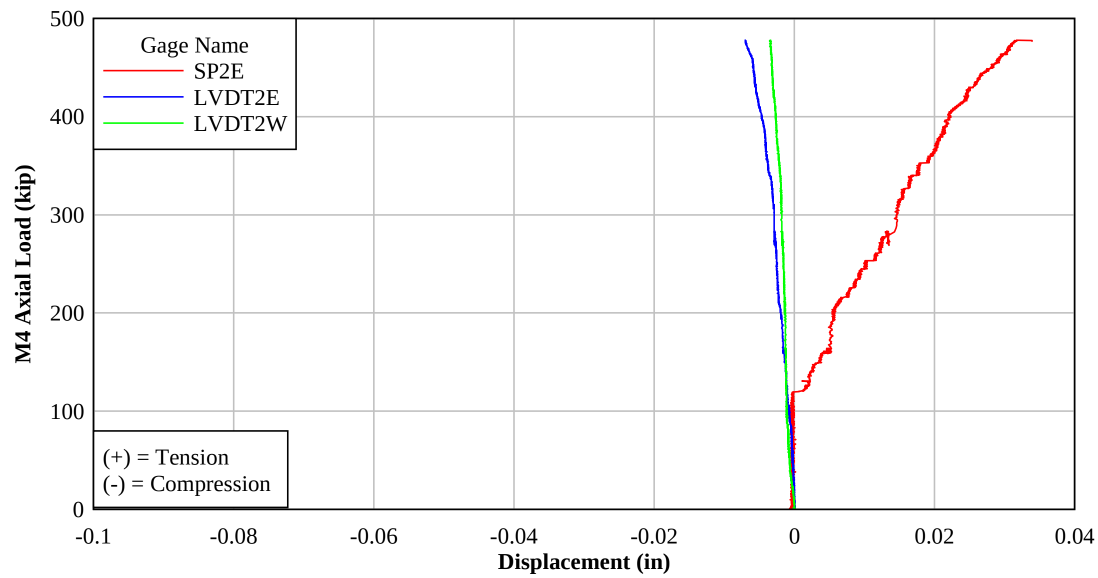

Fig. I-5: Member M2 bolt slip and relative member-to-work point displacement

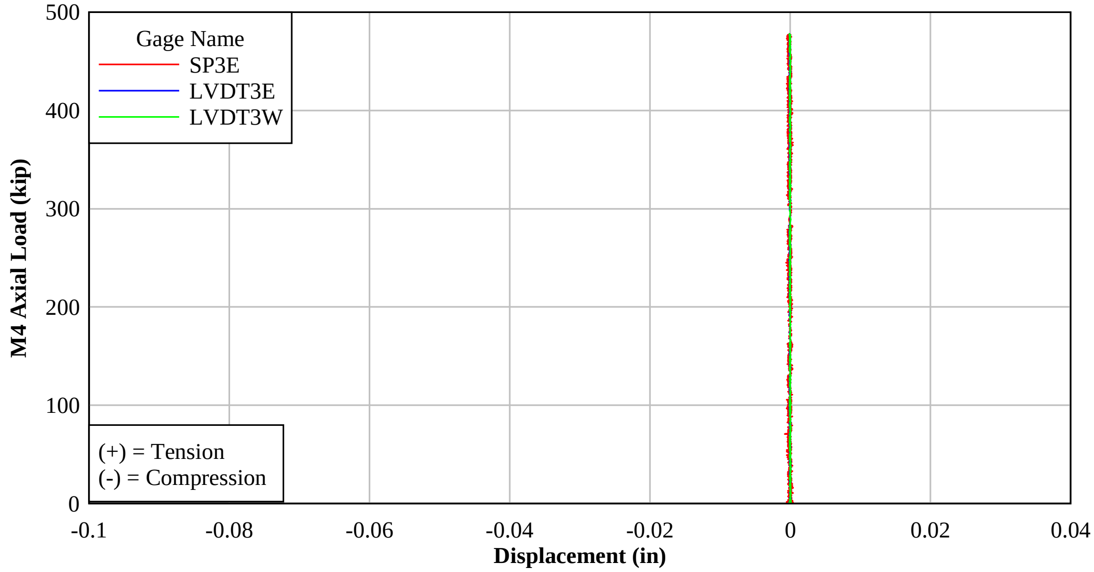

Fig. I-6: Member M3 bolt slip and relative member-to-work point displacement

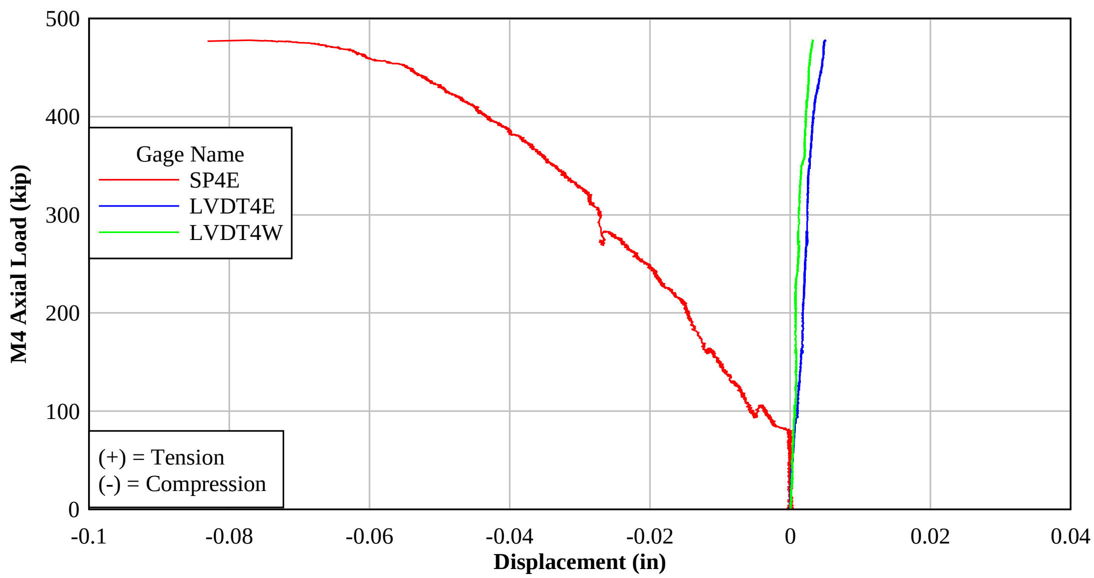

Fig. I-7: Member M4 bolt slip and relative member-to-work point displacement

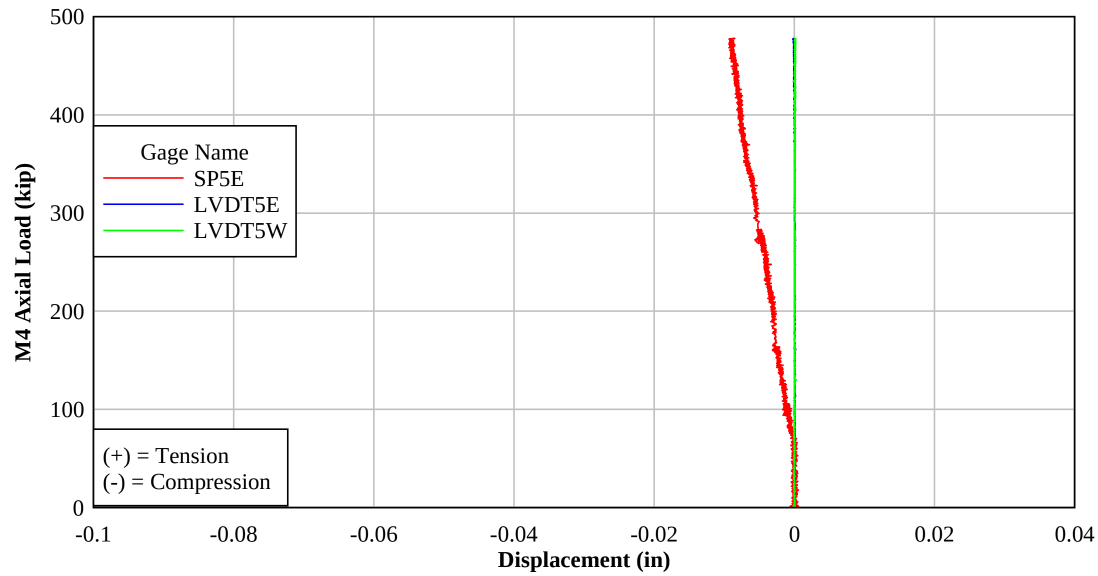

Fig. I-8: Member M5 bolt slip and relative member-to-work point displacement

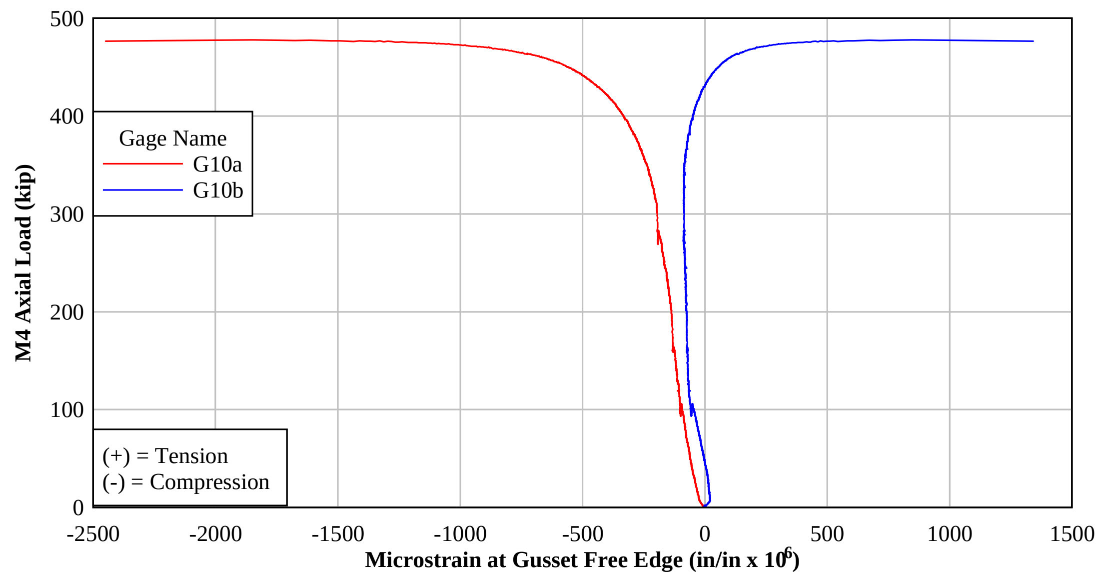

Fig. I-9: Gusset plate free edge strain versus M4 axial load

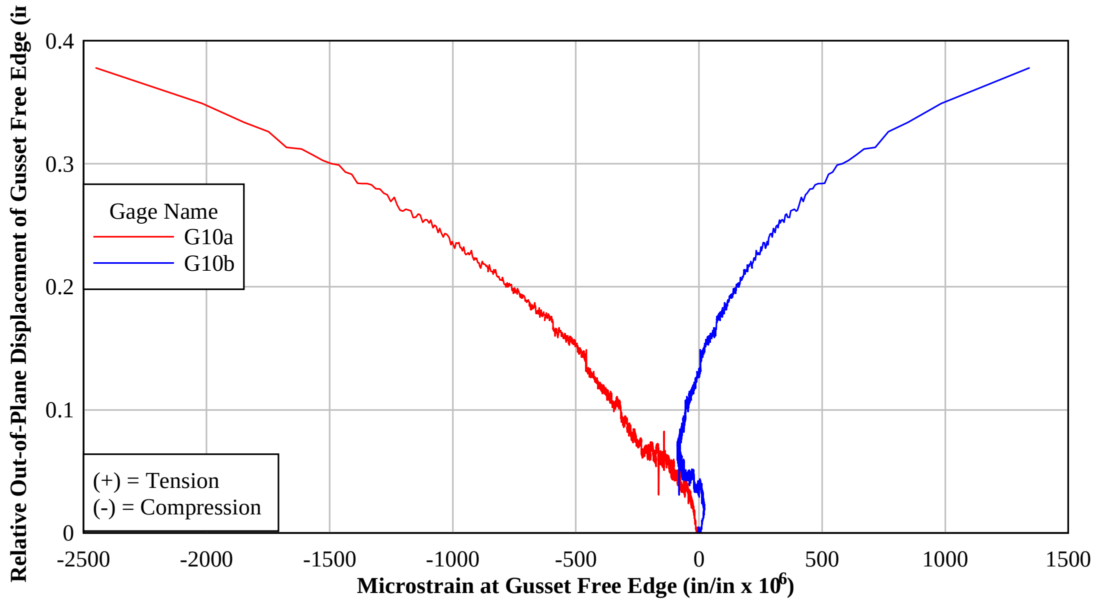

Fig. I-10: Gusset plate free edge strain versus out-of-plane displacement

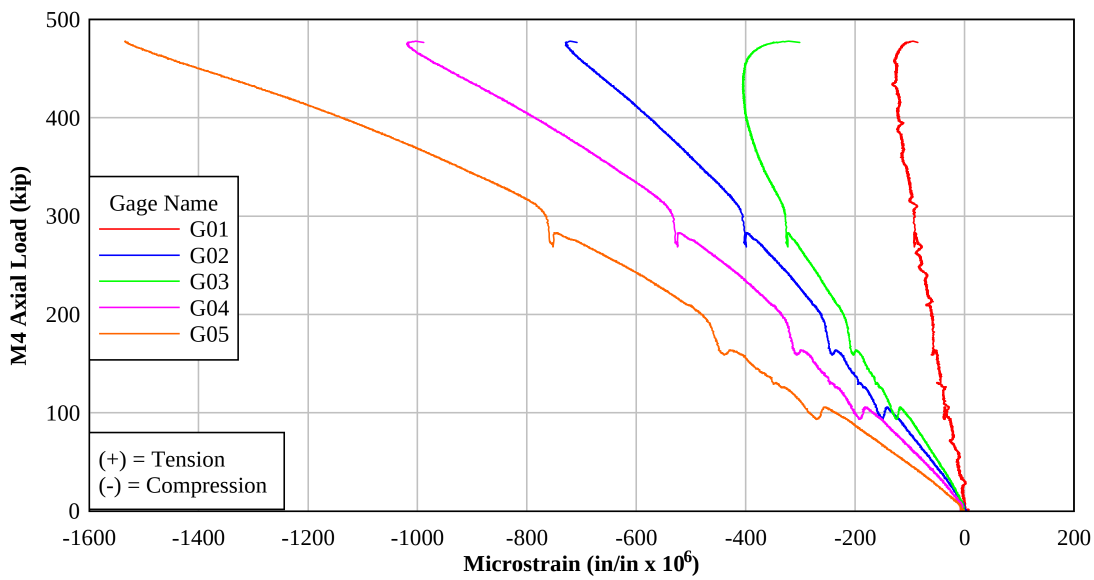

Fig. I-11: Strain in M4 connection versus M4 axial load

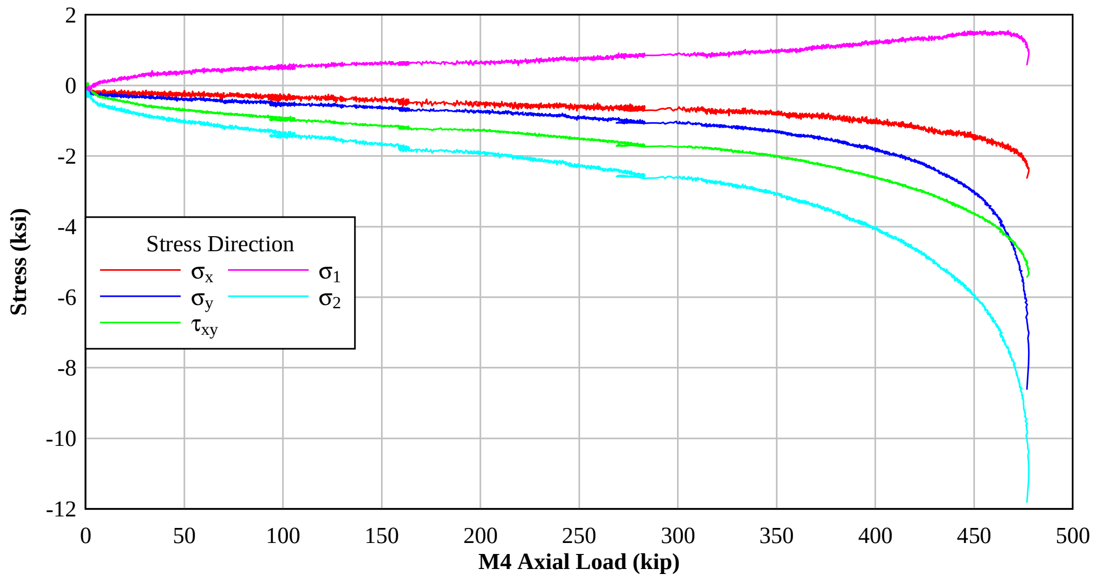

Fig. I-12: Retrofit plate stress at gage R12 versus M4 axial load

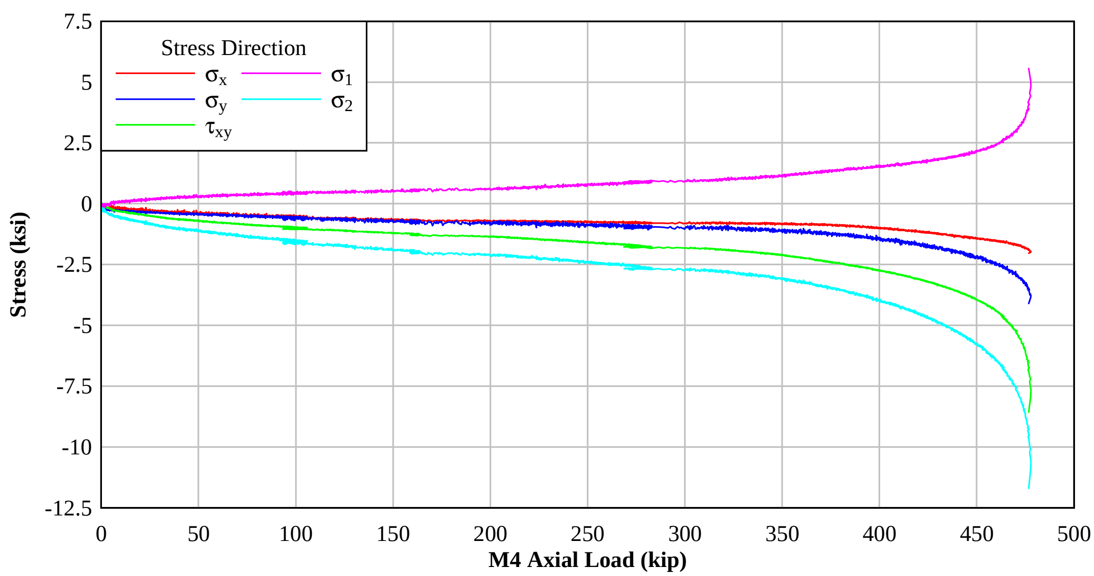

Fig. I-13: Retrofit plate stresses at gage R13 versus M4 axial load

APPENDIX J. STRESS COMPARISONS

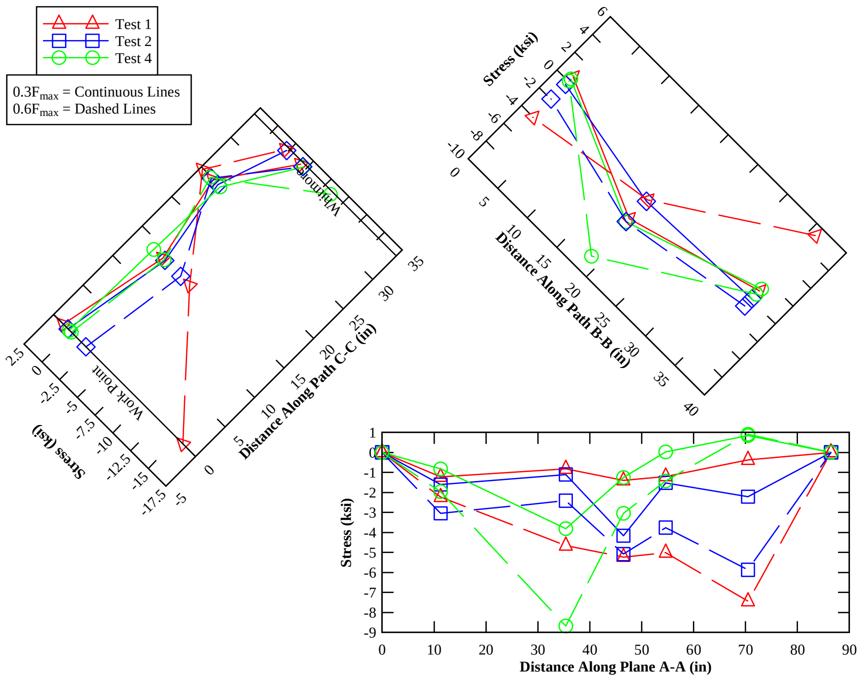

Fig. J-1: 1/4" plates, stress in global x direction

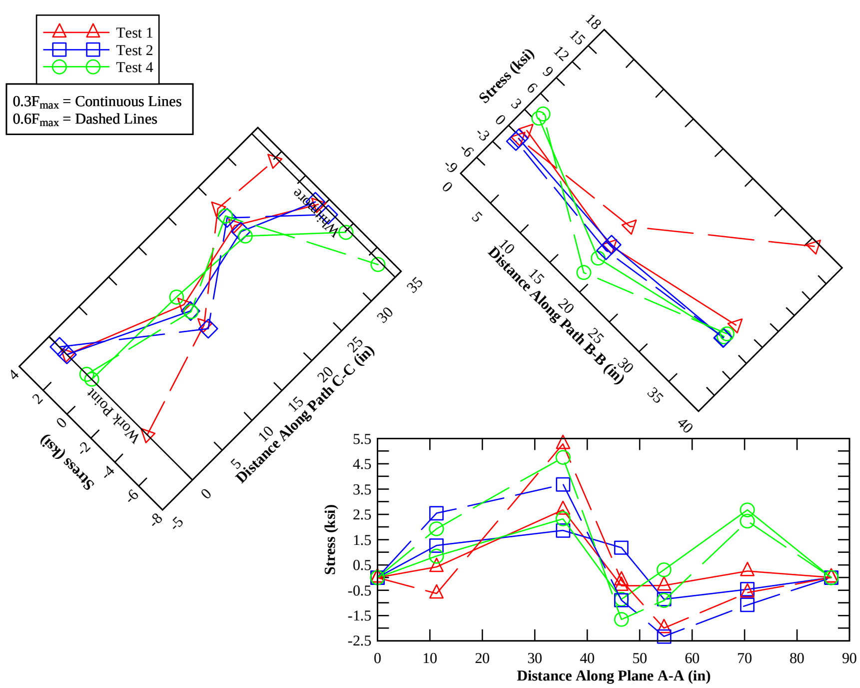

Fig. J-2: 1/4" plates, stress in global y direction

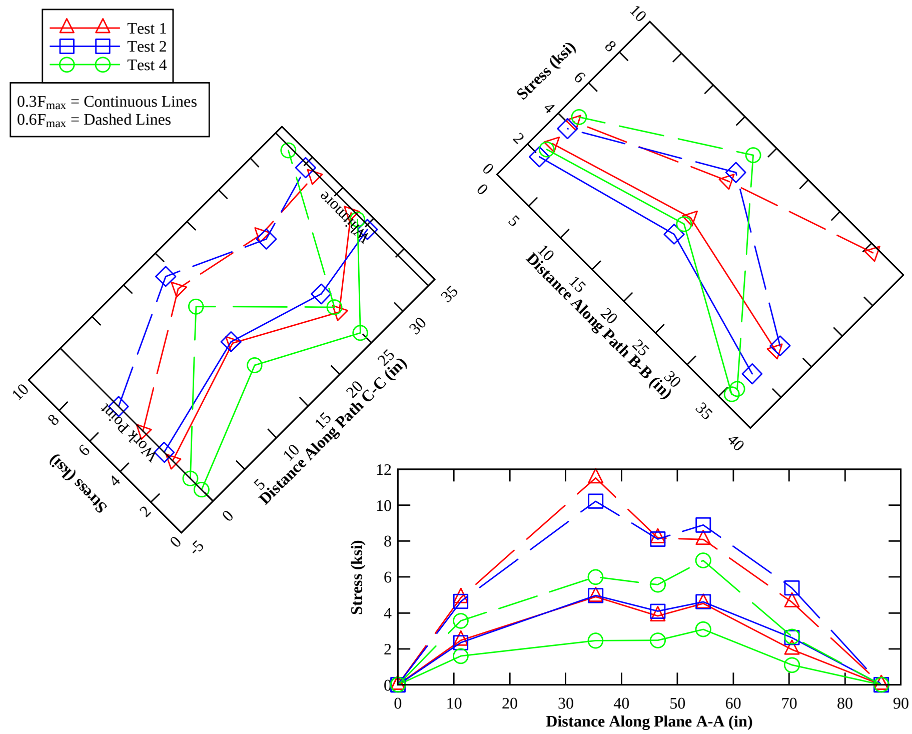

Fig. J-3: 1/4" plates, shear stress in global xy direction

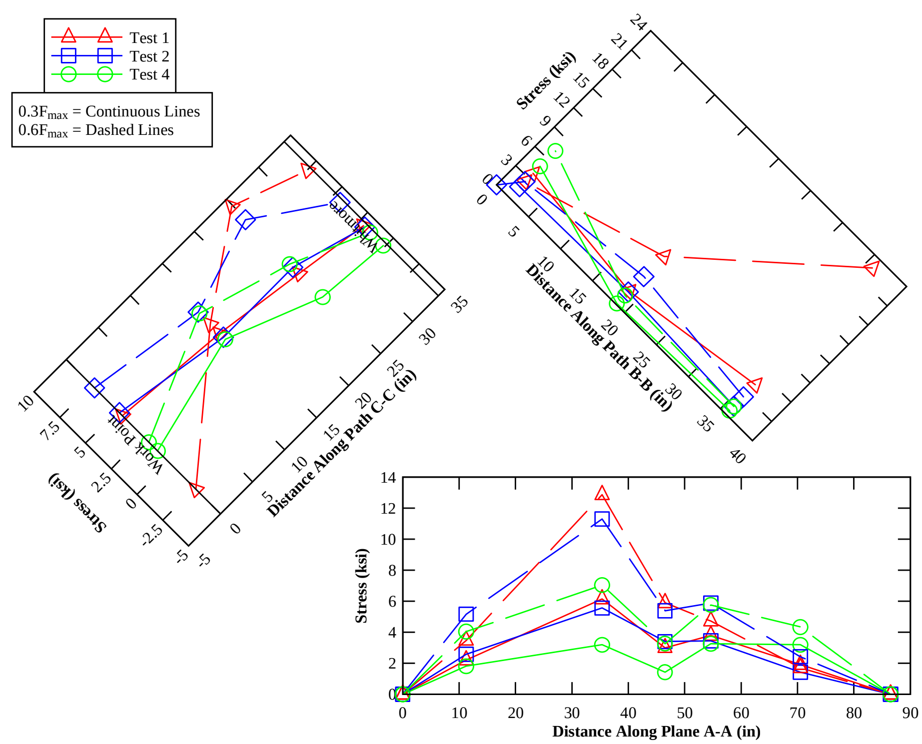

Fig. J-4: 1/4" plates, 1st principle stress

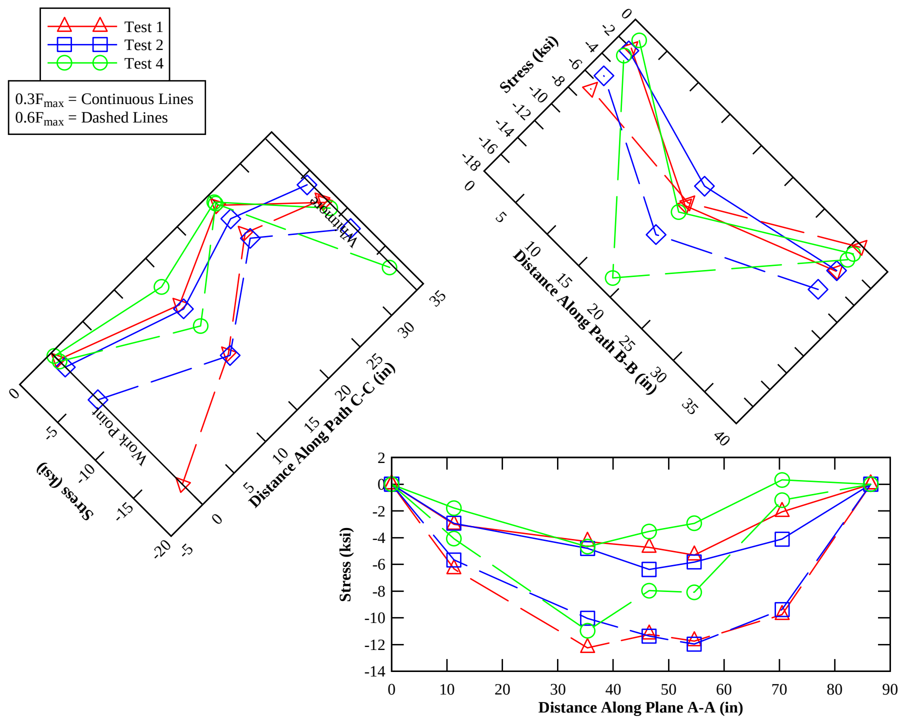

Fig. J-5: 1/4" plates, 2nd principle stress

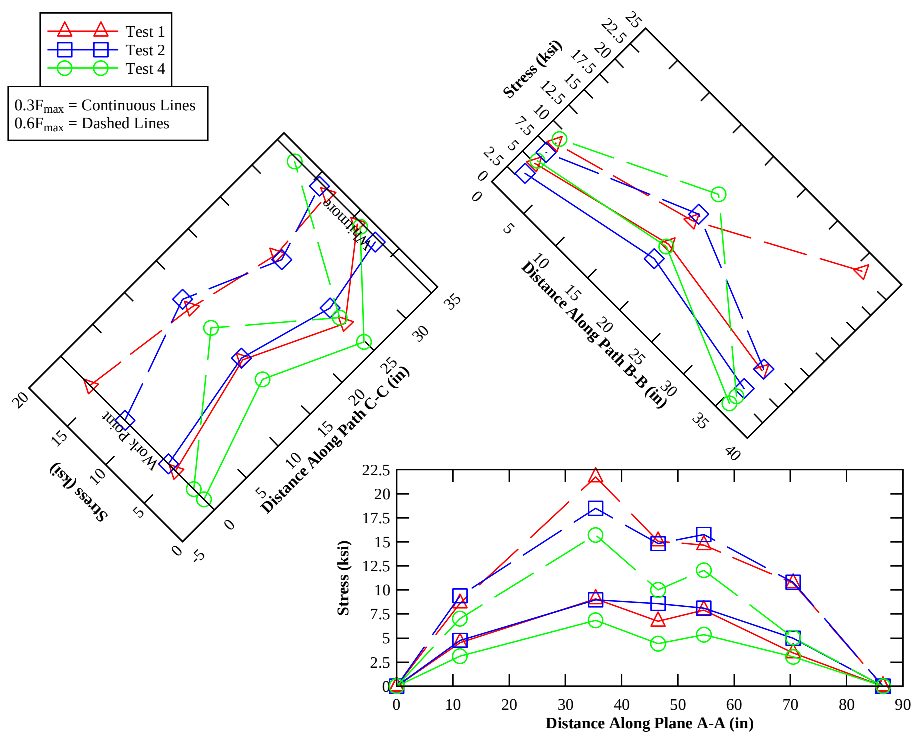

Fig. J-6: 1/4" plates, Von Mises stress

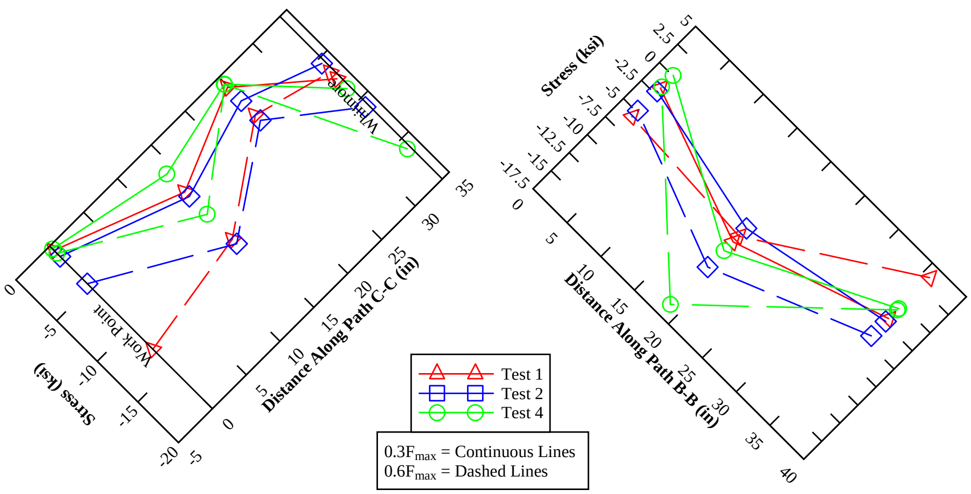

Fig. J-7: 1/4" plates, stress in M4 direction

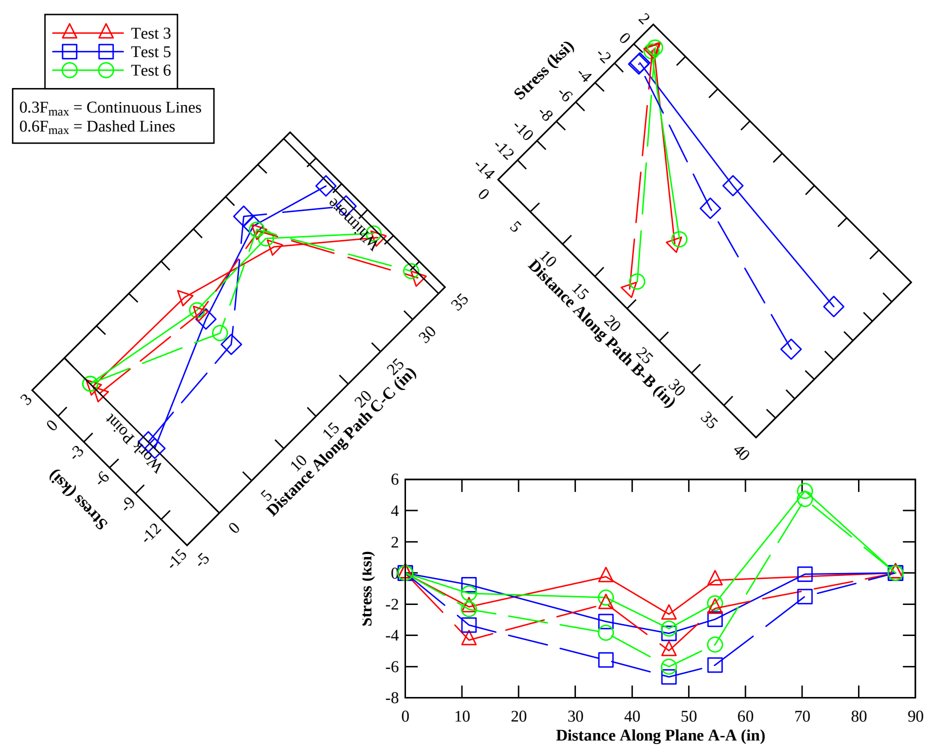

Fig. J-8: 3/8" plates, stress in global x direction

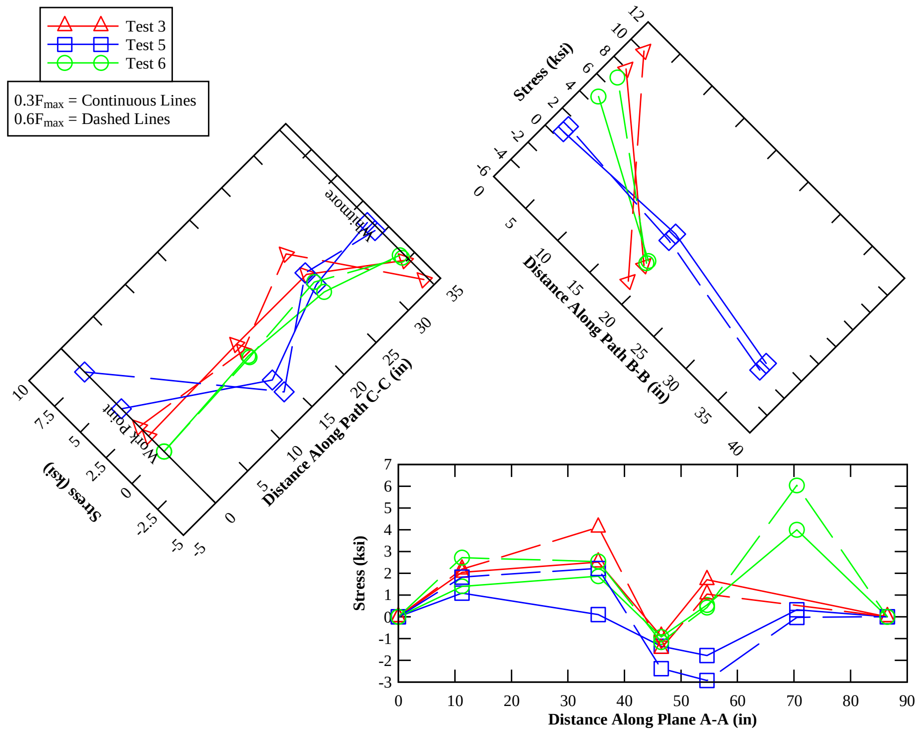

Fig. J-9: 3/8" plates, stress in global y direction

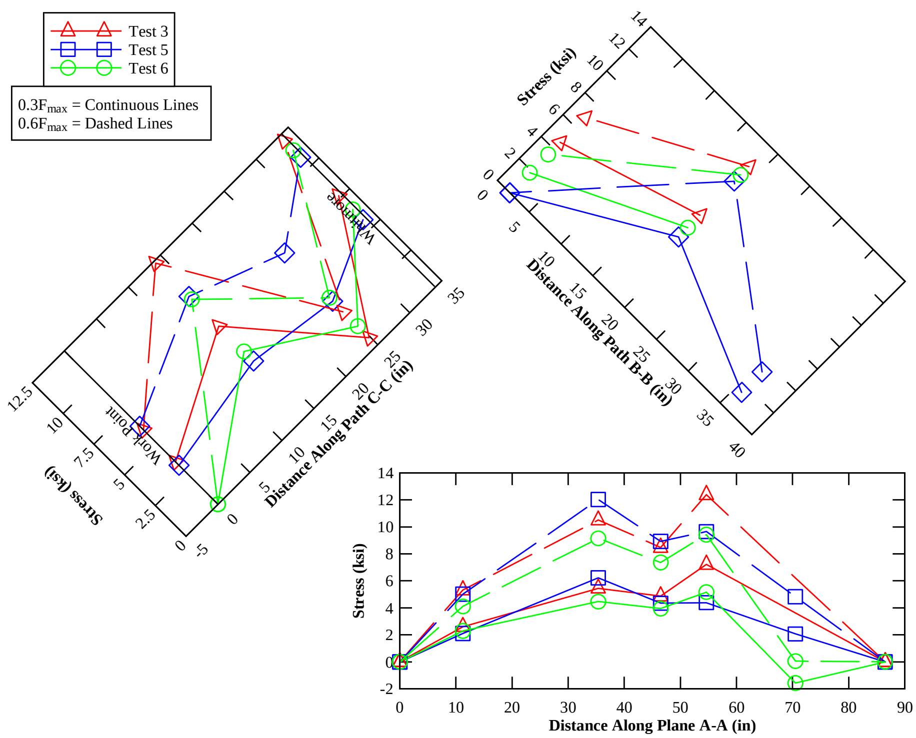

Fig. J-10: 3/8" plates, shear stress in global xy direction

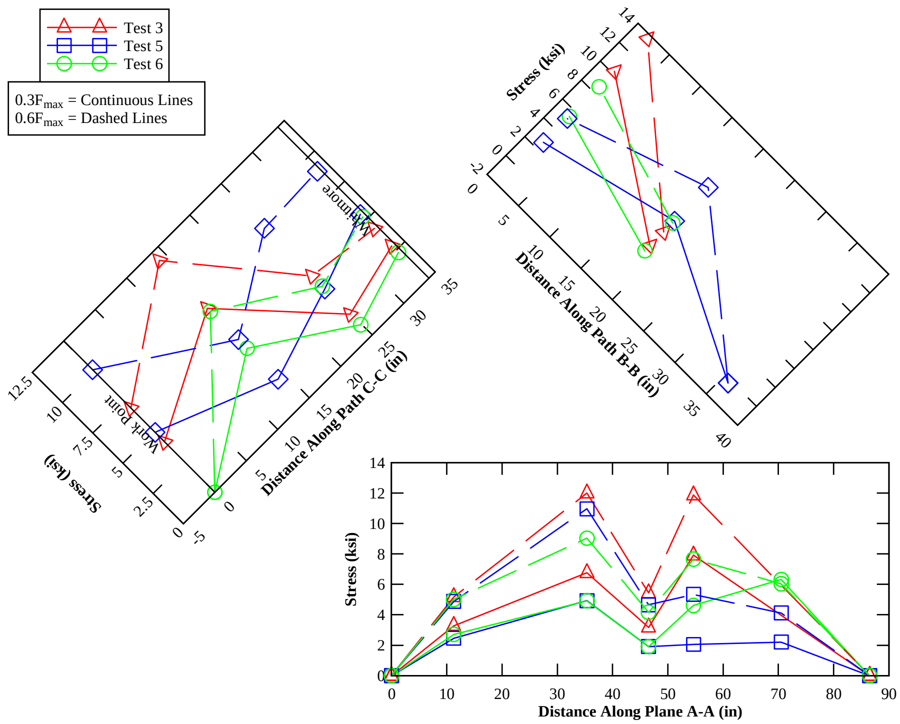

Fig. J-11: 3/8" plates, 1st principle stress

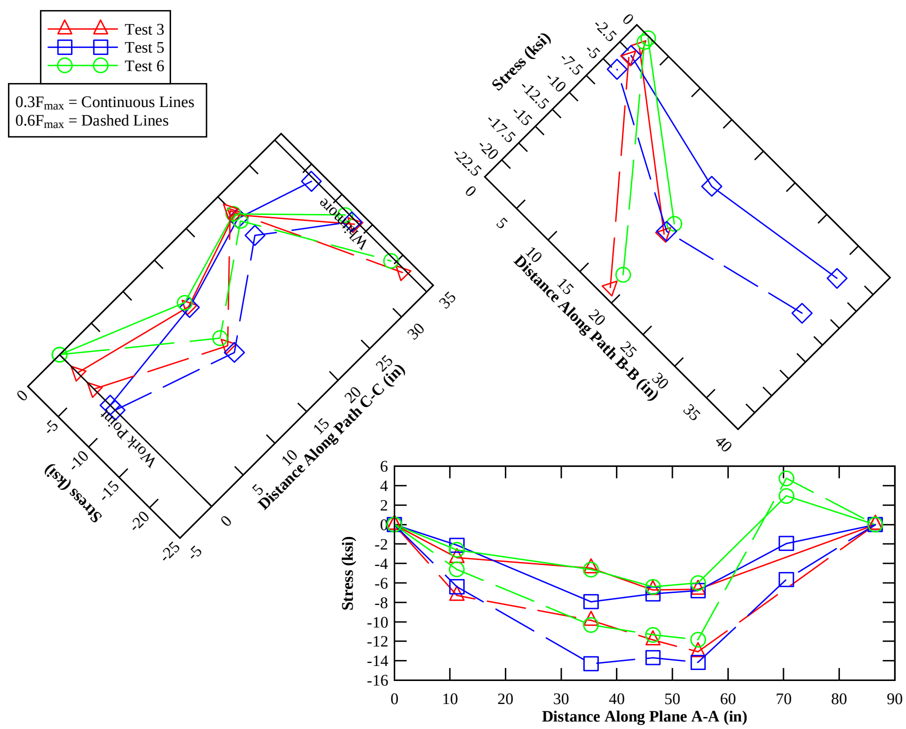

Fig. J-12: 3/8" plates, 2nd principle stress

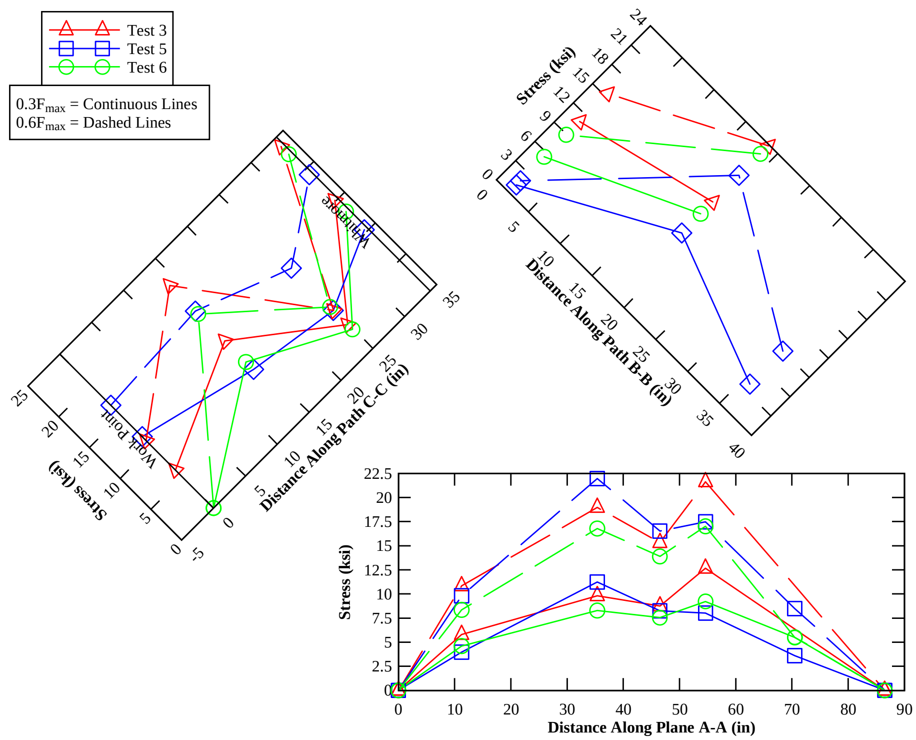

Fig. J-13: 3/8" plates, Von Mises stress

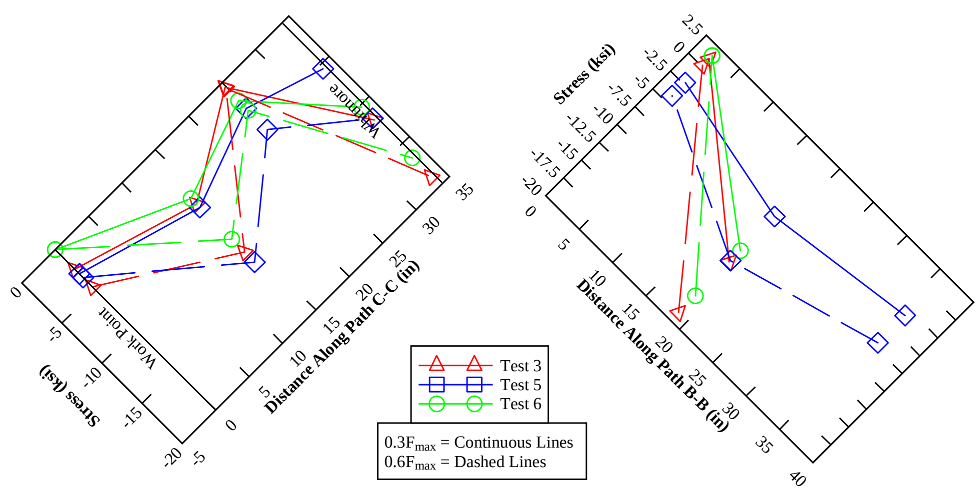

Fig. J-14: 3/8" plates, stress in M4 direction

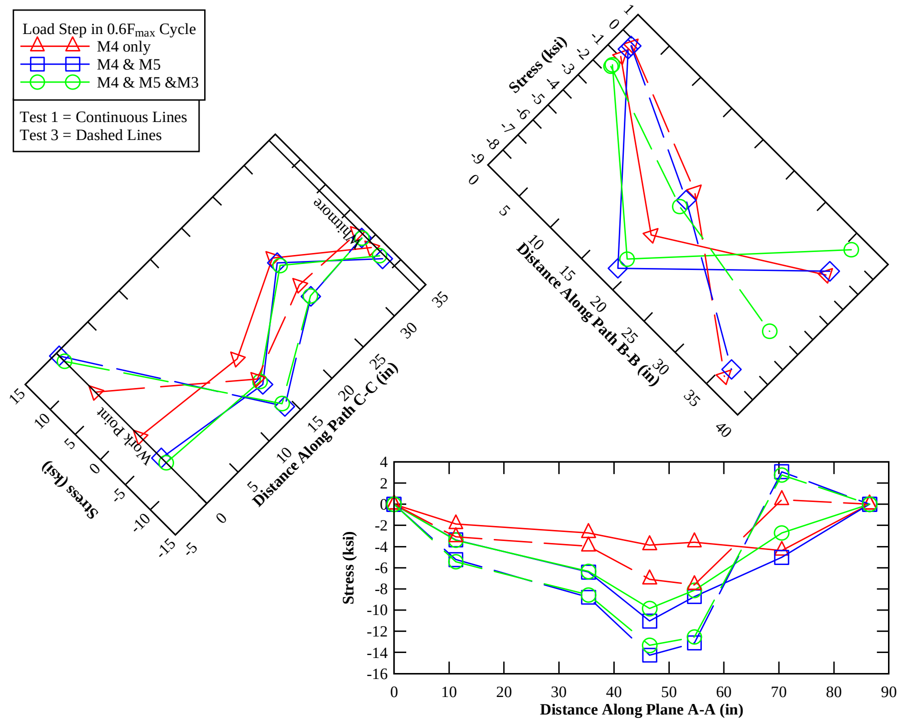

Fig. J-15: Combination loading, stress in global x direction

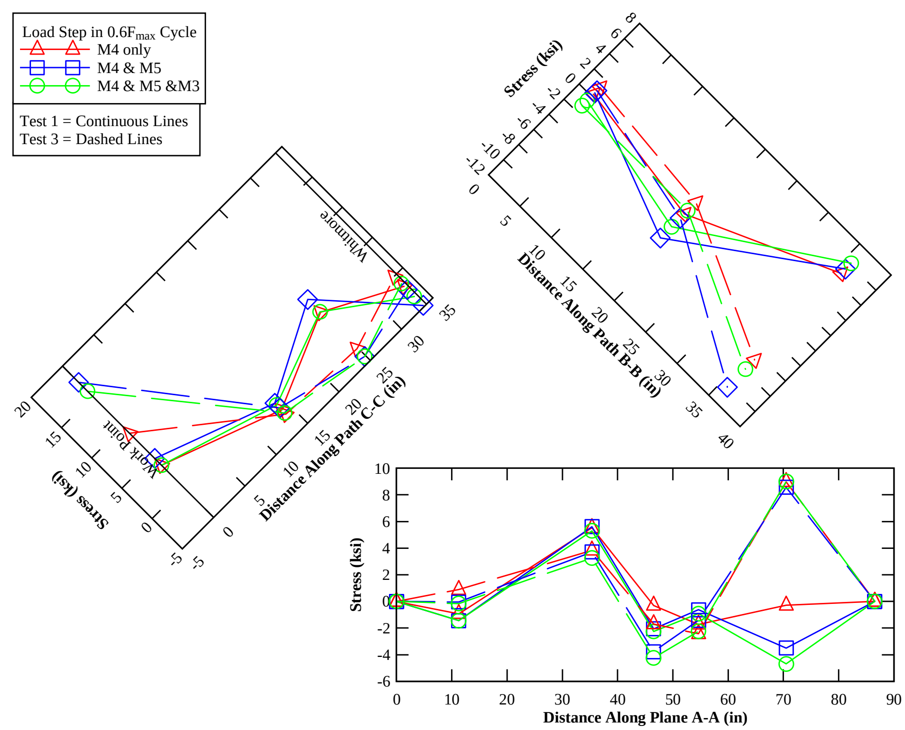

Fig. J-16: Combination loading, stress in global y direction

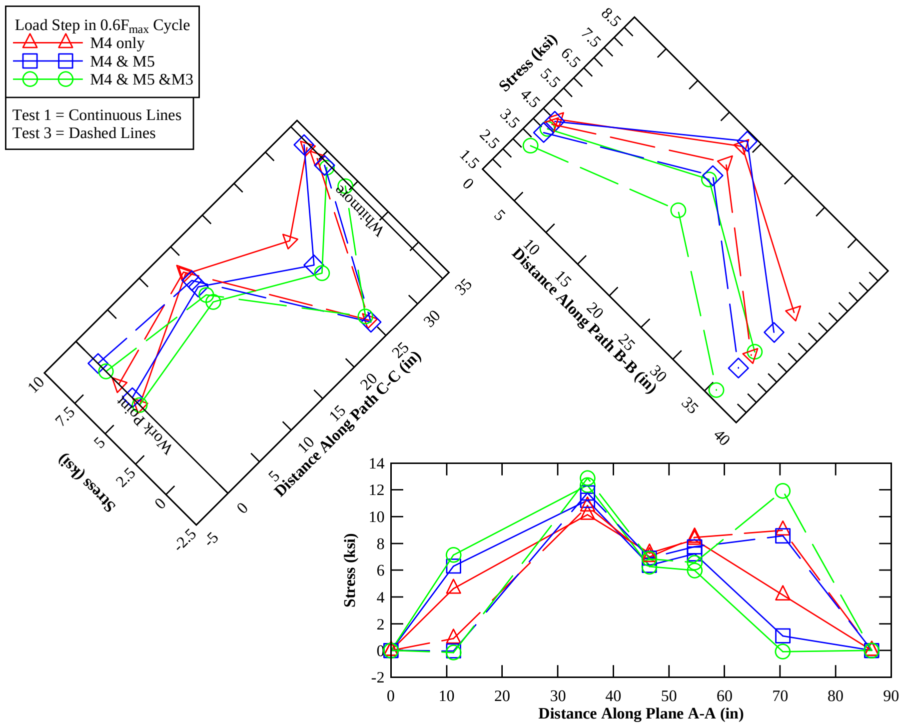

Fig. J-17: Combination loading, shear stress in global xy direction

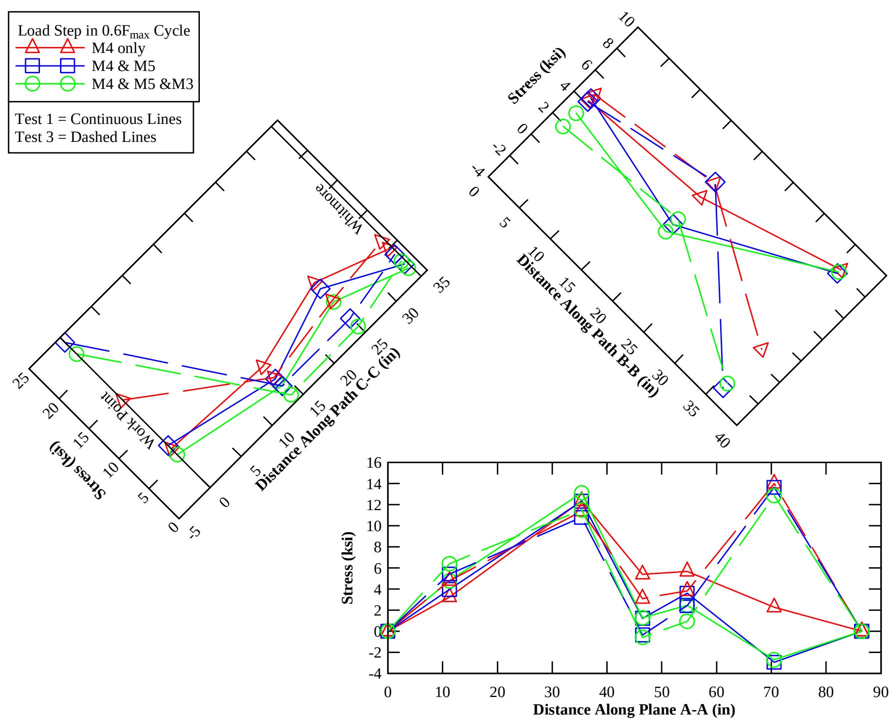

Fig. J-18: Combined loading, 1st principle stress

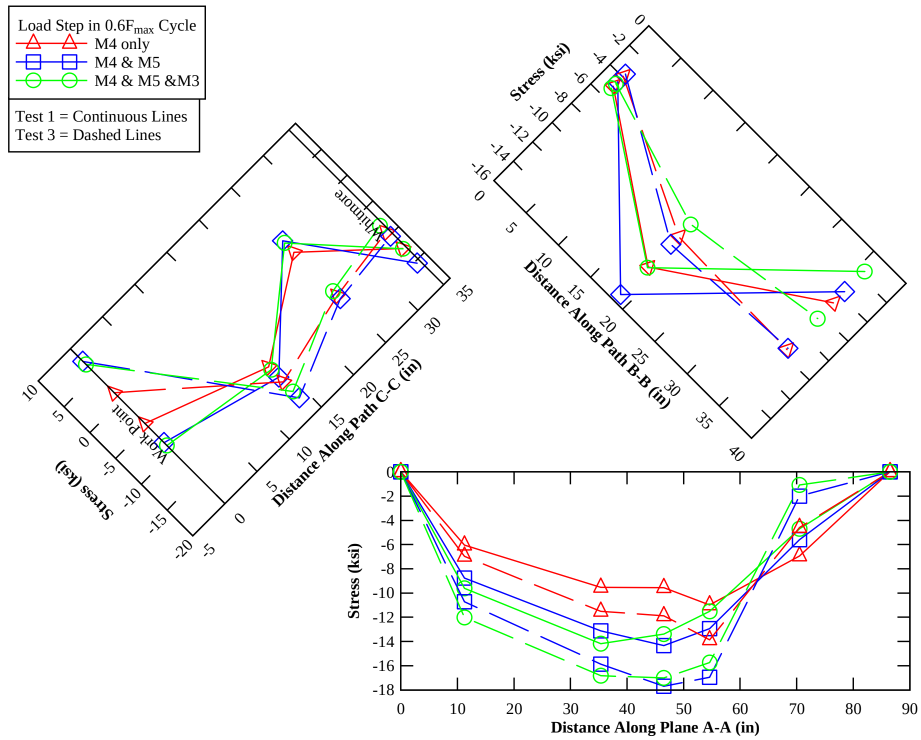

Fig. J-19: Combination loading, 2nd principle stress

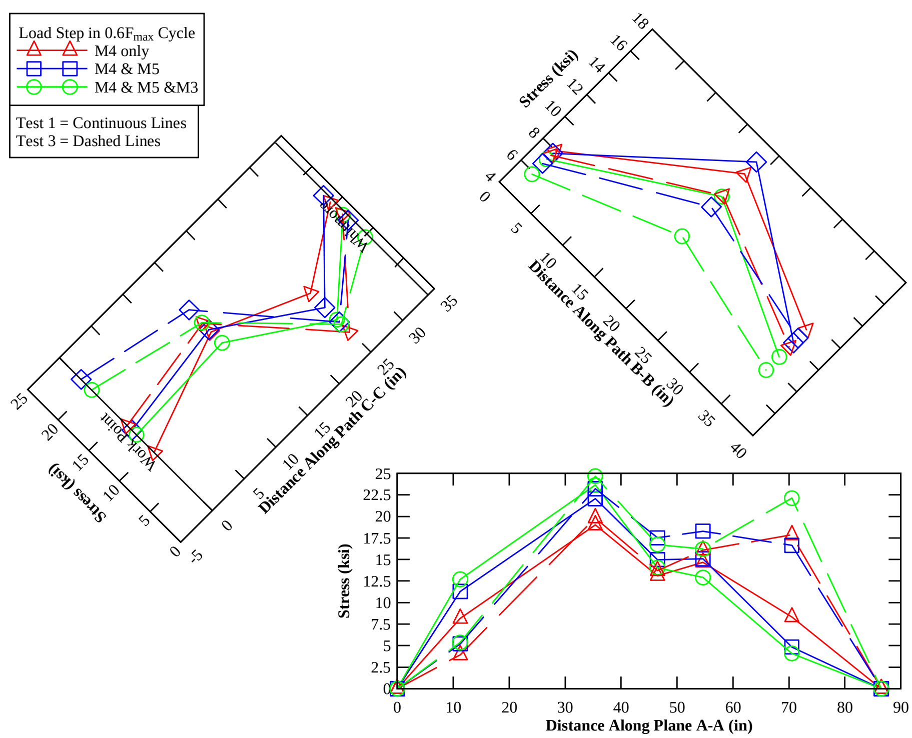

Fig. J-20: Combination loading, Von Mises stress

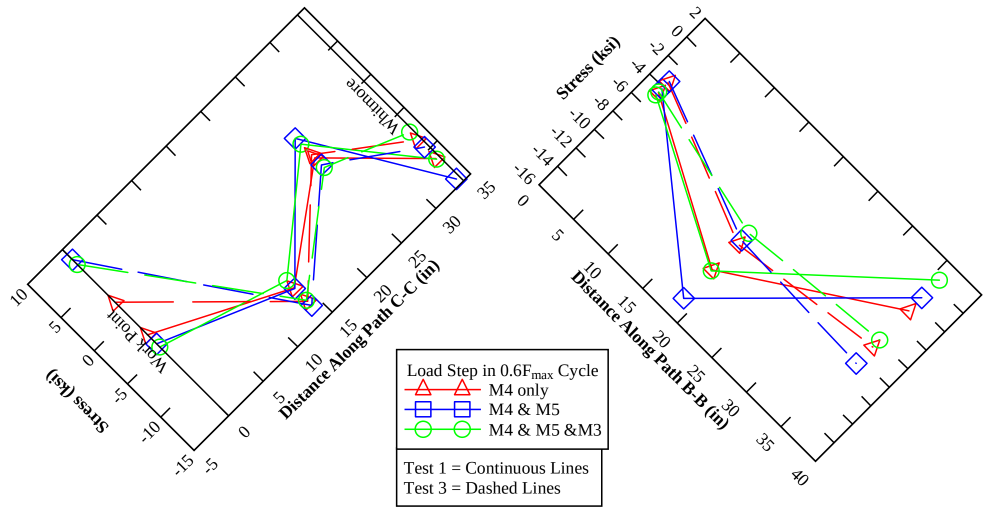

Fig. J-21: Combination loading, stress in M4 direction

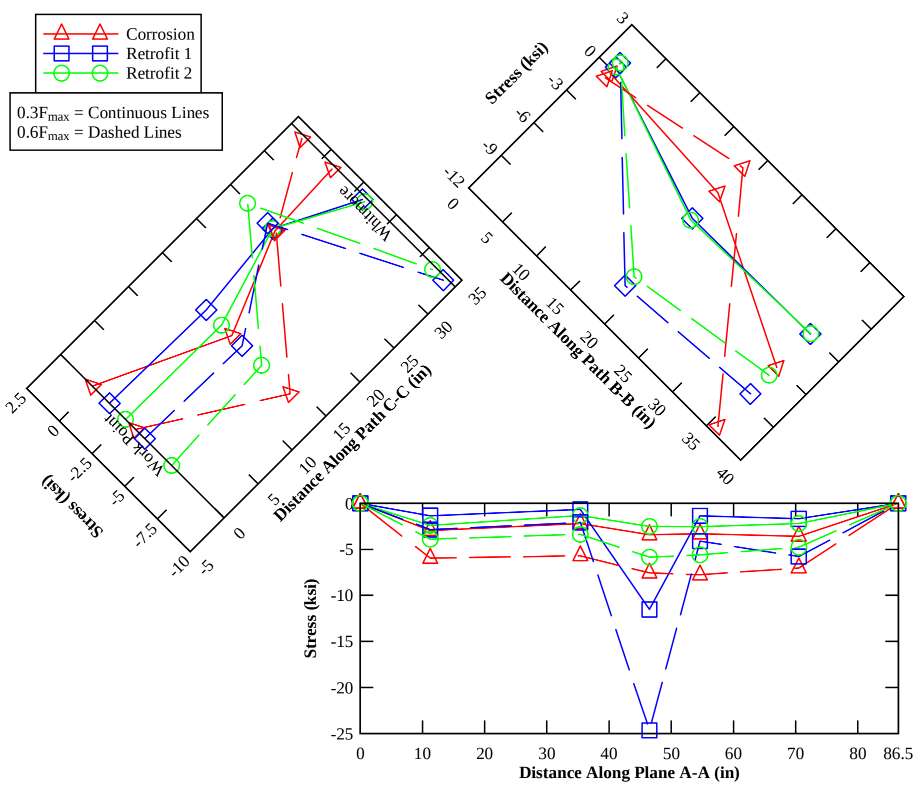

Fig. J-22: Phase 2 specimens, stress in global x direction

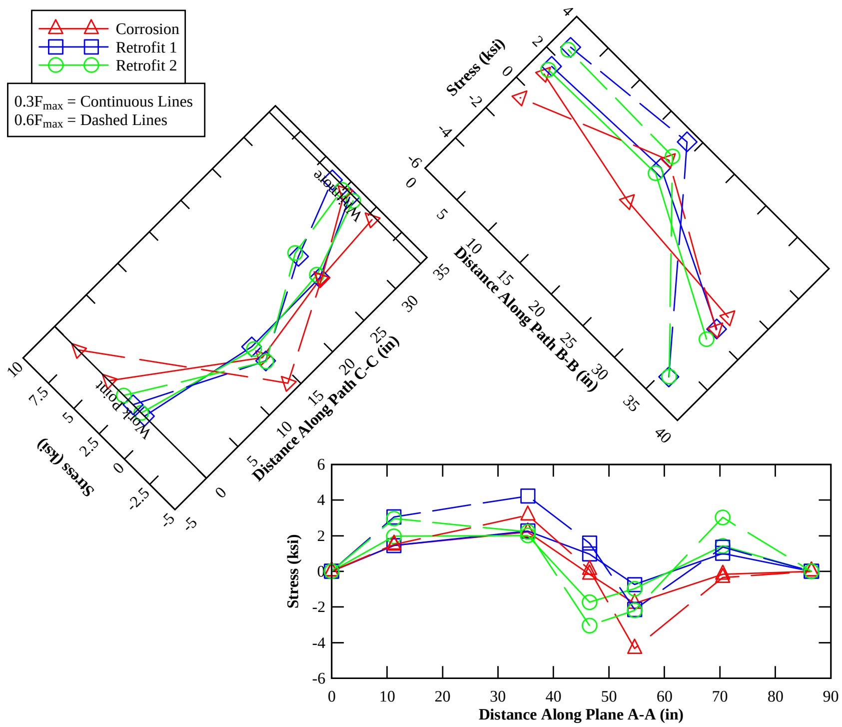

Fig. J-23: Phase 2 specimens, stress in global y direction

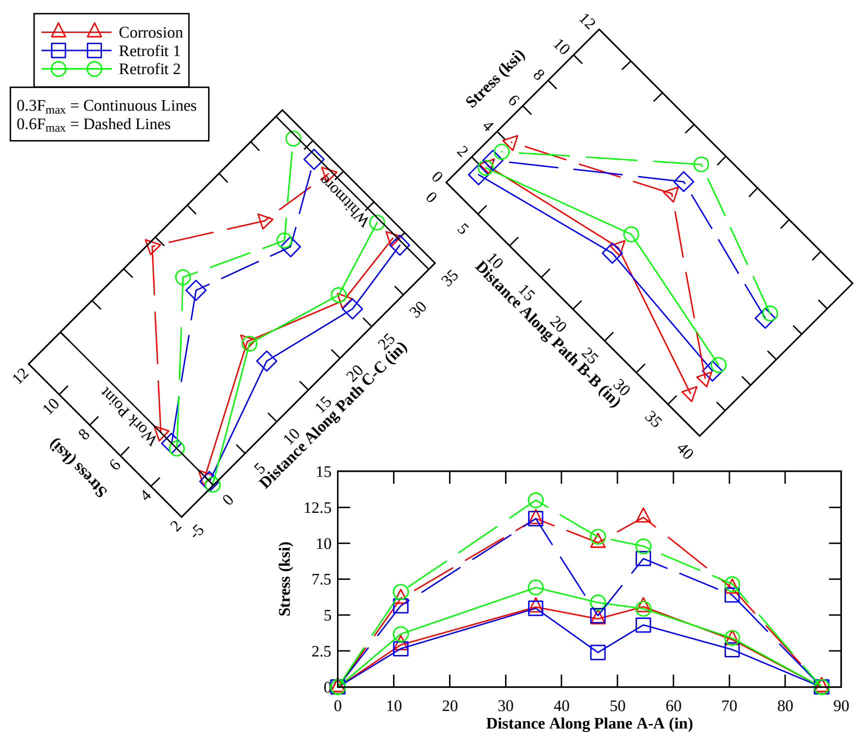

Fig. J-24: Phase 2 specimens, shear stress in global xy direction

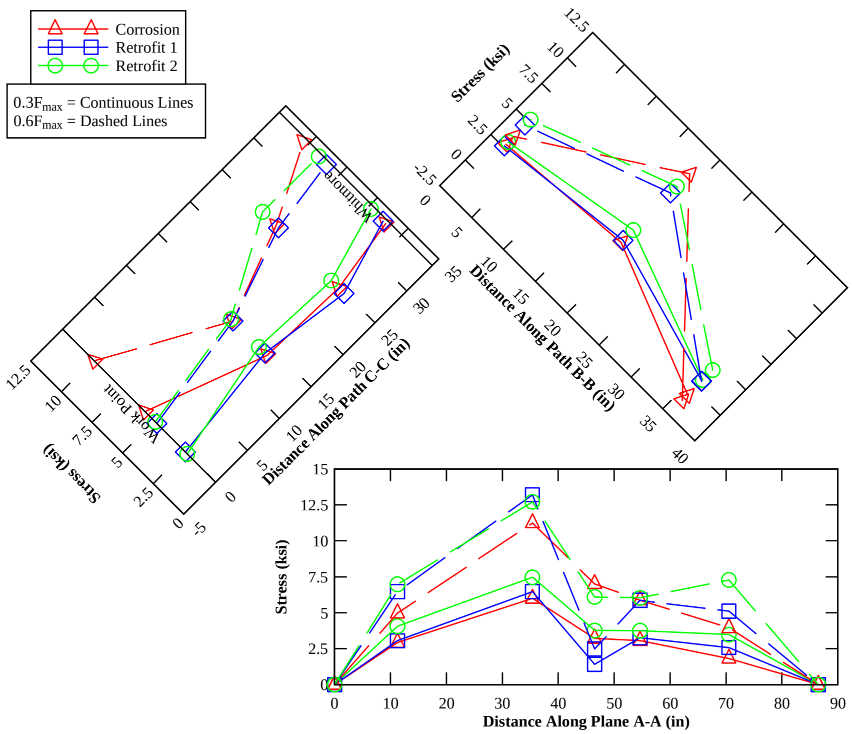

Fig. J-25: Phase 2 specimens, 1st principle stress

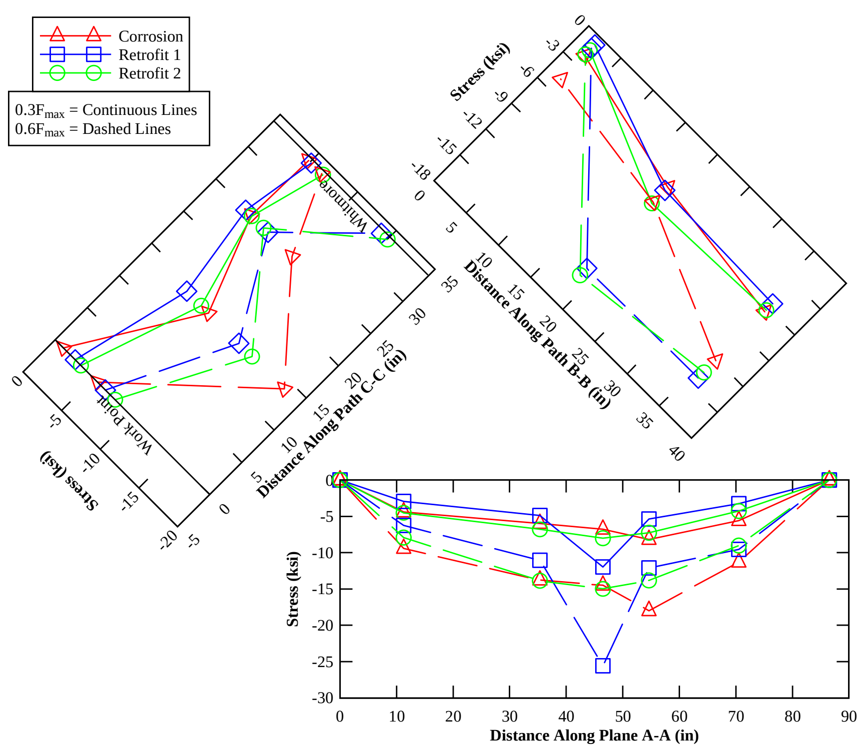

Fig. J-26: Phase 2 specimens, 2nd principle stress

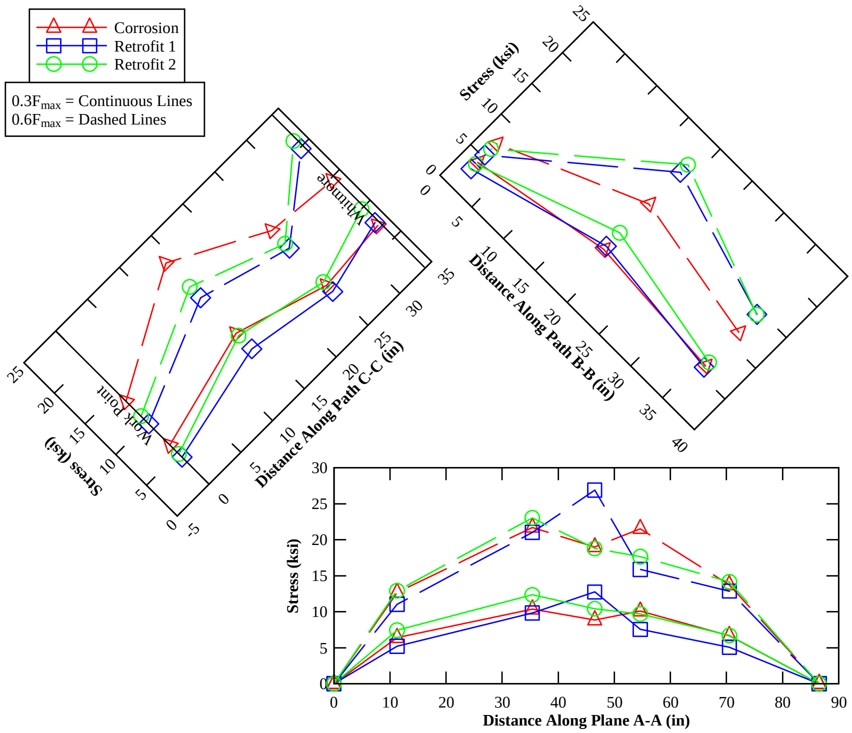

Fig. J-27: Phase 2 specimens, Von Mises stress

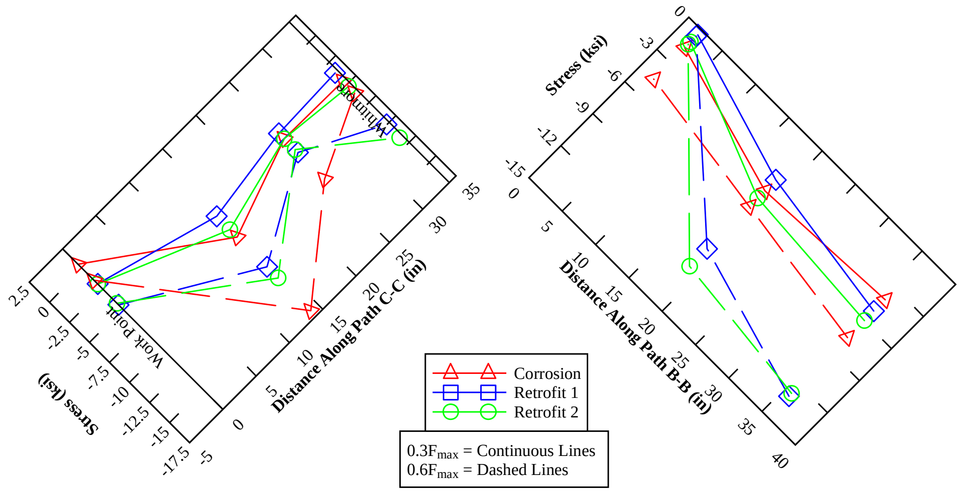

Fig. J-28: Phase 2 specimens, stress in M4 direction

APPENDIX K. NON-SPECIMEN SPECIFIC ADDITIONAL DATA

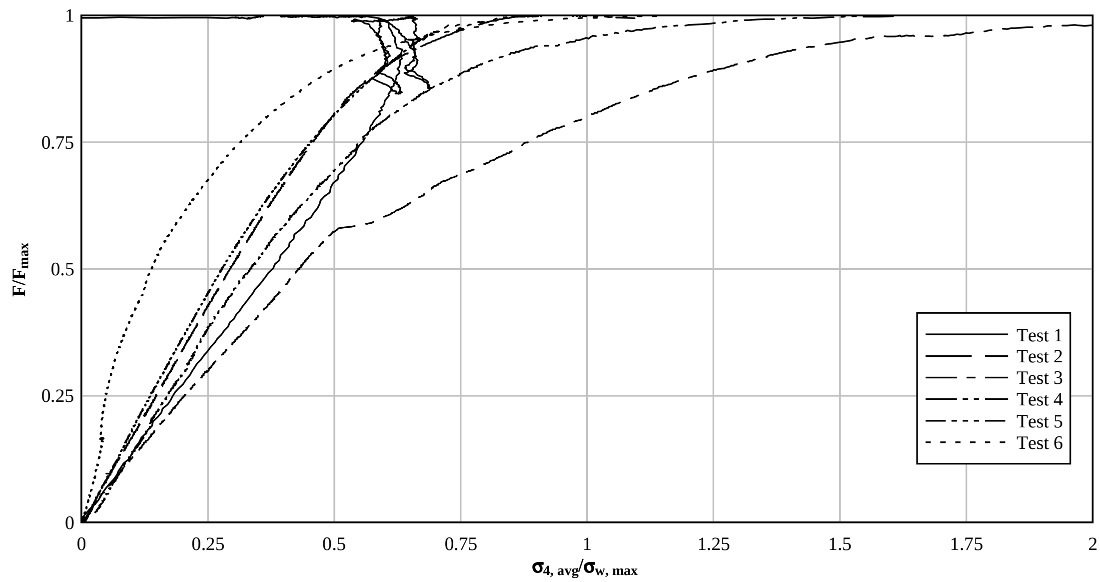

Fig. K-1: Stress in M4 direction normalized to maximum Whitmore stress at center of Whitmore width

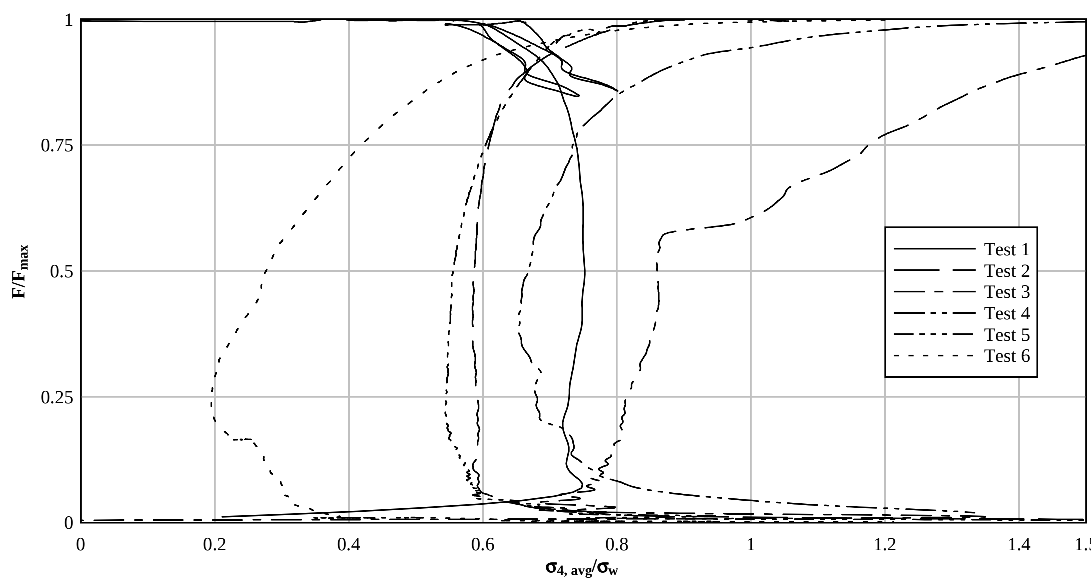

Fig. K-2: Stress in M4 direction normalized to Whitmore stress at corresponding M4 axial load at center of Whitmore width

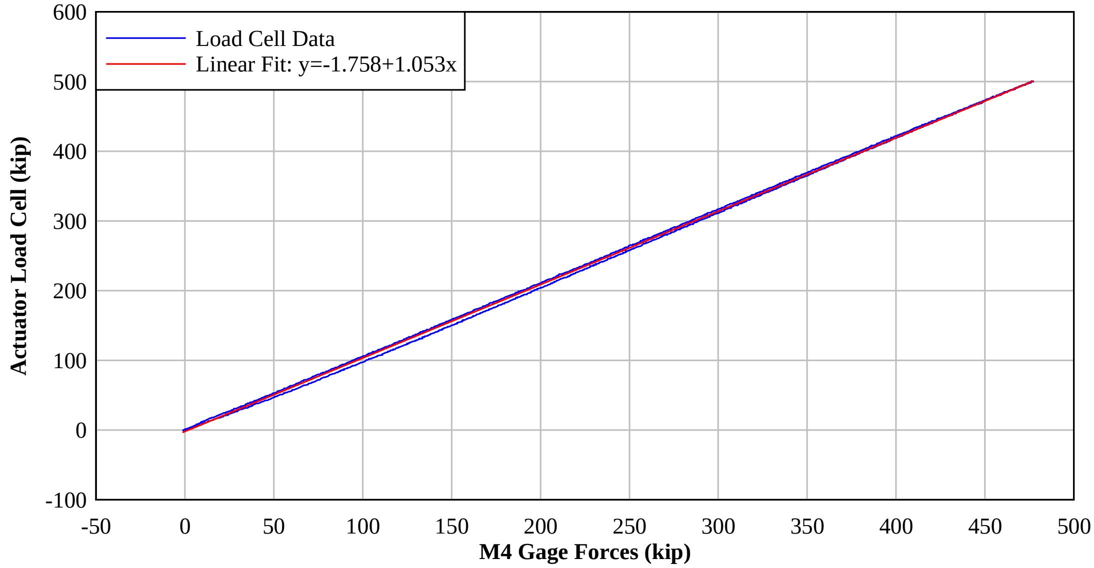

Fig. K-3: Calibration of uniaxial strain gages on M4 for stiff brace section

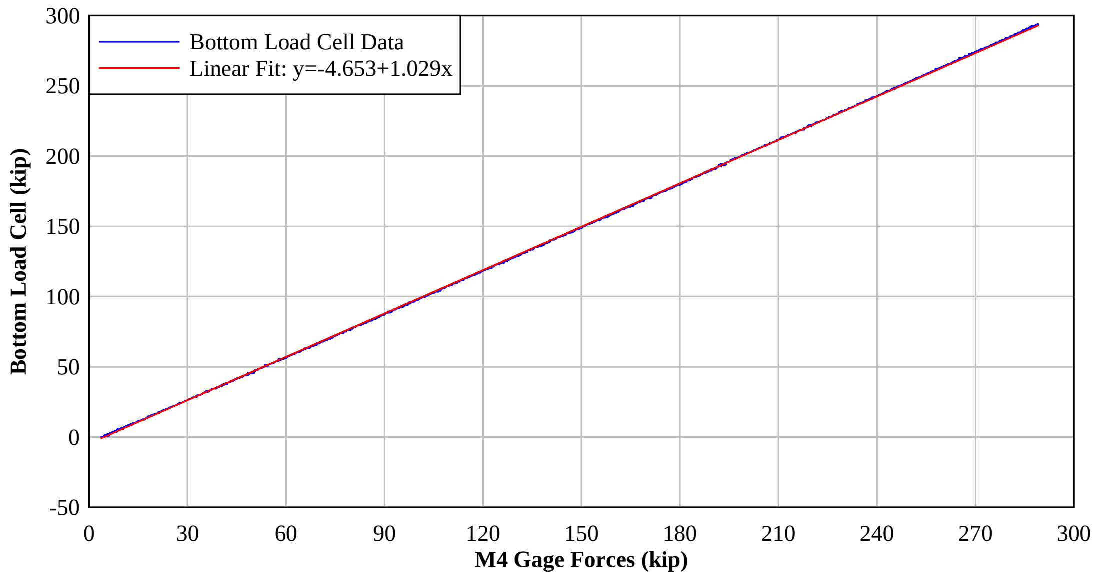

Fig. K-4: Calibration of uniaxial strain gages on M4 for soft brace section

Table K-1: Complete testing matrix with results for second manuscript including stress comparisons to Whitmore and Modified-Thornton

	Retrofit Control	Corrosion Control	Corrosion	Retrofit 1	Retrofit 2
Plate Thickness, mm (in)	6.4 (0.25)	9.5 (0.375)	9.5 (0.375)	6.4 (0.25)	6.4 (0.25)
Initial Imperfection, % thickness	43%	40%	34%	43%	40%
Gusset Free Edge Out-of-Plane Displacement at Failure, mm (in)	21.1 (0.83)	15.2 (0.60)	22.4 (0.88)	10.2 (0.40)	-0.8 (-0.03)
M4 Axial Load at Failure, kN (kip)	1139 (256)	2575 (579)	2504 (563)	1624 (365)	2126 (478)
σ_w at Failure, MPa (ksi)	101.4 (14.72)	152.9 (22.20)	148.7 (21.58)	144.6 (20.99)	189.4 (27.49)
$\sigma_{4,max}/\sigma_w$ at $0.6*F_{max}$	1.79	0.85	0.57	1.03	0.76
$\sigma_{4,max}/\sigma_T$ at $0.6*F_{max}$	2.20	1.05	0.75	1.27	0.94
$\sigma_{4,avg}/\sigma_w$ at $0.6*F_{max}$	0.69	0.57	0.46	0.62	0.51
$\sigma_{4,avg}/\sigma_T$ at $0.6*F_{max}$	0.41	0.59	0.60	0.69	0.56
σ_p/σ_w at $0.6*F_{max}$	1.89	0.98	0.91	1.24	1.16

All stresses measured at gages R1, R2, and R3 located along the Whitmore width.
$\sigma_{4,max}$ = maximum measured stress in the direction of member M4.
$\sigma_{4,avg}$ = average measured stress in the direction of member M4.
σ_p = maximum measured principle compressive stress.
σ_w = theoretical Whitmore stress across Whitmore effective width.
σ_T = theoretical Modified-Thornton stress across Modified-Thornton effective width.

APPENDIX L. FINITE ELEMENT ANALYSIS ADDITIONAL DATA

Table L-1: Complete Abaqus testing matrix showing $K_{retrofit}/K_{initial}$ for ¼” gusset plates with $K_{initial}$ = 11.33 kip/in.

	Stiffener Plate Thickness	1/4" angles	3/8" angles	1/2" angles	5/8" angles	3/4" angles
h = 24.875", h' = 0" (fixed base)	1/8”	2.49				
	1/4”	2.84	3.48	3.95	4.31	4.60
	3/8”	2.95	3.74	4.34	4.76	5.06
	1/2”	3.00	3.85	4.51	4.98	5.29
	5/8”	3.03	3.90	4.60	5.09	5.42
	3/4”	3.06	3.94	4.66	5.16	5.50
h = 24.875", h' = 2.375"	1/8”	2.12	2.42	2.72	2.99	3.22
	1/4”	2.33	2.77	3.12	3.39	3.60
	3/8”	2.40	2.93	3.34	3.63	3.84
	1/2”	2.44	3.00	3.45	3.77	3.98
	5/8”	2.47	3.04	3.51	3.84	4.07
	3/4”	2.49	3.07	3.55	3.89	4.12
h = 24.875", h' = 8"	1/8”	1.34	1.42	1.49	1.54	1.57
	1/4”	1.37	1.45	1.51	1.56	1.58
	3/8”	1.38	1.47	1.53	1.57	1.60
	1/2”	1.38	1.48	1.54	1.58	1.61
	5/8”	1.39	1.48	1.55	1.59	1.61
	3/4”	1.39	1.48	1.55	1.59	1.62
h = 24.875", h' = 13.625"	1/8”	1.08	1.09	1.10	1.11	1.11
	1/4”	1.08	1.09	1.10	1.11	1.11
	3/8”	1.08	1.10	1.11	1.11	1.11
	1/2”	1.08	1.10	1.11	1.11	1.11
	5/8”	1.08	1.10	1.11	1.11	1.12
	3/4”	1.08	1.10	1.11	1.11	1.12

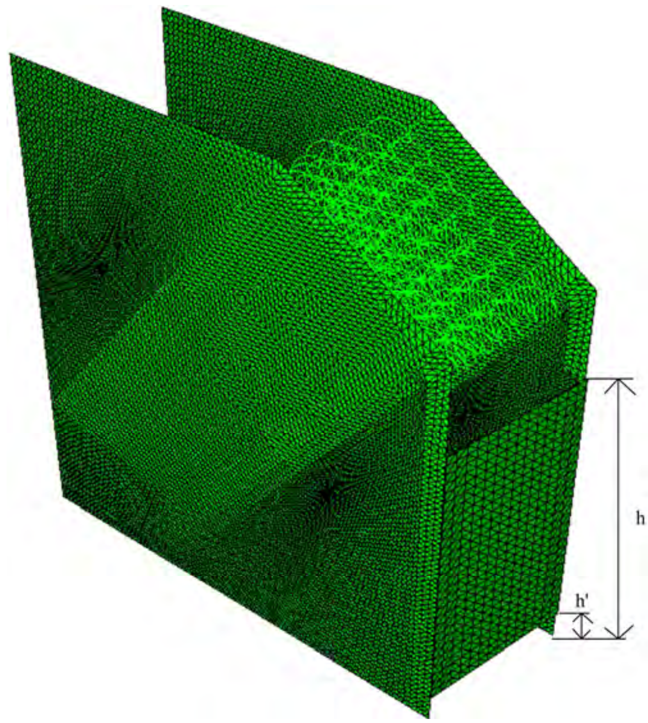

Fig. L-1: Retrofit #1 undeformed model with h and h' defined

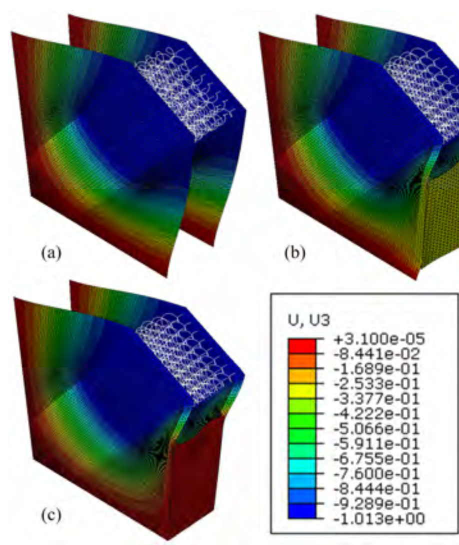

Fig. L-2: Deformed models showing out-of-plane displacement (inches), (a) unstiffened model, (b) retrofit #1 model, (c) retrofit #2 model

Table L-2: Spring analogy testing matrix with results

Translational Stiffness (kip/in)	Equivalent Plate Thickness (in)	Rotational Stiffness X (kip-in)	Rotational Stiffness Y (kip-in)	Trans. System Stiffness[a] (kip/in)	Total System Stiffness (kip/in)
1	0.00019	93.6	1.93E-07	12.06	12.07
5	0.00093	468	2.41E-05	14.64	14.70
10	0.00186	936	1.93E-04	16.55	16.68
50	0.00929	4680	0.0241	20.76	21.19
100	0.01858	9360	0.193	21.80	22.34
250	0.04646	23400	3.015	22.54	23.34
500	0.09292	46800	24.12	22.81	24.74
1000	0.18585	93600	193	22.95	27.78
1500	0.27877	140400	651	23.00	29.04
2000	0.37170	187200	1544	23.02	29.48
5000	0.92924	468000	24117	23.06	29.89
10000	1.85848	936000	192940	23.08	29.95
15000	2.78772	1404000	651171	23.08	29.96

a) System stiffness is only with translational spring (no rotational springs)
b) Total system stiffness with pinned boundary condition at springs = 23.10 kip/in
c) Total system stiffness with fixed boundary condition at springs = 29.98 kip/in